The Effect of Emulsion Chemistry on Rolling Contact Fatigue

A thesis submitted to the University of London for the degree of Doctor of Philosophy and to the Imperial College of Science, Technology & Medicine for the Diploma of Imperial College.

by

GARETH FISH

August 1989

Tribology Section
Dept of Mechanical Engineering
Imperial College
Exhibition Road
London
SW7 2BX

Abstract

This thesis describes work carried out into the rolling contact fatigue performance of water-based hydraulic fluids. Firstly relevant literature on rolling contact fatigue and water-based fluids is reviewed. This includes an examination of the influence of operating conditions on premature fatigue failure, and a consideration of statistical methods and the treatment of fatigue results.

Then the different types of water-based fluids and their comparative performance are described and the four mechanisms for the premature failure of bearing steels critically examined.

Test methods employed to study the rolling contact fatigue performance of lubricants are reviewed and deficiencies in the various test methods highlighted.

A new test rig, a rolling contact fatigue four-head rig, is introduced as a new test method for lubricant evaluation and a series of tests to quantify the performance of the test rig using commercial fluids (one of each type of fluid) are described. Further investigative test series into the effects of applied potential, dilution, loading and the performance of a new polymer thickened fluid are also presented and discussed.

As well as fatigue tests on the four-head rig an Admiralty Oil Laboratory vertical fatigue rig has been used to prepare specimens for chemical analysis and a rotating-bending fatigue rig employed to investigate the effect of water-based fluids on crack propagation rates.

The results of all these tasks have been collated and analysed to determine the effect of water on rolling contact fatigue. The new test method ranked the fluids in an order consistent with previous reports although lives were longer than predicted from theory.

The mechanistic study shows that the greatest influence on failure is the low film thickness formed though with longer lived specimens the contribution of corrosion and hydrogen embrittlement become more significant.

TABLE OF CONTENTS

LIST OF TABLES

7.9 Protocol for testing the polymer-thickened fluid

7.10 Calibration Data for the Reference Mineral Oil using the Optical EHD rig

7.11 Results for the polymer-thickened fluid in the optical EHD rig

7.12 Film growth observations for the various fluids

7.13 Comparison of the formulations of the aqueous glycol with the polymer-thickened fluid

7.14 Formulations of the dilute emulsions and the polymer-thickened fluid

LIST OF FIGURES

List of Symbols

C	dynamic capacity of the bearing/newtons
P	applied Load/newtons
K,n,k,C,m	constants
h_{min}	minimum)
h_{opt}	optical) elastohydrodynamic
$h_{central}$	central) film thickness
U mean speed	$[(U_1 + U_2/2]$
η	dynamic viscosity
D	film thickness parameter $(1/\lambda)$
λ	specific film thickness
σ_n	rms roughness of surface n
L_{10}	10% fatigue life
L_{50}	50% fatigue life
e	Weibull Slope
Po or Pmax	maximum Hertz stress
$\frac{da}{dN}$	crack propagation rate (13)
C,m	Paris materials constants
ΔK	Change in stress intensity factor
Hv	Vickers hardness
Ra	Centre Line Average Roughness
A_1	reliability factor)
A_2	materials factor) (36)
A_3	severity factor)
p	pressure
α	pressure-viscosity coefficient
a,b,c	Vogel Coefficients
T	absolute temperature
ln	natural logarithm
log	common logarithm
F_1)	
F_2)	Derating factors for modified bearing load-life equation
F_3)	
τ_{45}	maximum shear stress
σ_b	bending stress

Glossary

HF-A - dilute Emulsion (DE)
HF-B - invert Emulsion (IE)
HF-C - aqueous glycol (AG)
PTF - polymer-thickened fluid
VI - viscosity Index
PTFE - polytetrafluoroethylene
MEA - monoethanolamine (2-aminoethanol)
IPAE - isopropylaminoethanol
EHD - Elastohydrodynamic
IR - Infra Red
SEM - Scanning Electron Microscope
SIMS - Secondary Ion Mass Spectroscopy
SNMS - sputtered neutral Mass Spectroscopy
ASME - American Society of Mechanical Engineers
ASLE - now (STLE) American Society of Lubrication Engineers
WBF - Water-based fluids
MO - Mineral Oil
PE - Phosphate Ester
EP - Extreme pressure
KF - Karl Fischer
SF - Synthetic Fluid
BEA - Basic Electric Arc
VD - Vacuum Degassing
HE - Hydrogen Embrittlement
SCC - Stress Corrosion Cracking
trans- Transactions
JoLT - Journal of Lubrication Technology

ACKNOWLEDGEMENTS

These are featured in no particular order.

Dr Hugh Spikes for his supervision

Dr Philippa Cann for the IR Spectra

Reg Dobson, Tony Whymark, Paul Garden, Kevin Pickett and Mike Ottmann for Technical Support.

Dr John Kilner for the SIMS

Dr Sean Crofton for Hydrogen and the SEM

Mrs Pat Sharp and her colleagues for typing this thesis

Members of the Tribology Section for help and advice

British Coal for their generous support of this project

Mr Peter Kenny, Dr David Yardley and Mr Miles Talks of British Coal for advice and help

Dr Andy Olver of Westlands for the Rotating-Bending Rig

Mr Norman Hopkinson of RAE Pyestock for the AOL Rig

Mr David Hughes of Lubrizol for the Polymer-thickened fluid

Members of RCS and IC Unions, RCS Motor Club and the '22 Club.

Liz

My Parents

My Brother and Sisters

And finally to Dr Terry Moynehan, Mr Ian Harris and Mr Malcolm Sparks of the MOD for telling me to "Bloody Get it Done"

This Thesis is Dedicated to the Memory of my brother

Adrian Fish

who died before this came to fruition

1. Introduction

In many hydraulic fluid applications there is a risk of the fluid catching fire with disasterous results eg in Mining, steel processing and warships. Because of this, since the 1940's fire resistant hydraulic fluids have been developed to replace flammable mineral oils and common synthetic oils.

There have been two approaches in the quest for fire resistance, the first involving the use of special synthetic oils, and the second employing water-based fluids. The latter are used in confined spaces and in large scale applications, where health hazards and costs preclude the use of synthetics.

A major problem in their use is that water-based hydraulic fluids do not perform as well in a lubricating role as the mineral oils which they replaced. The major area of deficiency of water-based fluids is in rolling contact fatigue performance when lubricating the bearings of pumps and other moving machine parts. A number of likely mechanisms of this poorer performance have been identified in the past but arguments exist as to the relative importance of the different mechanisms in practical systems. This thesis describes work aimed at the elucidation of the causes of low fatigue lives with water-based fluids.

In chapter two the causes of rolling contact fatigue are identified and characterised. Because fatigue is a statistical process, special analytical techniques have to be applied to results and these are outlined. Factors promoting premature failure are examined, and mathematical models used to explain the failures are reviewed.

Chapter 3 introduces the three main types of water-based fluids and chronicles the historical problems of dissolved water in mineral oils. The four mechanisms for the promotion of premature failure of bearing steels are also described.

Test rigs used to evaluate fire resistant fluids are discussed in chapter four and test method deficiencies identified.

In Chapter five the test rigs used in this study are presented and the need for a new test method explained. Chemical techniques employed in this study to elucidate mechanistic effects are also introduced.

Chapters six and seven present the results of the tests and experiments into the causes of premature failure. These results are discussed and the conclusions drawn in chapter eight. Finally chapter nine proposes further work in areas highlighted by this study.

2.1 ROLLING CONTACT FATIGUE

2.1.1 Definition

Rolling Contact Fatigue is an important cause of failure of loaded, rubbing, lubricated contacts. According to Scott (1), 'Rolling Contact Fatigue is characterised by the sudden removal of surface material and in some cases by the catastrophic fracture due to repeated alternating stress. The process has three phases : preconditioning of the surface prior to cracking, crack initiation and propagation'.

2.1.2 Brief History of Rolling Contact Fatigue

This Section provides a very cursory history of our knowledge of rolling contact fatigue to illustrate the order in which the important factors influencing fatigue were recognised historically.

Over fifty years ago, Way (2) discovered that when two rollers were loaded together and run with a lubricant present, the surfaces of the rollers pitted. By contrast, when rollers were run dry, no pits formed. Way (2), experimented with a range of steels and loads, and various lubricants. He found that pitting could be postponed to at least twelve million cycles by using a high viscosity mineral oil or by employing nitrided and polished, and hence very hard and smooth, rollers. As there was no method, at the time, of measuring or estimating the lubricant film thickness, Way was unable to explore the correlation between film thickness, load and speed. This was not achieved until nearly 20 years' later. After the Second World War, research into rolling contact fatigue was resumed. Lundberg and Palmgren (3), suggested that fatigue life was related to the load

applied to the bearing and its load carrying capacity. Lundberg and Palmgren (3), produced a relationship between the factors shown below in Eq. 2.1.

$$\text{Life} = K\,(C/P)^n \qquad \text{Eq. 2.1}$$

where K,n are constants

C is the load-carrying capacity of the bearing

P is the applied load

An initial value of 10/3 was calculated for n but as will be shown later, this was adjusted with further work. Prior to 1954, all work was carried out using assorted mineral oils as lubricants. In that year Cordiano and co-workers (4) reported that a synthetic oil, an aqueous glycol promoted pitting in bearing steels.

The study of rolling contact fatigue mushroomed in the 1960s. Grunberg and Scott's work (5), demonstrated the premature rolling contact fatigue failures caused by water dissolved in mineral oils. Crook (6), measured the film thickness of various oils at a range of speeds and devised the following relationship between the lubricant film thickness and the viscosity of the lubricant and the speed of the surfaces, Eq. 2.2.

$$\text{Oil film thickness, } h_{min} = k\,(U\eta)^{0.7} \qquad \text{Eq. 2.2}$$

where k is a constant

Using this relationship, Dawson (7), investigated the effects of oil film thickness and surface roughness of rollers on pitting fatigue life. From this work he proposed that pitting life was dependent upon the ratio of the film thickness to the composite surface roughness.

Dawson (7), called this parameter the D-ratio, and suggested that below certain D values, no pitting took place because metal-metal contact was prevented.

$$\text{Film thickness parameter, } D = \frac{\sqrt{\sigma_1^2 + \sigma_2^2}}{h_{min}} \qquad \text{Eq. 2.3}$$

h_{min} = minimum film thickness

$\sigma_{1,2}$ = rms surface roughness of surfaces 1 and 2

At the same time, Rounds (8), looked at the effects of oil viscosity and chemical composition on the fatigue lives of ball bearings. Rounds found that, on the whole, fatigue life increased with viscosity for naphthenic oils but not with paraffinic oils. The same was true for other synthetic fluids tested.

The conclusions drawn from this is that the chemical reactivity of the lubricant is important. Rounds also found that the more stable the lubricant was to oxidation and high temperatures, the longer the fatigue lives obtained.

McKelvey and Moyer (9) looked at the relationship between the maximum compression stress (P_o) and the fatigue lives obtained under rolling contact and concluded that the relationship as given in equation 2.4 was only approximate.

$$\text{Fifty per cent survival life, } L_{50} = K(P_o)^m \qquad \text{Eq. 2.4}$$

where m ranges from 4.5 to 9

A more accurate figure for the value of m is given later in Section 2.4.

The early work of Way (2), was performed under conditions of pure rolling, with both rollers run at the same speed. Dawson, in a 1963 paper (10), demonstrated that slip promoted fatigue so that the slide-roll ratio is an important factor in fatigue life.

From the work outlined above, it can be noted that the most obvious factors affecting rolling contact fatigue are as listed in Table 2.1

Factors Affecting Rolling Contact Fatigue
Presence of Lubricant
Steel type/hardness
Oil film thickness
Surface roughness
Contact pressure
Speed
Temperature
Water content
Slip (Slide/roll Ratio)

Table 2.1

Subsequently, this list has been extended to incorporate other factors affecting rolling contact fatigue as will be discussed later (Table 2.4). The influence of some of the major factors in fatigue, steel, lubricant and film thickness will be further discussed in Section 2.4. The effect of water and water fluids, the most important aspect of this study is discussed at length in Chapter 3 but, prior to this, the modes of failure of rolling contact fatigue are briefly considered.

2.2 FAILURE MODES

Tallian, in 1968 (11), reviewed rolling contact failure and surface distress and outlined four failure modes as shown in Table 2.2.

Mode	Description
Wear	Mild and smearing
Plastic flow	Cold or due to overheating
Fatigue	Spalling and micropitting
Bulk or structural failure	Component failure away from the contact

Table 2.2 (11)

Rolling Contact Fatigue Failue Modes

More recently, Berthe and co-workers (12), have described five modes of surface produced in rolling contacts, listed in Table 2.3.

Mode	Description
Micropitting	Rashes of small pits ~ 20 μm in diameter
Sponges and flats	Worn areas a few mm in diameter
Macropits	Shallow voids of larger areas
Wear	Complete surface removal
Spalling	Small deep pits (orthodox pitting)

Table 2.3 (12)

Rolling Contact Fatigue Failue Modes

Of the above failure modes, wear is an enormous subject in its own right and is beyond the scope of this thesis and the other modes apart from structural fatigue, spalling and micropitting, are manifestations of wear. Structural fatigue is usually caused by poor component design or by incorrect fitting or misalignment and is also beyond the scope of this thesis. Micropitting and spalling are discussed in some detail below.

2.2.1 Spalling (pitting)

Spalling is the orthodox failure mode for rolling contact fatigue. Like most modes of failure, it is related to the inability of the lubricant to prevent asperity-asperity interaction between the two surfaces though spalling can eventually occur even in the absence of such interacation. In most occurrences of spalling, the asperity interactions promote the opening of small microcracks in the surface region of the contact. These cracks grow until a critical crack size is reached. This 'initiation' stage of rolling contact fatigue is discussed further in Section 2.2.4.1.

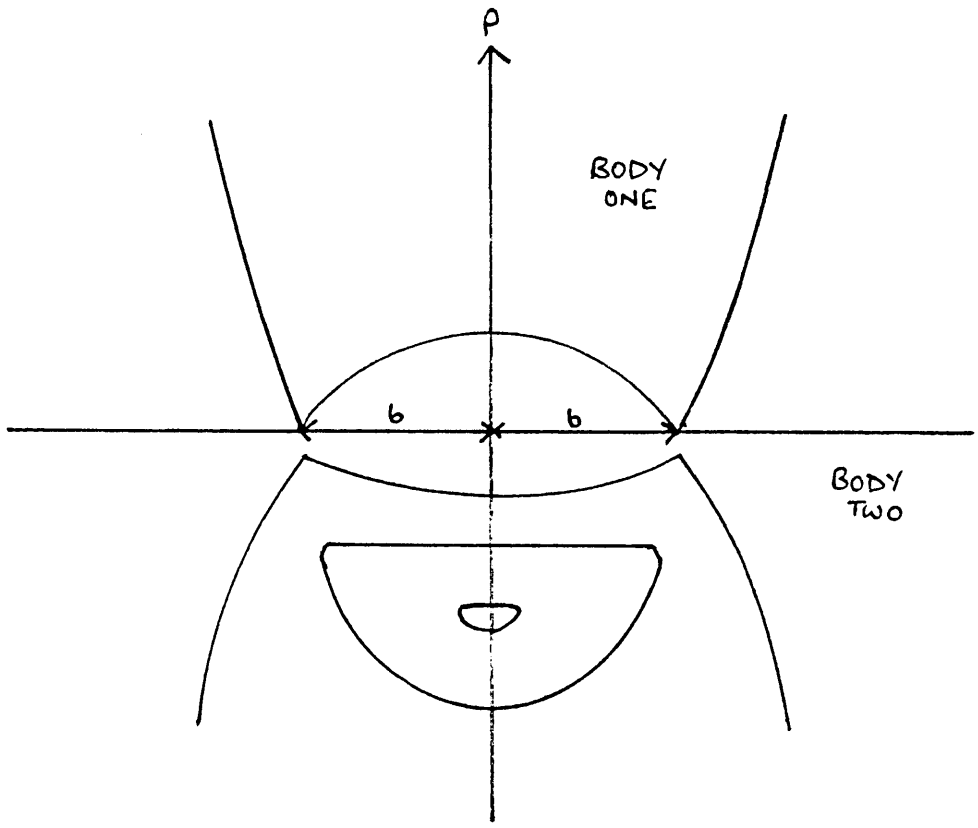

The macrostress field

Figure 2.1

The macrostress field, as shown in Figure 2.1, then causes the cracks to grow and propagate along the lines of stress. The crack branches and continues to grow at an ever increasing rate until a section of metal is undermined as in Figure 2.2.

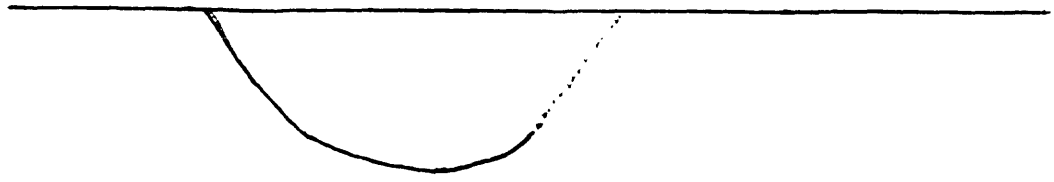

Figure 2.2

Cracking in a contact

Fracture then occurs along the dotted line and a whole section of metal breaks off to leave a cavity (spall or pit) as shown in Figure 2.3.

Spalling is usually surface initiated but, depending on the conditions employed, may also be sub-surface initiated. A mathematical model of spalling is given in Section 2.6.

2.2.2 Micropitting

Micropitting, as defined by Berthe and co-workers (12), is an area of rash-like pits whose individual diameters are small. Micropits are caused by an acute lack of lubricating film, so that a considerable amount of asperity interaction takes place and individual asperities undergo direct stressing due to the contact, Figure 2.4.

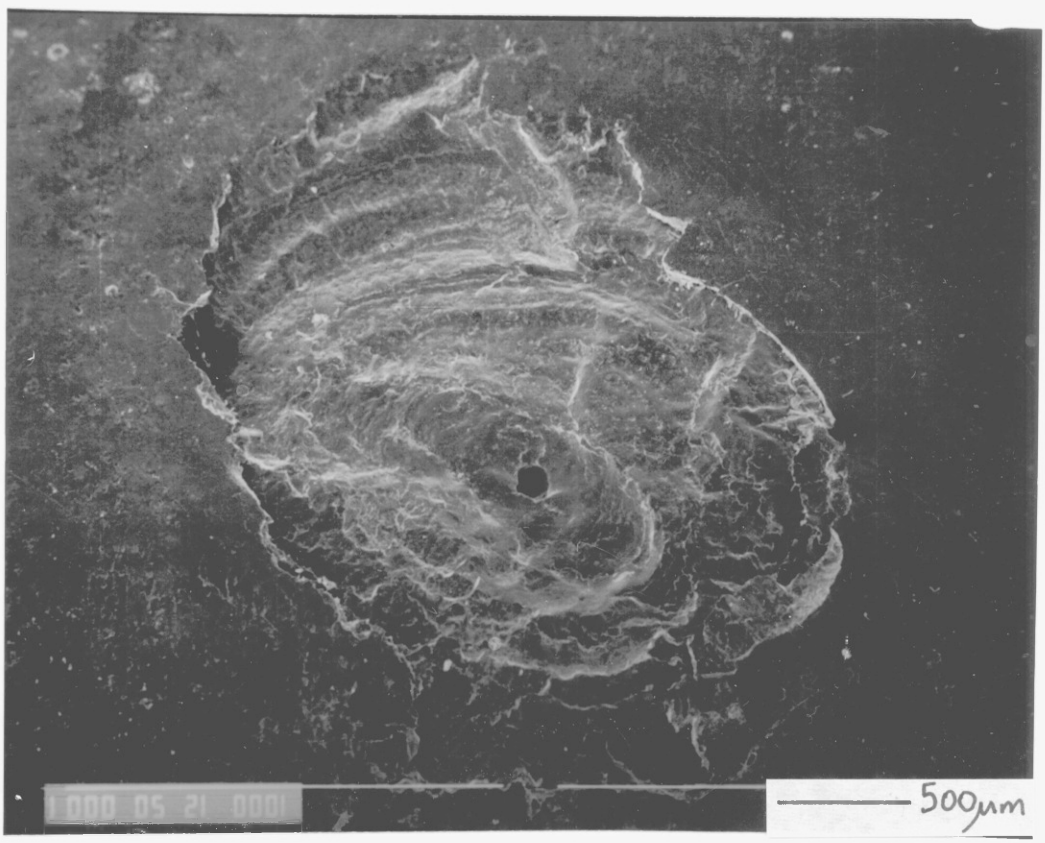

Figure 2.3

An electron micrograph of a ball having spalled, run in an invert emulsion for 12.84 million cycles.

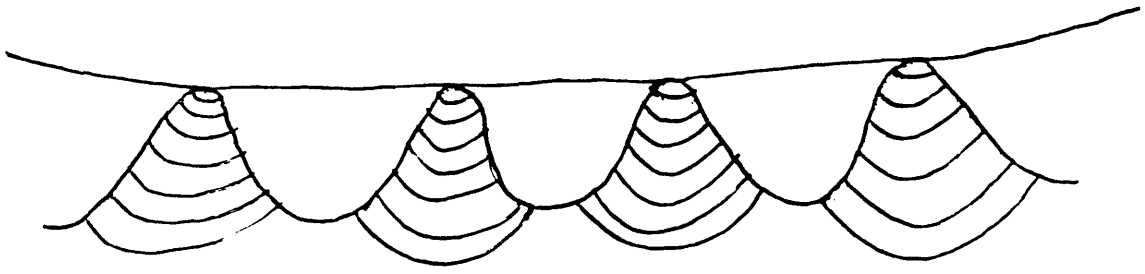

Figure 2.4

Microstress field on an asperity scale

This asperity stressing causes a high density of cracks to initiate and, as in spalling, these are propagated by the strain resulting from the stress cycle. Micropitting, has, in the past, been considered a form of wear but it is formed by a fatigue mechanism. A good example of micropitting is shown in Figure 2.5 where a small thrust bearing was run by the author for approximately 6 million cycles in a dilute emulsion.

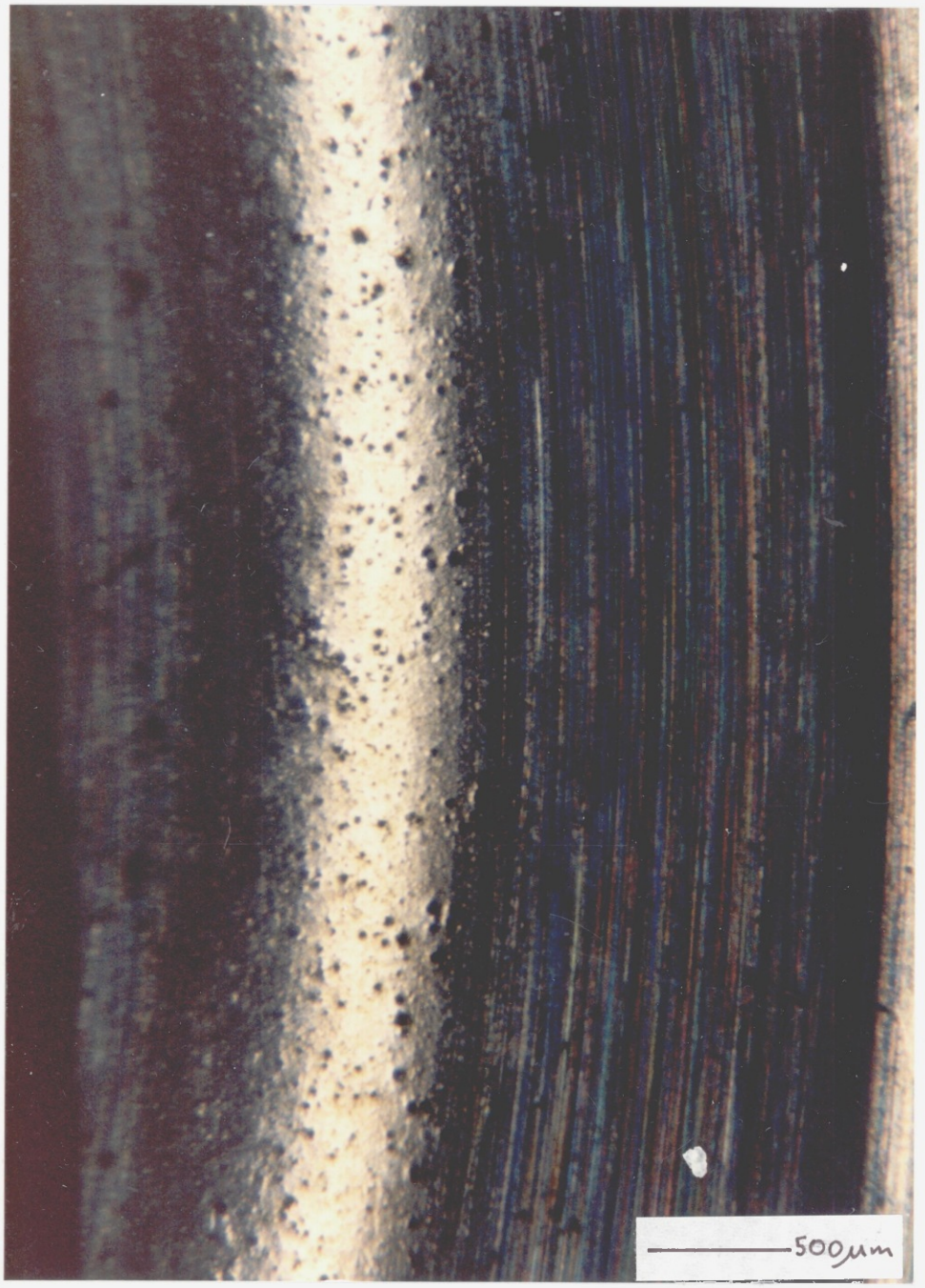

Figure 2.5

Micropitting

2.2.3 Micropitting versus spalling

In conditions of low film thickness there is competition between the two modes of fatigue failure and in some instances both spalls and micropitting are present. From Berthe and co-workers (12), and Tallian (11), it appears that micropitting is usually formed faster than spalling but this is because it is due to higher local stresses. At slightly thicker film thicknesses, life is longer but the mode of failure may again be a mixture of micropitting and spalling. Above a certain value of film thickness, micropitting is not formed except that after spalling has occurred the lubricant film collapses and micropitting may subsequently take place. In such a case, when examined, the failure looks like a combination of the two modes. The effect of film thickness on fatigue life is further discussed in Section 2.5.2.

2.2.4 Initiation and Propagation of Fatigue Cracks

The initiation and propagation of rolling contact fatigue cracks in the surface region of steels is a very important aspect of this study. If fatigue cracks can be prevented from forming or from growing to the critical crack size, then fatigue can be controlled.

In Section 2.1.2 the origins of rolling contact fatigue were discussed but the distinction between crack initiation and propagation was not. Depending upon the roughness and the cleanliness of the steel and the magnitude of the stresses involved, microcracks are formed in the surface or subsurface region. Surface cracks are those which start at the surface whilst, as the name implies, subsurface cracks grow and propagate wholly in the subsurface region of the metal. One or two things may happen to these cracks, either they may grow until the stress cycle is relieved and then stop growing or the stress may cause the crack to grow to the critical crack size. Crack growth is usually

in the direction of the maximum shear stress. Below this critical crack size, the cracks may be easily closed but above it, constant rate crack propagation commences. Up to the point where the critical crack size is reached, this zone is called, according to Paris (13), Region I crack growth or initiation. The steady state crack propagation is also called Region II crack growth or propagation. This crack propagation continues until a sufficient amount of the component has been undermined that the component fractures. This fracturing is the third region of crack growth. Paris and Erdogan (13), originally described these three stages in Figure 2.6 and the Region II crack growth rate which is approximately constant is covered by the Paris law of crack growth and it is discussed in Section 2.2.4.2.

There are two ways in which a lubricant can affect these events. The time to initiation or the initiation stresses can be lowered or the steady state crack propagation rate can be affected by the lubricant. Lockwood and co-workers (14), have studied the effects of additives and water on initiation and found that under certain conditions the initiation is affected, Figure 2.7.

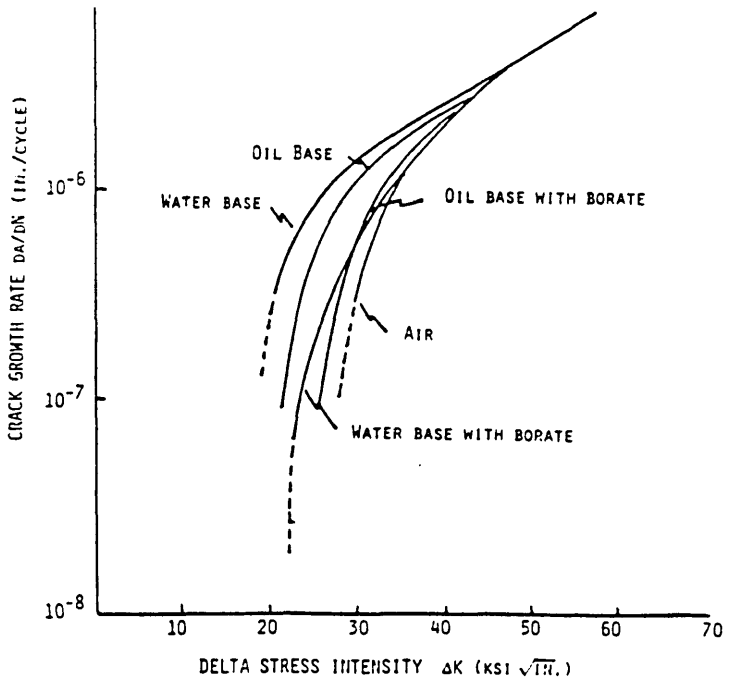

Figure 2.7

Effect of additives on initiation (14)

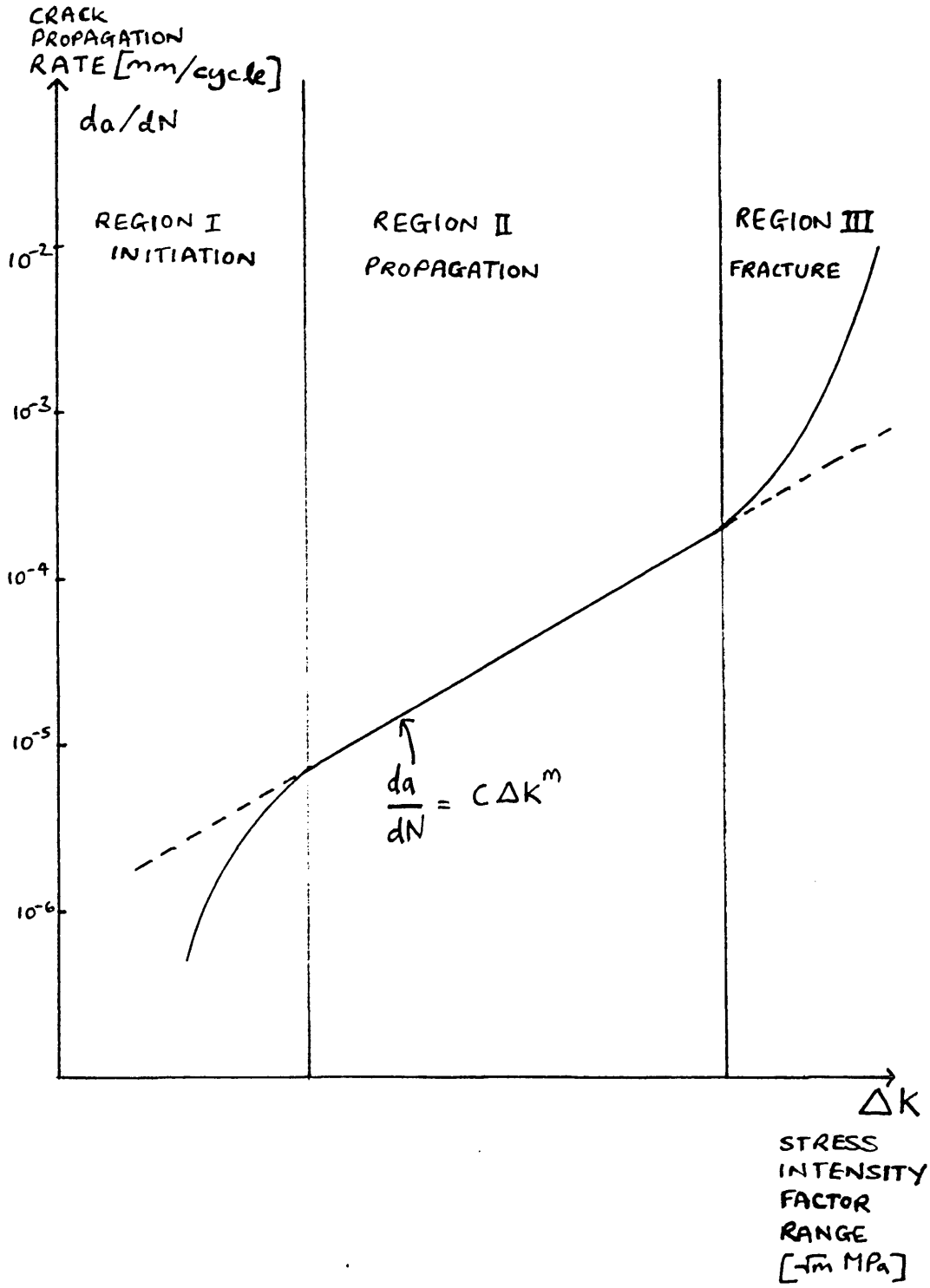

Figure 2.6

The rate of crack growth (13)

It is very difficult to study initiation and propagation behaviour in rolling contacts because there is no easy method of measuring the actual contact conditions whilst the bearing or raceway is actually running. Several techniques have been tried and some are discussed in Section 5.1. As a result of this, non-rubbing methods such as rotating-bending are often employed to study the influence of lubricants on crack growth. The use and operation of relevant fatigue test rigs is discussed in Sections 4.8 and 5.3.

2.2.4.1 Initiation

One method of separating initiation from propagation is to pre-crack the samples so that the initial crack is greater than the critical crack size, so that Region II cracking develops at once. The time to failure of precracked and unprecracked samples is measured and from the difference in the two results, the time to initiation can be calculated assuming the critical crack size can be reasonably estimated.

Lundberg and Palmgren (3), in their study of rolling element bearings, suggested that, in the mineral oils, the initiation stage took about 99% of the time to failure and the propagation stages were very short. Yoshioko and Fujiwara (15), who studied the acoustic emission of bearings in an effort to measure the times of initiation and propagation, reported results that agreed with Lundberg and Palmgren (3), such that initiation accounts for 98.6 - 99.9% of the time to failure and propagation times were between 1 and 25 minutes for lives of about 40 hours.

Lockwood and co-workers (14), investigated the effects of anti-fatigue additives on the initiation and propagation of a tool-steel in oil and water-based lubricants and concluded that water lowers the stress level from which steady-state crack propagation arises.

Final proof of this has not been presented but some of the results tie in well with Linear Elastic Fracture Mechanics (LEFM). LEFM is the

term used to describe the study of initiation and especially propagation of fatigue cracks as described in the next section.

2.2.4.2 Propagation

Steady state crack propagation appears to follow the Paris law of crack growth (13), shown below, Eq. 2.5.

$$\frac{da}{dN} = C(\Delta K)^m \qquad \text{Eq. 2.5}$$

where C, m are materials and environmental constants

In accelerated testing, the time of propagation is short due to the large ΔK but in service ΔK is generally quite small and the crack propagation rates depend greatly on the materials parameters C and m. Polk and co-workers (16), at Mobil used an interrupted stressing technique to measure crack propagation rates for an SAE 52100 in a series of fluids both drip fed and fully immersed. This is further discussed in Section 5.3.4.

Polk and Rowe (17), followed up the investigation into crack propagation rates by using an optical microscope method to count cracks and thus measure the extent of branching. From the amount of branching a crack severity parameter was calculated. This was correlated with the L_{10} fatigue of the failed samples and found to be a reasonable fit for a variety of steels and conditions.

Polk and Rowe (17), suggested that this correlation was independent of stress, lubricant chemistry and metallurgy but that the important factor was that the lubricant chemistry affected the crack branching.

To summarise, the study of the initiation and propagation of rolling contact fatigue cracks is important but has rarely been studied under normal service conditions. When the crack propagation rates are usually measured they are done under accelerated conditions when initiation accounts for 99% of the failure time, (15), and crack propagation rates are very high. It does not necessarily follow that this is true in bearing service conditions due to the vast differences in stress levels.

2.3 THE STATISTICAL NATURE OF FATIGUE

Fatigue failure is a random process which occurs when a time-varying stress greater than a limiting value is applied to a component or structure. This limiting value is called the fatigue limit and failure will only occur at stress levels above this value no matter how many cycles are run.

2.3.1 Fatigue Life Distributions

The distribution of the lives, or times to failure, at given stress cycle conditions, follow a left-handed skew distribution curve as shown in Figure 2.8.

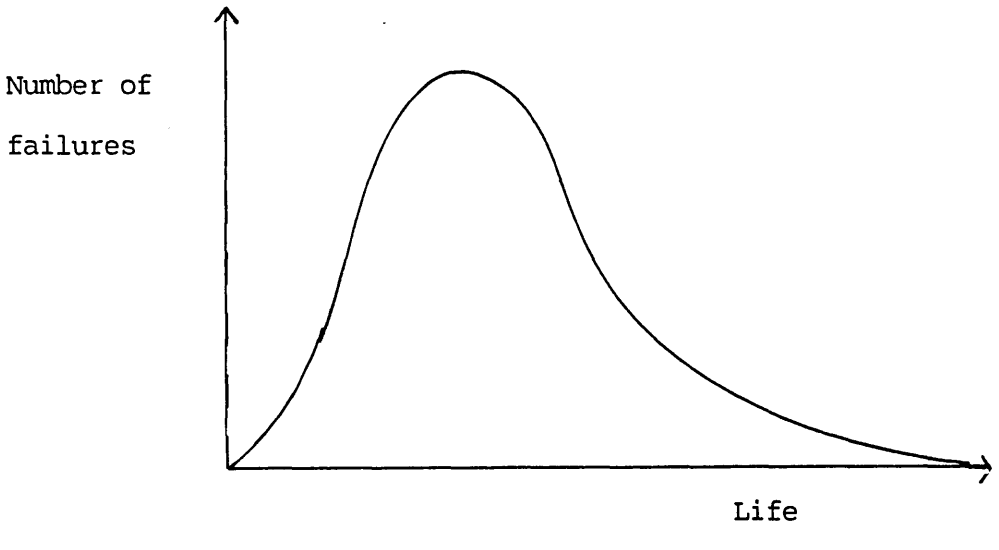

Figure 2.8

Weibull distribution

To generate precisely a distribution shown in Figure 2.8, a very large number of failures would have to be obtained. Since fatigue failures have life times to failure of the order of days, the cost of producing an accurate failure map would be enormous as well as the time very lengthy.

For this reason statistical methods have been developed which allow fatigue failure plots to be compared by performing a small number of tests rather than hundreds. The larger the number of failures the greater the accuracy and reliability of the result but the greater the cost in time and money. For any fatigue study these parameters need to be properly balanced.

2.3.2 Statistical Analysis

The requirement of statistical analysis of a few samples is, according to Johnson (18), that the graphical presentation of the data is reliable and that if one set of failures is found to be superior to another set, the same is true of the whole populations.

Straight line graphs of fatigue data are obtained by plotting the log log (1/1-F) as ordinate, where F is the median rank, against the common logarithm of the life, as in Figure 2.9.

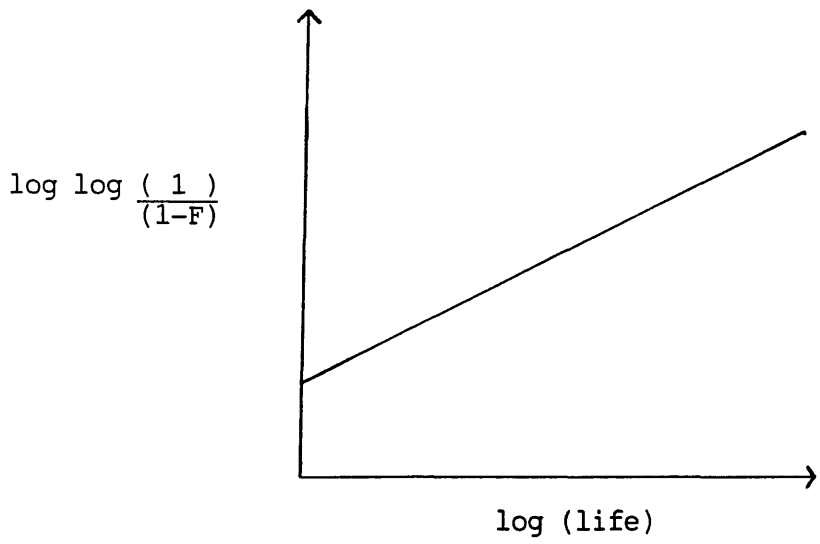

Figure 2.9
Weibull plot

The median ranks, (F), for a set of lines depends on the number of failures and the method of testing, sequential or simultaneous. Median ranks are calculated from formulae depending on the number of failures, n, and are shown in Appendix 1.

This type of plotting was devised by Weibull (19), and his name is given to the special paper on which graphs of this type are drawn and is shown in Figure 2.10.

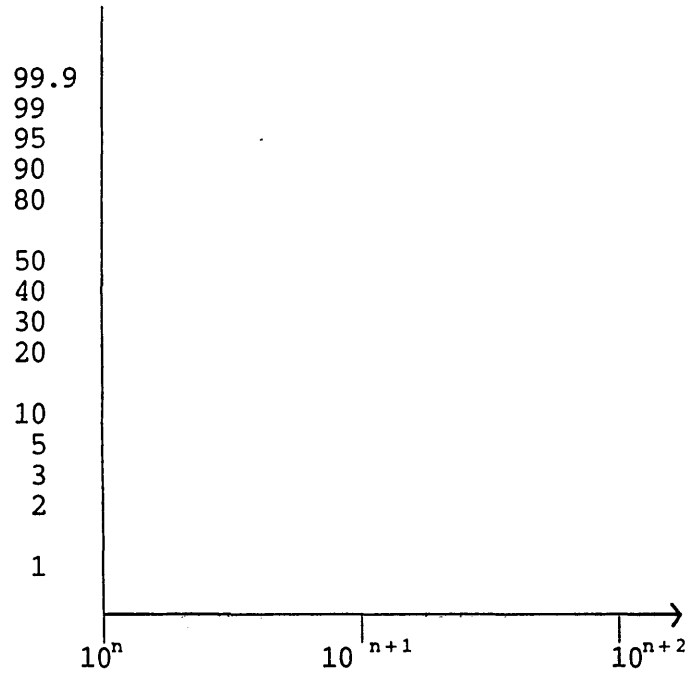

where n is an integer, usually 5 or 6

Figure 2.10
Weibull paper

From these plots, the Weibull slope, e, an important parameter in the statistical analysis is calculated using eq. 2.6.

$$\text{Weibull slope, } e = \frac{\log \{\log (1/S_1)\}}{\log \{\log (1/S_2)\}} \qquad \text{eq 2.6}$$
$$\{N_1\}$$
$$\{N_2\}$$

where S_1 is the probability of survival after N_1 cycles (normally $S_1 = 0.5$)

S_2 is the probability of survival after N_2 cycles (normally $S_2 = 0.9$)

2.3.3 Statistical Significance

In order to compare two plots, to find out if data has any meaning, the statistical significance of the data must be established. This is obtained from the confidence limits for the two sets of data. The calculation of confidence limits is described by Johnson (18), and can be found in Appendix 2.

When the Weibull slopes are equal the calculation of the statistical significance is relatively simple. The ratio of the L_{10} or mean lives is calculated and then using the value of the Weibull slope, the confidence level is established from the graphs of Johnson (18). If this confidence level is greater than 90%, then statistical significance is achieved.

In the case of unequal Weibull slopes, the confidence limits for the two sets of data are calculated at both Weibull slopes and then an average taken. If the joint confidence level is greater than 90% achieved, then the two sets of results are statistically significant. Statistically, methods based on this are used to analyse the results of the four-head rig in Section 6.2.

2.4 FACTORS AFFECTING ROLLING CONTACT FATIGUE

Table 2.1, the nine factors understood to affect rolling contact fatigue in 1963 were shown. In 1976, Howes and co-workers (20), published a list of eleven factors which they suggested were the important variables in rolling contact fatigue. These are listed with some of the current examples of materials and conditional variables, in Table 2.4.

Factor	Descriptive Example
Steel type	EN 31 or Stainless Steel
Processing	Vacuum degassed or electrode remelt
Surface finish	Ground/honed/polished
Load	
Speed	
Temperature	
Slip	0% (pure rolling) 3% to 30% (found in gears)
Lubricant type	Paraffinic, naphthenic, synthetic
Viscosity	High/low
Additives	With or without package
Humidity	Moisture content of the lubricant

Table 2.4

Factors affecting Rolling Contact Fatigue (20)

The two tables are not exhaustive in their listing of important variables in rolling contact. Combining the two lists in Tables 2.1 and 2.4 gives twelve factors. Other important factors not included are the pressure-viscosity behaviour of the lubricant (important in elastohydrodynamic film thickness generation) and the viscosity-shear behaviour of the lubricant. The shearing of mineral oils generally has very little effect on viscosity up to quite high values of shear rate, but is of very great importance to the study of invert, dilute and polymer thickened emulsions. This gives a total of fourteen factors that are important in rolling contact fatigue. Each of these factors are discussed in turn below.

2.4.1 Steels, Processing and Surface Finish

Way (2), tested three types of steels and concluded that of the three, hard, smooth, nitrided steels offered the best resistance against the deleterious pitting failure.

In the United Kingdom, a series of steels were developed for the range of bearing applications where fatigue life is a particularly important consideration. EN 31 steel, (21), and its current equivalent is described in Table 2.5.

Name	Country	Composition
EN 31 S 135 AISI M52100 SAE 52100 SLkL 15	UK (old) UK (new) USA USSR	1% Carbon 3/2% Chromium 1/2% Vanadium 1/2% Manganese + traces Silicon, Sulphur & Phosphorus

Table 2.5

EN 31 Steel and its equivalents

The steels are temper-hardened and quenched at a variety of temperatures depending on the final hardness required. When these steels were first manufactured one of the major problems was the presence of a large number of metallic and non-metallic inclusions in the steel. Littmann and Widner (22), showed that these were responsible for the nucleation of microcracks in cyclically stressed components. Fatigue cracks then propagated from these points. They also showed that flaws in the surfaces of machined components could act as stress concentration points from which cracks grew. Improvements in steel manufacture have produced increases in fatigue lives. Initially, Martin and co-workers (23), observed that surface finish improvements switched the life-limiting region from the surface to subsurface inclusions as described by Littmann and Widner. Then, as the quality of the steel improved with the introduction of vacuum degassing and other remelting processes, the origins of fatigue shifted back to the surface. Martin and Eberhardt (24), then noted that changes in the surface structure and separation of the grains allowed microcracks to be nucleated in the surface region. Nowadays, rolling contact fatigue is thought to be largely a surface-initiated process and surface treatments and abuse seem to cause the greatest material-related variations in the performance of bearing steels. From the work of Way (2), it is clear that the hardness of the steel is very important. Hard steels running together have been shown to give far longer fatigue lives than soft steels, (25). Current metallurgy suggests that bearing steels should be hardened to a minimum value of 750 Hv50, otherwise premature failure will arise.

The surface finish is also very significant. From the work of Dawson (7), the surface roughness is an important factor in rolling contact fatigue. If the film thickness is held constant, then the composite roughness of the two surfaces contributes greatly to the fatigue life. This is further discussed in Section 2.5.2. At the hardnesses involved, bearings have to be ground into the correct shape. A finer surface finish than grinding can be obtained by honing and polishing but these are expensive processes. The extra cost has, however, to be set against improved performance but for most applications, the extra expense is uneconomical.
Approximate surface roughnesses for a variety of surface finishing techniques are shown in Table 2.6.

Technique	Ra roughness	
	μm	μ in
Rough grinding	> 1.2	> 45
Grinding	1.2 → 0.4	45 → 15
Honing	0.8 → 0.08	30 → 3
Polishing	0.4 → 0.05	15 → 2

Table 2.6

Surface roughnesses for a variety of finishing processes.

2.4.2 Other non-lubricant factors

The five other non-lubricant factors are shown in Table 2.7.

Speed
Temperature
Contact Pressure
Load
Slip

Table 2.7
Non-lubricant factors

These factors are inter-related and will be discussed together. The temperature in the contact depends largely on the speed, the load and the amount of slip or sliding present. However, it is widely recognised that when the load, speed and the amount of slip are high, the mode of failure is not pitting but rather scuffing, due to the collapse of the lubricant film rather than pitting, with localised welding, smearing and extremely high rates of wear of the contacting surfaces. Temperature also affects the viscosity of the lubricant and thence the elastohydrodynamic film thickness.

In Section 3.4 it can be seen that temperature is important in controlling boundary lubrication. The load is an important parameter in determining the maximum Hertzian stress along with the geometrical and materials parameters of the contact. The calculations used in this study for determining the maximum stress are given in Appendix 3.

From Section 2.1.2 it was shown that both load and stress are important in determining life. Harris (26), followed up the work of Lundberg and Palmgren (3), and suggested that the power, n, of equation 2.1, was equal to 3. This was found to be satisfactory for

mineral oils in favourable conditions but modifications were required for more harsh conditions. Severity parameters, A_1, A_2, A_3 were introduced as shown in eq. 2.7.

$$L_{10} = A_1 . A_2 . A_3 . (C/P)^3 \qquad \text{Eq. 2.7}$$

where A_1 = reduction factor for reliability (Reliability parameter)

A_2 = reduction factor for materials (Materials parameter)

A_3 = reduction factor for severe conditions (Severity parameter)

This equation 2.9 is adequate for mineral oils under the majority of conditions but is inadequate for use with fire-resistant lubricants. Kenny and co-workers (27), modified the formula further as discussed in Section 3.2.5.

The contact stress is particularly important because, for rolling contact fatigue to take place, high cyclic stresses must be present. From the materials parameters and the load, Johnson (28) calculated the shakedown limit. This is an important parameter as above this stress limit, plastic flow occurs. For rolling contact fatigue to occur, the stress must be between the fatigue limit and the shakedown limit. This is shown again in Figure 2.11.

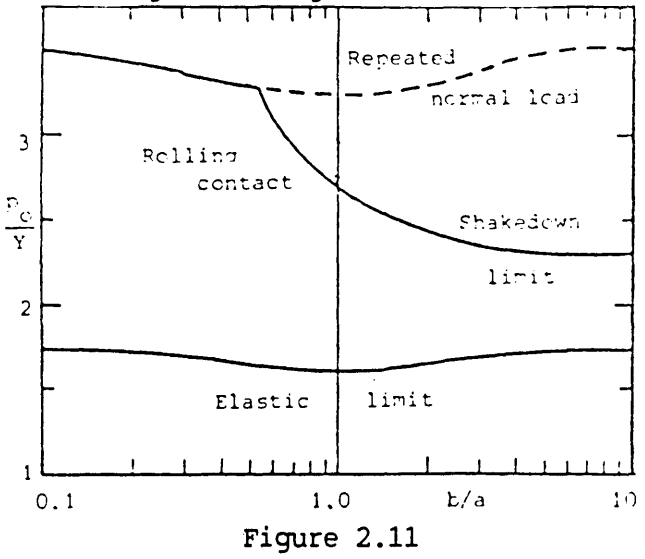

Figure 2.11

Elastic and shakedown limits under normal loading with eliphical contacts (28)

Under normal operating conditions, many lubricated components are stressed above the fatigue limit to maximise load-carrying ability. It should be noted that for fatigue testing much higher loads and stresses are used, well above the fatigue limit, so as to reduce the time to fatigue failure. This is further discussed in Section 4.7. The amount of slip is very important, especially in relationship to the fatigue performance of gears and cams and tappets, (1), but in this study the condition employed is nominally pure rolling.
From the equation of Crook (6), it is clear that the speed of the two surfaces is a large contributor to the film thickness. The speed of the contacting is also important in the shear rate endured by the lubricant. These are discussed in the next section.

2.5 LUBRICANT FACTORS

From Sections 2.1 and 2.4, it is clear that the lubricant is of very great importance in rolling contact fatigue. From Table 2.4 it is evident that there are seven basic lubricant factors which affect rolling contact fatigue. These are shown in Table 2.8.

Property	Effect
Type	Physical behaviour
Viscosity	Film thickness
Pressure - Viscosity	Film thickness
Shear - Viscosity	Effective viscosity, film thickness
Temperature - Viscosity	Effective viscosity
Additives	Chemical behaviour
Moisture	Chemical behaviour

Table 2.8
Lubricant factors

The actual contributions of lubricant behaviour are extremely complex especially in the contact. The chemical and physical properties of the lubricant can be modified or changed completely by additives. As

can be seen from Table 2.8, the use of high pressure, temperature and shear affects the viscosity and the film thickness. Each of the effects are outlined in turn but first the effects of composition are reviewed.

2.5.1 Lubricant Type

Originally, animal fats and vegetable oils were used as lubricants but with the discovery of crude petroleum oil, the use of mineral oil lubricants developed rapidly. Mineral oils consist of four chemical types of compounds, shown in Table 2.9.

Name	Compound Type
Paraffinic	Alkanes
Aromatic	Substituted benzene di and polyaromatics 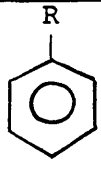
Naphthenic	Saturated rings 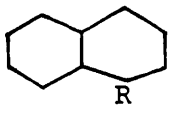
Non-hydrocarbon compounds	S, N, O compounds

Table 2.9
Mineral Oil Components

Variations in the proportions of the four types of compounds in a mineral oil gives rise to differing chemical and physical properties. The composition depends upon the source, with mineral oils from the Middle East being different from those from the North Sea or Alaska. During the Second World War, the Germans suffered acute shortages of crude oil and were forced to turn to synthetic oils. This led to the development of phosphate and other esters as high temperature engine lubricants.

Subsequently, only specialised uses were found for these lubricants when crude oil was once more in plentiful supply. With the sharp increases in oil prices since 1973, synthetic lubricants have become viable for a wide range of applications. The main classes of lubricants, their compositions and current uses, are shown in Table 2.10.

	Composition	Use
Mineral oils	Hydrocarbon	General
Natural fats	Fatty acid esters	Low friction, rolling oils
Esters (Type I & II)	I Diesters	Gas turbines, compressors greases
	II Polyolesters	
Phosphate Esters	$(RO)_3\ P = O$	Aircraft hydraulics
Polyglycols	$R(-O-CH_2CHR-O-)R$	Mining hydraulics, gear lubricants
Silicone oils	$R_3(-SiR_2-O-)SiR_3$	Electrical oils
Halogenated oils	$(-CX_2-CX_2-)_n$	Space lubricants, vacuum oils
Synthetic hydrocarbons	$(-CH_2-)_n$	Traction fluids, compressors, crankcases

Table 2.10
Lubricant types and uses

According to Goldblatt (29), the different components in mineral oils have vastly differing properties and stability to oxidation. The mixing of proportions of the different types of lubricants gives base stocks without the wear-promoting behaviour of polyaromatics and poor

lubricity of paraffinic base stocks. The mixing and blending of lubricant fractions is a science in its own right and is beyond the scope of this study.

In Section 2.1 the work of Rounds (8), on the effects of lubricant reactivity were described but only properties of base oils was discussed. In the next two sections, the properties resulting from type and composition are reviewed. The way in which these properties may be modified by the use of additives are outlined in Section 2.5.3.

2.5.2 Viscosity and Viscosity Linked Properties

From the early work of Crook (6), and Rounds (8), it is clear that the viscosity of the lubricant is very important in relation to the thickness of the lubricant film thickness. With the advent of elastohydrodynamic theory, the pressure-viscosity, viscosity-temperature, and viscosity shear behaviour of the lubricant have been recognised as critical parameters. In concentrated contacts the local pressures are extremely high, resulting in the importance of the pressure viscosity-coefficient, α. The pressure-viscosity behaviour is described approximately by Barus equation 2.8.

$$\eta_p = \eta_o e^{\alpha P} \qquad \text{Eq. 2.8}$$

From the elastohydrodynamic equations of Dowson and Hamrock (30), it can be shown that the film thickness is proportional to both the viscosity and the pressure-viscosity coefficient, α, as in Equation 2.9.

$$h_{min} \simeq K (\eta)^{0.7} (\alpha)^{0.5} \qquad \text{Eq. 2.9}$$

The full equation is given in Appendix 4.

The viscosity-temperature behaviour of lubricants is well documented. The most widely applicable relationship is the Vogel equation 2.10.

$$\eta_T = a e^{b/(T-C)} \qquad \text{Eq. 2.10}$$

where a, b, C are constants, T is the absolute temperature.

In order to calculate the viscosity of a lubricant at a temperature, three measurements need to be made at either side of the required temperature and calculated from the modified relationship, Eq. 2.11.

$$\ln \eta_T = \ln a + \frac{b}{T-C} \qquad \text{Eq. 2.11}$$

The values of viscosity obtained are only valid within the range measured. In elastohydrodynamic contacts there are flash temperature rises caused by the friction in the contact but these do not influence film thickness directly which depends solely upon the inlet viscosity and temperature.

The shear behaviour of mineral oils is dependent upon the rate of shear. At low shear rates, all fluids are Newtonian and mineral oils behave in this manner up to shear rates of at least 10^6 s^{-1}. Water-based fluids behave differently with most shear thinning between 10^2 and 10^6 s^{-1} but some shear-thicken . The shear behaviour of fluids is discussed in Section 3.4.1.

2.5.3 Additives

Mineral oil lubricants contain a number of additives which modify or enhance the physical and chemical properties of the fluid so as to meet the requirements of service. Nine important classes of additives are shown in Table 2.11.

Oxidation Inhibitors Corrosion Inhibitors Rust Inhibitors Friction Modifiers Pour point depressants Detergents Dispersants Foam inhibitors Viscosity Modifiers

Table 2.11

Classes of lubricant additives

These additives are blended in small quantities up to a total of about 15% depending on the use for which the oil is intended. Other additives are sometimes used in more severe conditions such as anti-wear, anti-fatigue, emulsifying and extreme pressure additives. The study of additives and additive behaviour is a major branch of lubrication science in its own right and is only discussed in this thesis where relevant to the lubricants under study.

One of the main problems with additives is that, whilst they may be good protection against fatigue or corrosion in their operation range relative to the same conditions without the additive,they may under other conditions enhance corrosion or fatigue. This is especially true of extreme pressure additives.

The use of surface active agents in oils and emulsions and the way these influence rolling contact fatigue performance is further discussed in Section 3.5.

2.5.4 Moisture

The influence of moisture on rolling contact fatigue is of great significance. There are several different levels at which moisture can affect contact fatigue. As this is the major topic of this study, the effects of moisture on rolling contact fatigue are discussed in some detail in the next chapter.

With regard to composition, different types of oils have different water suitabilities and so behave differently or similarly in a wide range of humidities.

In Section 3.1 the influence of dissolved water on fatigue is discussed followed by the influence of water-based lubricants on fatigue in Section 3.3.

2.6 MATHEMATICAL MODELS

Mathematical models have been developed to describe rolling contact fatigue. There are a wide variety of different models based upon different approaches to the problem. These will each be discussed briefly below but it should be noted that because they are devised using mineral oils they have only limited relevance to this study.

2.6.1 Finite Element Model of Rolling Contact Fatigue

Bhargava and co-workers (31), used a plane strain elastic-plastic finite element method to produce pressure distributions for single contacts. The model gave pressure distributions which were close to those of Hertzian theory predictions, (28). The model was then extended to take into account repeated contacts by reapplying the pressure for each contact. Values of the shakedown limit were

compared to those of Meervin and Johnson (32), and were found to be in agreement. Bhargava and co-workers (33), found, however, that some of the results for residual shear strain were not in agreement. A modified model has not been published.

2.6.2 Statistical Model of Rolling Contact Fatigue

Tallian (34), first proposed a model for rolling contact fatigue in 1968 based upon the weighted statistical probabilities for a series of factors tied together to produce life predictions. Since then the model has been updated and modified. In its most recent form, in 1982 (34) it is described by the author as a unified model for rolling contact fatigue, but it appears only to work for standard and not extreme conditions. The model is based on combining crack growth rates with local plastic strain and ductility and applying this to failure probabilities of the contact material and at the contacting surfaces. In summarising the model, Tallian (34), points out its weaknesses and deficiencies but suggests that the model gives reasonable results for non-extreme conditions. However, failure to work at extreme conditions is often a sign of a deficient model, but with further improvement may give results closer to that found in practical situations.

2.6.3 Asperity Interaction Model of Rolling Contact Fatigue

Chow and Cheng (35), examined the film thickness between lubricated rollers of varying surface roughness. From this they developed a mathematical model based on the interaction of surface asperities and the transient and residual stresses induced into the surfaces. From their investigation into the theoretical behaviour of asperities, they suggested that the specific film thickness, λ, was the most important

parameter in EHD lubrication. Their model predicted that at low λ ratios, asperities interactions caused severe subsurface plastic flow which allowed crack growth to occur very easily and as a result spalling. Their model agreed with a good deal of early work on film thickness ratios and metallic contact of Dawson (7), Rounds (8) and others (36).

2.6.4 Fracture Mechanics Crack Growth Model of Rolling Contact Fatigue

Mathematical models based on the analysis of cracks in surfaces have been studied in great detail. Results have been recently published for a variety of crack geometries and positions. The contacts are generally for elastic half-spaced surfaces. Keer and co-workers (37), published models for a subsurface horizontal crack, a surface breaking vertical crack and for a combination of the two cracks. They concluded that the propagation of the cracks depended on the local stress intensity factors and upon the magnitude of the mode critical stress intensity level. Keer and Bryant (38), followed up this earlier work and that of Way (2), in an attempt to model the mechanism of Way (2). This mechanism suggested that it was lubricant which is forced into the openings of surface breaking which when restressed caused crack extension and propagation. This is further discussed in section 3.5.4 Keer and Bryant (38), concluded that this hydraulic mechanism did not seem to fit their data but it may be that their model is deficient.

Murakami and co-workers (39), also employed a cracking model by using a 3d stress analysis of a vertical crack and one inclined at an angle to the surface of 45°. They also calculated stress intensity factors and applied them to the Paris law of crack growth (13). From this they concluded that a change of one order of magnitude in the maximum value of the stress intensity factor would change the crack propagation rate by four orders of magnitude. As a summary of their model they concluded that the hydraulic mechanism of Way (2), was responsible for the crack propagation and that without surface fracture the lubricant would not get into cracks as they were closed up. This does not explain the rolling contact fatigue of components in pure rolling and is contrary to the models of Keer and co-workers (37), (38).

2.6.5 Summary of Mathematical Models

The region of application of all the four models reviewed is very limited. Some of the more recent models are not yet at the stage where they can be applied realistically to rolling contact fatigue.

3.1 EFFECT OF DISSOLVED WATER IN MINERAL OILS AND FATIGUE

Almost thirty years ago, Grunberg and Scott (5), using a rolling four-ball fatigue test rig, discovered that small amounts of water dissolved in mineral oils promoted pitting failure of the upper ball compared to dry mineral oils. They tested five different oils with five differing additive packages and viscosities at four levels of humidity. The four levels of humidity were as shown in Table 3.1.

CONDITION	WATER CONTENT
Dried over Sodium	< 100 ppm
'As received'	220 - 550 ppm
Saturated	350 - 1500 ppm
Supersaturated	4 - 7% by weight

Table 3.1

Levels of water content in oils used by Grunberg and Scott, (5)

The values of the water content used by Grunberg and Scott (5) seem to be extremely high. Water has very slight solubility in mineral oil but does not apparently dissolve up to the level indicated. The reason for the apparently high level of water may be due to the inaccuracy of the method used for determining the water content.

Grunberg and Scott (5), found that the four lubricants when used 'dried' gave marginally longer mean lives than the 'as received' samples which were in turn, similar to those 'saturated' with water. Owing to the small number of tests run under each condition, the 'as received' and the 'saturated' samples were indistinguishable statistically. The results of tests run under the 'supernatant water' condition, gave mean lives of only 20-40% of those run under the 'dried' condition. These initial results led to further work on the effects of water, both dissolved and emulsified, on the fatigue lives of bearing steels. Grunberg and Scott (5), repeated their tests on stainless steel balls but found no reduction in the mean lives of the 'as received' and 'supernatant' water conditions when compared to the dried oils. In 1960, Grunberg and Scott (40), reported further work on the effect of water on the fatigue lives of bearing steels, using two different oils, of two very different viscosities, Table 3.2.

OIL	VISCOSITY AT 25°C/cSt
A	636
B	14.4

Table 3.2

Viscosities of the two oils as used by Grunberg and Scott (40)

Similar moisture conditions were employed to the earlier work (Table 3.1), although the 'supernatant' level was split into approximately 3% and approximately 6% water content. The results were very similar to the early work, with the 'dried' oil giving the longest life, the 'as received' and the 'saturated' very similar lives and the two with supernatant water giving only 10-20% of the mean lives of the dried samples. This shows that the effect of water is independent of film thickness. Grunberg and Scott (40), then tested the effects of several additives on fatigue life and found that some of them improved it whilst others reduced the mean lives still further. This is further discussed in Section 3.1.2.

Mantel and co-workers, noting that the use of very hard steels was becoming commonplace, investigated the effects of atmospheric moisture on hardened steels in 1961 (41). Using a reversed bending test, they found that the median lives of SAE 52100 steels of hardness, Rockwell C60 in moist argon, were approximately 10% of those tested in dry argon under otherwise identical conditions. They found similar results for moist air and moist nitrogen as compared to dry nitrogen using a unidirectional bending machine.

In 1968, Schatzberg and Felsen (42), employed a rolling four-ball fatigue rig to investigate the effects of both water and oxygen on ten percent fatigue life (40). They used squalane (IUPAC name (2,6,10,15,19,23-hexamethyltetracosane) as the lubricant in silicagel dried (< 10 ppm H_2O) and wet (0.01% (100 ppm) H_2O) conditions at four different stress levels. At the highest stress level (8.94 GPa) the reduction in L_{10} fatigue life produced by water was 43% and at the lowest stress level the reduction was 36%. The reduction in L_{10} fatigue for all the stress levels is shown in Table 3.3. These stress levels are very close to the shakedown limit of Johnson (28).

Stress Level GPa	Reduction in Fatigue
8.94	43%
8.25	32%
7.56	48%
6.36	36%

Table 3.3

Reduction in fatigue life for rolling fourball tests for a variety of stress levels (42)

Schatzberg and Felsen (42), also reported that the L_{10} fatigue lives for both wet and dry conditions were proportional to the applied stress raised to a power. The influence of oxygen was investigated by replacing the air used to dry or moisten the squalene by argon gas which purged the oxygen from the system and led to a slight loss of the L_{10} fatigue life but to a greatly improved fifty percent survival life (L_{50}). The wet and dry L_{50} fatigue lives were also brought closer together indicating that oxygen does play an important role in the premature failure of bearing steels.

Further work by Schatzberg and Felsen (43), examined the regions of the balls when the failure pits occurred and concluded that the water was reacting with the more chemically active regions of the ball's surface and that this was the cause of the premature failures. They also noted that the wear of the balls increased with the increase in water content.

Felsen and co-workers (44), investigating the problem of lubricant contamination by water and especially sea water, for naval applications, obtained values of fatigue lives using a rolling four-ball machine. They examined a series of five mineral oils, two emulsifying oils and one synthetic fluid at various levels of water content. Reductions in L_{10} fatigue life of between 35 and 66% and 57-80% for L_{50} fatigue life were obtained. The reduction in fatigue lives for the mineral oils and the emulsifiable oils is given in Table 3.4.

Lubricant		Kinematic Viscosity at 66°C/cSt	L_{10} Dry	Percentage Reduction in L_{10} %			L_{50} Dry	Percentage Reduction in L_{50}		
				.1% H_2O	.5% H_2O	1.0% H_2O		.1% H_2O	.5% H_2O	1.0% H_2O
Mineral Oil	A	26	132.5	60.6	55.2	–	605	79.7	79.5	–
Mineral Oil	B	12.5	76.6	–	–	–	237	–	–	–
Mineral Oil	C	8.3	33.1	–	–	66	933	–	–	71
Mineral Oil	D	8.0	21.6	–	–	35	51.3	–	–	57
Mineral Oil	E	4.7	35.4	–	–	62	132.9	–	–	78
Emulsifiable Oil	with Sea Water	31	130.5	43	64	–	374	64	64	–
	with Distilled			45	56	–		56	71	
Emulsifiable Oil	G	14.2	68.5	–	22.5	–	180	–	46	–
Synthetic Fluid	H	15.8	82.3	–	–	–	284	–		

Table 3.4 (Lives in hours)

Reductions in fatigue life for a variety of oils at differing water contents, (44)

From Table 3.4, the results for the emulsifiable oil F, show that there is almost no difference between using sea water and distilled water for the fluid make-up. The other emulsifiable oil G, gave lower overall fatigue lives compared to emulsifiable oil F in the dry condition but at a 0.5% water content there was no significant difference between the lives obtained for the two fluids. The synthetic fluid (SF) H, was a triaryl phosphate, and despite having a water content of approximately 550 ppm, gave a better fatigue performance than most of the wet mineral oils with much lower water contents. Further tests on the same fluids were carried out using thrust-loaded angular contact bearings and it was reported that the zones of pitting shifted from the ball to the raceway surface for the tests with water-containing lubricants.

Also in 1972, Penfold (45), working at the Admiralty Oil Laboratory on a new vertical fatigue test rig, experimented with adding 10% sea water to an emulsifying hydraulic oil and compared the fatigue lives to those of the water-free oil. Penfold obtained a 58% reduction in L_{10} and a 48% reduction in L_{50} fatigue life.

Richie and Eastaugh (46), continued the work of Penfold (45), on emulsifiable hydraulic oils using the same Admiralty Oil Laboratory vertical fatigue and the Unisteel fatigue rig. These authors compared the mean, L_{10} and L_{50} fatigue lives of dry oil and with 1% and 10% emulsified sea water. The lives obtained for the conditions employed on the Unisteel fatigue rig are shown in Table 3.5.

Fatigue Life	Reduction in fatigue life at 1% Sea Water	Reduction in fatigue life at 10% Sea Water
L_{10}	54	56
Mean	23.5	73.5
L_{50}	31	69

Table 3.5

Reduction in fatigue life at 1 and 10% Sea Water for the Unisteel Rig

The lives and percentage life reductions for the same conditions as employed on the AOL vertical fatigue rig are shown in Table 3.6.

Fatigue Life	Reduction in fatigue life at 1% Sea Water	Reduction in fatigue life at 10% Sea Water
L_{10}	7.5	93
Mean	21.4	66
L_{50}	41	73.5

Table 3.6 AOL

Reduction in fatigue life at 1 and 10% Sea Water for the AOL rig

In the Soviet Union, Stepurenko and co-workers (47), used a rotating-bending fatigue rig to compare the fatigue limits of a steel in various atmospheres including air, dry oil, 'as supplied' and with various amounts of water. Using five million cycles as a run out, values for the fatigue limit were obtained, $\pm$ 30.5 kg/mm^2 for the dried oil, $\pm$ 29.5 kg/mm^2 for air and $\pm$27 kg/mm^2 for oil with 2 and 5% water. Further tests were then carried out with other atmospheres and water contents but the oils had been dehydrated with hot air instead of argon. The effect of the dissolved air/oxygen was to reduce the fatigue limits of steels by 15-25% compared to the oxygen-free samples, and with some samples to remove any fatigue limit.

In 1972 Cantley (48), in the United States, examined previous results of Schatzberg and Felsen (42), (43), and other workers at the Naval Research Laboratories (44), and at the results of Grunberg and Scott (5), and then conducted some fullscale bearing tests with water concentrations of 25,100 and 400 ppm. Cantley compared the $L_{15.9}$ of the three concentrations of water in an SAE 20 mineral oil. He found a 61% decrease in the $L_{15.9}$ fatigue life with 100 ppm and 80% reduction in the $L_{15.9}$ fatigue life with 400 ppm, when compared to 25 ppm water content.

The work of Cantley (48), highlighted a problem encountered in the study of rolling contact fatigue. No proper comparisons can really be made between results and water contents unless very similar conditions are employed. Cantley used a fully formulated oil whereas Grunberg and Scott (5), (40) and Schatzberg and Felsen (42), (43) all used unformulated base oils, and Cantley's work on the water content of oils at a variety of humidity levels also indicates problems that unless oils used are very similar in terms of chemical composition, vast differences in water content and as a result, fatigue lives may occur.

3.1.1 Effects of Additives on the deleterious effect of dissolved water

After the discovery of the deleterious effect of water on rolling contact fatigue, Grunberg and Scott (5), attempted to find additives to counteract the effects of the water. They tested the four main classes of additives as shown in Table 3.7 (40).

Aliphatic alcohols
Fatty acids, amines, commercial 'dewatering' agents'
Detergents
Water soluble anti-corrosion additives

Table 3.7

Classes of additives tested by Grunberg and Scott (40)

For the first two classes, small amounts were dissolved directly into the oil but the latter two classes were dissolved in water and then added to the oil. The same mineral oils, A and B, were used and the same conditions as in the original paper(5), (Table 3.1). Of the additives examined, a 3% w/w addition of isoamylalcohol (IUPAC name 2-amino-2-methylpropan-1-ol) caused slight reductions in the viscosities of the two oils but under the 'saturated' condition

improved the mean life by 90% with Oil A and by 14% with Oil B, when compared to the oil without additives. This was still, however, only 77% of the life in the dry oil without additives for Oil A and only 77% for Oil B. It also gave significant improvements under the supersaturated conditions of 26% for Oil A and 340% for Oil B. The fatty acids and amines proved to be no use at counteracting the effect of the water under the 'saturated' condition but offered some improvement under the 'highly supersaturated' conditions. In further work, Scott (49) attempted to find additives to improve the fatigue lives under saturated conditions. Scott followed up the idea that additives behave differently under differing saturation levels. He reported that short chain alcohols improved fatigue life with 3% water but that with an imidazoline '0' which, according to the two authors is a strong alkali, it gave a longer fatigue life than with the dried mineral oil. At the 6% water saturation, however, single additives were useless in combating the worst effects of the water but mixtures of additives worked quite well. Scott reported that a mixture of a sarcosine derivative and a N-methylglycin improved fatigue life considerably.

Schatzberg (50), also experimented with additives under the same conditions as his earlier work (43), and concluded that although some of the earlier additives showed considerable improvement, isopropyl-aminoethanol (IPAE) (IUPAC name N-ethoxy-2-aminopropane) at 0.1% w/w concentration gave very similar L_{10} and L_{50} fatigue lives to the dried mineral oil. Rowe (51), also reviewed the effects of additives on the water-induced premature failure of angular thrust bearings and again concluded that IPAE was efficacious. Rowe compared the results obtained from a rolling four-ball and Unisteel fatigue rigs and concluded that proper formulation of the oils with additives could

substantially negate the worst effects of the water. Under the less severe Unisteel test, the L_{10} and L_{50} fatigue lives of the formulated oil + 0.5% water, were substantially increased over the lives in the dry base oil. More recently, Lockwood and co-workers (14), looked at the effects of anti-fatigue additives on an emulsion and an oil based product. They used a series of test machines and measured the crack propagation rates for various conditions and concluded that the anti-fatigue additives reduced the crack propagation rates for the with-additives conditions.

They also summarised the effects of a series of additives on fatigue and concluded it is very important to match additive with the conditions to be employed in service. These results are shown in Table 3.8 taken from Lockwood and co-workers (14).

The mechanism explaining the behaviour of these additives are discussed in Section 3.5.

Additive Type	Fatigue Effect	Test Method	Reference
ZDDP	Harmful	Wohler	(113)
ZDDP	Harmful	Geared roller Test Machine	(20)
Dibenzyl sulphide	Harmful	Wohler	(113)
Chlorinated Wax	Harmful	Wohler	(113)
Olecic Acid	Beneficial or Harmful depending on concentration	4 ball	(8)
IPAE	Beneficial	4 ball	(50)
Dodecyl phosphate	Harmful	4 ball	(8)
Trioresyl phosphate	Harmful	4 ball	(8)
ZDDP	Beneficial	4 ball	(8)

Table 3.8

Effects of Additives on Fatigue (14).

3.2 FIRE RESISTANT LUBRICANTS

As a result of a tragic accident and fire in Belgium in 1956, in which over 200 lives were lost (52), mining authorities around the world set about replacing mineral oils in mining and other fire-hazardous environments with fire resistant fluids in the late 1950s. Fire resistant lubricants have been increasingly employed and new applications implemented. Another major area for fire resistant lubricant use is in naval applications where the prevention of fire is of the utmost importance, and, recently, in the steel making and forming:

The Institute of Petroleum (IP) and the American Society for Test Materials (ASTM) with the International Standards Organisation (ISO) have established classifications for the various types of fluids and these are shown below in Table 3.9.

Class	Description	Other Name
HF-A	Oil-in-water emulsions containing a maximum of 20% combustible material. These usually contain 95% water.	Dilute emulsion (DE)
HF-B	Water-in-oil emulsions containing a maximum of 60% combustible materials. These usually contain 40-45% water.	Invert Emulsion (IE)
HF-C	Water-glycol solutions. These are solutions of monomer and polymer mixed together. They usually contain at least 35% water.	Water or Aqueous Glycol (WG or AG)
HF-D	Water-free fluids. These usually refer to fluids containing phosphate esters (PE), other organic esters or synthesised hydrocarbon (SHC), fluoro (FHC) - or chloro (CHC) - hydrocarbons.	

Table 3.9

ISO classifications for fire resistant fluids

The three classes of water-containing fluids will be described in detail below.

Since the ISO designations were set up over twenty years ago, much research into fire resistant lubricants has been carried out and, with improvements in additives and formulation, the HF-A classification has become divided into several groups. These are described below in Table 3.10.

Class	Description	Other Name
HF-A/e	Dilute emulsions of droplet size 1-10 μm. These are the Standard emulsions of the original designation.	Dilute Emulsion (DE)
HF-A/m	Microemulsions. These are similar to HF-A/e but the droplet sizes are < 1μm (typically 0.5 μm) and are usually clear pale brown liquids. They are much more stable than the HF-A/e liquids (53).	Micro-Emulsions (ME)
HF-A/s	These are solutions of additives in water and usually contain no oil. They are not really water lubricants but corrosion protection solutions (54).	Oil-Free Solutions (OFS)
AF-A/t	These are polymer thickened fluids typically containing about 90% water, 5% oil and additives as with the AF-A/e but also 5% of a high molecular weight water soluble polymer to act as thickener (55).	Polymer thickened emulsions (PTE)

Table 3.10

Sub-groups of the HF-A ISO classification

Further description of all the above fluids, their fatigue performances, lubricity, stability and other important properties are described below.

3.2.1 HF-A Dilute emulsions

These fluids were developed from the need for hydraulic fluids in 'static applications' such as pit props where there are no highly loaded moving parts. One of the major problems with fluid under high pressure is that if a leak develops the fluids is sprayed out in a fine mist. If the fluid were mineral oil then a dangerous, potentially explosive mist would be formed. British Coal specify that the requirement for a high water based hydraulic fluid is as shown in Table 3.11.

Cheap
Non-toxic
Have a degree of corrosion resistance
Be compatible with local water

Table 3.11

Required properties of a high water based fluid

As a result of the above requirements, two concentrate specifications have been developed for use. The first, NCB specification 18 (56), is for use in waters containing up to 250 ppm calcium carbonate equivalence and the second, NCB specification 19 (56), for use in waters containing up to 750 ppm calcium carbonate equivalence. These concentrates are usually slowly added to a stirring or mixing chamber containing the water, to ensure complete homogenisation of the emulsion. This is normally carried out on site. It has been suggested that microemulsions (HF-A/m) are better able to cope with higher calcium carbonate equivalent concentrations, work at very high dilutions (~ 98% water) and remain stable, uniform emulsions. Recent work by Baker and co-workers (53), have shown that specially formulated microemulsions pass corrosion tests at these very high dilutions in Laboratory tests but no field performances have yet been reported.

The oil free solutions, (HF-A/S), were experimented with in the 1970s but gave much poorer performances than the dilute emulsions (54), and with the advent of micro-emulsions, appear to have been discarded. The new polymer-thickened fluids are still under development and their general performances are being improved. Until formulations are completed, an accurate appraisal of their overall behaviour is not possible.

One of the problems with orthodox dilute emulsions is that they are prone to microbial degradation (57). Bacteria feed on the hydrocarbon of the oil and emulsifying agents to generate scums, noxious gases and corrosive residues. The scum tend to block filters and the bacteria can cause dermatalogical problems. Mattison and co-workers (57), investigated the effects of the microbial degradation of a soluble oil emulsion on the fatigue lines of an EN 31 steel using a rolling four-ball fatigue rig. They determined the average fatigue lives from 20 tests on three emulsions. One emulsion was a sterile batch used as a control, the second was the same as the first but plus a small amount of biocide and the third was an amount of the same emulsion after three months microbial degradation. Mattison and co-workers (57), found that the mean lives for the sterile and the microbially degraded sample were very similar but the mean fatigue life for the emulsion containing the biocide was increased by 18%. The number of bacteria in the emulsions were measured as was their growth rates. Corrosion tests were also carried out on the emulsions and the microbially degraded emulsion was found to be somewhat corrosive but the emulsion with biocide showed no corrosion. On statistical analysis of the rolling contact fatigue results, a large amount of scatter was obtained in the results and no statistical significance was obtained. Further tests were necessary to obtain a proper account of the effect of microbial degradation on emulsions but no further work has been published in this field.

3.2.2 Invert Emulsions - HF-B

For applications where a reasonable degree of lubricity is required, HF-As do not generally provide sufficient performance and invert emulsions are used. These contain water droplets dispersed in an oily phase. The oil phase provides the lubrication and the water the fire resistant properties. The emulsions are usually supplied ready-mixed. The major problem with most fluids is that if the level of water falls below about 35%, then the emulsions become flammable. Invert emulsions are widely used only in the UK and some parts of the USA.

3.2.3 Aqueous Glycols - HF-C

On the continent of Europe, in Japan and for Naval applications, solutions of glycols are used in place of HF-Bs (58). Water glycols consist typically of about 15% high molecular weight polyalkylene glycol, about 40% monomer (alkylene glycol) which acts as a co-solvent because polyalkylene glycols are largely insoluble in water and 5% anti-corrosion and other additives dissolved in the remaining 40% of water. Unlike emulsions, water glycols are single phase solutions, which avoid many of the stability and filtration problems of emulsions. The monomer also acts as a low temperature stabiliser for the water glycols which gives them enhanced low temperature capability. Because of this low temperature stability, water glycols are used in a few applications in the United Kingdom mining industry and their use in ship hydraulic systems for arctic use is under investigation.

3.3 Rolling Contact Fatigue Performance of Fire Resistant Lubricants

In 1954, Cordiano and co-workers (4), reported that fire resistant hydraulic fluids greatly reduced the pitting lives of bearings. Using a bearing test rig, they compared the fatigue lives of a phosphate ester, a phosphate ester base and a water glycol to a mineral oil. The reduction in modal (mean) life for the aqueous glycol, compared to the mineral oil was 94%.

Cordiano and co-workers (4), also introduced derating factors for use in equipment designed for mineral oils operated with fire resistant lubricants based on equations 3.1.

$$F = \sqrt[3]{\frac{\text{Modal life (Mineral Oil}}{\text{Modal life (Fire Resistant Fluid)}}} \qquad \text{Eq. 3.1}$$

The derating factor for the aqueous glycol tested was given as 2.6. The further use of derating factors is discussed at the end of the section.

Hobbs and Mullett in 1968 (59), used a series of four test rigs each containing four plane roller bearings, partially immersed in the test lubricant and loaded up to a maximum Hertzian stress of 2.9 GPa on the inner raceway. They tested a series of fire resistant lubricants and compared their performance to a mineral oil which was also tested. The lubricants tested were synthetic fire resistant lubricants consisting of phosphate esters and halogenated hydrocarbons mixed with petroleum fractions, a chlorinated aromatic hydrocarbon, an invert emulsion with 40% water, a water-glycol and a fire resistant insulating transformer lubricant which was a mixture of two chlorinated aromatic hydrocarbons. The L_{10} and L_{50} fatigue lives were compared for the five fluids. Compared to the mineral oil the invert emulsion gave a 56% reduction in L_{10} fatigue life and a 66% reduction in the L_{50} fatigue life whilst the aqueous glycol gave a 74% reduction in the L_{10} fatigue life and an 85% reduction in the L_{50} fatigue life.

The authors also produced a table of relative capacities of the fluids when compared to the phosphate ester fluid. The invert emulsion had an 87% relative capacity and the aqueous glycol 74% relative capacity when compared to the phosphate ester.

Also in 1968, Turski (60), (61), examined the wear performances of the fluids and using various wear test machines became concerned at the relatively poor performances of the invert emulsion and the aqueous glycol.

In a related project, Bietowski (62), used a bearing test rig with the maximum Hertzian stress 3.3 GPa on the inner race and 2.75 on the outer race. For the fluids which produced short bearing lives, further tests were carried out with reduced loads and thus reduced maximum Hertzian stresses to give much more realistic fatigue lives. Under higher load both the glycol and the invert emulsion, within 400 hours (36 million cycles), failed nine times (out of ten) but under the lower load the invert emulsion failed only three times, whilst under the same lower load, the aqueous glycol failed seven times. The L_{10} fatigue lives at the higher stress was 4 million cycles for the aqueous glycol and 9 million cycles for the invert emulsion with the L_{50} fatigues lives 15 and 22 millions of cycles respectively. Since there were no failures with the mineral oil and only two with the phosphate ester, no comparison between these and the two aqueous fluids was possible.

Kenny and Yardley (63), following up this earlier work of Turski (60), (61) and Bietowski (62) used a Unisteel fatigue rig to compare the fatigue performance of a mineral oil, a phosphate ester, two invert emulsions and two aqueous glycols. The operation of the Unisteel fatigue testing rig is described fully in Section 4.2. They also investigated the effect of the six fluids on samples of differing surface finishes and hardnesses from two different manufacturers in

four different batches. The details are given in Table 3.12.

Source	Batch	Hardness Range/ HV	Finish	Roughness, Ra/μm
Manufacturer 1	I	750 - 780	longitudinally ground circumferentially ground	0.09-0.47
	II	750 - 780	circumferentially ground	0.09-0.47
Manufacturer 2	III	775 - 860	lapped	< .20
	IV	775 - 860	circumferentially ground	0.09-0.47

Table 3.12

Materials variables for Unisteel specimens

The mineral oil was used as the reference lubricant. Test runs were carried out to assess the effect of the various surface finishing methods on fatigue life and to establish a datum from which the loss of reduction in fatigue lives of the fire resistant fluids could be compared. For the batch II specimens, percentage reductions in the fatigue lines compared to the mineral oils are given in Table 3.13.

Fluid	% Reduction in L_{10}	% Reduction in L_{50}
Phosphate Ester (PE 14)	84%	71.2%
Invert Emulsion (OA 20)	89.5%	92.4%
Aqueous Glycol (AG 4)	93.4%	94.1%

Table 3.13

Reduction in fatigue lives of various fluids compared to mineral oils for Batch II Unisteel specimens (63)

For batch III, the percentage reductions in the fatigue lives for the fire resistant fluids as compared to the mineral oil are given in Table 3.14.

Fluid	% Reduction in L_{10}	% Reduction in L_{50}
Phosphate Ester (PE 14)	86.1%	77.8%
Invert Emulsion (OA 20)	94.9%	96.8%
Invert Emulsion (OA 43	93.0%	95.7%
Aqueous Glycol (AG 4)	96.1%	95.4%

Table 3.14

Reductions in fatigue lives of various fluids compared to mineral oils for Batch III Unisteel specimens

Kenny and Yardley (63), found no correlation between the grinding direction and fatigue lives but the slightly harder and smoother samples did give significantly higher fatigue lives than the slightly softer, rougher samples.

Kenny and Yardley (63), then attempted to correlate results between different machines in the same and in different laboratories. To reduce the number of variables they used an aqueous glycol from the same batch for all tests and the metal test specimens were all from the same batch with nominally identical treatments, hardnesses and surface finishes. They found significant differences from machine to machine and laboratory to laboratory but not on the same machine done at different times. It was suggested that the variations were due to slight differences in the various machines and the environment in each laboratory. They suggested that the same machine or set of machines must be employed to obtain any worthwhile comparison of fluids.

Hobbs (54), continuing the earlier work of Hobbs and Mullett (59), used the same bearing test rig to examine other series of fire resistant lubricants. There were four aqueous glycols included in the list, one was a fully formulated hydraulic fluid, whilst the other three selected for their low, medium and high viscosities. An invert

emulsion was also included. The bearings tested were made from two steels, both conforming to the EN 31 specification. One was prepared by the basic electric arc (BEA) process and the other was prepared byc the vacuum degreasing (VD) processing. The fatigue lives for the various fluids for the two steels were compared to a paraffinic high viscosity mineral oil. The reduction in fatigue lives for the two types of steel lubricated by the fire resistant fluids when compared to the mineral oil are given in Table 3.15.

Fluid	% Reduction in Fatigue Life			
	Basic Electric Arc Steel		Vacuum Degassed Steel	
	L_{10}	L_{50}	L_{10}	L_{50}
Aqueous Glycol	74	85		
Low viscosity Medium viscosity High viscosity	-	-	96	98
Invert Emulsion	56	62	79	96

Table 3.15

Reduction in fatigue times for differently processed steels in a bearing test rig

Hobbs suggested that the reduction in fatigue life caused by the aqueous glycol was as a result of the lack of calculated film thicknesses but he was unable to measure or estimate the film thickness for the dilute emulsion and no mechanism was suggested. Yardley, Kenny and Sutcliffe (65), continuing the earlier work of Kenny and Yardley (63), looked at the effects of different loads on the rolling contact fatigue lives of various fire resistant lubricants. They used a rolling four-ball fatigue rig, a Unisteel

fatigue rig and a bearing test rig to assess the L_{10} and L_{50} fatigue lives and the Weibull slope of a mineral oil, a phosphate ester, an aqueous glycol, an invert emulsion and a dilute emulsion. The work on the first four fluids was largely as described previously (63), but included further work using other test rigs and using the dilute emulsion. Using the load life relationship (Eq. 3.2) and the dynamic capacity of the system (Appendix 6), a theoretical L_{10} fatigue life for the given loads for a mineral oil was calculated and values of experimental L_{10} lives were compared to these figures.

Analysis of the results showed that the amounts by which the lives were reduced for the fluids were inconsistent for different conditions of load. This demonstrated the importance of the applied load/ dynamic capacity ratio. Some statistical fitting of the data was attempted but insufficient data was obtained to give reasonably statistically significant factors for the load life relationship March (66), again using a Unisteel and a rolling four-ball fatigue rig, compared fluids from each of the four classes of fire resistant fluid against a mineral oil. The results obtained on the Unisteel rig were compared to those of Yardley and co-workers (65), using the four fire resistant fluids and yielded the results in Table 3.16, L_{10} fatigue lives in millions of cycles.

	YARDLEY et al (65)	MARCH (66)
Mineral Oil	26	6.3
Phosphate Ester	3.62	5.0
Aqueous Glycol	1.02	1.1
Invert Emulsion	1.33	1.3
Dilute Emulsion	0.71	0.4

Table 3.16

L_{10} fatigue lives (millions of cycles) for different fluids on the four-ball (65) and Unisteel (66) fatigue rigs

The reason for the big difference in the mineral oil lives is that Yardley and co-workers employed an oil of much higher viscosity. Hobbs (64), used a mineral oil of intermediate viscosity and obtained an L_{10} fatigue life of 9.8 million cycles. The reductions in the L_{10} fatigue lives for the three water based fluids were again in keeping with those reported earlier of 83% for the Aqueous Glycol, 79% for the Invert Emulsion and 94% for the dilute emulsion. The reduction for the dilute emulsion was, however, slightly more than had been reported earlier. At the same time, Knight (67), reported data taken from pump tests lubricated with various fluids. He reported the fluids were not a problem in most moving parts of the pump but were severe on the fatigue life of the rolling element bearings of the system. Knight found that invert emulsions gave about one quarter, dilute emulsions about one twentieth and aqueous glycols one sixtieth of the lives of those operated with mineral oils. The percentage reductions are given in Table 3.17.

Fluid	% Reduction in Fatigue Life
Invert Emulsions	76
Aqueous glycols	93
Dilute emulsions	98

Table 3.17

Reduction in fatigue life for fire resistant fluids in pump tests (67)

Culp and Widner (68), used a tapered roller bearing test rig to exercise the effects of various fire resistant fluids on mineral oils and their $L_{15.9}$ fatigue lives were compared to those of a mineral oil.

The reduction in $L_{15.9}$ lives when compared to a standard mineral oil is given in table 3.18.

Fluid	% Reduction in Fatigue Life
Invert Emulsions	47 - 69%
Water Glycols	76 - 86%

Table 3.18

Reduction in L_{15} fatigue lives for tapered roller bearing tests (68)

3.3.1 Synthesis of the Rolling Contact Fatigue Performance of Fire Resistant Fluids

As can be seen from the previous section, a great deal of related but fragmentary fatigue work had been carried out on fire resistant fluids by 1977. In that year Kenny and co-workers (27), collected results from three types of rolling contact fatigue tests from manufacturers and users and pooled results for the three types of aqueous fluids. The aim of the work was to complete the earlier correlation of data of Yardley and co-workers (65), but with sufficient data to make proper analysis and weighting of the results possible. Kenny and co-workers (27), acquired three sets of results for the three types of water fluids under investigation. The L_{10}, L_{50} fatigue lives and the Weibull slopes for every set were calculated along with the type of test, the number of failures and the dynamic capacity-load ratios were obtained.

Using Yardley and co-workers (65), modified load life predictions, Eq. 3.2.

$$L_{10} = (C/KP)^n \times 10^6 \text{ revolutions} \qquad \text{Eq. 3.2}$$

the factors K and n were calculated for the three water-based fluids.

The final estimates of the values for n and K are shown below in Table 3.19.

Fluid Type	Estimated Parameters	
	n	K
HF-A	2. 5109	2.0210
HF-B	2.7090	1.4349
HF-C	2.4598	2.0122

Table 3.19

Estimated values for n and K, adjustment factors for Load-life prediction equations

The results obtained from the literature along with the C/P ratios are presented in Table 3.19 and from the results in Table 3.16, a theoretical rankings of the types of fluid is obtained.
The ranking is given in Table 3.20.

Order	Fluid
First	MO ≃ PE
Second	IE
Third	DE ≃ AG

Table 3.20

The ranking of fluids

This ranking is drawn up within the constraints of the fact that this ranking is based on moderate loads (65). At very low or very high loads this ranking may change. Further discussion on the ranking of fluids is in Chapter 7.

3.4 LUBRICATION BY FIRE RESISTANT LUBRICANTS

As was described in Sections 2.1.2 and 2.5, the lubrication of bearings depends on many factors. The lubrication regimes of hydrodynamic, elastohydrodynamic (EHD), mixed EHD and boundary lubrication depend on these same factors. Hydrodynamic lubrication is a purely physical phenomenon where only the bulk properties of the materials and conditions involved are taken into consideration. It is also only concerned with low loads and thick separating films. The other three regimes EHD, mixed and boundary lubrication are concerned with surface properties, high speeds and loads and are of special interest to this study. The elastohydrodynamic and boundary lubrication of water-based lubricants are discussed below in the next two sections.

3.4.1 The Elastohydrodynamic lubrication performance of water based lubricants

From Section 2.5, it appeared that at least part of the reason for the poorer rolling contact fatigue performance of water based lubricants is due to their inability to form thick elastohydrodynamic films. Some early work by Hobbs (64), suggested that aqueous glycols produced slightly thinner films than those of similar viscosity mineral oils. With the advent of the elastohydrodynamic theory of Dowson and Hamrock (30), importance of the pressure-viscosity behaviour of a lubricant became clear, Eq. 3.3.

$$h_o = K (\alpha)^{0.49} \qquad \text{Eq. 3.3}$$

where h_o is the film thickness

K is a constant

α is the pressure-viscosity coefficient

The reason for the low film thickness estimated by Hobbs (64), was thus due to the low α-value of the aqueous glycol which was about 6 GPa^{-1} as opposed to a value of 20 GPa^{-1} for a typical mineral oil. This means that for identical other conditions, the aqueous glycol would produce a film only 45% the thickness for the mineral oil. For the invert emulsions, however, Hobbs (64), could not measure any film thicknesses. In 1977, Hamaguchi and co-workers at Imperial College (69), used an optical interferometric technique (see Appendix 7) to measure film thicknesses of invert emulsions. After a series of tests on the emulsions and their base oils, it became clear that the EHD films formed by invert emulsions depended on the viscosity and α-value of the base oil rather than on the viscosity of the emulsion. These and others attempted to look at films formed by dilute emulsions but without success. The reason for the failure was that the EHD films, if formed, would be very much smaller than the surface roughness and the ensuing contact removed the surface from the glass plate and prevented any film from being measured. Dalmaz and Godet (70), in Lyon, looked at film thickness in sliding rather than rolling contacts for a mineral oil, an invert emulsion, an aqueous glycol and a chlorinated diphenyl. The mineral oil and the aqueous glycol gave good agreement with theory but the invert emulsion did not. However, they found that at high shear rates the viscosity of the invert emulsion dropped to that of its base oil and formed film thicknesses similar to those calculated for the base oil. This agrees with the findings of Hamaguchi and co-workers (69). After this pioneering work, it has become common practice to use the base oil viscosity and α-value for the calculations for film thicknesses.

3.4.1.1 Film thickness improvers

Tokarzewski and co-workers (71), performed a large number of experiments to find additives to increase the film thicknesses of water-based ethylene glycol hydraulic fluids. They synthesised some complex phosphoryl amide derivatives and found that one phosphoryl tris(diethanolamide) (DAP) increased the viscosity of the fluids markedly and as a result increased fatigue lives of 10 minutes for water and 30 minutes for ethylene glycol to 120 minutes for pure DAP, whilst a 5% solution of additive in water gave a 95 minute life and a 90 minute life in ethylene glycol. The welding load also increased with increasing concentration of DAP in both water and ethylene glycol but the fatigue life with DAP in water went down.

Tokarzewski (71), also noted that adding sugar to water improved the life against welding loads but not against pitting. This was pioneering work in the development of HFA/t fluids.

A more recent development in the field of film thickness improvers for water fluids was reported by Hughes and Forsberg (55), when high molecular weight water-soluble polymers were added to a dilute emulsion. The viscosity increases markedly with only 5% by weight polymer added and the polymers give reasonably good EHD films. The behaviour of polymer thickened fluids is discussed further in Section 7.3.

3.4.1.2 Behaviour of emulsion particles in contact zones

One important aspect of the EHD behaviour of water fluids is what actually happens in the contact. Wan (72), used the interferometric technique (Appendix 7) to look at invert emulsion particles in contacts and with the equipment that was available concluded that the emulsified water particles were dragged round the contact and only the mineral oil passed through the contact. This supported the earlier

work of Hamaguchi and co-workers (69). In some later work, Wan and his co-workers (73), used ultra high speed cameras to photograph emulsion particles passing through the contact. Small particles, even if many times the height of the contact could, in some circumstances, pass through the contact to give increased separation of the two contacting surfaces. With emulsified water particles this was found to depend on emulsion stability and contact geometry.

3 4.1.3 Shear behaviour of water fluids

Emulsions are non-Newtonian fluids and as a result of this, behave rather differently from either water or oil when under shear. The viscosity of water and mineral oil do not change significantly to very high rates of shear but emulsions shear-thin. Whether the loss of viscosity is permanent or temporary it has important implications for lubricant behaviour. As reported by Dalmaz and Godet (70), invert emulsions shear thin to the viscosity of the base oil, whilst dilute emulsions do not lose all their viscosity, although some is lost due to the alignment of surfactants in the direction of shear (72). Aqueous glycols behave similarly to water but polymer-thickened emulsions suffer from loss of viscosity due to the temporary shearing of the thickening agents. Prolonged shearing may lead to permament loss of viscosity.

Taylor and Wang (74), used an ultrasonic shearing device to demonstrate these effects of shearing on water fluids. They also used a Stribeck curve to demonstrate that for the most part, water fluids operate in partial EHD and boundary lubrication.

3.4.1.4 Film thickness measurements

Because mineral oils give such thick films they are very easy to measure by standard techniques such as optical interferometry and electrical resistance measurements (69). The latter technique is ruled out with water fluids because the emulsions conduct and the former technique is ruled out for all water-based fluid except invert emulsions because the minimum thickness measurable by this method is

about 200 nm. Using calculations from Wan (72), the estimated film thickness for an aqueous glycol is only marginally above that of water and dilute emulsions. Due to the inability to measure such thin films, it is not possible to prove the validity of Dowson and Hamrock's (30), elastohydrodynamic film thickness equation. Recently two new techniques have been published which should be capable of measuring film thicknesses down to about 5 nm for the most sensitive method. Kimura and Okada (75), reported in July 1987, a method of X-ray absorption which they suggested could with good calibration measure down to 70 nm. With some of the emulsions they did not give any measurable films but one gave a 350 nm film at 40% water, which is several times larger than the theory predicts. Kimura and Okada (75), explained this by the ability of the emulsion to form large globules on the metal surfaces and thus separate them quite well.

Guangteng and Spikes (76), also recently reported a method for looking at very thin films but as yet have not applied the method on emulsions. Their method was an optical interferometric one with a wedged spacer layer on top of the reflecting surface. Guangteng and Spikes (76), suggested that film thicknesses down as far as 50 Å (5 nm) can be measured. If this method is successful with water fluids, then it should be possible to prove or disprove elastohydrodynamic theory for very thin fluid films, as the estimated film thickness for water is of the order of tens of nanometres, (76).

3.4.1.5 EHD of Dilute Emulsions

Stable oil-in-emulsions, especially microemulsions, behave very similarly to water (74), and may well form very thin films similar to those to water. However, unstable emulsions form films on rolling surfaces. These films are formed by the surfactants and oil plating out in layers on the metal surfaces. Wan (72), also looked at this

and, using a highly unstable emulsion, obtained a film which was almost measurable by optical interferometry. This is further discussed in Section 7.5.

3.4.2 Boundary Lubrication

In this section the boundary lubrication properties of water based lubricants are considered.

When an elastohydrodynamic or hydrodynamic film fails to separate contacting surfaces completely, catastrophic failure may be prevented due to 'boundary lubrication'. This arises from the adsorption or reaction from the lubricant of reactive molecules onto the rubbing surfaces. The use of surfactants in lubricants has been studied in some depth and organic sulphur compounds have been added to oils to improve their severe condition performance since the turn of the century. The use of long chain surfactants and sulphur organics to illustrate boundary lubrication is made because they represent the extremes of the two chemical mechanisms by which boundary lubrication takes place, namely physical adsorption (physisorption) and surface chemical reaction respectively.

3.4.2.1 Physical Adsorption

Physisorption is the reversible adsorption of a surface active molecule onto an interface. In the case of boundary lubrication, surface active molecules adsorb onto the exposed metal surface. This is a dynamic process in which surfactants are continuously being adsorbed onto and desorbed from the surface. The degree of lubrication depends upon and thus the concentration of surfactants in the oil, the concentration of vacant sites on the surface and the temperature. Cameron (77), reviewed the topic of boundary lubrication and suggested that the mechanism of physisorption had been well established and explained known phenomena. A stick-slip model was used to characterise the effects of temperature. At low temperature, no scuffing took place because adsorbed surfactants prevent surface interaction. As the temperature rises surfactants have more energy

and more easily desorb from the surface. Above a certain temperature virtually no surfactants can remain adsorbed to the surface, there is no protective film and scuffing takes place. This temperature is usually above 150°C. At even higher temperatures, EP additives can react at the surface to prevent scuffing. Thus slip at low temperature stick when the surfaces scuff because all surfactants have desorbed and then slip as the EP additives start to react as the temperature is raised further. Other effects concerning the boundary lubrication of contacts are largely time and temperature dependent and are beyond the scope of this brief review. One important effect is, however, chain matching. If the tail (the hydrophobic part) of the surfactant is of similar length to that of the carrier oil, then interaction occurs between the two and thicker surface layers are formed.

3.4.2.2 Surface Chemical Reaction

Surface chemical reactions occur when an irreversible chemical reaction takes place at the surface of the contact. Examples of this are surface oxidation by adsorbed oxygen and the behaviour of the extreme pressure lubricant additives. There is, however, one major problem in that there must be sites available on the metal surface for the additives to adsorb onto and then react. It is for this reason that lubricant additive packages are carefully mixed to ensure that one additive does not prevent another from operating by blocking all available sites. Another problem with the lubrication by reactive chemical films is that the temperature in the contact needs to be high, above 130°C (77), a temperature which is beyond the scope of this study. The boundary lubrication by water fluids is discussed in the next section.

3.4.2.3 Boundary Lubrication of Water Fluids

There has been very little work related to the boundary lubrication of water fluids. Yahagi (78), in 1979, investigated the behaviour of extreme pressure agents in emulsions and concluded that the water was such a good coolant that it suppressed the vast majority of reactions between the organo-sulphur additives and metal surfaces. The presence of water may also have caused the organo-sulphur molecules to hydrolyse.

Spikes and Cameron (79), had shown that at medium and at slow speed, it was the temperature giving rise to additive reaction which was responsible for the prevention of scuffing.

A recent study by Wan and co-workers (73), investigated the elastohydrodynamic lubrication of water fluids and also of unstable emulsions. They showed that when an emulsion was unstable physical adsorption of surfactants and emulsion particles onto the the metal surface took place and these gave a considerable degree of boundary protection. The problem is that these films are extremely thin (< 100 nm) and until recently were immeasurable although with the techniques of Spikes and Guangteng (76), and further investigation into the boundary performance of these fluids should now be possible. The boundary lubrication of water fluids is further discussed in Section 7.5.

3.5 MECHANISMS

In Section 2.1, rolling contact fatigue was introduced but the various mechanisms for the premature failure of bearing steels in a water-based system were not discussed. There are three main schools of thought as to the mechanisms by which water might promote short fatigue lives. These are listed in Table 3.21.

1. Low elastohydrodynamic film thickness and thus low lambda ratio.
2. Chemical effects promoting crack growth.
3. Pressure pulsing of the lubricant in cracks, (The hydraulic mechanism).

Table 3.21

Three mechanisms of failure

The chemical effects mechanism can be sub-divided into two closely related ones, hydrogen embrittlement and corrosion. The above mechanisms go some way towards explaining the reasons behind the premature failures but with different fluids, different mechanisms may operate or the contribution of each mechanism to the overall reduction in fatigue may be different. Each of the mechanisms is discussed below.

3.5.1 Film Thickness Mechanism

Dawson (7), in his pioneering paper in 1962, reported that, for the most part, when film thickness in a bearing contact was low, fatigue life was low. He suggested that the reason for this was that low film thickness permitted metallic contact. Dawson introduced a parameter, D, the ratio of the surface roughness at the start of the test to the oil film thickness and found that there was an approximate logarithmic life to D ratio relationship. He experimented with assorted

roughnesses and viscosities for the same steel and mineral oil. Since then an engineering guide has been drawn up which charts the influence of film thickness on life for mineral oils (36). The guide has converted Dawson's 'D' parameter and called it lambda (λ), the specific film thickness, Eq. 3.4.

$$\lambda = \frac{\text{Minimum EHD film thickness}}{\text{Composite surface roughness}} \qquad \text{Eq. 3.4}$$

The effect of specific film thickness on life can be seen in Figure 3.1.

When the specific film thickness falls to less than 2, metallic contact occurs. At $\lambda < 1$ significant part of the load, is borne by the surface asperities and the fatigue life drops off rapidly. When surface asperities interact they are generally elastically or plastically deformed due as a result of spalling, or micropitting occurs depending on the severity of the interactions. This was discussed in Section 2.2.4.

In Section 3.4.1 it was shown that many water fluids give significantly lower film thickness and this is part of the reason for premature failure with water based fluid lubrication.

The thin film mechanism does not, however, explain the reason for the loss of fatigue performances suffered by mineral oils with as little as 50 ppm of dissolved water so there must be other effects operating in these cases.

3.5.2 Chemical Effects promoting Crack Growth

The presence of water aside, the chemistry of the lubricant was shown in Section 2.4 to be very important. Additives, which may be only present in amounts up to 0.5% and thus have no significant effect on the physical properties of the lubricant, may change the fatigue life

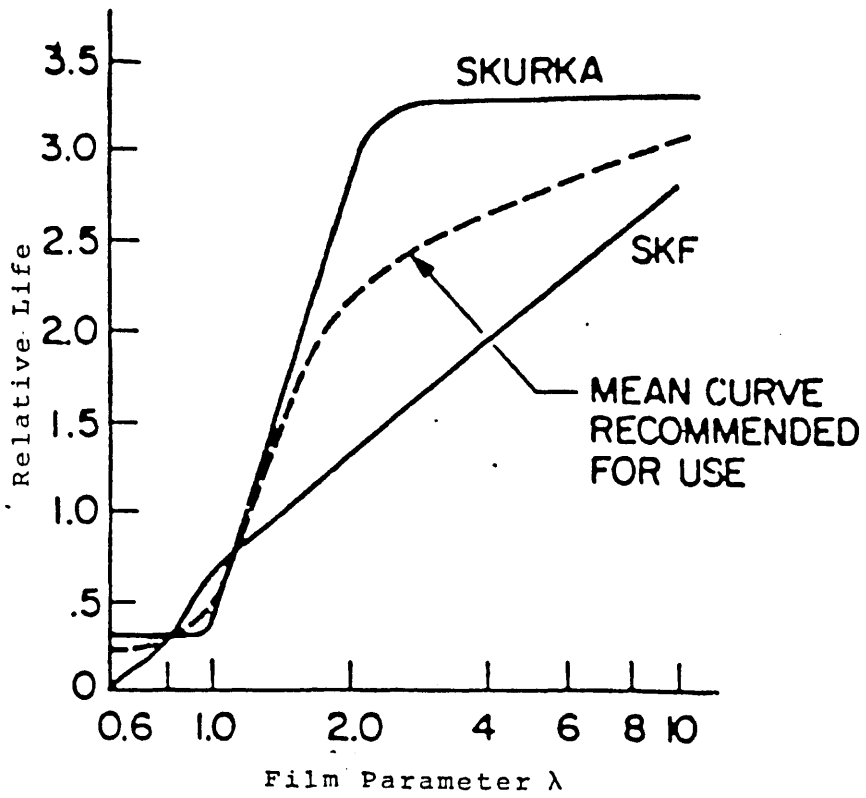

Figure 3.1

Life specific film thickness relationship

considerably. Rounds (8), in 1962, reported that the viscosity of a lubricant was its primary property in Rolling Contact Fatigue but nearly as important was its chemistry, in terms of its composition and its reactivity or polarity. Littmann and co-authors (80), reviewed the effects of lubricant chemistry on bearing fatigue life and concluded that lubricant chemistry was by far the most important effect in rolling contact fatigue. Water behaves like an additive and is responsible for chemical effects such as hydrogen embrittlement and chemical corrosion that are almost certainly responsible for the premature failure.

Hydrogen embrittlement is further discussed in Section 3.5.4 and chemical corrosion in section 3.5.5.

3.5.3 The Hydraulic Mechanism

Way (2), in his pioneering paper of 1935, suggested that the contact fatigue was due to the seepage of oil into microcrack openings so that when these were closed, the stressing caused the cracks to propagate and promote pitting. This mechanism seemed to explain the premature failure of components lubricated by mineral oils but, with the advent of the work of Grunberg and Scott (5), this mechanism seemed deficient as there is no difference in the bulk physical properties of wet and dry oils.

A modified version was published by Littmann and co-workers (80), who suggested that the lubricant viscosity has to be sufficiently low to penetrate microcrack openings. Since low viscosity also tend to promote low λ values, it is difficult to separate the two mechanisms of low film thickness and hydraulic effects.

Michan and co-workers (81), used a horizontal disc machine to investigate the influence of a mineral oil on the hydraulic mechanism. The horizontal test disc was run at 200 rpm and the oil was drip fed into contact. The disc was run until surface cracks opened up. The oil was forced into these openings by the contacting discs and the lubricant was observed to cause crack propagation. This was shown by a series of high speed photographs. This showed that for mineral oils the hydraulic mechanism was valid.

Murakami and co-workers (39), produced a mathematical analysis of a rolling contact and suggested that the hydraulic mechanism of Way (2), was the one responsible for rolling contact fatigue.

This mechanism has been inferred by some authors to explain the effect of water on rolling contact fatigue. Several workers have suggested that one of the important effects of water was that it was very much more surface active than the oil and condensed out of the oil onto the metal surface (40), (41), (47), (64).

Sullivan and Middleton (82), reviewed the mechanisms for the premature failure of bearings and after having completed some rolling contact fatigue tests on a series of aqueous glycols proposed that pitting was caused by the ingress of water into the crack opening, which is then restressed and closed up. Water is virtually incompressible and its viscosity is insensitive to pressure and transmits the pressure down the length of the crack. It would thus promote extension of the crack, branching and eventually pitting. Rudston and Whitby (84), also suggested that water ingressed into the crack but could not explain what happens in the crack, whether the water transmits the pressure down the crack or reacts with the fresh metal surfaces so that corrosion and/or hydrogen embrittlement take place.

The hydraulic mechanism is very plausible for the earlier failure of rolling contacts but it is not possible with present instrumentation to prove or disprove it as the mechanism in realistic systems.

3.5.4 Hydrogen Embrittlement

Grunberg and Scott (40), in their 1960 paper, suggested that one possible mechanism for the early failure of bearing steels was the hydrogen embrittlement of the steel. The hypothesis put forward is that the straining of the surface layers produce a high concentration of vacancies into which hydrogen ions or atoms could diffuse, provided that there was a ready source of hydrogen available. In the case of rolling contact fatigue it has been suggested that the mechanism for hydrogen embrittlement is that water diffuses into the tips of microcracks caused by the stressing, reacts with the fresh metal surfaces and liberate to form metal oxides reactive hydrogen, Eq. 3.5.

$$H_2O + M \rightarrow MO + 2H \qquad \text{Eq. 3.5}$$

This hydrogen diffuses into the plastic zone ahead of the crack tip and causes embrittlement which allows the crack to grow further. Grunberg and co-workers (84), experimented using tritiated water to investigate the hydrogen diffusion into the highly stressed steel balls. They supersaturated with 6% tritiated water a rolling four-ball fatigue test rig with mineral oil and then used a scintillation counter to measure the ball activity caused by radioactive tritium. They found that on the ball away from the tracks, the count rate was just above the background count but that in the track area, the counts were about 30 to 60 times higher than the background count. They suggested that tritium diffused into the stressed surface areas and caused embrittlement. Grunberg and co-workers (85), followed up their earlier work quantitatively and found similar results as before but concentrations of hydrogen and

tritium were measured and the maximum depth of tritium penetration was measured (< 1 μm). They also reported that the concentration of hydrogen/tritium is proportional to the time of stressing and also the load. A short period after the test, the H/T concentration levels had declined so they concluded that most of the hydrogen diffused out of the stressed area but some was retained in the matrix of the metal as interstitial metal hydrides.

Grunberg and co-workers (85), concluded that hydrogen penetration occurred causing hydrogen embrittlement but that most of the hydrogen came from the lubricant rather than the water and that both water and oxygen were necessary for the reactions to take place. There were no definite conclusions as to the mechanisms of the production of hydrogen but hydrogen peroxide can be formed at metal surfaces from water and oxygen and hydrocarbons can be cracked at 400°C on hot metal surfaces. Between 1962 and 1973, it appears that this mechanism fell into disuse and it was not, until renewed interest in water fluids, that hydrogen embrittlement of bearing steels was studied again. During the late 1960s, it was discovered that hydrogen gas stored under very high pressure was causing failure in high strength steels. Gray (87), in his opening remarks to a conference on hydrogen embrittlement testing, described the three types of hydrogen embrittlement. In rolling contact fatigue only 'Internal Reversible Hydrogen Embrittlement' and 'Hydrogen Reaction Embrittlement' are of interest. Internal Reversible Hydrogen Embrittlement, also known as slow strain rate embrittlement and delayed failure, is the oldest recognised failure mechanism. It is the classical type of embrittlement failure associated with electroplating, melting, pickling and with stress corrosion. For fully reversible internal hydrogen embrittlement to occur, no chemical reaction must take place between the hydrogen and the metal lattice.

Where the hydrogen is absorbed and it reacts with the lattice or with foreign bodies or inclusions in the lattice, it is termed Reaction Hydrogen Embrittlement. This method of hydrogen embrittlement is very common in high carbon steels where the hydrogen reacts with the carbon in the lattice to form methane which bubbles into the grain boundaries weakening the metal. The type of hydrogen embrittlement in rolling contacts is difficult to determine although run samples may give off hydrogen as a result of reversible internal hydrogen embrittlement. Ciruna and Szieleit (88), renewed interest in the investigation of the effects of hydrogen embrittlement on Rolling Contact Fatigue in 1973. Using a modified rolling four-ball fatigue test rig, they looked at the effect of hydrogen content on AISI 52100 steel and 440C stainless steel. They carried out a series of tests in air, hydrogen and helium with treated and untreated balls. Two types of treatment were used. The first involved storing the balls in hydrogen gas at 400°F under 1000 psi for 40 hours whilst the second electrolised the balls in 10% sulphuric acid solution with a 100 mA current for 1 hour. For the AISI 52100 steel balls, no difference was obtained between the the untreated and the high pressure hydrogen treated balls in air but the untreated balls run in helium and hydrogen gave considerably longer lives. The electrolised balls gave lives of less than 1% of the untreated balls. The others were analysed very closely for evidence of corrosion and other effect but none were detected. Further tests were done to investigate the effects of the electrolysis on both AISI 52100 and the AISI 440C stainless steels. The hydrogen content of the balls were proportional to the time of electrolysis with the stainless steel having a lower hydrogen content than the AISI 52100 steel. The effects of hydrogen content on fatigue was then studied. Significant reductions at varying concentrations of hydrogen were reported with

the greater the concentration of hydrogen the greater loss of fatigue performance. Further ageing tests were done with most of the hydrogen having diffused out but still gave very poor fatigue performance. From this it would appear that the embrittlement damage is permanent but precise quantitative effects cannot be measured due to the low inaccuracies of hydrogen concentration measured. Some tests were also done using hydrogen sulphide gas as the source of hydrogen but owing to the presence of the corrosive sulphur severe loss of fatigue performance are due to the sulphur rather than to the hydrogen was reported. In concluding their work, Ciruna and Szieleit (88), suggest that it is oxygen and hydrogen from the lubricant and the water that is important in the hydrogen embrittlement of bearing steels.

Ray and co-workers in France (89), looked at the effect of hydrogen embrittlement on the same AISI 440C stainless steel using rotating-bending and tensile tests. They used a cathodic charging method similar to Ciruna and Szieleit (89), to embrittle the samples and then examined at the failure modes after varying time periods between charging and running.

The main source of failure was the breakage of carbide grains. An autoradiograph method for detecting tritium indicated that hydrogen and tritium were trapped at carbide-martensite and carbide-carbide interfaces causing weaknesses from which easy fracture occurred.

Frisch and Thiele (90), studied the effects of hydrogen on steels and its passage through mildly worn surfaces and reported that oxide layers blocked the passage of hydrogen and the removal of these layers allows the passage of hydrogen again. A modified model for the behaviour of hydrogen adsorbing of a surface was presented but the results presented are not very useful for studying hydrogen embrittlement. Hydrogen embrittlement as a mechanism for the premature failure of bearings is further discussed in Section 7.5.

3.5.5 Chemical corrosion

Corrosion of metals occur when they are exposed to reactive media and as a result oxides or other salts are formed which are then dissolved by the media and the process continues to remove the metal. With some metals the oxide layer is very strong and dense so that once it has grown to a critical depth, further reaction is inhibited. Aluminium is a good example of this type of behaviour. With iron, the oxide/hydrated oxide films formed are resistant to further oxidation. However, these films do not bind very strongly to the metal surface and cracking of the film allows further corrosion to take place. This is especially common in exposed stressed structural steels where corrosion is promoted at the highly stressed areas, causing component failure. It is for this reason that the two most famous iron structures, the Forth Bridge and the Eiffel Tower must be continually painted to prevent the onset of corrosion.

Corrosion is an electrochemical reaction where two points on the metal surface are at different potentials with the medium acting as the electrolyte and the steel acting as the two electrically connected electrodes, Figure 3.2.

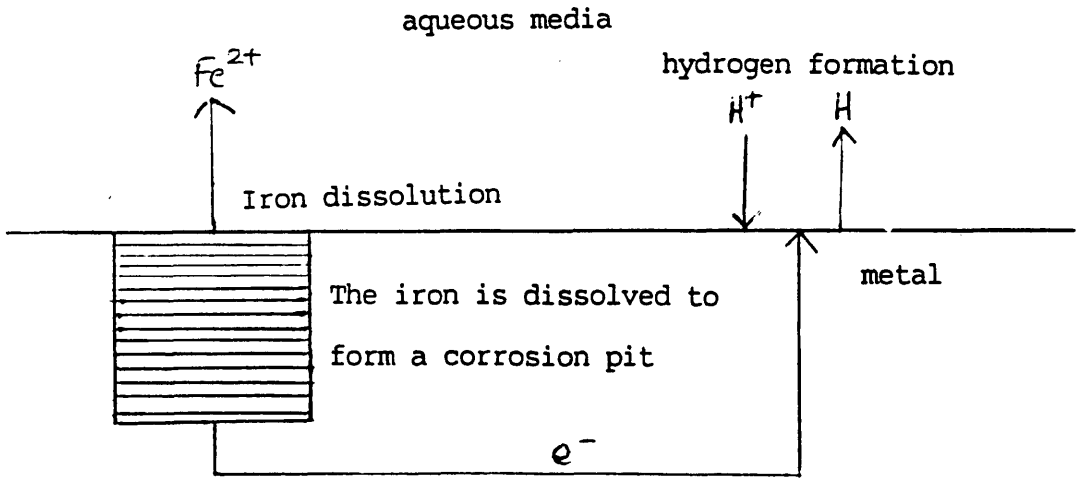

Figure 3.2

A schematic diagram of corrosion

In stressed iron or steel components, corrosion is generally characterised by the formation of small deep pits on the exposed surface. These pits are formed by the localised dissolution of the iron at the anode of the cell. At the anode, ferrous (Fe^{2+}) ions are formed which dissolve into the media and leave fresh metal which is in turn dissolved shown by Eq. 3,6. Eventually pits are formed by the loss of the metal from the surface. In stressed components, these small pits act as stress concentrations and when the pit has reached sufficient depth, the crack may be extended by the stressing until failure occurs. At the cathode, hydrogen is formed by the reaction shown by eq. 3.8.

$$Fe \rightarrow Fe^{2+} + 2e^{-} \qquad \text{eq. 3.6}$$

$$2H_3O^{+} + 2e^{-} \rightarrow H_2\uparrow + 2H_2O \qquad \text{eq. 3.7}$$

In strongly oxidising acidic media, however, the ferrous salts formed inhibit the reactions of the acidic media with the metal and instead of dissolving the anode, oxygen is formed by the following reaction shown by eq. 3.8.

$$2O^{2-} \rightarrow O_2\uparrow + 4e^{-} \qquad \text{eq. 3.8}$$

This occurs with concentrated nitric and sulphuric acids whose ferrous salts act as passive layers.

An important aspect of the water corrosion of iron is the presence of oxygen in the water. According to Schatzberg and Felsen (42), and Ciruna and Szieleit (88), the noted reduction in fatigue lives caused by water and hydrogen did not occur in the absence of oxygen.

An explanation for these observations is given in

Cotton and Wilkinson (91), in their review of the behaviour and properties of dioxygen (0_2). When dioxygen is dissolved in water, its stability is decreased and it becomes more reactive. This gives the appearance that water containing dissolved oxygen is a much more aggressive oxidising agent and why water, in the absence of oxygen does not apparently cause corrosion. One observation that the reaction was, however, very slow and a considerable length of time was required before corrosion became apparent. As a consequence of this, corrosion it would appear, has no effect on very short life failures but only on longer fatigue lives. This agrees with the rotating-bending results of Armstrong and co-workers (82),and Harris (119), as shown in Figure 4.1, where when corrosion occurs no fatigue limit is obtained.

Much of this initial work of corrosion is from the work of Evans (95), in third edition of his pioneering work. Subsequently, various workers have looked at corrosion aspects of rolling contact fatigue and their work is reviewed below.

Endo and Komai (92), looked at the corrosion fatigue strength of a high strength steel under controlled potentials and pH values to investigate the electrochemical behaviour of the steel under such conditions. They used a rotating-bending fatigue test rig with the majority of the specimen coated in a protective rubber layer but with a small area exposed to the buffer solution. A platinum electrode in the buffer and a slip ring on the sample, provided the polarising voltage. The presence of corrosion was detected by the use of a photoelectric colorimeter which detected the presence of ferrous ions above a concentration of about 0.05 mg/dm^3. Endo and Komai (92), reported that the degree of anodic or cathodic protection and the the amount of corrosion depended upon the pH and the applied voltage.

Cathodic protection was found to occur slightly above -800mV for pH = 1, with considerable protection above -800mV at pH = 4 and good protection at pH = 6. However, at -1200mV, large amounts of OH^- were formed and alkalinic rather than acidic corrosion took place. Anodic protection was found not to work very well because the stressing caused the protective films formed to break off the surface and metal dissolution took place. The work of Endo and Komai (93), showed how important the controlling of both pH and potential are in water solutions but as no work was done with alkali solutions (pH > 7) this work can not be applied to fire resistant hydraulic fluids whose pH values are between 8 and 12.

Another important area of rolling contact fatigue is that, as a result of wear and electrochemical reaction, debris is generated; little is known about how this debris behaves inside cracks. In some follow-up work, Endo and co-workers (94), investigated the influence of corrosion products on the crack propagation rates of a high tensile strength plate specimen in a 1% sodium chloride solution and concluded that the effect depended on the ratio of the maximum and minimum stresses, and the frequency of stressing. At high stress ratio (R = 0.5) no effects were found but at a low stress ratio (R = 0.1) considerable wedge damping was observed at 5 Hz. By accounting for the effective stress intensity factors, however, they eliminated the effect of the wedge but it can be concluded that the wedge may reduce the stress intensity factor or change the material constraints slightly by introducing this damping effect.

Vijh (95), looked at the electrochemical mechanism for the dissolution of metals and the concomitant oxidation of lubricating oils caused by high temperature friction. He concluded that the loss of metal from engine components was caused by the electrochemical dissolution of the

metal and completely discounted other wear mechanisms. His main suggestion was that the amount of metal lost by corrosion was proportional to the amount of oil oxidised but did he not offer any evidence for this. In his review of the subject, Vijh (95), supported the idea of Bjerk (96), of oxygen as an EP additive but failed to take into account the effect of sulphur in the oil. Again no account was taken of possible water reactions in oils as a possible corrosion indicator.

Corrosion and corrosion fatigue has been studied extensively with special reference to marine environments but very little has been published with the effects of fire-resistant lubricant on metals. For a fire-resistant fluid to be used it must pass the IOP corrosion test (97), IP 329 but apart from some work by Leach and Talks (98), very little has been published on the effect of these fluids. The corrosion and electrochemical behaviour of dilute emulsions as investigated by Leach and Talks (98), is further discussed in Section 7.5.

One of the problems with corrosion is that hydrogen is a major product so that hydrogen embrittlement can never be discounted as a constricted effect. Once hydrogen is present it is almost impossible to identify the source of the hydrogen as coming from the lubricant or from the water as a result of lubricant decomposition or as a result of corrosion respectively.. This makes the study of the problem quite difficult. The exchange of hydrogen, deuterium and tritium between lubricants, water and additives is facile. (90)

3.5.6 Rebinder Effect

In 1954, Rebinder and his co-workers (99) reported that the adsorption of surfactants onto metal surfaces lowered the endurance fatigue limit of hardened steels. These surfactants, especially alcohols, lowered the fatigue limit by up to 20% according to Rebinder. In some follow-up work twenty years later, by Stepurenko and co-workers (47), and by Lobioko and co-workers (100), two different interpretations of the so-called 'Rebinder Effect' developed. Stepurenko and co-workers (47), looked at the effect of water in mineral oils on fatigue lives and fatigue limits using carefully dried oils then dried oils with surfactants. They found that the surface energy was lowered by 10-15% and the fatigue limit by 7-75%. However, the 'Rebinder Effect' does not account for water and addition of only 2% water, the oils gave a 26% reduction in fatigue life. The others also reported the lack of proper fatigue limit with high water concentrations, suggesting corrosion as described by Evans (92), on (Figure 2.11.). Lobioko and co-workers (100), came down firmly in favour of the 'Rebinder Effect' by suggesting that water was strongly surface active and that no evidence of corrosion was found on their tests specimens. Again rotating-bending fatigue tests were carried out and a slight loss in fatigue limit for the surfactant containing conditions was reported with over a 50% loss for the same oil and surfactants but in moist air. In their following paper, Lobioko and Karpenko (101), looked at the effects of the same alcohols and water on the kinetics of crack development and once more concluded that water, acting as a very strong surfactant, was responsible for these findings. Stepurenko and co-workers (102), in their second paper on the subject, could not prove either the mechanism of Rebinder (99), and that suggested by Lobioko and co-workers (100), (101) and Stepurenko and co-workers, and they concluded that the 'Rebinder Effect' is important but how important the contribution of the water is, is not known.

3.5.7 The Mechanism of Additives

Rowe (51), in his review of rolling contact fatigue of 1979, suggested that there were three mechanisms by which the deleterious effect of water on bearings could be counteracted by additives. They are shown in Table 3.9

1.	Proton neutralisation
2.	Hydrophobic surface film formation
3	Water Sequestration

Table 3.22

Mechanisms of additive action for water containing fluids

Grunberg and Scott (40), having tested the effect of various additives concluded that isoamyl alcohol acted as a proton neutraliser, whilst surfactants such as oleic acid acted by the second mechanism and commercial 'de-watering' agents by the third. Grunberg and Scott (40), did not, however, have a way of actually proving any of these mechanisms though their ideas accelerated the study of the mechanisms concerned.

The additive Isopropyl aminoethanol (IPAE), identified by Schatzberg (50) was thought to act via the first mechanism and all small, strongly basic amines and alcohols would appear to act in this way. The details of this mechanism, as outlined by Schatzberg (50), was that IPAE condensed from the bulk phase of the lubricant into small microcracks in the metal surface and captured protons (hydrogen ions) that were formed with the reaction of fresh metal surfaces with the water from the lubricant. By trapping these protons, hydrogen embrittlement of the metal surface was prevented or considerably reduced until the additive was exhausted. Hydrogen embrittlement has been further discussed in Section 3.5.4.

Of the second mechanism, Scott (49), thought that oleic acid and other long chain surfactants formed hydrophobic monolayer surface films on the rubbing surfaces which prevented the water molecules from reaching the surfaces.

The third mechanism involves commercial 'de-watering' agents which were added by Grunberg and Scott to their saturated and supersaturated water levels but unfortunately, apart from an imidazoline derivative, however, was strongly basic and it would appear to operate by mechanism one rather than by water sequestration.

Grunberg and Scott (40), came to the conlcusion from their work that it was not the amount of water that affected the fatigue lives but the nature of the additives in preventing the worst effects of the water.

3.5.8 Cavitation Erosion

Cavitation occurs in fluids when extremely high rates of shear are applied, found near to the surface of a ship's propeller blade or the rotating parts of a pump.

Voids form in the fluids under extreme pressures. These voids burst and cause high pressure shock waves which travel through the liquid until they strike a surface and have their energy absorbed or reflected. With some surfaces, these shock waves cause a break-up of the surfaces and thence erosion. This is called 'cavitation erosion'.

According to Riddei and co-workers (103), who studied the problem of cavitation erosion, the intensity of the shock waves depends upon the vapour pressure of the fluid and the quantity of dissolved gas present. If the liquid has a high vapour pressure (above 0.013 MPa) or has a high concentration (above 5%) of dissolved gas (a silicone oil for example) then cavitation damage drops to almost nothing. They also noted that viscosity does not seem to affect cavitation and that

stainless steels behave very similar to ordinary steels suggesting that the mechanism is mechanical rather than chemical. Despite the above drawbacks, Riddei and co-workers (103), suggested that a cavitation method is a good way for looking at lubricant behaviour and compared a series of cavitation tests with rolling four ball tests using mineral oils and a variety of controlled atmospheres and different steels. They found similar results for wet, dry and inert atmospheres for base mineral oils but when tests were done with additives present, agreements were not obtained for most of additives. They suggested the differences were caused by the unrealistic conditions employed in four ball tests. In concluding, Riddei suggested that cavitation erosion testing might be another way of testing lubricants but that further work on comparison and suitability of the method was required. Since then no further work has appeared in the published literature.

Okada and co-workers in Japan (104), looked at the effects of cavitation on corrosion fatigue and on resistant coatings. They used a corrosion fatigue test equipment with a piezoelectric oscillator attached to generate the cavitation. They tested two carbon steels and one stainless steel and found that, in general, samples fractured in the corrosion areas without cavitation taking place but that with cavitation the fracture was more facile owing to severe corrosion and erosion taking place. They suggested that this was due to the formation of localised corrosion cells on the test piece.

When the surface was coated with corrosion resistant coatings the effects of the cavitation erosion and corrosion were somewhat reduced. The results show how important it is to separate effects when looking into aspects of cavitation erosion and corrosion fatigue, especially in corrosive environments. This cavitation work examined an aspect of water behaviour which is especially important in the wear and fatigue of pumps.

Leach and Talks (98), followed up the earlier work on cavitation erosion of Riddei and co-workers (102), and Okada and co-workers (104), by investigating the effects of cavitation erosion in water-based lubricants. Leach and Talks (100), reported that adding up to 5% emulsifiable oil to distilled water had little effect but the addition of 5% oil to hard water reduced the steady state erosion by 30%. From this observation and related work, they listed four mechanisms that might prevent the erosion from taking place, Table 3.23.

1. Oil changes the physical properties.
2. The cavitation interacts with the oil droplets.
3. Emulsion inhibits corrosion,.
4. The emulsion forms an energy adsorbing layer on the surface.

Figure 3.23

Mechanisms preventing cavitation erosion

The first three proposed possible mechanisms were then discounted on the basis of observations made by the authors. The first two mechanisms, if valid, would have found no difference between the hard and distilled water and the third was found invalid since cavitation erosion also affecting the brass tip. These observations suggested that the fourth mechanism was acting and an energy absorbing layer was formed on the surface of the specimen tip by the emulsion. This layer would appear to be similar to that found by Wan (72), and is in fact caused by the instability of the emulsion in high hardness water which causes plating-out of the emulsifying agents onto the metals surfaces.

Rudston and Whitby (84) also investigated the cavitation erosion properties of dilute emulsion hydraulic fluids and concluded, similarly to Leach and Talks (98), that surface active fatty acids reduced the erosion damage but the effects were due to their physical properties rather than by surface film formation. However, no data was published on the stability of the emulsions. Rudston and Whitby (84), also suggest that, in emulsions, only bubbles which burst close to the surface cause erosion damage but no proof of this is offered. The lower compressibility of water fluids is partially to blame for the greater cavitation erosion arising in them and as before, it appears that cavitation erosion is a mechanical and not a chemical effect.

4. SURVEY OF TEST METHODS FOR STUDYING ROLLING CONTACT FATIGUE

Most lubricant test machines were originally designed to run on mineral oils rather than on synthetic or water-based fluids. The main criteria of a lubricant evaluation bench test rig are shown in Table 4.1.

Quick results
Easy to use
Cheap to run
Cheap test pieces
Consistent results
Good repeatability
Good reproducibility
Discrimination between lubricants

Table 4.1

Requirements of a lubricant test method

A whole series of test rigs have been developed to study many aspects of rolling contact fatigue. The main rigs which have been applied to the study of water-based lubricants are described below.

4.1 THE ROLLING FOUR-BALL

This rig was developed from the sliding four-ball wear test rig (105), used to evaluate the ability of lubricants to limit wear in a sliding ball bearing contact. This fatigue rig, in its standard operation, is described in detail in the Institute of Petroleum Test Methods (106). One upper ball is loaded against three lower balls held in a cup, separated by a central divide. The three lower balls are free to rotate when driven by the upper ball and the whole arrangement is lubricated by circulating test lubricant. The test is run until the upper ball pits and a consequent increase in vibration level trips the motor and timer. This rig has been extensively used and results obtained using water-based fluids are outlined below.

Grunberg and Scott (5), found that the rig gave quick results and was able to differentiate between dried, wet and water-saturated mineral oils. Other workers followed up this pioneering work with varying degrees of success. Felsen and co-workers (43), (44), employed the rolling four-ball rig to investigate the effects of water, oxygen and synthetic sea water on fatigue life. Yardley and co-workers (65), used the rig in conjunction with other fatigue test methods and concluded that the method was too severe for testing fire resistant fluids owing to the very low C/P ratio attained when the rig was used at the recommended load. Kenny and co-workers (27), showed that the ratio of the dynamic capacity of the standard rig to the standard load of 600 kg (C/P ratio) is only 0.41. This compares to typical bearing operating conditions of C/P ratios between 10 and 20. The lowest load level reported by Kenny (27), on the rolling four-ball machine was 280 kg, which corresponded to C/P ratio of 0.91 which is still very severe. Martin and Eberhardt (24), have suggested that, under normal service conditions, elastic strain takes place but that under very high loads, plastic strain and gross plastic deformation of the balls occurs. This gross plastic deformation, it is suggested, is responsible for the very short fatigue lives found using four-ball machines (less than one hour). Despite this limitation, rolling four-ball fatigue rigs are still in use today for lubricant and fire resistant fluid evaluation but the results are generally interpreted in conjunction with other test machines having higher and thus more realistic C/P ratios.

4.2 THE UNISTEEL FATIGUE RIG

The Unisteel Rolling Testing Fatigue Machine was originally designed to test the quality of different steel test specimens when lubricated with a standard mineral oil (107). This rig, when employed under its standard operating procedure, is fully described by an Institute of

Petroleum Test Method (107). The fatigue specimen is a flat steel washer used in place of the upper race of a thrust bearing. As this is commercially available and, indeed, has two surfaces so that it can be used twice, the specimens are relatively cheap.

The dynamic capacity of the system is 5700 N (65), and the standard load used is 3340 N, giving a C/P ratio of 1.71. The contact stress for each point of contact is 3.9 GPa (see Appendix 3 for calculation) which is slightly above the elastic limit but below the crucial shakedown limit (28), for the steel used. Kenny & Yardley (63), carried out extensive testing using the Unisteel machine and found it to be satisfactory for lubricant evaluation. However, different machines were found to give different results and so they recommended that all rigs be calibrated with a standard mineral oil before use. The main problem with these calibration tests is that they take a very long time to complete, because the mean life for a mineral oil is about 170 hours (7 days) (107). Kenny (108), also recommended that about thirty tests should be carried out to produce a statistical set of results, implying 7 months per calibration. If less than ten tests are carried out the error in the L_{10} fatigue lives is of the order of $\pm$ 60%. Eastaugh and Ritchie (46), also carried out extensive testing on a Unisteel test rig to investigate the performance of emulsifying oils on rolling contact fatigue. Their results were described in Section 3.1.

Some work has also been carried out on the Unisteel machine at much lower loads, with a C/P ratio of 3.10 but Yardley and co-workers (65), reported that under these conditions it takes more than three months to complete just one test set of results.

4.3 ADMIRALTY OIL LABORATORY (AOL) VERTICAL FATIGUE RIG

The operation of this rig will be fully described in Section 5.2 since it has been employed in the current study. The rig was designed as a compromise, intermediate step between the rolling four-ball with a very low C/P ratio and the Unisteel with a quite high ratio of 1.71 to 4.78 depending upon the load used. The rig consists of a rolling four-ball fatigue machine modified to accept standard thrust bearing races.

According to Eastaugh and Ritchie (46), the AOL rig operates at a C/P ratio of 1.5 and it gives results similar to those of the Unisteel rig, but much more rapidly. The set-up used by Penfold (45), Eastaugh and Ritchie (46), and Onions (109), consisted of six vertical fatigue rigs to generate data rapidly.

4.4 DISC MACHINES

These are probably the earliest form of rolling contact fatigue test rig and Way used one in his pioneering work on rolling contact fatigue (2). Disc machines generally consist of two driven discs, hydraulically or mechanically loaded against one another.

Unlike most other test rigs they permit a controlled degree of sliding. Historically, they were designed to test scuffing of gear steels and gear lubricants but the relatively cheapness of discs and ease of use has led to their application in rolling contact fatigue studies. A recently published application of a disc machine to study rolling contact fatigue was by Sullivan and Middleton (83), who examined the pitting and cracking of bearing steel discs lubricated by an aqueous glycol. The two discs employed were of 750 and 250 VPN for the fast and slow discs respectively, with 10% slip.

Sullivan and Middleton (83) reported that pitting took place only in the partial elastohydrodynamic region suggesting that the lack of film was the cause of the pitting but the presence of water also promoted

pitting by the hydraulic mechanism. One of the problems with using two discs of very different hardness rates is that the conditions for failure are not realistic, as hardened materials have a much longer fatigue life than soft specimens. Only a few tests were carried out at each load, speed and viscosity condition by Sullivan and Middleton (83), and so Weibull analysis (18), of the results is impracticable.

4.5 BEARING TEST RIGS

Hobbs and Mullett (59), used a full scale roller bearing test rig to obtain realistic results for the fatigue lives of the bearings as did Hobbs (64), in later work with the same test rig. Cantley (48), also employed a bearing test rig, using tapered rollers, and found good agreement with the earlier work of Grunberg and Scott (5), Schatzberg and co-workers (41), (42), and Hobbs and Mullett (59). Culp and Widner (68), used a similar rig to Cantley (48), and found similar reductions in the fatigue lives caused by water-in-oil emulsions and other fire resistant lubricants. Overall, bearing test rigs give good reproducible results.

However, tests are very expensive since in most bearing test machines, eight sets of bearings need replacing after each run. Hobbs and Mullett (59), also found that running bearings under their usual C/P ratio of 10 to 20 took hundreds of hours to fail and reported that their tests on seven fluids took three years to complete.

4.6 NASA FIVE-BALL FATIGUE RIG

Parker and co-workers (110), employed a NASA five-ball test rig to examine the rolling contact fatigue of mineral oils and bearing steels. This rig is similar to the four-ball rig except that there are four lower balls instead of three. In a modification common to the four-ball fatigue rig, Stickels (111), removed the upper ball and replaced it with a tapered cone specimen. This removed the problem, common in the rolling four-ball, of the upper ball sliding in its collet. No results have yet been published by Stickels on the performance testing of fire resistant lubricants.

4.7 PUMP TESTS

The tests described above are all accelerated tests but clearly the true test of a lubricant is its operation under its 'service' conditions in the equipment to be lubricated. It is not uncommon for lubricants to pass small scale screening tests and then to result in premature failure in actual service. One of the most widely used types of test for water-based fluids are pump tests. These are employed to assess the wear and fatigue caused by the test fluids when run under service conditions in pumps. The method of testing is to visually inspect, weigh and measure the moving parts of the pump before the commencement of test, then run typically for 1000 hours at 13.8 MPa pressure or until the pump fatigues. At the end of the test the pumps are stripped, the parts reweighed and rated for damage. Fluids are ranked by the amount of wear (weight loss) and the number of hours to failure of the pumps.

Four types of pumps are commonly used -

i. vane pumps;
ii. axial piston pumps;
iii. plunger pumps;
iv. gear pumps.

Of these, the 'Vickers' vane pump test is an IP standard test (112). The major disadvantage of pump testing is the cost of the pumps and the length of time required to obtain a full set of results (1000 hours is 41 days 16 hours of continuous running). With dilute emulsions, plunger pumps appear to give the best performance, especially when powering hydraulic pit props, but when testing fluids that have superior performance, the more demanding axial piston pumps and gear pumps are preferred so that failure or damage occurs in a realistic time. Pump tests tend to be performed after other cheaper screening methods have been employed.

In 1977, Knight (67), reported the results of some hydrostatic pump tests on various fluids and found similar reductions in fatigue lives and the same ranking order as in Tables 3.5 and 3.9.

4.8 NON-CONTACTING TEST METHODS

Other fatigue test methods, which do not involve a lubricated contact, are often employed to study the influence of lubricants on fatigue. These include biaxial-bending, tension-compression, rotating-bending fatigue rigs and other cracking and crack propagation rigs.

For many years classical fatigue studies have been carried out using high cycle fatigue rigs. These studies usually involve the repeated stressing of the components under differing cyclic loads until failure. From a series of about eight to ten tests including run-outs at low stresses, a stress-life plot (S/N plot) is drawn as in Figure 4.1.

From these plots, the fatigue limit of the steel under the appropriate environmental conditions is obtained. The fatigue limit is the stress level below which no fatigue failure should occur, provided the conditions are maintained.

The method has been shown to give good discrimination between various conditions and, provided the stresses are of not too high values, sensible run-out lives of the order of 20×10^6 cycles may be obtained. The use of this type of bending rigs is further discussed in Sections 4.8.2 and 5.3, as there is a large amount of work on these rigs using fire resistant lubricants.

4.8.1 Fracture Mechanics Techniques

From Section 2.2.4 it is clear that it is far easier to investigate the initiation and propagation of rolling contact fatigue cracks by using fracture mechanics techniques than by using full scale S/N type fatigue tests. The most common type of fracture mechanics technique

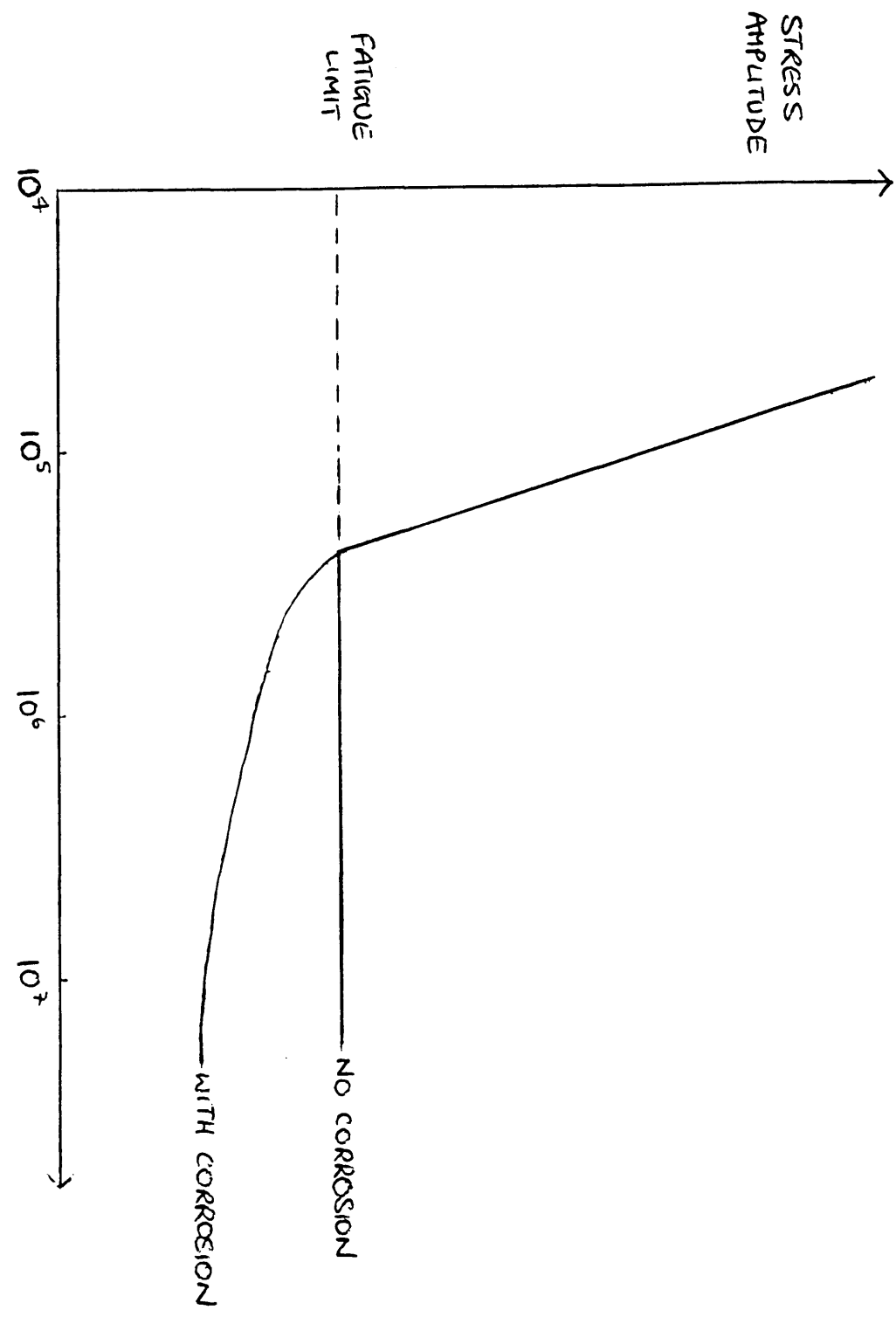

Figure 4.1

Load-life fatigue plot

involves the use of plate specimens as in Figure 4.2, where one of the boltholes is anchored and

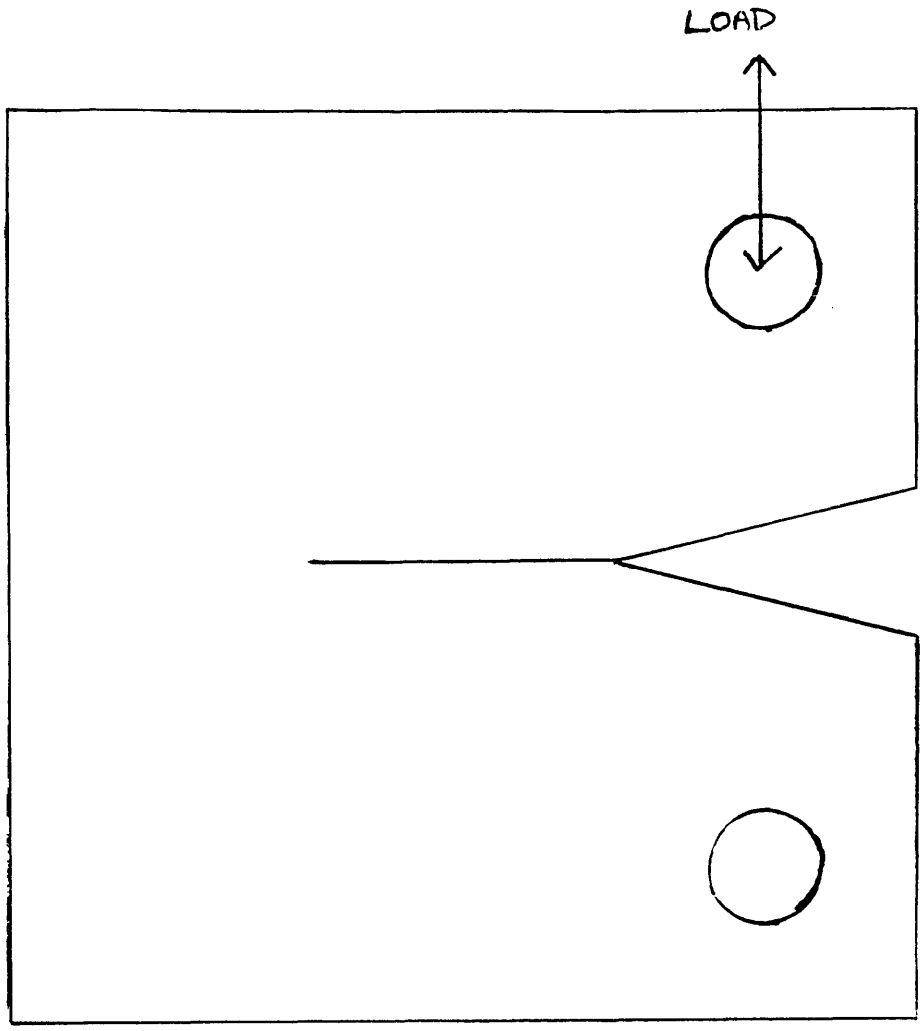

Figure 4.2
Fracture Mechanics plate specimen

the other is cyclically displaced to cause strain and cracking at the tip of the notch. If the specimen and mounting equipment is immersed in a temperature and environment-controlled chamber, the test conditions can be easily maintained to give reliable data. A considerable amount of work on the corrosion fatigue of stainless and other high strength steels has been published, but very little has been published using lubricants as the medium (93). This is further discussed in Chapter 9.

4.8.2 Rotating Bending Fatigue Rig

This type of non-contacting fatigue test machine has been used extensively to study the influence of lubricants and fire resistant hydraulic fluids on the fatigue limit and fatigue life of bearing steels. The rigs were initially employed to investigate mineral oils (113), but from 1974 work has been carried out using standard water-based systems (16). Since this type of rig was used in the current study, further details will be given in Section 5.3 along with previous experimental work using this method.

4.8.3 Summary of Non-contacting Methods

The use of rotating-bending fatigue rigs for the investigation of lubricant-steel interactions is well documented but that of fracture mechanics techniques less so. The major problem with using non-contacting test methods is that there has been no systematic attempt to correlate contacting and non-contacting methods with respect to fatigue in the presence of lubricants. This is further discussed in Section 6.3.

4.9 SUMMARY OF TEST METHODS

Some methods used to investigate the rolling contact fatigue life and the influence of lubricants on fatigue have been outlined above. Numerous other test configurations have also been employed in isolated studies. Alternative test methods have been employed by Law (114), a modified four-ball fatigue test rig and Blanplain (52), a reciprocating sliding test rig. Other workers, Rowell (115), Stanton and Whitwell (54) and Baker and Riley (53), have used actual pit prop equipment for the assessment of fluids under laboratory conditions. The use of such tests is further discussed in chapter 7.

Test methods used in the current study are described in further detail in the next chapter.

5. DESCRIPTION OF EXPERIMENTAL TEST RIGS EMPLOYED IN THIS STUDY

Three fatigue test rigs were used in this study to evaluate the rolling contact fatigue performance of commercial water-based fire-resistant lubricants. These are described in detail below, after which there are brief descriptions of other test equipment employed during the research program.

5.1 ROLLING CONTACT FATIGUE FOUR HEAD TEST RIG

This test rig was specifically designed and built for the evaluation of fire resistant lubricants. Firstly the rationale behind the design of this rig is outlined, and then its main features are developed and described.

5.1.1 Reasons behind the New Test Rig

As indicated in the previous chapter, the most widely used test equipment for lubricant evaluation are the rolling four-ball and the Unisteel test rigs. The rolling four-ball test rig, as discussed in Section 4.1, operates under very severe contact conditions. The Unisteel fatigue rig, Section 4.2, is a lot less severe than the four-ball but, because of this, fatigue test series take a very long time to complete.

The background investigation to this work was carried out by Dousinas (25), who developed a single headed rolling contact fatigue rig to investigate the effects of mineral oils and the pitting of hard and soft steels. The results of his investigations showed that using the rig, it was possible to obtain reasonable fatigue lives for bearing steels under high loads. From this work it was also clear that as the rig had only one head, it was very unsuited to an extended fatigue programmme since it generated data slowly and also since progress was critically susceptible to mechanical failure in the single head. To overcome this limitation, the four-head rolling contact fatigue rig was designed to operate under intermediate conditions of load and

speed and to have four identical test heads. The four identical heads were built so as to keep the variations in life due to the different heads to a minimum. Had the method of Kenny (108), been followed, then extensive calibration tests on the rig would have been carried out to establish any variation between heads. These calibrations would probably have been taken about 1 year to complete without breakdowns and it was estimated that no significant differences between the heads would have been found. Thus a full Weibull plot could hopefully be obtained in a relatively short space of time, and only slightly longer if a breakdown occurs.

5.1.2 Nature of the test

The test simulates the rolling of a lubricated ball on a raceway. A steel ball bearing is loaded by hydraulic pressure against a rotating bearing steel bar, as shown in Figure 5.1.

The samples are run to pitting failure and when 11 to 15 failures have been recorded without suspensions, the results are analysed and a Weibull plot of the failure data drawn. From the Weibull plot the L_{10} and L_{50} fatigue lives are calculated, as is the Weibull slope, e. These values are used to compare the fluids and to rank them. The fluids are also compared by their modes of failure.

5.1.3 Test Rig Details

The rig is shown in Figure 5.2.

5.1.3.1 Lubricant Supply

The basic contact consisted of a ball hydrostatically loaded and free to rotate against the curved side of a rotating steel bar. The steel bar thus drives the ball in nominally pure rolling. The contacts were lubricated and the balls loaded by test fluid pressurised by an axial piston pump. The piston pump was Model Number PO7MAPONXY supplied by RHL Hydraulics, Newcastle-upon-Tyne, and was recommended by British Coal for use with water-based fluids, (56). It was important to select a pump able to withstand prolonged use pumping water-based fluids without failure. From the pump the fluid passed through

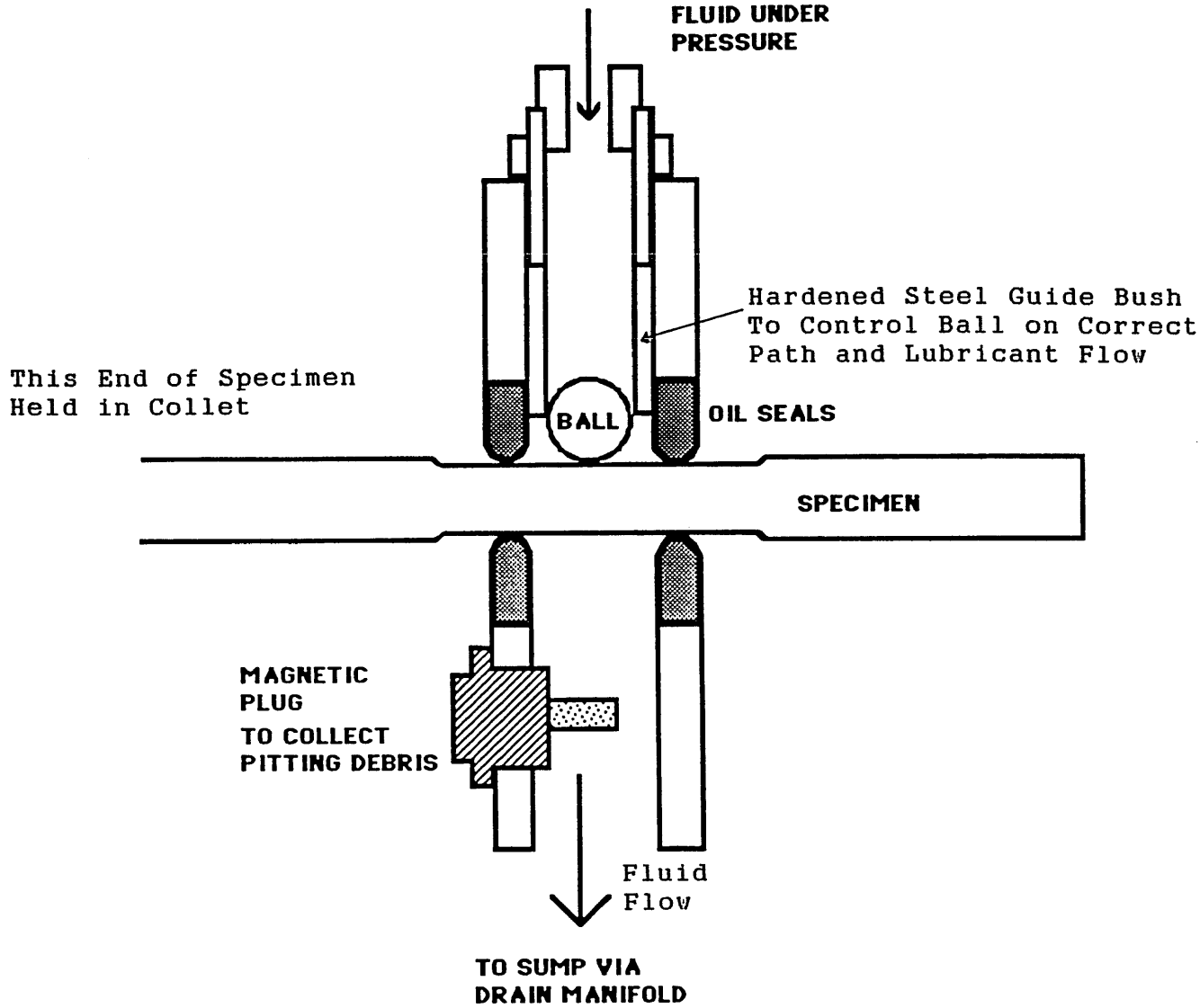

Figure 5.1

A test head from the four-head rig

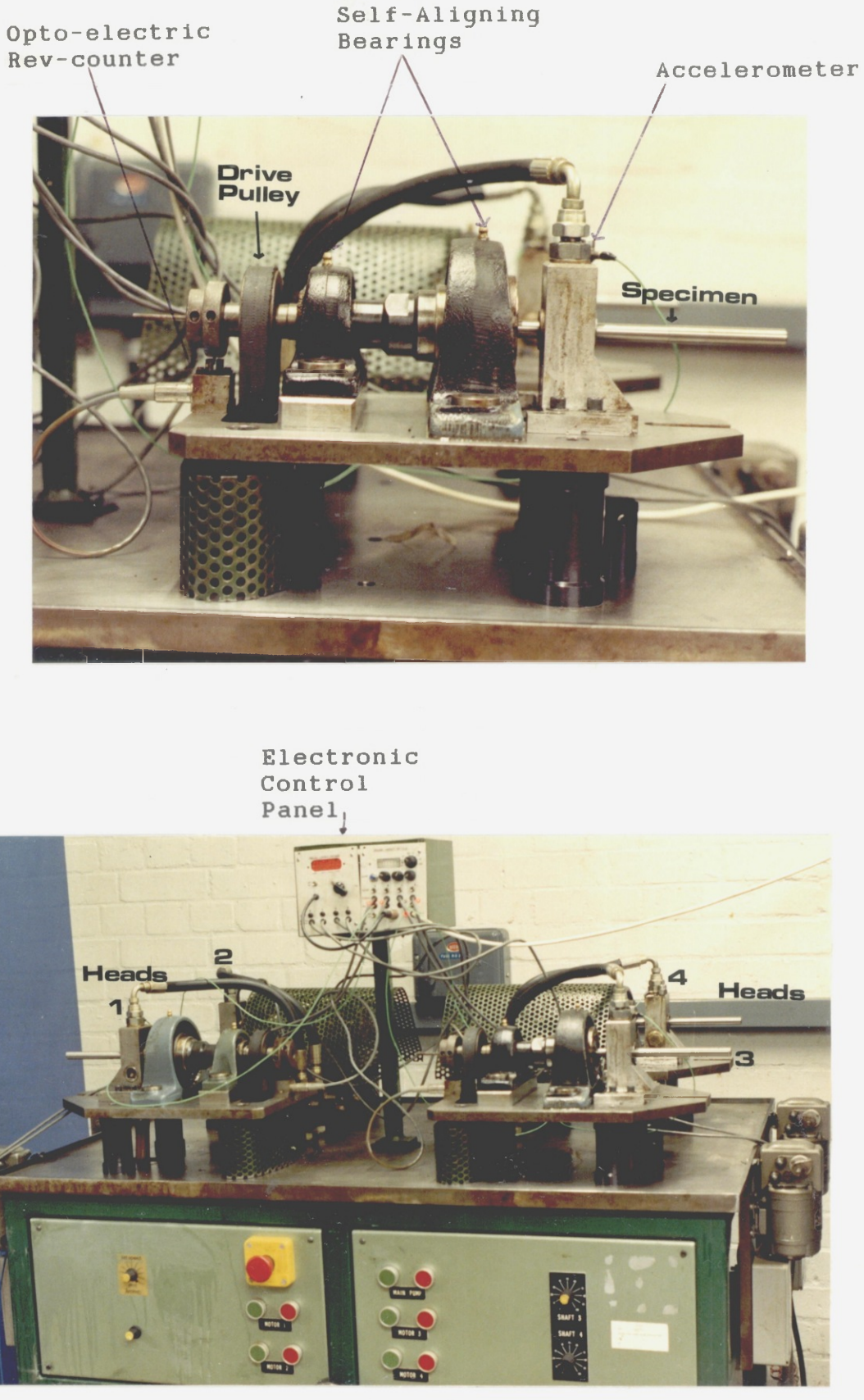

Figure 5.2

Part of the four-head test rig

a flow smoother and pressure reducing valve, which was set out so as to minimally restrict flow and only slightly reduce pressure in the system. The fluid then passed into a manifold which fed the fluid to each of the four heads. Between the pressure release valve and the manifold was a pressure gauge which gave the fluid pressure. The filtration employed in the fluid circuit was a 50 micron paper filter.

5.1.3.2 Lubricant Supply and Cooling System

The axial pump was run to give a pressure of 1800 psi (12.41 MPa) for the highly loaded runs, 1600 psi, (11.03 MPa) for the first test run and 1200 psi (8.27 MPa) for one low load run. A secondary gear pump was used, at low pressure, to drive the mixture through a heat exchanger both to maintain the temperature a 35°C and to circulate the emulsion to prevent settling or separation of the two phases. A diagram of the lubricant circulation system is shown in Figure 5.3. In the sump there was a depth switch so that if the level fell below a volume of four gallons, the pump cut-out and the head motors stopped. Also in the sump was an electric heater which, in conjunction with the fluid cooler, maintained the bulk lubricant temperature at the required 35°C.

5.1.3.3 Bar Locating and Driving System

Each head was driven by a single-phase motor through a pulley to the back of the head. Behind the pulley was a flagged wheel which passed through an opto-electrical detector to register a signal one for each shaft revolution. A control box counted the number of revolutions and displayed this based on tens of thousands of revolutions, on a four digit display. The bearing steel bar specimens were fitted with a locating rod of 2BA steel studding which was fed through the centre of the chuck. A specimen was held in place and the larger of the two wheels was then tightened up aginst the back of the holder until the specimen was firmly held. The smaller of the wheels was then tightened up against the first to lock the specimen in position finally, the locating bar was tightened up against the end of the specimen holder with two small nuts.

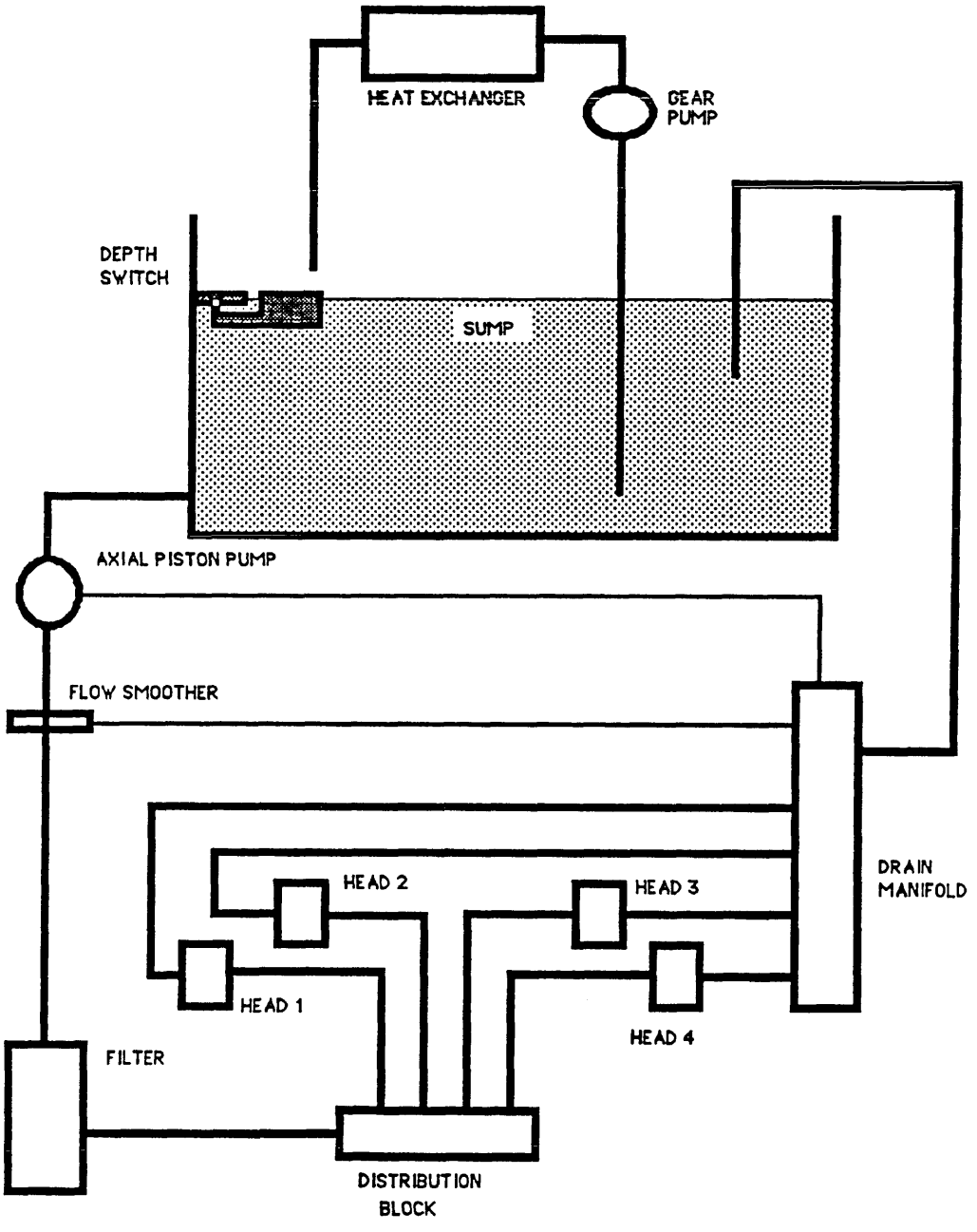

Figure 5.3

Lubricant system of the four-head rig

If the specimen was not tightened up properly in the collett, then it rotated and fractured due to fretting fatigue. this happened very early in the study in the first and second test runs. As a result of this the collett was modified to prevent this fretting taking place in the zone where the bar specimen emerges from the collett.

5.1.3.4 Ball Holder

Once the sample was tight in the head, the ball was loaded into the top of the head and allowed to drop onto the sample. There was a small clearance (less than 0.04mm) between the ball and the bush that when it was located it allowed the passage of lubricant over the sample bar.

The loading of the ball against the sample bar caused it to rotate at the same speed. Provided that the ball was free to rotate in the end of the bush, then a pure rolling contact is obtained. Before each test this free movement and the clearance was checked as well as the ball to ensure its free rotation.

5.1.3.5 Failure Detection System

Underneath the sample bar on the head outlet was a magnet to attract ferrous debris and filter it out of the system. After every failed test run the magnet was cleaned and the ferrous debris removed. An accelerometer cut-out connected to the head motor was fitted to every head. The ball and specimen were loaded up, the fluid was turned on to load the specimen up slightly and then the motor was started and the fluid turned on to full pressure. Once the motor was running satisfactorily, the motor cut-out was switched to running and the level was set to cut-out at a rise in vibration to a level of about 8dB, but varying slightly from head to head depending on the background noise and the fluid in use. When the vibration reaches the cut-out level, the head was stopped automatically. The sample was examined for signs of failure. If no failure was found then the head was restarted but if pitting had occurred, then the sample was removed, the reading on the cycle counter was noted down and the life of the sample calculated.

One single test sequence was carried out using combined bending stress (Figure 5.4), in consequence of an earlier study on rolling contact fatigue by Dousinas (25). However, this first sequence showed that the benefit of shorter life obtainable by the application of combined stress was outweighed by the complications incurred in applying external stress. This is further discussed in sections 6.1 and 7.1.

5.1.4 Controlling the Variables of the Test Method

The first two set results from the test rig were used to establish the method and standardise the operation of the rig. The outcome and the consequences of the two results are given in Section 6.1. In order to control scatter of the results, the variables of the test had to be controlled as tightly as possible. The method by which the variables were controlled is described below.

The first two runs were performed on two different batches of specimens but then a large number of ball bearings and a large batch of specimens were ordered so as to limit the materials variables. The main variables in rolling contact fatigue as listed in Section 2.4, are the lubricant, the steel, the load, the speed and the temperature. By using identical conditions and specimens from the sample batch, the five main variables are maintained constant. As the main variables are held constant, the minor variables become important. The surface finish and the hardness of the balls are very important but they were closely controlled. The water content of the lubricant was monitored and controlled. The water content of the test fluid was measured daily at the initial stage of using the test rig and then at regular intervals once the behaviour of the fluid had been established. The water content was measured by means of Karl Fischer titrimetry (72). Typical variation was 3 to 4% loss of water per week for Aquacent Light when three heads were running together. The operation of this equipment is described in Appendix 5. The eleven

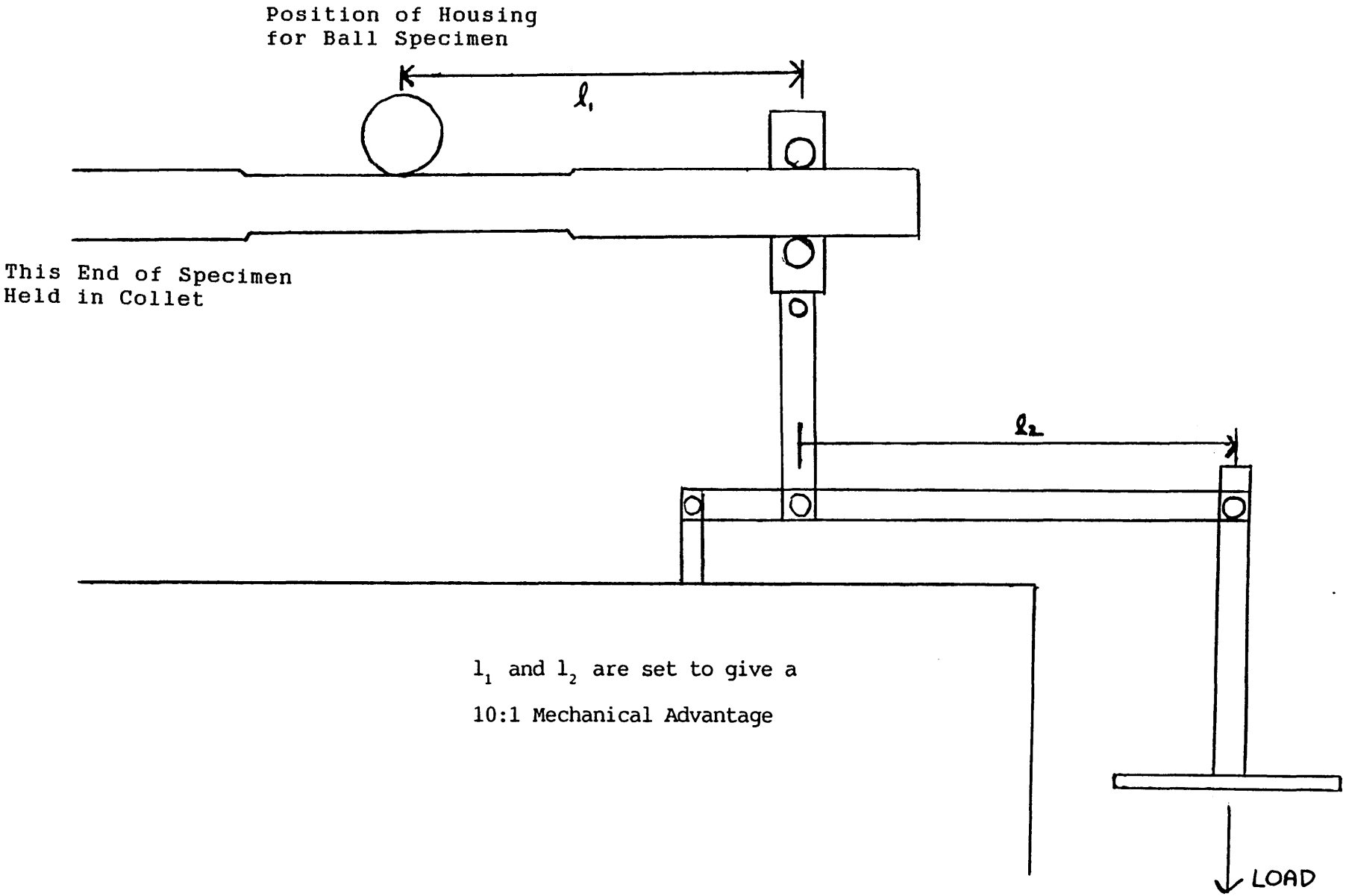

Figure 5.4
Application of Bending Stress

variables listed in Table 2.4 were considered important in rolling contact fatigue with the above restrictions operating, and all were controlled for the same lubricant within on test series.

One possible shortcoming covering the control of variables involves the presence of chemically reactive lubricant additives. During a test, as leaks and spillages of the lubricant occurred, so more fluid was periodically added. Reactive additives may be consumed during a test however, so concentrations may have fluctuated in an irregular fashion. There was no easy method of measuring additive content and so it was assumed that there was always sufficient additive available in the lubricant to give a constant performance level. The role and amounts present of additives is further discussed in Chapter 7.

For different lubricants under the same load conditions, the only variance from identical conditions was the lubricant and for different loads with the same lubricant the only variant was the load .

Other possible external factors such as surface scratches and other blemishes were screened, as far as possible, by the careful examination of the specimens under a microscope and the proper removal of packing grease with toluene and acetone prior to loading up.

The effect of the control of the variables on the method and its repeatability and reliability is discussed in Chapter 7.

5.1.5 Comparison of the Test Method in the IP 300 and IP 305

The rolling four-ball (IP 300) and the Unisteel (IP 305) fatigue test rigs were described in Section 4. The main differences between the methods are the test pieces used and the contact severity.

The dynamic capacities of the rolling four-ball and the Unisteel are obtained from Eastaugh (117) and Penfold (45), and from March (66). The value of the dynamic capacity for the four head rig has been calculated from first principles using the formulae of Harris, (26), and is described in full in Appendix 6. The values of the dynamic capacities, the normal levels and the C/P ratios are compared in Table 5.1.

Rig	Dynamic Capacity/N	Load/N	C/P ratio
Four-ball	2220 (45,117)	5890	0.38
Unisteel	5710 (66)	3340	1.71
Four head	2043	1570	1.30

Table 5.1

Comparison of load, dynamic capacity and C/P ratio for the three rigs

As can be seen from Table 5.1, the value of the C/P ratio for the four head rig is more realistic than that of the four ball and slightly less than that of the Unisteel.

Some idea of the implications of this C/P ratio on life can be obtained as follows.

If the load life equation for mineral oil is used (eq 5.2)

$$L_{10} = (C/P)^3 \times 10^6 \text{ cycles} \qquad \text{Eq. 5.2}$$

the theoretical L_{10} and L_{50} fatigue lives for the three rigs can be compared.

The approximation of the ratio of L_{10} to L_{50} fatigue lives, equation 5.3 is used.

$$L_{50} \simeq 3L_{10} \qquad \text{Eq. 5.3 (66)}$$

Predicted life values are given below in millions of cycles in Table 5.2.

Rig	Four-ball	Unisteel	Four head
Theoretical			
L_{10} lives	0.055	5.0	2.2
L_{50} lives	0.165	15.00	6.6

Table 5.2

Predicted Life Values from Theory

The difference in theoretical testing times for mineral oils can be clearly seen from the above table and demonstrates the thinking behind this new test method.

Results obtained on the four-head fatigue rig are outlined in Sections 6.1.1 through to 6.1.3.

5.2 ADMIRALTY OIL LABORATORY (AOL) VERTICAL FATIGUE RIG

In the current study, this rig was used to generate a selection of failed raceways which were sectioned and used for scanning electron microscope (SEM), Infra-Red Spectroscopy (IR) and Secondary Ion Mass Spectroscopy (SIMS). The reasons behind this use of the rig for qualitative work rather than quantitative fatigue studies is described later in the following sections.

5.2.1 Development of the Rig

This rig was introduced by Penfold (45), in 1972 as an alternative to the rolling four ball and Unisteel fatigue test rigs. The basic design of the rig is the same as the rolling four-ball rig but the balls are replaced by a small commercial thrust race assembly (Figure 5.5). The assembly consists of a 29 mm diameter shallow grooved upper raceway, a ball holder containing eleven 6.35 mm diameter steel balls and a 30 mm diameter shallow grooved lower raceway. The loading mechanism is by a series of pivoted bars and a dead weight which can be hung in various alternative positions to vary the amount of force on the raceway. As the testing is not an IP Standard method, the load is varied to suit the lubricating performance of the fluids on test.

According to Penfold (45), Onions (109) and Eastaugh and Ritchie (46), the AOL rig offered several advantages over the other two test machines. The varying of the load and thus the C/P ratio is an important advantage. Under the loads recommended by Penfold, the C/P ratio is midway between the rolling four-ball and the Unisteel rig, and as with the four head rig, offers results more realistic than four-ball results but in a shorter time than the Unisteel rig.

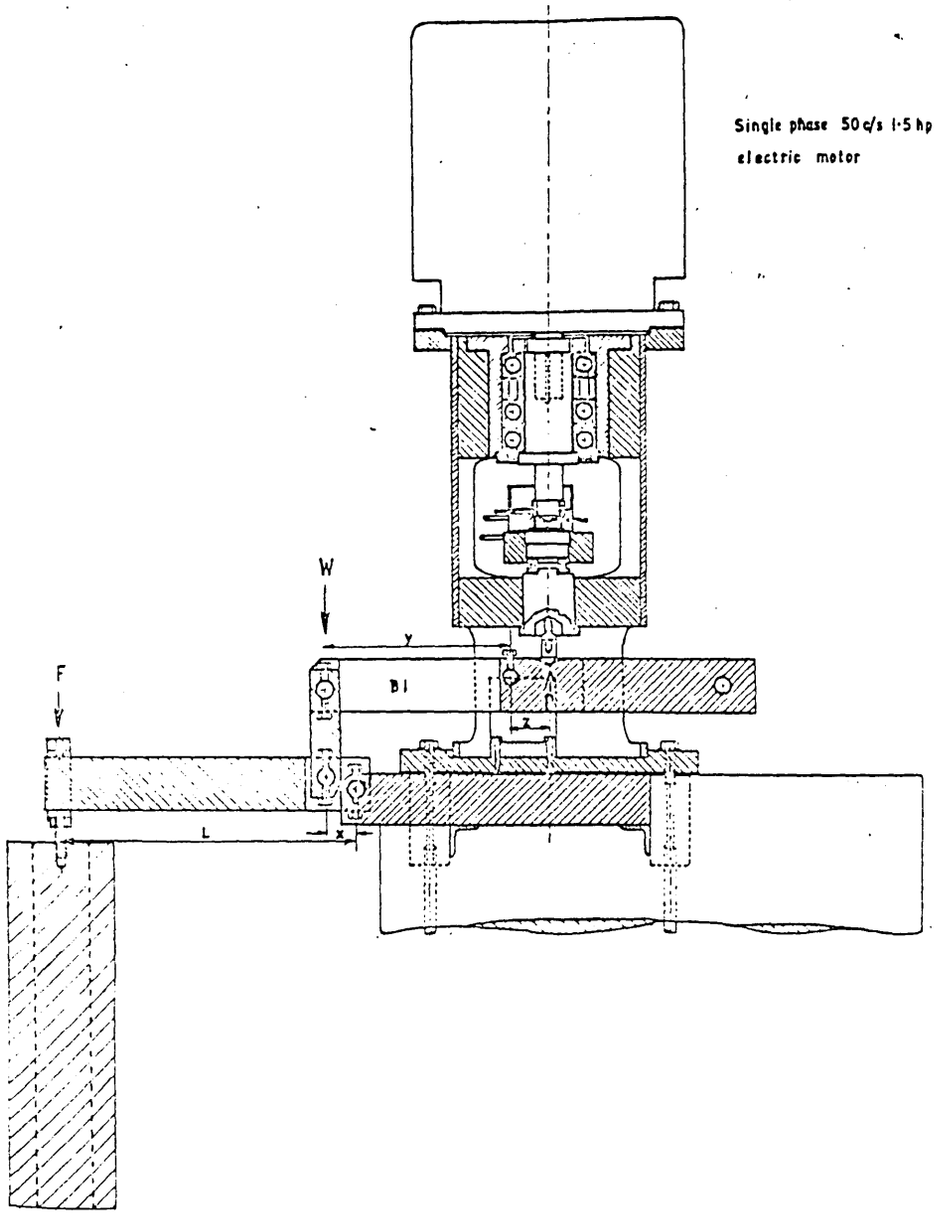

Figure 5.5

The AOL Vertical Fatigue Test Rig

5.2.2 Rig Modifications

The rig used in this study was provided by the AOL along with a large batch of specimens. As it had not been used for some time and some of the parts of the rig were missing, a considerable amount of time was spent preparing the machine for operation. The loading mechanism was remade from drawings and a new loading thrust race fitted. The rig was commissioned using Century 'Aquacent Light' as the test fluid. Initially, fluid was added to the chamber by syringe with the upper outlet sealed with PTFE tape and the chamber was filled at hourly intervals. This method did not, however, allow the system to be run overnight. A gravity feed system using two beakers was then devised (as shown in Figure 5.6) which provided a flow rate of about 1 dm^3 per 12 hour period. A magnet was glued into the side of the lower beaker where the outlet was positioned so as to filter out any ferrous debris from the system.

This system worked satisfactorily for the moderately viscous 'Aquacent Light' but proved to be ineffective for the low viscosity dilute emulsion used. This was because the fluid either drained extremely rapidly from the chamber or flowed too rapidly in and flooded over the top of the chamber. For the dilute emulsion, a beaker was used as a sump and the fluid was pumped from there using a peristaltic pump into the test chamber whence it flowed back into the sump under gravity, as shown in Figure 5.7. This system also proved satisfactory when an aqueous glycol was used as the test fluid. With polymer- thickened fluid, this system did not work. The high viscosity of the fluid resulted in low flow rates out of the chamber outpipe which led to overflow and total loss of the fluid from the sump in a very short time. Another problem with the polymer-thickened fluid was that when the chamber reached its normal operating temperature of about 35°C, the water evaporated off and a thick

residue was left, which on cooling, set solid. As a result of this, the supply method employed was to fill up the chamber with fluid using the peristaltic pump, switch off the pump and then allow the chamber to drain under gravity. This meant that only daytime hour running was possible. Only two completed tests were carried out using this fluid. Two tests were also carried out with the lubrication system disconnected and no fluid used.

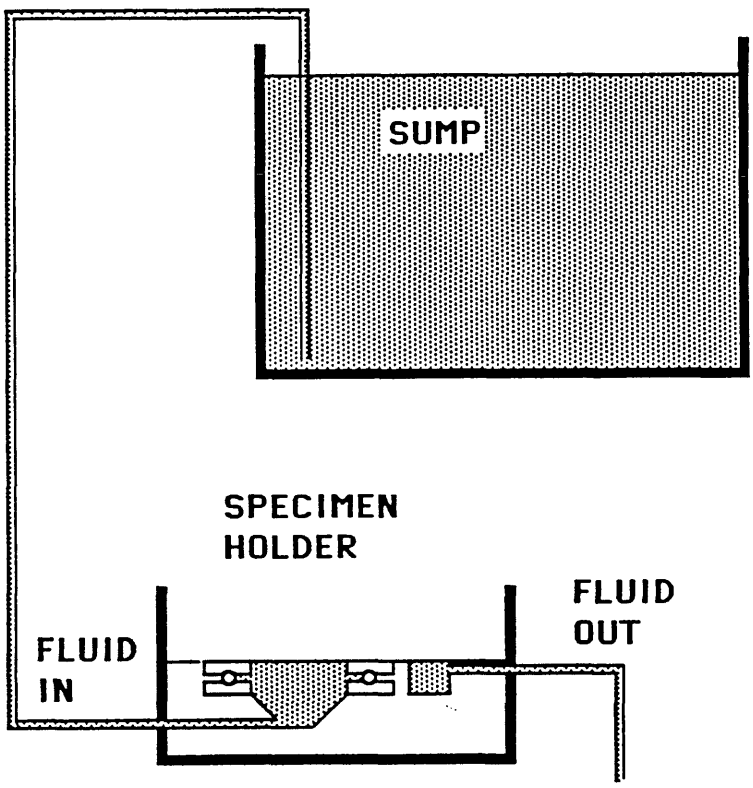

Figure 5.6

AOL Gravity Feed System

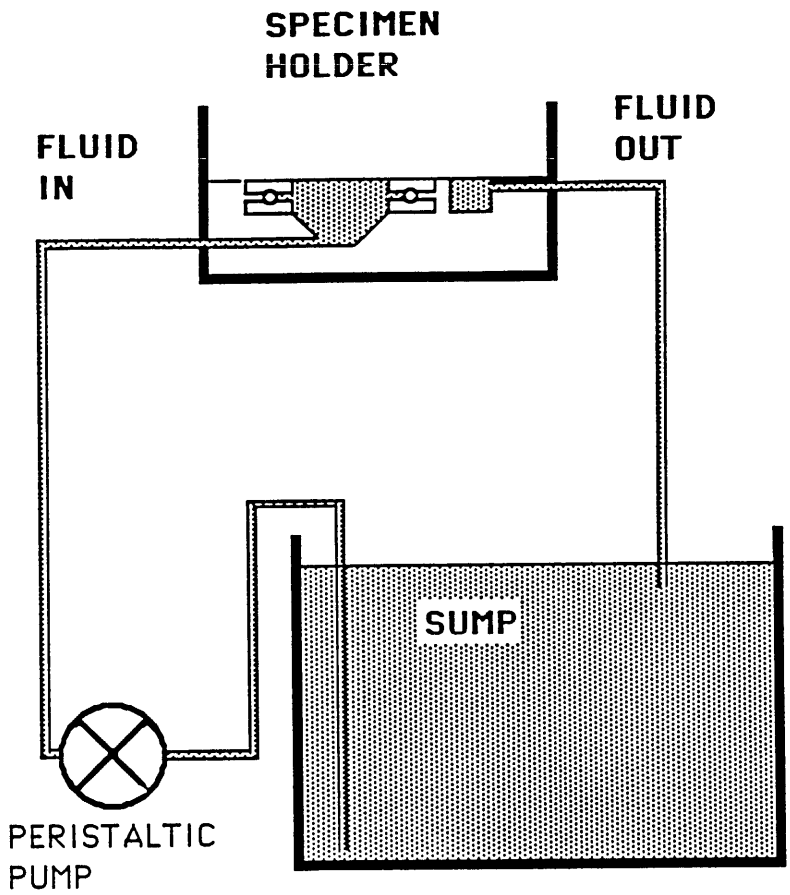

Figure 5.7

AOL Pump System

5.2.3 Operational Details

A communication by Hopkinson (116), concerning the operation of the rig, suggested that large numbers of cage failures would occur during rig operation especially with low viscosity fluids. As a result of this, it was decided not to use the rig for statistical fatigue work, but instead simply to use it to produce failed specimens for examination by various test methods as described in Section 5.2 . Before commencement of a test the chamber was removed, wiped and then ultrasonically cleaned in a 50:50 mixture of chloroform and methanol. The chamber was then dried, reassembled and flushed with the test fluid. The race specimens were coated in a packing grease which was difficult to remove and the following procedure was adopted for cleaning the specimens, as shown in Table 5.3.

Stage	Cleaning Process
1	Wipe off excess grease with cloth
2	Ultrasonically clean in chloroform and methanol
3	Dry with cloth
4	Examine under microscope for traces of grease

Table 5.3

Stages used for cleaning AOL specimens

This cycle was repeated until no grease could be detected. Normally two cycles were required. Once cleaned, the specimens were loaded into the chamber and covered with the test fluid using a small syringe, or if the pump were connected, using the pump. The upper race and the lower loading/vibration plate were positioned. Slack in the lever loading system was taken up by pressing gently onto the end of the loading level whilst ensuring that the bearings and housing were in the correct position. Once lightly loaded, the pump and motor were started. If the raceway assembly were fully loaded before the motor was switched on, the motor stalled and bruising of the raceways took place. Once the motor had reached full speed, the dead weight was lifted into position and the fluid flow checked. An accelerometer cut-out control was built for the rig but, due to problems with the power supply, it was never employed. As a result of this, failure examination was by trial and error based on the number of cycles completed. The tests were run until pitting or micropitting of either of the two raceway surfaces had taken place or the test was stopped at the end of a day and upon examination, was found to have pitted. Cage failures were a common problem and if this occurred or the test prematurely stopped for other reasons, then the test was disregarded. The large number of cage failures occurred confirmed the advice of Hopkinson (116), in this respect.

Another problem with the rig was that no revolution counter was attached and so the time to failure could only be estimated from the running speed which appeared to depend on the amount of load applied since, at low levels, speeds slightly above 1450 rpm were recorded. However, this was considered to be adequate for life estimation. The results from this rig are further discussed in Section 6.2.

5.3 ROTATING-BENDING FATIGUE TEST RIG

In section 4.8.2, the rotating-bending fatigue test rig was introduced as a method of fatigue testing without lubricated rolling contact. The origins of the test method, the differences between the rubbing and the rotating-bending test methods and the types of results are outlined in the following sections.

5.3.1 Origins of the Test Method

Galvin and Naylor, (113), used a rotating-bending fatigue rig to discriminate between the effects of contact and those of environment in 1964. They then reviewed the work of others in the rolling contact fatigue field (5), (7), (8), and concluded that lubricant viscosity had a major effect on the premature failure of bearing steels. Galvin and Naylor (113), tested a series of lubricants of different viscosities and types and also a water glycol. An inert medicinal white oil (MWO) was employed to investigate the effects of various additives on the fatigue limit.

The apparatus used was a 'Wohler type' rotating bending device and is shown in Figure 5.8.

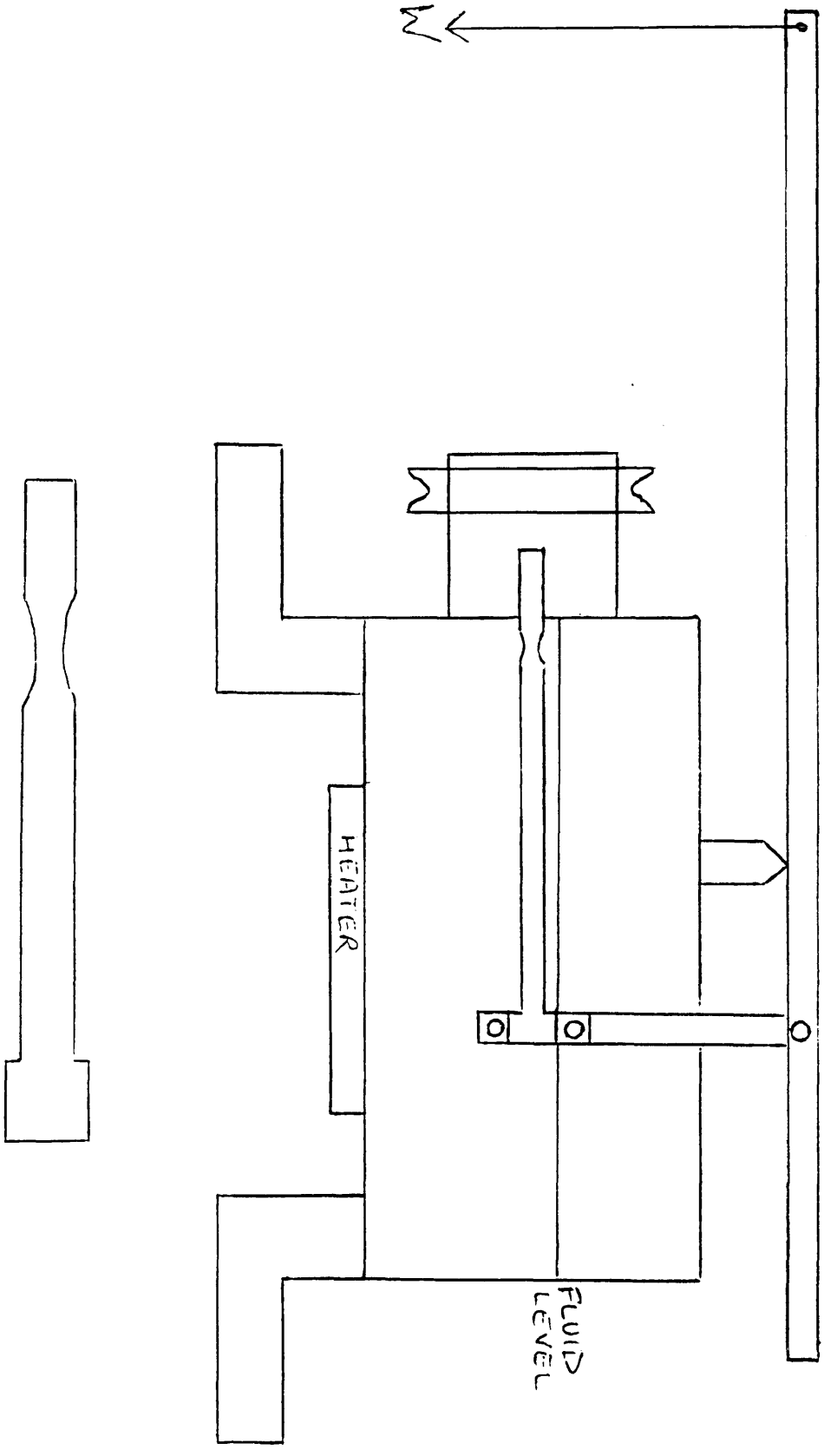

Figure 5.8

Wöhler type Rotating-Bending Fatigue Rig and Specimen

The type of steel employed was a 3% nickel steel made to specification EN33 with an hourglass test area area as shown in Figure 5.9.

The test conditions employed by Galvin and Naylor (113) were 1560 rpm and 70°C and they obtained the fatigue limits given in Table 5.4. From Table 5.4 it can be seen that no differences were detected between the three mineral oils and the medicinal white oil but in all cases the presence of additives lower the fatigue limit.

Fluid	Fatigue limit/MPa
High VI MO	275
Medium VI MO	275
Low VI MO	275
Medicinal White Oil (MWO)	275
Castor oil	240
di-2-ethylhexyl sebacate in MWO	265
Amyl phosphate in MWO	270
Silicone fluid	255
Water glycol	245

Table 5.4

The fatigue limits for a variety of media (113)

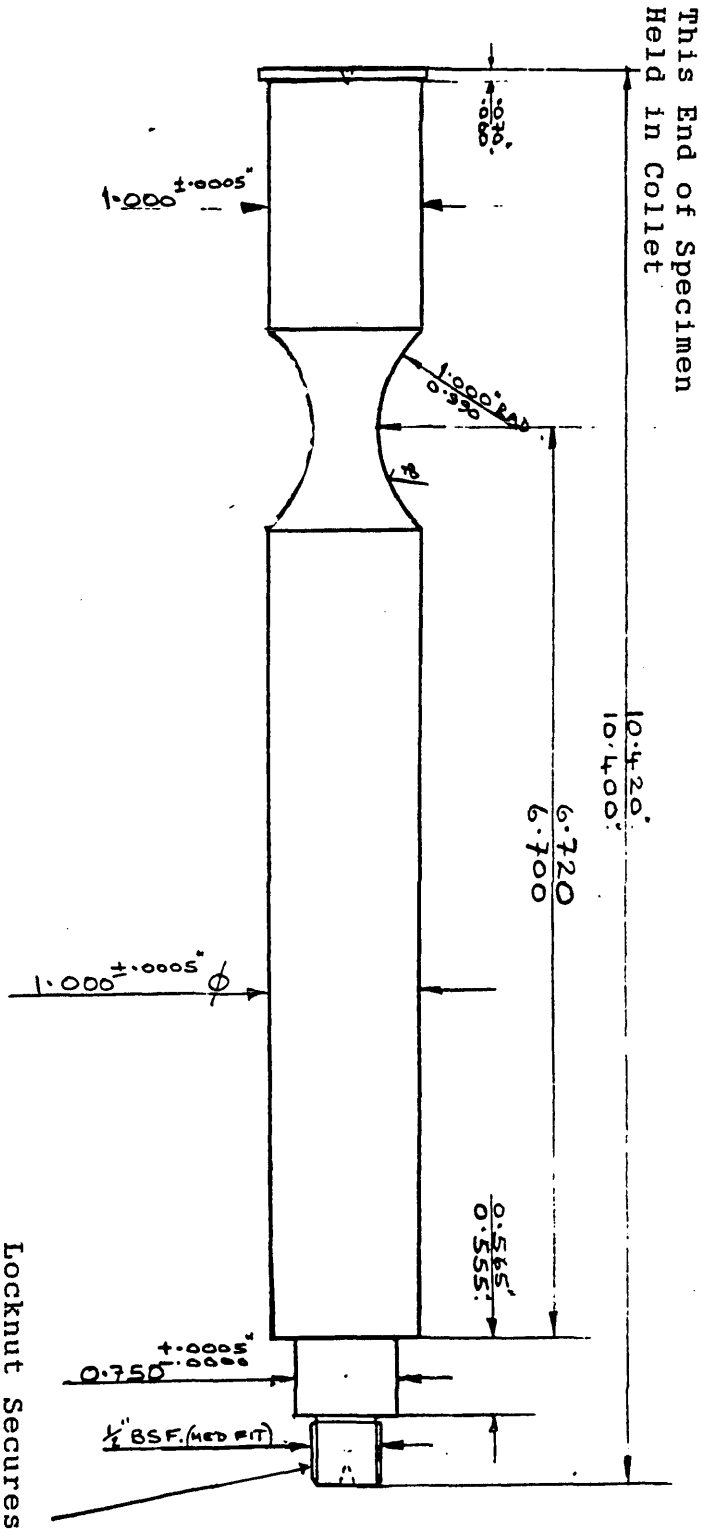

Figure 5.9

Hourglass Rotating-Bending Specimen

Galvin and Naylor also looked at the effects of dry and wet air on the fatigue limit and compared them to that of the medicinal white oil (Table 5.5).

Fluid/media	Fatigue limit/MPa
Medicinal White Oil	275
Dry air	275
Moist air	265

Table 5.5

Rotating-Bending results for wet and dry media (113)

When these results are compared with that of the water glycol, fatigue limit 245 MPa, clear differences can be seen in the effects of the water.

Galvin and Naylor (113), reported no visible evidence of corrosion or corrosion fatigue on the specimens run in water-containing media. Between 1964 and 1974 little work was published using this type of approach but Polk and co-workers (16), noting an upsurge in the use of fracture mechanic techniques, revised the method of Galvin and Naylor (113), and Eisenstadt and Fuller (118), to calculate crack propagation rates for bearing steels in a variety of media (see next section). The results of Eisenstadt and Fuller and the techniques of Polk and co-workers (16), will be outlined in section 5.3.2.

Various Soviet workers, following up the work of Rebinder (99), also used classical rotating-bending fatigue rigs to study lubricant-steel interactions.

In Section 3.1, the work of Stepurenko and co-workers (44), (102), and Lobioko and co-workers (100), (101), was briefly mentioned. Both groups of workers used dissolved and free water in mineral oils and other media in an attempt to respectively prove and disprove the Rebinder effect (99). All results tied in with the work of Galvin and Naylor (113), in that, with different mineral oils, very little difference between fatigue limits was observed. The most dramatic effect was with large amounts of free water present, (up to 5% by weight), where no fatigue limit at all was obtained. Stepurenko (47), suggested that the lack of a fatigue limit was caused by corrosion in the stressed region and the formation of rusted patches in the hourglass portion of the specimen. This tied in with the work of Harris (119), who reported that water caused the corrosion of the longer-lived specimens, Figure 5.10. Differences in the behaviour of notched and pre-cracked specimens were reported by Lubioko and co-workers (101), but no explanation of the significance of this was reported.

Stepurenko and co-workers (102), also investigated the effects of surface structure on fatigue, the results of which are shown in Table 5.6.

Steel State	Fatigue limit in MPa				
	Air	MO	Mineral Oil MO+1% H_2O	H_2O	H_2O+MEA
Pearlite-ferrite	290	300	245	-	-
Sorbite	380	385	315	280	385
Troosite	640	640	425	-	-
Martensite	770	725	120	185	660

Effect of Surface Structure on Fatigue Limit in Various Media (102)

Table 5.6

MEA ≡ Monoethanolamine (IUPAC name 2-aminoethanol)

In Table 5.6, the deleterious effect of water can be clearly seen. This table illustrates clearly the usefulness of the rotating-bending test method in differentiating between the fatigue effects of steels and water containing media.

5.3.2 The Interrupted Stressing Technique

In 1970 Eisenstadt and Fuller (118), constructed a new type of rotating-bending fatigue rig, which utilised small test pieces. Specimens used in traditional rotating-bending fatigue rigs were as shown in Figure 5.9.

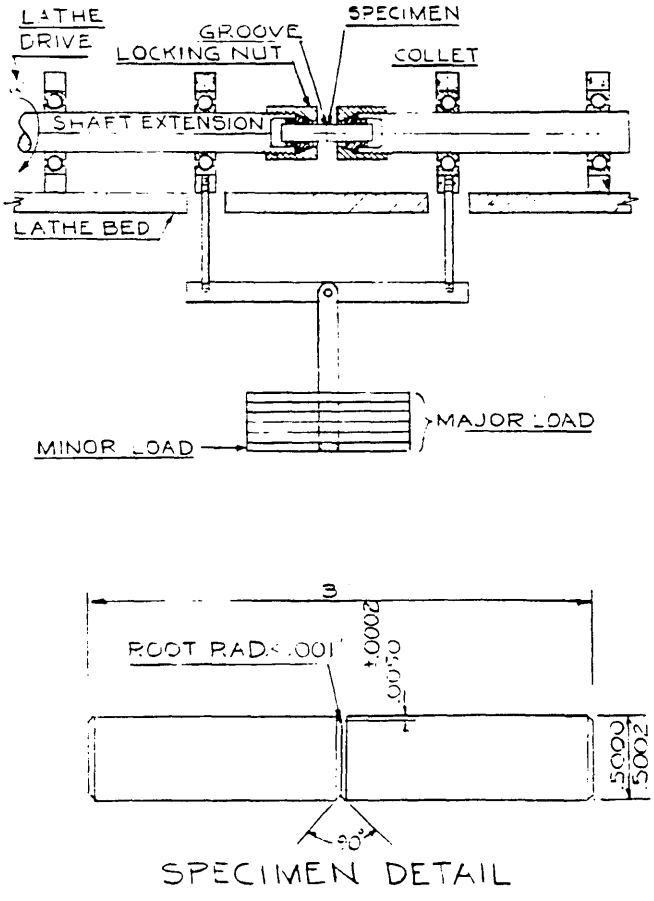

Figure 5.10

Rotating-Bending Rig of Eisenstadt and Fuller (118)

The ones used by Eisenstadt and Fuller (118), were only 76 mm long by 12.7 mm diameter, with a 90° circumferential notch ring round the centre of the specimen. This specimen was held on both ends in collets and mounted on a lathe bed with weights cantilevered onto the specimen. This is shown in Figure 5.10.

Eisenstadt and Fuller (118), also devised a novel method of measuring crack growth rates in their rotating-bending fatigue rig by using an "interrupted stressing" technique. The technique consisted of a high level stress for a short time followed by a low stress for a longer period. The higher level stressing caused rapid crack growth whilst the lower level stressing caused slow crack growth.

The two conditions were alternated until the specimen fractured. This gave the fractured specimen a ringed fracture face with the different stress levels giving a slightly different appearance. An example is given in Figure 6.29. These bands were measured with an optical microscope and from these measurements, the crack propagation rate calculated. Stress intensity factors for the specimens were calculated using the method of Neuber (120), Harris (121), and of Paris (13), and are given in Appendix 8.

One problem with the technique is that of achieving sensible and reliable fatigue initiation. This problem was overcome by the use of pre-cracked specimens. The pre-cracking was performed on the specimens at the root of the notch, so that the cracking propagated in the correct plane. The duration of the loading cycles is given below in Table 5.7.

% of Expected Life	No. of Cycles	% of Max Loading
30	12,000	100%
40	15,000	23%
50	24,000	100%
55	25,000	23%
65	25,000	100%
70	20,000	24%
72.5		
75		
↓		
Fracture		

Table 5.7

Loading cycles for interrupted stressing technique (118)

The narrow dark bands are the points of low stress, low order growth rate and the wider lighter bands are regions of high stress, high crack propagation rate. From the measurement of band widths and the calculated stress intensities, rates of crack propagation can be calculated for the bands. In Section 2.2.4.2, the Paris law of crack growth, eq. 2.1, was introduced. The two materials constants used in these equations, C and m, are calculated using the data obtained from the band widths. The crack propagation rates are also calculated from the band widths and the number of cycles.

This technique of Eisenstadt and Fuller (118), proved to be very satisfactory for measuring crack propagation data of steels in air but was not suited to using oil or fire resistant fluids as the medium. However, Polk and co-workers (16), developed the interrupted stressing method for use on an orthodox rotating-bending fatigue rig. Similar circumferentially 90° notched specimens were used but these were 450 mm long instead of 76 mm. The loading schedule used by Polk and co-workers (16), is given in Table 5.8.

Load (lbs)	Cycles at High Load	Cycles at low Load	Ring No.
40	20,000		
14		250,000	1
40	5,000		
10		100,000	2
40	5,000		
10		100,000	3
40	2,000		
10		100,000	4
40	2,000		
10		100,000	5
40	2,000		
10		50,000	6
40	2,000		
10		50,000	7
40	2,000		
10		50,000	8
40	2,000		
10		50,000	9
40	2,000		
10		50,000	10
40	2,400	-	Fracture

Interrupted Stressing Technique Loading Cycles (16)

Table 5.8

From Tables 5.7 and 5.8, the main differences between the two techniques is the number of cycles run at each load level . Eisenstadt and Fuller ran approximately the same number of cycles at each load but Polk and co-workers (16), ran for very short periods of time at the high load and very long periods at the low stress level. This gave the fractured end of the specimen a very similar appearance to Figure 6.29 but the actual band spacings were slightly different. Values of stress intensity factors, crack propagation rates and materials constants m and C were again obtained. The conditions employed and crack propagation rates calculated are given in Table 5.9, for various types of oil, oil and water mixtures and emulsions as well as in distilled water and air for two levels of stress intensity factor.

Lubricant/media	Lubrication Method	Crack Propagation rate μin/cycle	
		Stress intensity factor level	
		ΔK_1=50 ksi-in$^{\frac{1}{2}}$	ΔK_1=100ksi-in$^{\frac{1}{2}}$
SAE 20 Mineral Oil	Drip	5.64	27.5
Invert Emulsion	Drip	6.16	38.0
Air	Drip	12.4	78.9
Distilled Water	Drip	15.7	232
SAE 20 Mineral Oil	Immersion	7.17	40.3
Antiwear hydraulic oil	Immersion	7.27	44.4
Mineral Oil + 0.05% H_2O	Immersion	6.29	38.2
Antiwear Hydraulic oil + 0.05% H_2O	Immersion	6.93	46.1

Table 5.9

Crack Propagation Rates for Two Stress Intensity Levels and a Variety of Media (16)

In Table 5.9 it can be seen that the crack propagation rate varies by almost an order of magnitude at the higher stress intensity level for the mineral oil as compared to the distilled water under drip conditions.

Under immersion conditions, very similar rates were obtained for all four lubricants used but no explanation as to the reasons for this were given, despite the obvious differences between the mineral oil and the antiwear hydraulic oil and especially since, according to other workers (47), (119), the amount of water in the fluid has a significant effect on the fatigue limit of rotating-bending specimens. This will further be discussed in Chapter 7, as are the application of fracture mechanics techniques to study rolling contact fatigue. The validity of such test methods are also discussed there.

5.3.3 Experimental Method

As the method of studying crack propagation rates devised by Eisenstadt and Fuller (118), and modified by Polk and co-workers (16), seemed to have been tried and tested, it was decided to try to use this interrupted stressing technique.

The modified cycling plan of Polk (16), with short high loading periods followed by longer lower loading periods to give light and dark banding, was chosen as the best approach and it was decided to attempt initially to use also similar loadings and durations to Polk, followed by different cycling patterns. The actual operational details and cycle times and loads are given in the next section.

5.3.4 Rig Operation

The rotating-bending fatigue test rig used in this study was borrowed from Westland Helicopters. It accepted the traditional hourglass specimens as in Figure 5.9. The rig was fitted with an hydraulic loading system and load was measured by strain gauges attached to either side of the loading mechanism as shown in Figure 5.11.

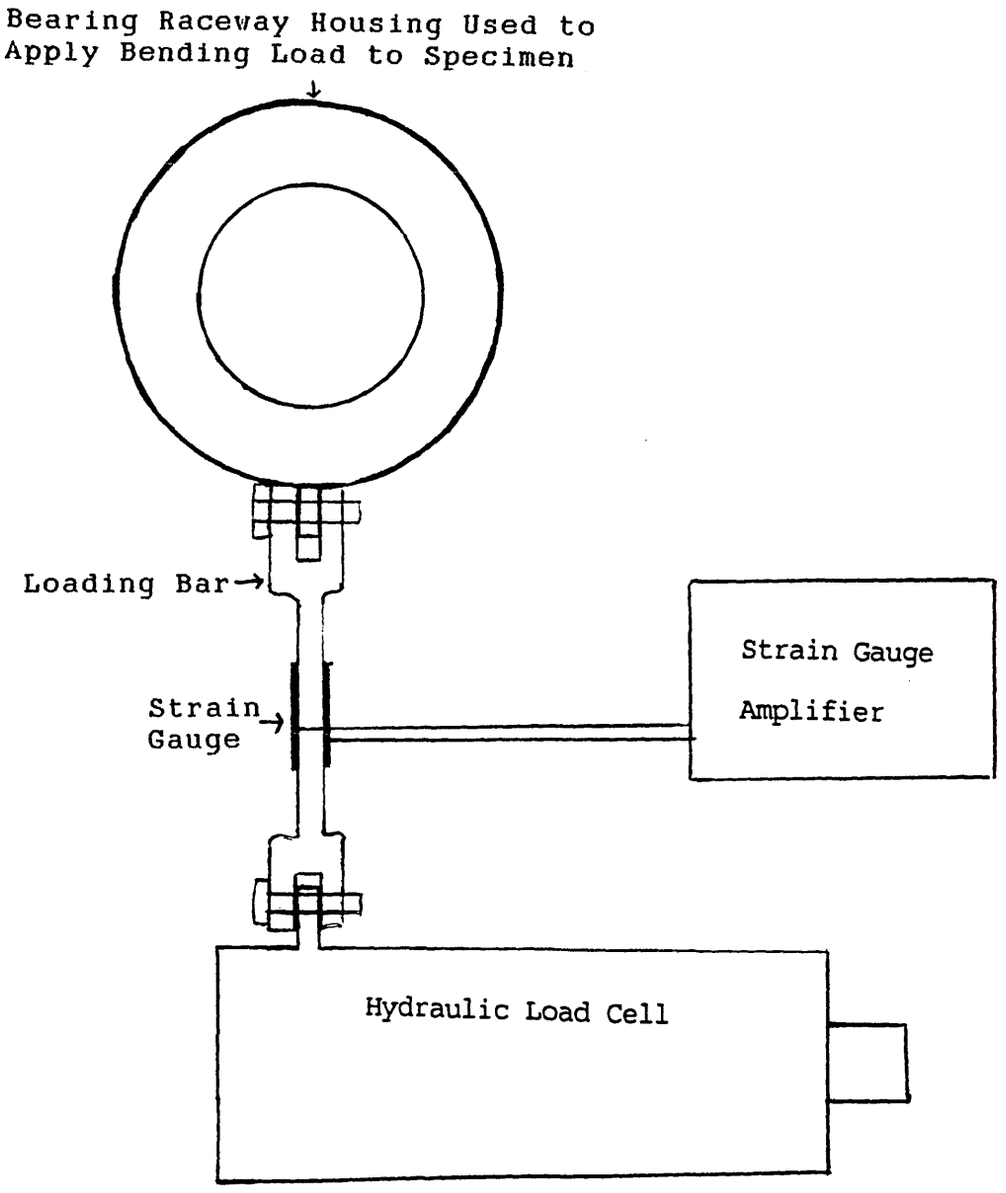

Figure 5.11

Hydraulic loading system for the rotating-bending rig

The first time an invert emulsion was run, the specimen fractured unexpectedly and the cut-out operated correctly. However, emulsion ran down the fractured end of the specimen and dissolved the protective coating on the strain gauge and the weight of the attached wires ripped the strain gauge off the tension bar.

Shortly after this the strain gauge was refitted and recalibrated but under a high loading cycle, the tension bar sheared and the test was aborted. As a result of this the rig was modified to remove the hydraulic loading system and fitted with a level dead weight loading system as in Figure 5.12.

The length of the loading arm was chosen to give a 10:1 mechanical advantage in the loading of the bar. This system appeared to work satisfactorily. A loading cycle was devised and is shown in Table 5.10.

Load Stage	Bending Moment Nmm	No. of cycles	Time @ 3000 rpm
High	Depended on Test Load used.	50,000	16 min 40 s
Low	8721	200,000	66 min 40 s
High	Depended on Test Load used.	50,000	16 min 40 s
Low	8721	200,000	66 min 40 s
↓			
Repeated until Fracture			

Table 5.10

Loading cycle for the test method

All timings were measured with a stopwatch.

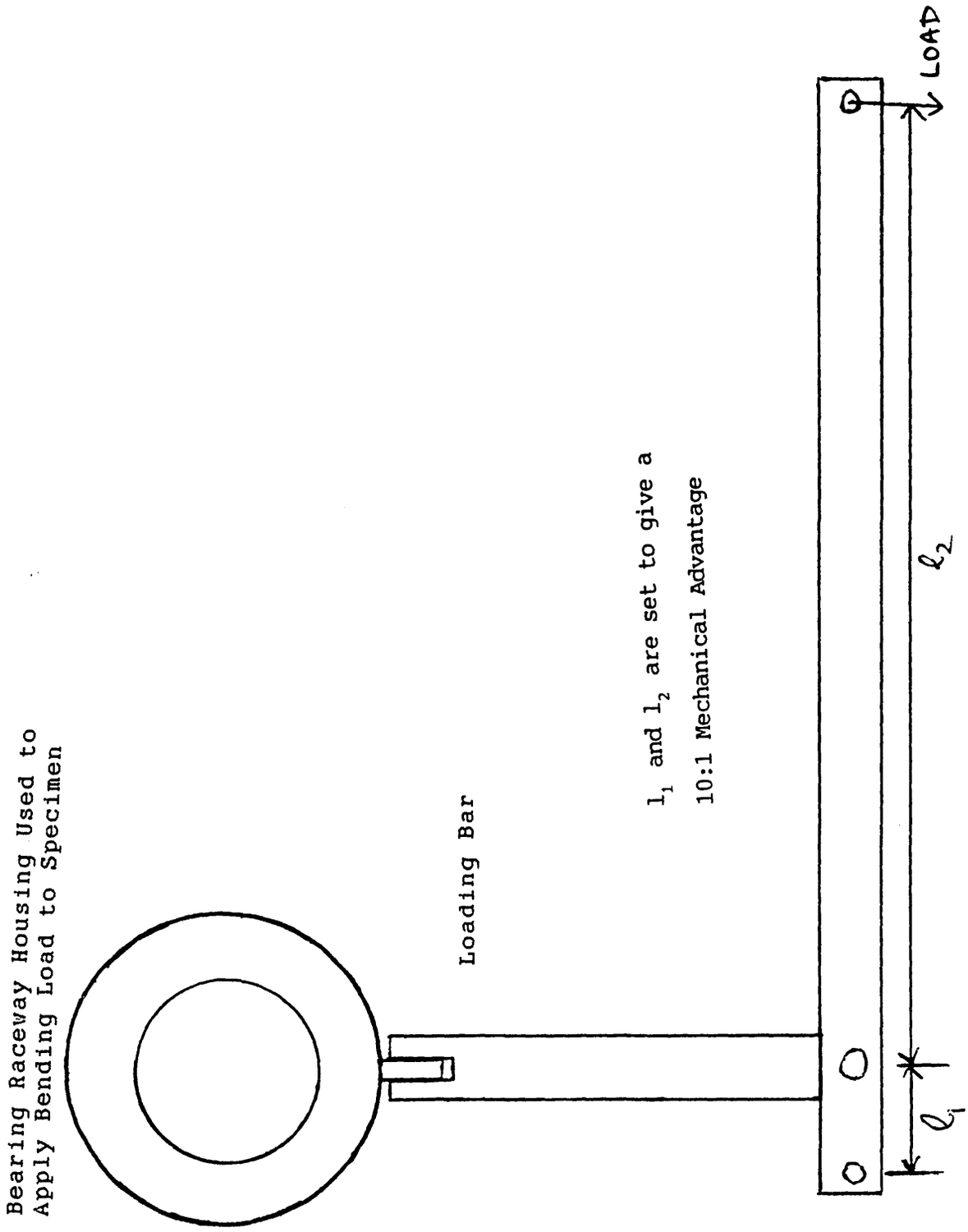

Figure 5.12

Dead weight loading mechanism for the rotating-bending rig

The problem with the loading with uninitiated specimens was extreme sensitivity to load. At high loads the specimens failed to initiate during the first period but would fracture under longer periods of initiation or under slightly higher loads. It was considered that this may have been due to variability of specimens but the specimens were from the same batch and had undergone the same treatment and processing. It was decided that the higher loads were well above the fatigue limit for the specimens and so the remaining ones from the same batch were notched using a very sharp 90°C tool to a depth of 0.010" (0.39 mm), initiated at the lower load. This method was used for some of the remaining specimens. The results obtained on this rig and data arising from those results are given in the next Chapter.

6. RESULTS

The fatigue results from each test rig are presented in this chapter. The results from the four-head rig which are described first, are divided into four sections. Firstly, initial rig commissioning or shakedown tests are described and the way that these determined final test conditions, explained. Then general results and observations found in each fatigue test series are briefly outlined to provide an overview of tests carried out. The third subsection looks at results obtained from different types of commercial test fluids. Finally results from investigative test runs into the effects of polarising potential, load and other factors along with a test series on special fluid are examined. The results for the AOL vertical and the rotating bending fatigue test rigs are contained in separate single sections.

6.1 FOUR-HEAD FATIGUE TEST RIG RESULTS

All fatigue lives for all fluids and test conditions tested lay between 1 and 86 million cycles.

In section 2.3, the statistical analysis of fatigue results was introduced. From the number of failures obtained, the median ranks were calculated as per Appendix 2. Weibull plots, as per figure 2.5, were drawn up for all ten sets of results and are shown in Figures 6.1 to 6.10. From the graphs drawn, the ten and the fifty per cent fatigue lives were measured and the Weibull slopes for the test series were calculated. The tabulated results are described and analysed in sections 6.1.2 through to 6.1.4.5 and summarised in Table 6.1. From this data the statistical significance of the results were established and different fluids were ranked in order of performance.

Series	Number of Failures	Fatigue lives/millions of cycles			Weibull slope, e
		L_{10}	L_{mean}	L_{50}	
1	11	2.3	28.0	21.0	1.39
2	15	0.73	8.2	6.4	1.42
3	12	11.5	36.0	35.0	2.99
4	13	1.35	21.0	13.0	0.82
5	14	4.5	19.5	16.5	1.45
6	11	21.0	37.0	36.5	3.41
7	14	4.3	16.5	14.3	1.57
8	13	2.35	22.5	15.5	1.00
9	15	2.4	13.5	10.8	1.25
10	15	11.2	28.0	27.0	2.14

Table 6.1

Summary of four-head Test Results

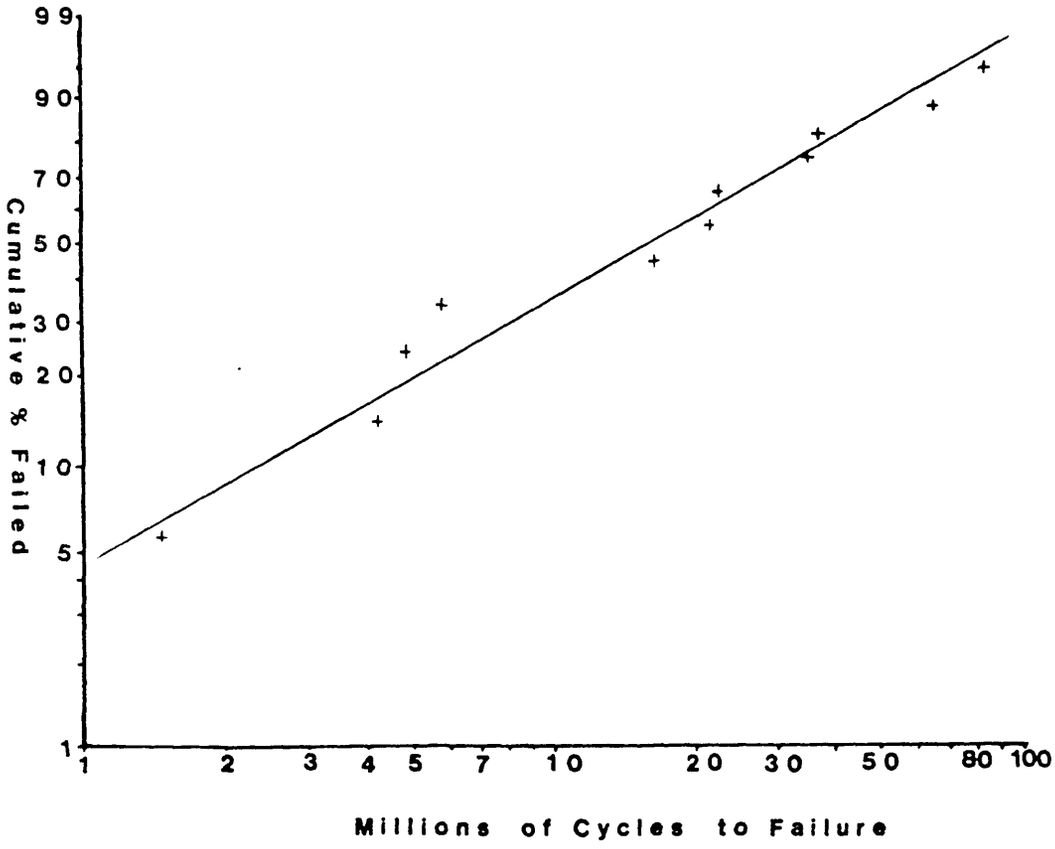

First Shakedown Run (Series 1)

Figure 6.1

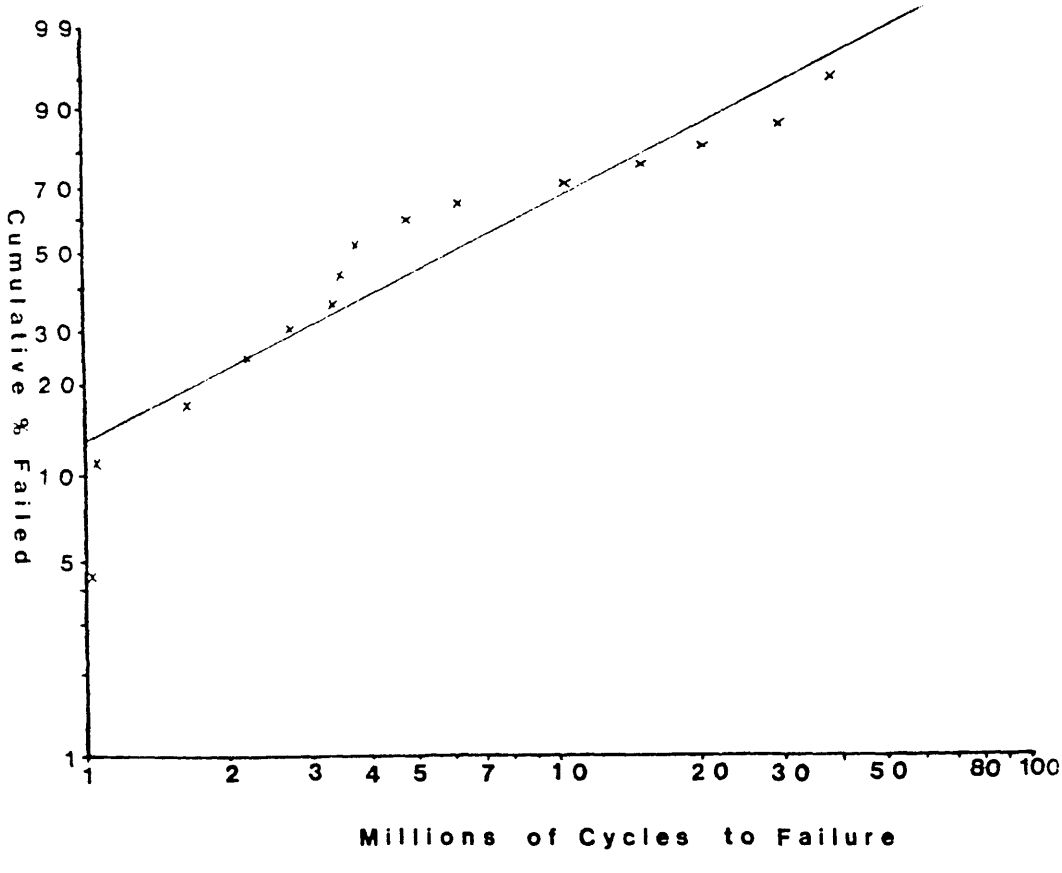

Figure 6.2

Second Shakedown Run (Series 2)

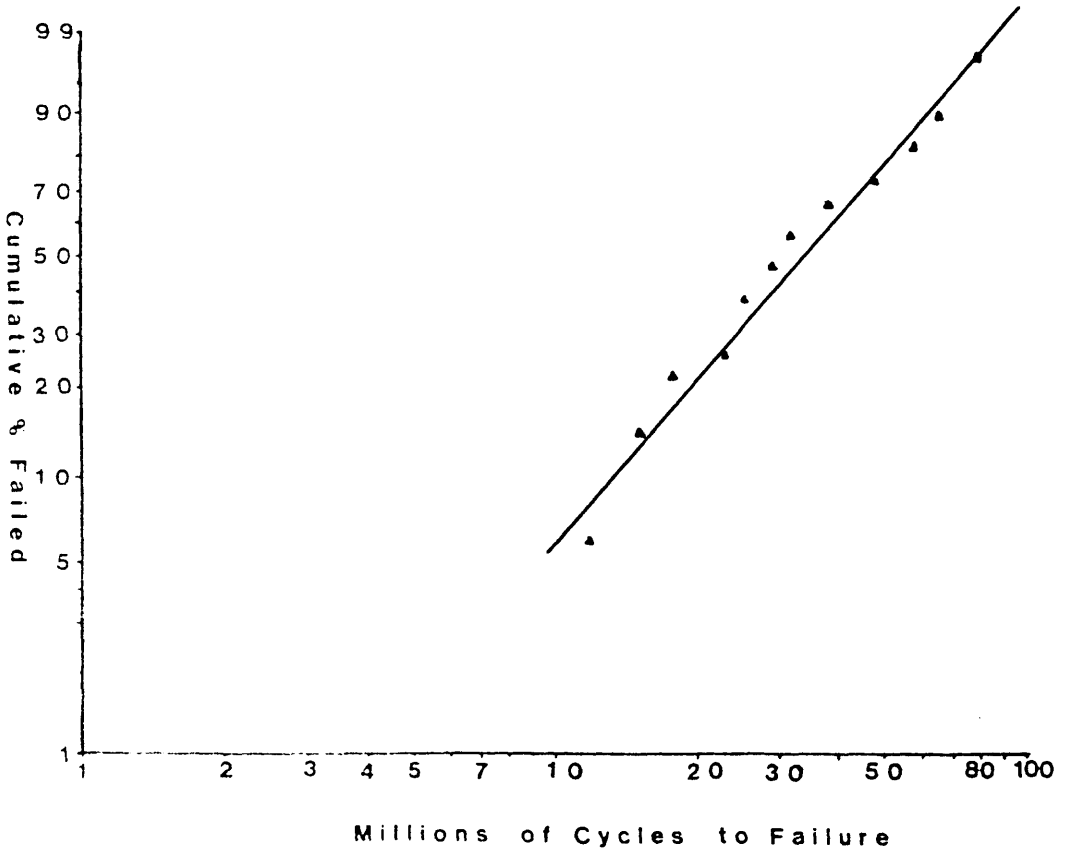

"Aquacent Light" (Series 3)

Figure 6.3

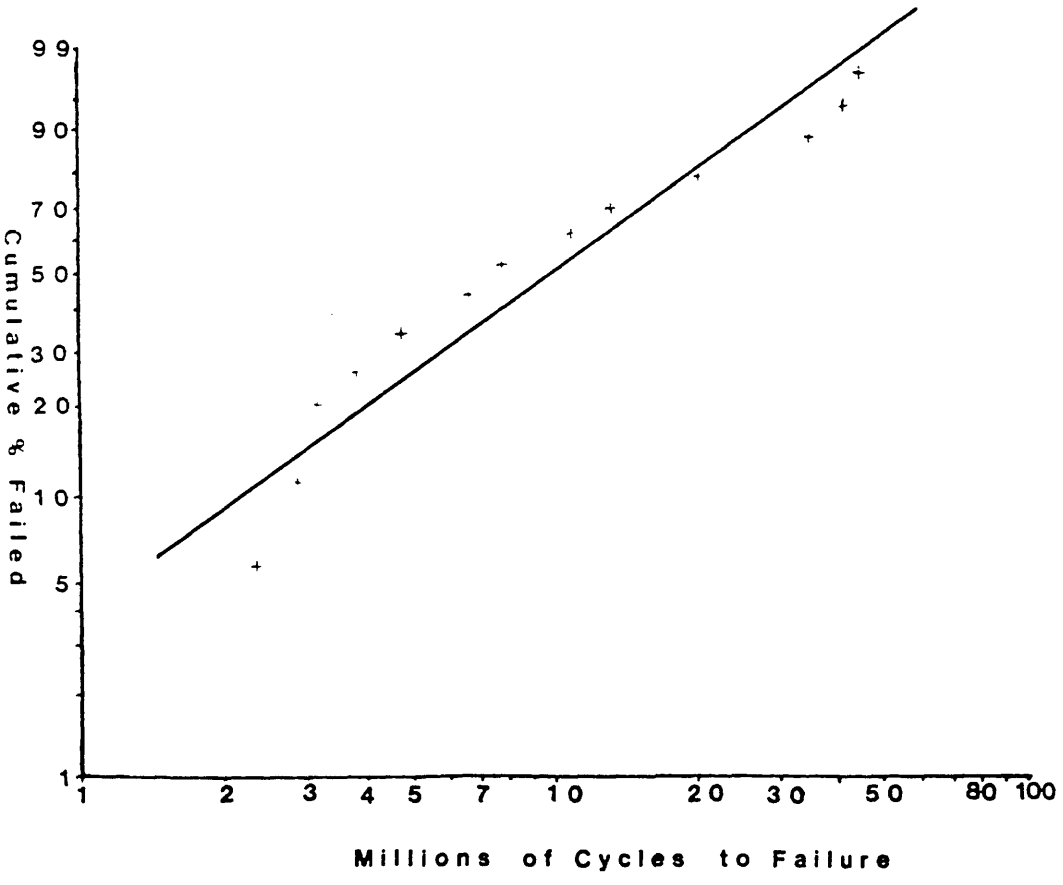

Figure 6.4

Dilute Emulsion (Series 4)

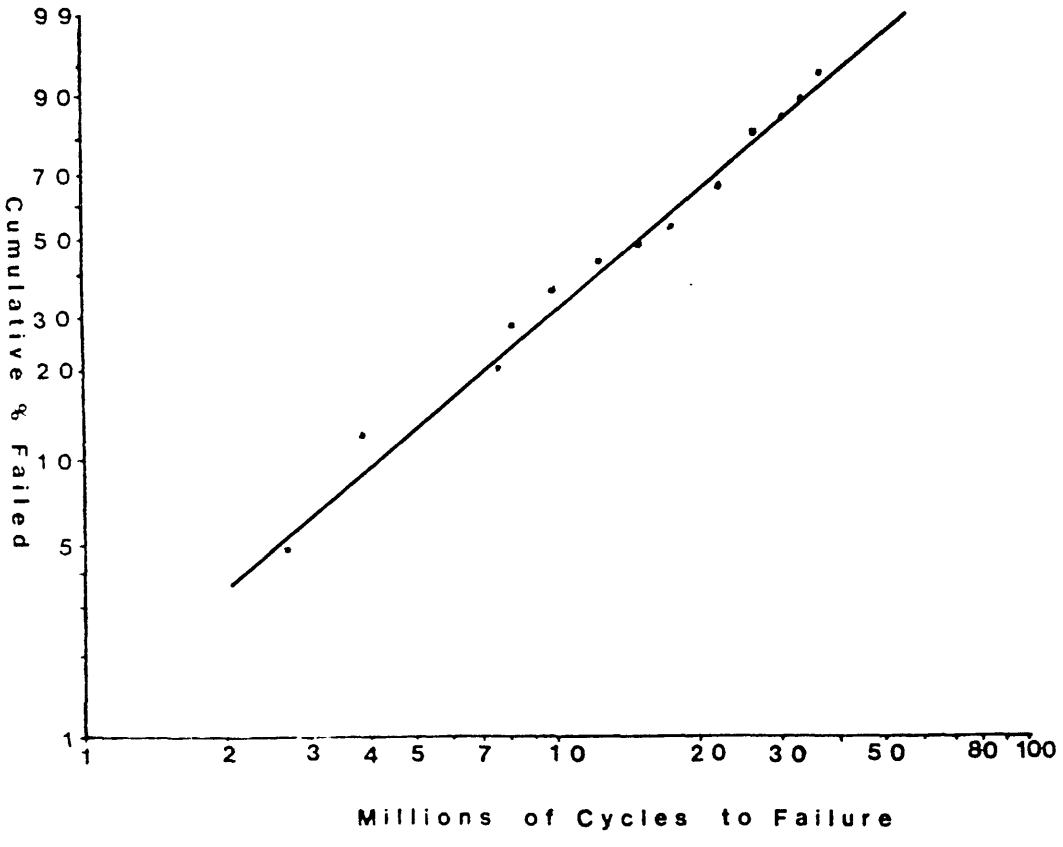

Figure 6.5

the polarised + 200mV (Series 5)

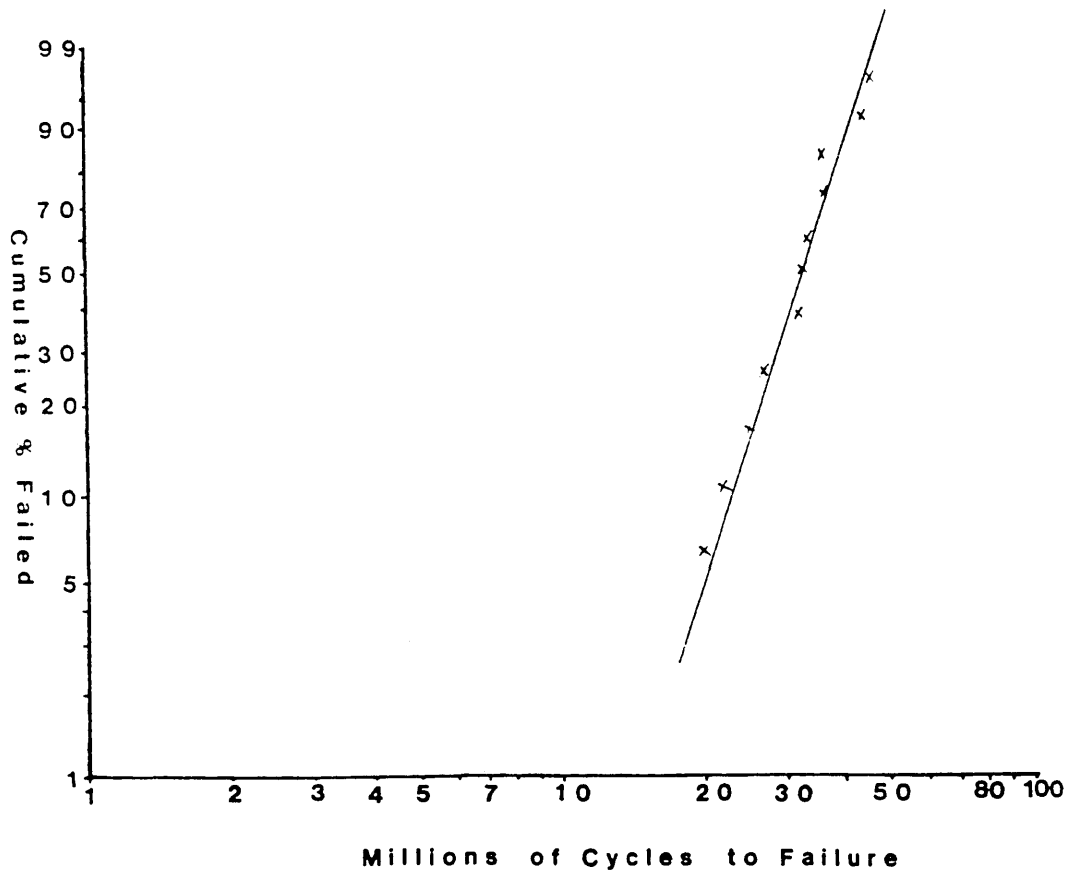

Figure 6.6

the -200mV Series under load (Series 6)

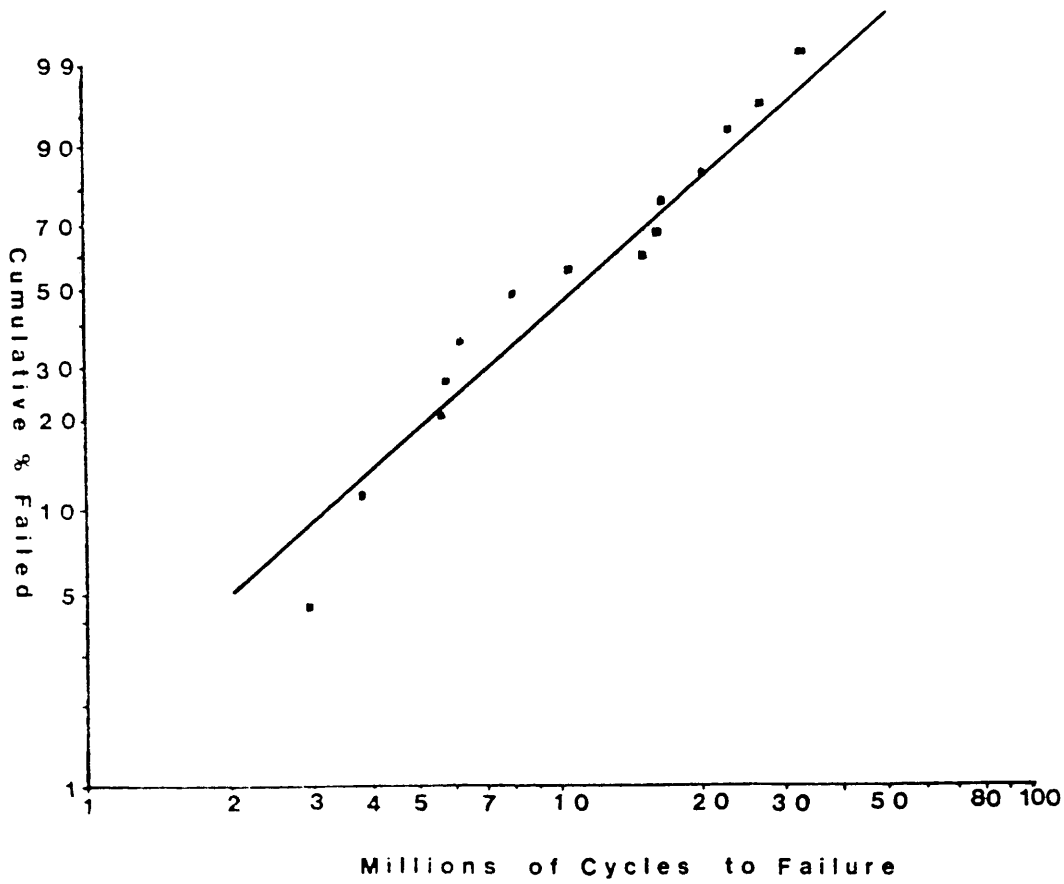

-200mV under the standard High Load (Series 7)

Figure 6.7

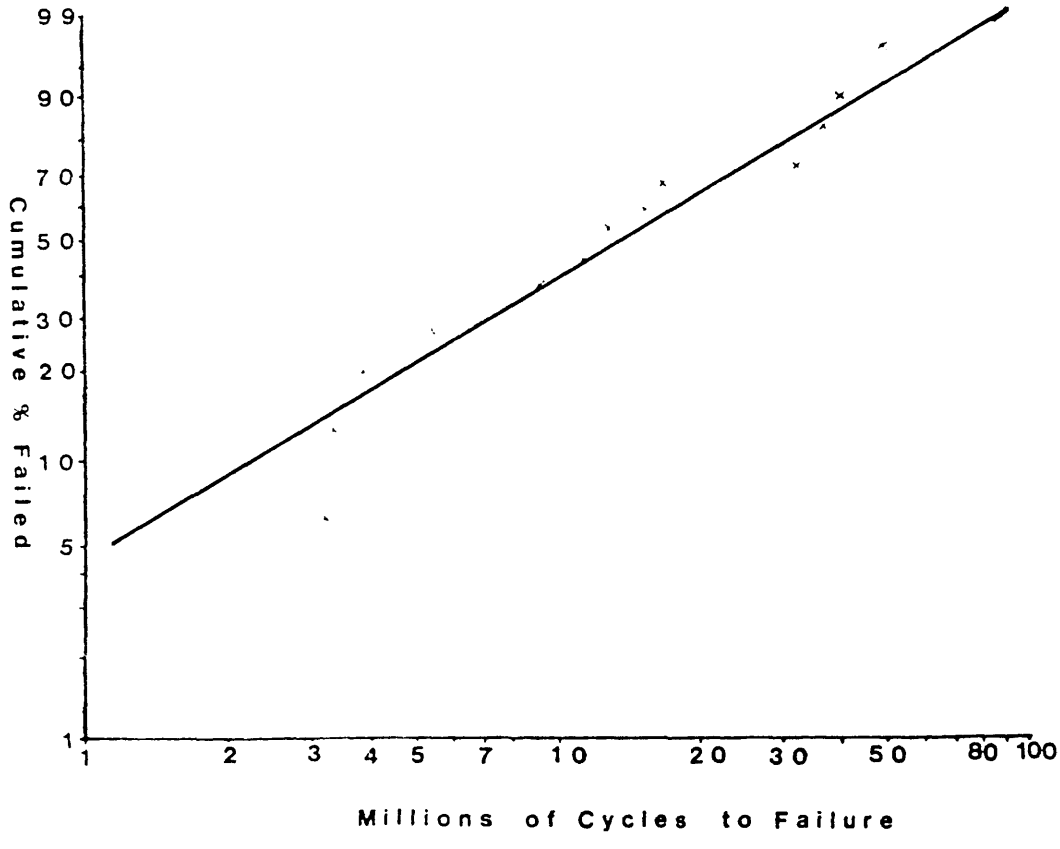

the HF-C Fluid, ("Glycent FRX"
@ 46 H_2O by Weight) (Series 8)

Figure 6.8

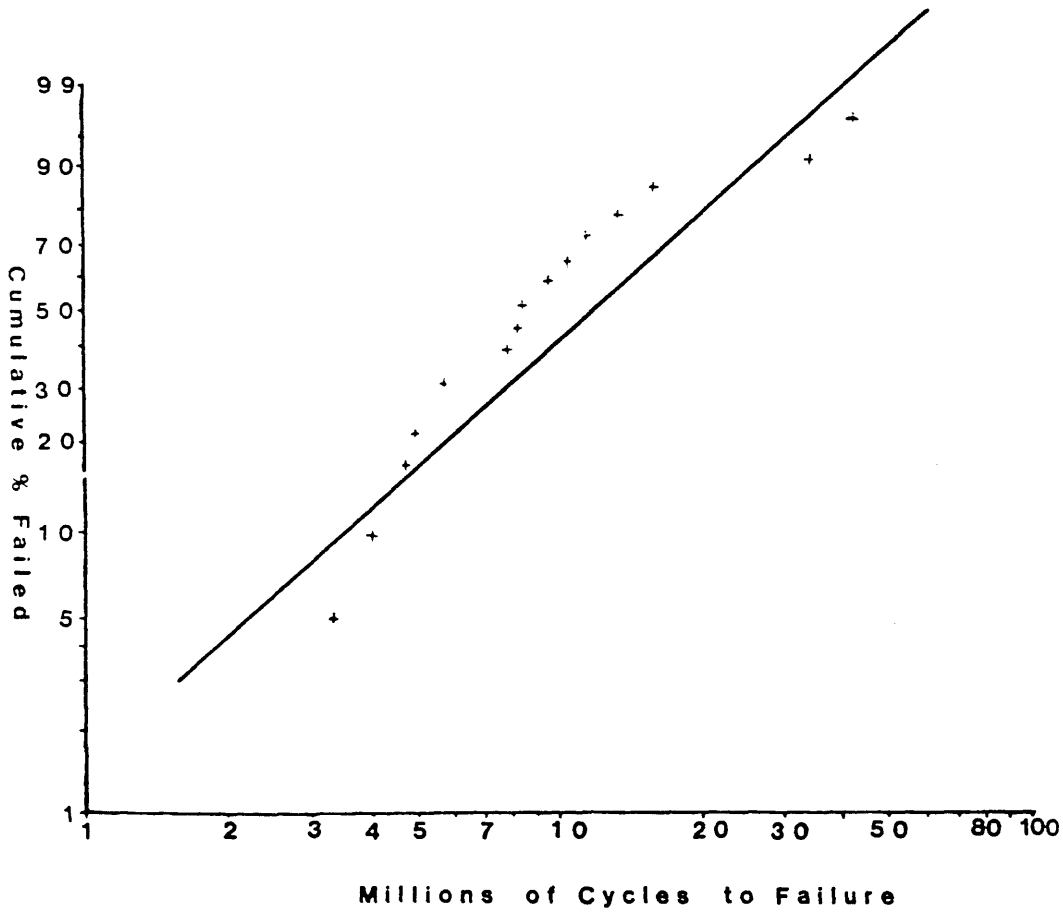

the HF-C Fluid mixed 50/50 by weight with water (water content 73.5%) (Series 9)

Figure 6.9

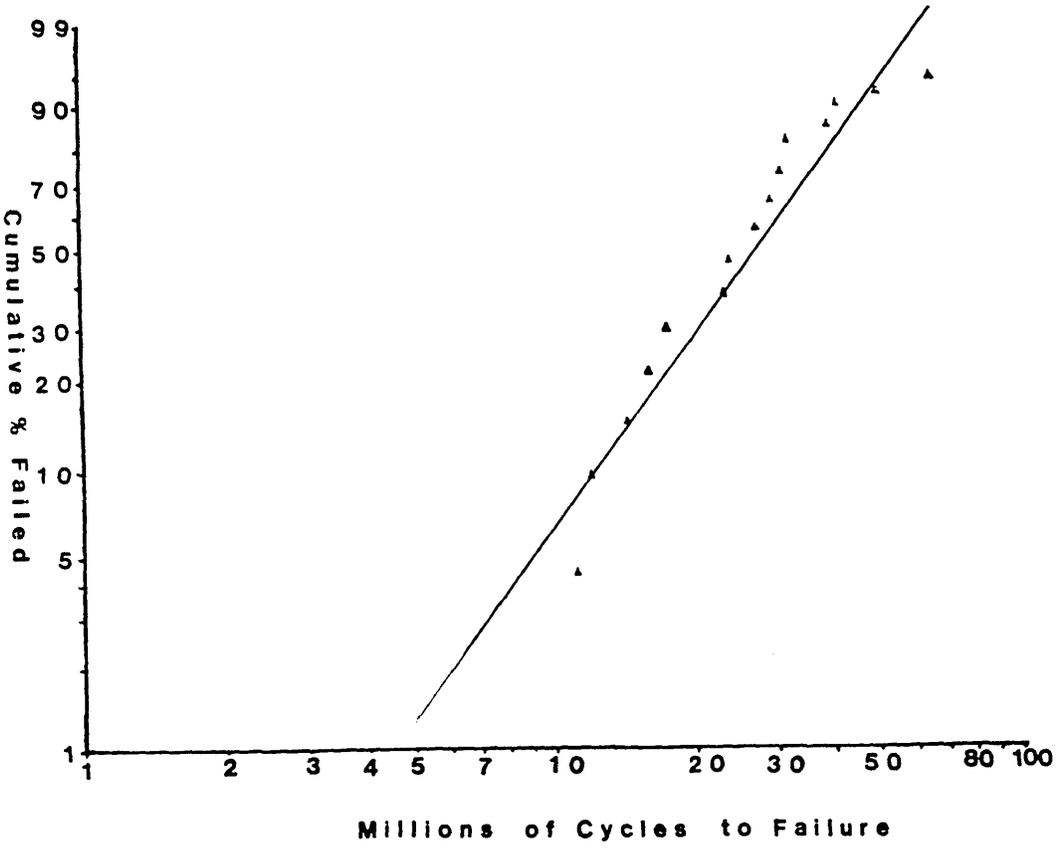

the polymer thickened dilute emulsion @ 90% water (Series 10)

Figure 6.10

6.1.1 Development of the Test Method and Conditions

6.1.1.1 First Shakedown Series

Two shakedown series were carried out initially. As the rig was intended to be used with fire resistant fluids, a standard invert emulsion HF-B, 'Aquacent Light' was employed as the test fluid, the properties of which are described in Table 6.2. This first shakedown run combined four purposes. It was intended to be (i) a break-in run; (ii) a test of the findings of Dousinas (25), that applied tensile stress could significantly shorten the fatigue life of the bearing steel; (iii) test of the similarity between the four heads, and (iv) a proof of the test method.

The conditions employed are described in Table 6.3 and the results are given in Table 6.4. The stylus of a Rank Taylor Hobson 'Talysurf 4' was tracked on the surface specimen after running and the trace is shown in Figure 6.11.

A number of problems were noted in the initial runs. Firstly, failure of the ball as well as the specimen bar occurred due to over-hardness of the bar specimens. Another area of concern was caused by the publication of a report by Nakajima (123), which indicated that where two specimens of the same dimension are rolled repeatedly against each other at the same speed, they rapidly wear or deform to fit one another, ie to 'conform'. This should extend the fatigue life. As a result of this work and the first test series, it was decided to reduce the diameter of the bar specimens in the contacting area, and also to soften them to about 650 Hv 50. The reduction in diameter meant that the ball and bar no longer had simple ratio diameters and thus would not conform circumferentially.

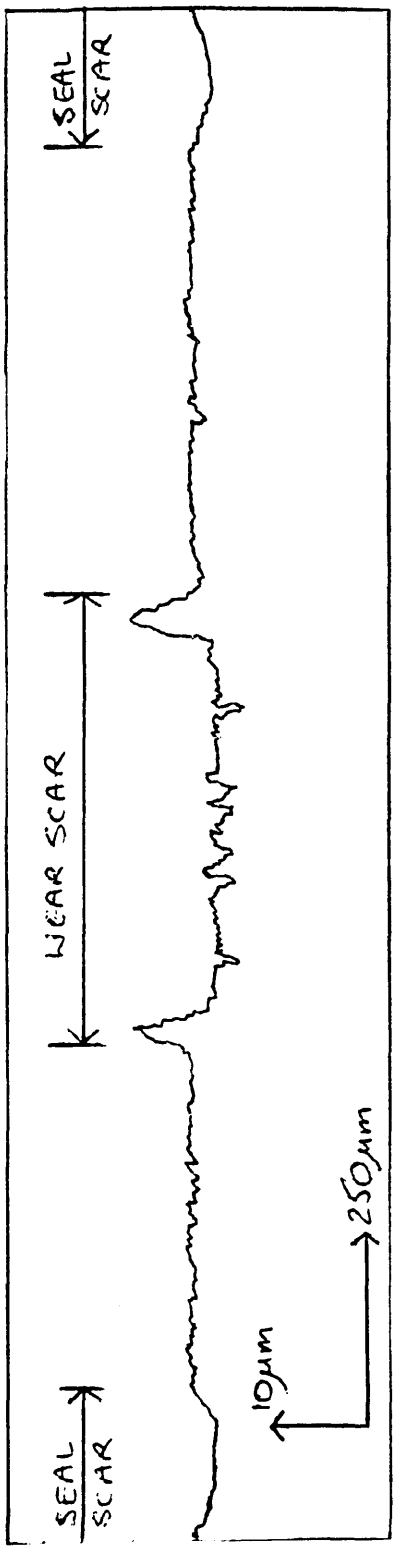

A track length was 4 mm and the filter cut-off 0.8 mm

Figure 6.11

Talysurf trace of the surface of the specimen after running

"Aquacent Light"	
Specification Water content % Water particle size Remulsifiable on remixing Seals	570/1981 35-40 < 0.5 μm Compatible
Kinematic viscosity at t °/c 25 40 50 60	Centistokes 128 68 47 34.4
Corrosion Tests: Copper Brass Silver Cast Iron Aluminium Hydural Steel	Pass Pass Pass Pass Pass Pass Pass

Table 6.2

The Propereties of 'Aquacent Light'

Loading pressure	1600 psi (11 MPa)
Maximum Stress, P max	5.6 GPa
Sump temperature	25°C
Speed	3000 rpm 2.0 ms^{-1}
Ball: Hardness 800-850 Hv50 diameter 12.7mm Rq roughness 0.15 μm	
Bar: Hardness 770-850 Hv50 diameter 12.7mm Rq roughness 0.25 μm	
Estimated EHD film thickness, (30), $h_{mean} = 9.4 \times 10^{-8}$m	
Specific film thickness λ = .63 Composite surface roughness, Rq = 0.152 μm Applied tensile Bending - 90mm x 15 lb (20 Nm)	
Fluid : "Aquacent Light"	

Table 6.3

Test Conditions for the first Series

Test No	Life/millions of cycles	Failure Site	Failure mode
1	6.75	bar	spalling
2	18.36	bar	spalling
3	24.84	ball	spalling
4	26.65	ball	spalling
5	43.20	bar	spalling
6	1.62	bar	spalling
7	4.70	bar	spalling
8	42.94	ball	spalling
9	5.21	ball	spalling
10	71.36	bar	spalling
11	80.68	bar	spalling

Table 6.4

Results for First Shakedown Run (Series 1)

	Series 2	Series 3
Loading pressure	1600 psi (11 MPa)	1800 psi (12.4 MPa)
Maximum stress	5.6 GPa	5.8 GPa
Sump temperature	35°C	35°C
Speed	3000 rpm $1.8\ ms^{-1}$	3000 rpm $1.8\ ms^{-1}$
Ball		
Hardness	800-850 Hv50	800-850 Hv50
Diameter	12.7 min	12.7 min
RMS roughness	0.025 μm	0.025 μm
Bar		
Hardness	600-650 Hv50	760-800 Hv50
Diameter	11.5 mm	11.5 mm
RMS roughness	0.150 μm	0.150 μm
Composite surface roughness	Rq = 0.152	Rq = 0.152
Estimated elastohydrodynamic film thickness, (30)	$h_{mean}=7.3\times10^{-8}$m	$h_{mean}=7.2\times10^{-8}$m
Specific film thickness	λ = 0.49	λ = 0.47
Fluid 'Aquacent Light'		

Table 6.5

Standard Test Conditions

The first run also showed that there was no apparent difference between three of the heads, (head number 3 suffered a motor failure) as all gave fatigue results over the same ranges. The test method itself appeared to be valid from the results obtained and the subsequent Weibull plot, Figure 6.1. The run also showed that the monitoring of the water content of the fluid was very important. In the manufacturers specification of the fluid, it was suggested that the fluid should show no loss of water at temperatures below 40°C. After two weeks running, however, the fluid was found to have lost about 2% of the water content. This was made up with distilled water poured into the recirculation stream in the sump. The water content was subsequently measured every day or two days to establish a pattern of water loss and then made up to the correct level. Periodic monitoring of the water level was also carried out to maintain the water content at 40 $\pm$ 1%.

6.1.1.2 Second Shakedown Series

The second shakedown run was carried out using the modified specimens described above under the conditions in Table 6.5. The resultant fatigue lives are presented in Table 6.6.

For the second set of tests, the rig was once again undergoing a proving run, as well as trying to establish a reasonable set of test variables. If Table 2.4 is considered then the 11 parameters affecting rolling fatigue can be assessed for their influence on each test run. By maintaining the lubricant the same, the lubricant parameters are constant. The only parameter changes are actually to the load, geometry and the hardness of the contacting surfaces. The

Test No	Life/Millions of Cycles	Failure Mode
1	3.94	Spalling
2	1.01	Spalling
3	1.74	Spalling
4	5.23	Spalling
5	12.07	Spalling
6	1.10	Spalling
7	17.51	Spalling
8	2.49	Spalling
9	2.80	Spalling
10	3.50	Spalling
11	29.35	Spalling
12	23.00	Spalling
13	45.45	Spalling
14	3.58	Spalling
15	6.73	Spalling

Table 6.6

Results for Second Shakedown Run (Series 2)

hypothesis was that increasing the load slightly and reducing the diameter would increase the contact stress and therefore reduce the life of specimens. Making the specimen bars softer than the ball specimens should also promote pitting in the bars rather than the balls.

One problem which was not foreseen was that the reduction in the diameter of the central section caused a marked softening of the specimens. This caused the high incidence of very early failure which was considered to be due to the specimens being too soft. The result was the very short fatigue lives seen in Table 6.6. It has been suggested that for valid bearing tests, a minimum hardness of 750 Hv 50 is required (124).

As the overall time allowed for the project was limited, the system of changing test variables by small amounts and then testing to produce a full Weibull plot was not possible, so variations to more than one test parameter had to be introduced together and often these changes caused very significant differences between test series.

6.1.1.3 Summary of the First Two Test Series

The first two test series showed that, provided the test variables were reasonably controlled and suitable specimens used, then the rig offered a new test method for the assessment of fire resistant lubricants. As a result of these two shakedown runs, a large batch of one hundred and twenty specimens of hardness about Hv 750 was ordered. These specimens were manufactured on a Computer Numerically Controlled (CNC) lathe to ensure that they were as uniform as engineering tolerances allowed.

One of the problems with the first two runs was that it became clear that only two or three of the specimen heads on the rig could be used at any one time due to reliability problems which prevented the use of one of the heads for the majority of the test work. This added considerably to the length of time required for a full test series to be completed.

Despite this problem, a test program to compare and contrast the performances of the three main classes of fire resistant lubricants listed in Table 3.1. The conditions employed and the results obtained for these fluids are described in section 6.1.3.
A Talysurf trace of the surface of one of the new specimens was obtained and is given in Figure 6.12.

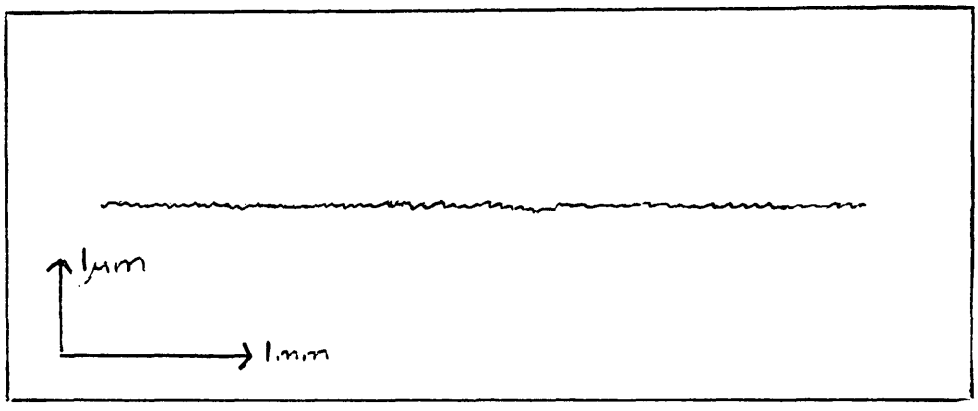

Figure 6.12

A track length of 4 mm and an ISO filter cut-off of 0.8 mm was employed

6.1.2 Observations on Each series of Results

6.1.2.1 First Shakedown Series

The first shakedown series which employed invert emulsion was used primarily to investigate the performance of the test rig itself. Some failures in this series were on the ball and not on the bar specimen. The spall shown in Figure 2.3 was found on a ball run in this series. The use of the applied tensile stress did not appear to contribute to the reduction in fatigue lives caused by this fluid. This is further discussed in Chapter 7.

The wear track on the bar specimens were brightly polished with no evidence of corrosion on visual microscope inspection. On the ball specimens that pitted, there was only one polished wear track indicating that the ball had maintained a single axis of rotation in its holder. On the other balls, which did not pit, there was more than one wear track indicating that there had been axial rotation. The wear tracks on the bars were approximately the same at about .75 mm wide. On the balls that pitted, the wear track approximately matched that of the bar, but on those that did not pit the wear scar was less wide. Unfortunately it was not possible to obtain 'talysurf' traces for the spherical balls and so this difference could not be quantified. The reasons for the rotation or lack of rotation could not be positively ascertained but it may be that, as the collar holding the ball became worn, it allowed the ball to rotate slightly until the ball, which was not perfectly spherical, became partially jammed and rotated only in the longitudinal direction of the bar. The conclusions drawn for the first shakedown run were that the bar specimens were too hard and incorrectly the same diameter as the balls, that the water content of the fluid required careful monitoring, and the applied tensile stress did not appear to shorten the fatigue lives of the bar specimens. These points are further discussed in Section 7.1.2.

6.1.2.2 Second Shakedown Series

The failure mode in this series was, in all cases, by spalling of the specimen bar. This suggested that moderate film thickness occurred in the contact zone which ties in with the value of the specific film thickness of 0.49 given in Table 6.5. The wear scars were brightly polished on first removal from the holders and were about 0.75 mm in diameter. The scars tarnished somewhat on storage, suggesting that the surface was fresh metal when first removed. Again, some of the balls showed multiple wear tracks and greater the number of scars, the less pronounced each was. In some test runs the vibration cut-out level on the accelerometer was not set quite correctly and the specimens often cut-out before failing or did not cut-out immediately on failure. Those that cut-out without failure had their cut-outs reset but the others were more of a problem.

Two short-lived specimens with lives less than 4 million cycles had multiple failures but as there was no evidence of failure less than 2 million cycles, it was decided in these two instances to record their actual failure lives when stopped.

It was anticipated that with some fluids, surface films would be formed on the test specimens but in this series using invert emulsion, no films apart from slight oiliness due to the fluid which wiped off with a soft cloth were seen. There were no areas of corrosion or rusting visible in the track regions between the two oil seals when examined by optical microscope at 40X magnification. No damage, apart from the wear scars, were seen on the balls run in this series. One problem with the reduction in shaft diameter was the oil seals. It was not possible to obtain internally correctly fitting oil seals and

so slightly undersized seals had to be run-in to prevent severe heating of the surface of the specimens and melting of the contacting area of the seals. The other major problem discovered during this second series was the poor reliability of the four heads. This meant that between each specimen being run, heads had to be cannibalised to facilitate operation of two to three heads at any one moment. This problem dogged the programme throughout the whole of the period of use of the rig.

As a result of these first two series, the test parameters given in Table 6.6 were decided upon and maintained rigidly during the standard test runs, so as to facilitate comparison between the three main classes of fluids.

6.1.2.3 'Aquacent Light' Invert Emulsion Test Series

The observations made during this test series were very similar to the 'Second Shakedown Series', which was to be expected since the fluids were the same. The major differences were that with the bar specimens being much harder and much more uniform than those used in the previous series, the fatigue lives were much longer. There were no early failures in this series, in fact 75% of the failures had occurred in the second shakedown run before the first failure in the 'Aquacent Light' series at just over 12 million cycles. This is further discussed in Chapter 7. The wear scars on the bars were of similar width to the previous series (approximately 0.75 mm) but the wear scars on the balls were much more pronounced, Figure 6.13.

Figure 6.13

Wear Scar on ball

A 'Talysurf' trace of a failed run was also taken and is shown in Figure 6.14.

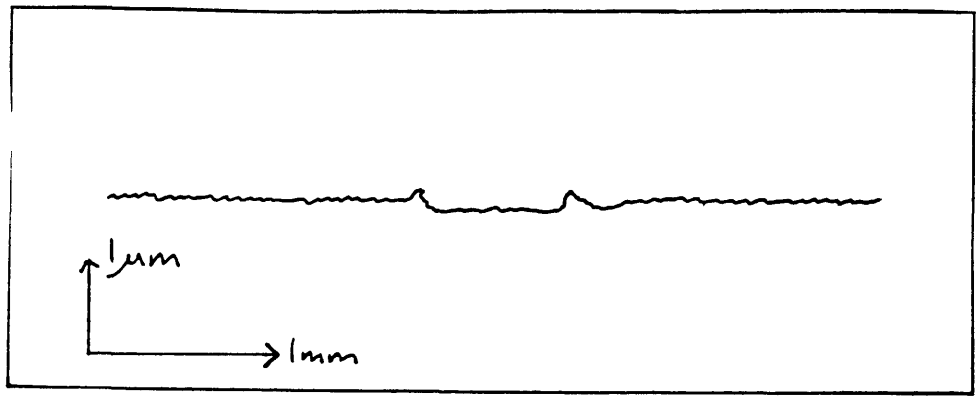

A track length of 4 mm and an ISO filter cut-off of 0.8 mm was employed

Figure 6.14

A failed bar having run for 60.74 millions of cycles is pictured in Figure 6.15, and the polished nature of the wear scar can clearly be seen. Some slight corrosion of the region either side of the wear track was visible in the 85 million cycles life specimen but no evidence was found on any other specimens. This was probably due to the fact that this specimen failed at the start of a holiday period and it was left for several days in the head after failure. No films were found to have formed during the running of any specimen but the emulsion formed a dark residue with the seal material in the seal areas. This residue could be wiped off with a small amount of acetone to leave polished areas in the seal zones.

In this test series, the vibration levels responded correctly to the first pit, in all cases, though there were some sympathetic cut-outs when one head cut-out after another had failed, perhaps due to 'spikes' in the vibration monitoring equipment.

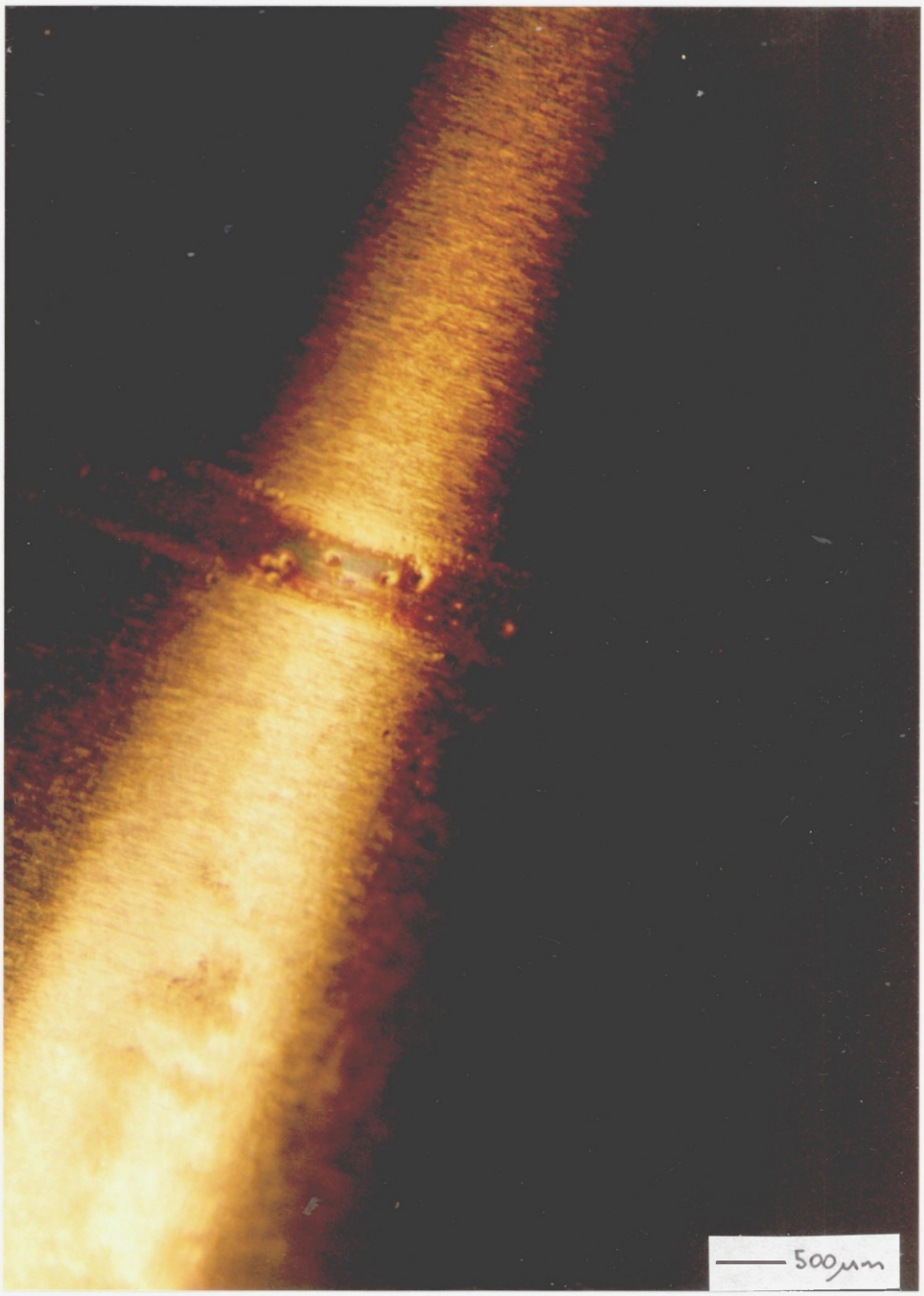

Figure 6.15

Failed bar run for 60.74 million cycles

Overall this test series proved a success but the whole series took far longer than anticipated to complete, and this delayed the completion of the originally planned test series. At the end of the tests the equipment was stripped and examined. The two pumps showed no signs of corrosion and seemed to be in good working order. Unfortunately, no weighings of parts had taken place and so no study into the effects of the pumps was possible. Full implications of this test series are discussed in the next chapter.

6.1.2.4 Dilute Emulsion 'Specification 19' (56) Series

Testing of this fluid produced a great deal of audible noise and other vibration in the contact and this made the setting of the accelerometer levels difficult. Frequent cut-outs of the heads occurred with no apparent failures. After every shut-down, the wear track was examined visually and if no sign of pitting was present the trip was reset and the head restarted. Micropitting was the major mode of failure, so that was difficult to see failure with the naked eye and often the specimen was removed from the head and examined under the optical microscope to confirm the onset of significant surface damage. With the longer fatigue-lived specimens, corrosion on the surface of the non-contacting area of the specimens was seen, and with the three longest lives, both micropitting and spalling were observed.

Some thin surface films formed on the balls and specimens run with the dilute emulsion. These films appeared to be produced soon after the start of running-in but did not grow to any great thickness (< 0.5 mm). These films were largely insoluble in water but removable by organic solvents on soft cloths. The films did not always form to the same degree but they are very likely to be responsible for the longer than expected lives survived by some of the specimens. The formation of these films is further discussed in Section 6.4 and their possible effects on the fatigue lives of the specimens in Chapter 7.

6.1.2.5 Dilute Emulsion with +200 mV Applied Potential

Many of the problems of the orthodox dilute emulsion series were observed with this +200 mV series. The most significant characteristic of this series was the formation of thick white films in the contact zone on the specimen bars. The films formed appeared to be somewhat time-dependent as the longer live specimens times had apparently thicker films although this was not confirmed quantitatively. The films were analysed by reflective infra-red spectroscopy and the results are discussed in Section 6.4. The setting of the vibration level was again a problem but the films formed appeared to damp the vibrations and allowed the levels to be set correctly.

The failure mode for this series was again micropitting indicating that only minimal effective film thickness was present in the contact zone. The wear track was much duller than in previous runs but was the same width at about .75 mm. The implications of this series are further discussed in Chapter 7.

6.1.2.6 Dilute emulsions with -200 mV (low stress)

The first observation noted was the absence of films formed on the contact zone of the bar specimens but instead, built-up deposits on the ball and the guiding bush of the loading assembly, Figure 5.1. Under the low load conditions the lives were considerably longer than expected. The failure mode was again micropitting in all cases but the wear track was much less marked at about only 0.5 mm wide. Rusting areas of corrosion were also found in the contacting zone of the bar specimens in some of the longer lived test runs. The vibration level was not as high due to the lower load and so the setting of the vibration cut-out levels was much easier and micropitting will be eventually picked up . The implications of these observations and results are discussed in Chapter 7.

6.1.2.7 Dilute Emulsion with -200 mV (high stress)

The observations of this series are a combination of the previous two series. There was no film formation on the bar specimen but there was on the ball and on the guiding collet. The wear scar was approximately 0.75 mm wide and the failure mechanism was by micropitting. The wear track was once again dull rather than bright and shiny. In Chapter 7 the results from these three tests involving polarising currents are analysed.

6.1.2.8 Aqueous Glycol - 'As received' Condition

The vibration levels were much lower using this fluid than those of the dilute emulsion. This is very probably due to the higher bulk viscosity of the fluid and its consequent damping effect. After the specimens had run, a very thin white layer was formed on the surface which was water-resistant but soluble in toluene, indicating that it is probably organic. Infra-red analysis of the layer was carried out and is reported in Section 6.4. The failure mode was, as with the dilute emulsion, a mixture of spalling and micropitting for the longer lives, whilst the short-lived specimens failed by micropitting.
The main difference between the aqueous glycol and the other fluids was that the wear track appeared scorched. This is shown in Figure 6.16 There was also some visible corrosion.

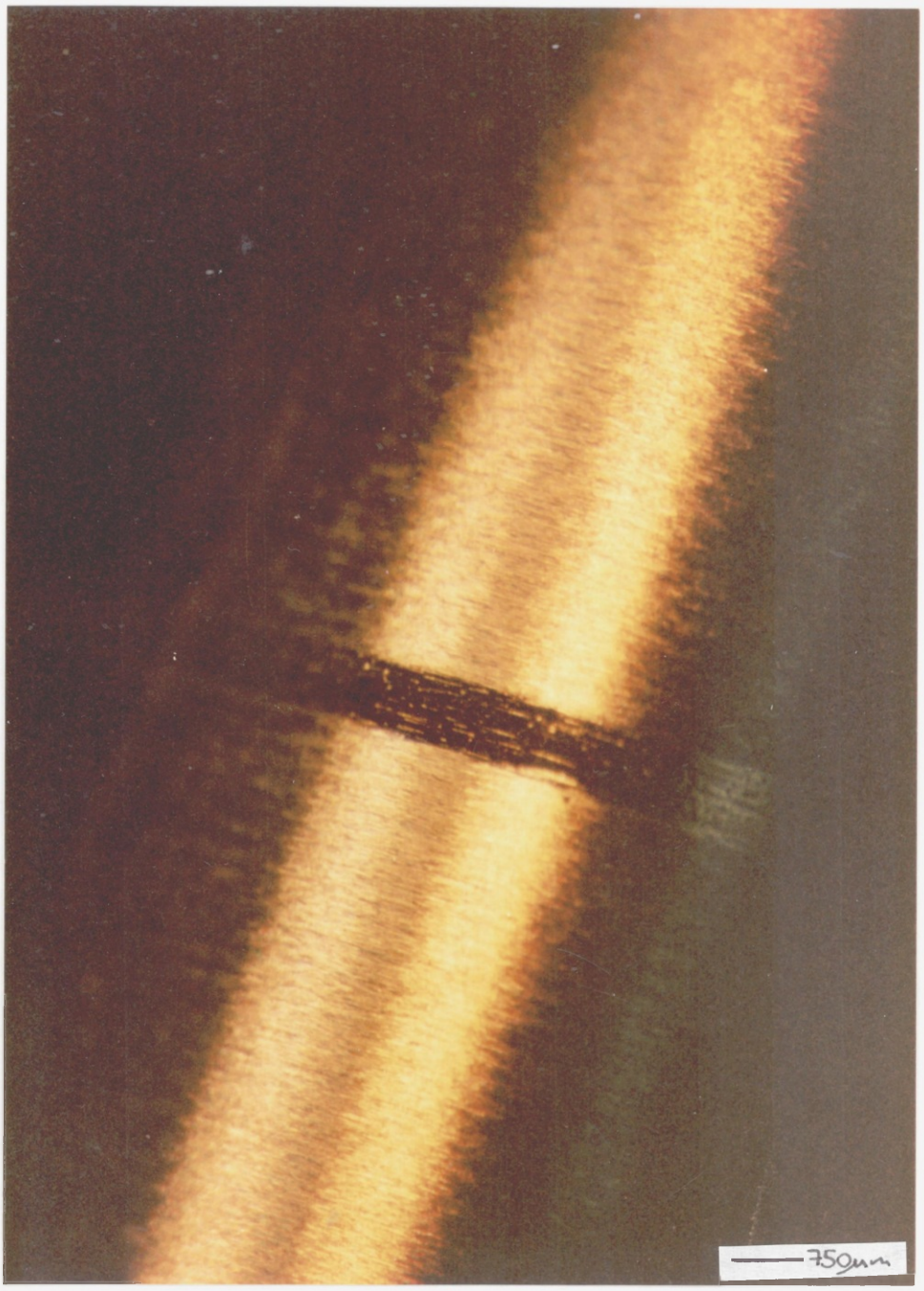

Figure 6.16

A specimen run in 47% Aqueous Glycol for 43.20 cycles

6.1.2.9 Aqueous Glycol - diluted to 73.5% Water

Problems were encountered with the vibration cut-out due to the low viscosity of the fluid. Very thin white films, similar to the 47% water glycol, were formed. The failure mode was purely micropitting in this case, indicating that only thin separating films were forming in the contact.

Some corrosion was again seen on the longer lived specimens. Overall there was very little difference between the results for the two aqueous glycol fluids despite the difference in water content. The wear track was once again burned or darkened in appearance but it was the same width at about 0.75 mm wide. The pumps had a similar although less rusty appearance on stripping at the end of the test. This may be due to the shorter time interval using the aqueous glycol fluids.

The reasons for the similarities of result despite the differences in water content are discussed in Chapter 7.

6.1.2.10 Polymer Thickened High Water-Based Fluid

Operationally, this fluid behaved very similarly to the invert emulsion, with low vibration levels. The main differences were that the fluid formed thick viscous deposits on all surfaces coming into contact with it. These films were again analysed by infra-red spectroscopy.

Full water-analysing experiments were conducted into the fluid and are reported in Chapter 7. The track width was the familiar 0.75 mm suggesting further that this was due primarily to ball loading and elastic/plastic coantact geometry rather than the fluids. The failure mode in all cases was spalling with some micropitting present, indicating that the film may have broken down on spalling and allowed the micropitting to take place. With some of the longer life specimens, corrosion areas were seen on the area surrounding the

track, close to the oil seals. On the magnetic filter at the head drain, plastic growths formed during running and had to be scraped off at the start of every test. Another observation made was the formation of a plastic substance on the filter element, indicating that the fluid may have filter-blocking tendencies and also the formation of similar plastic-type 'stalactites' on the pipe-joints where leaks had occurred. One other problem with this fluid was that it was difficult to wash off components and specimens.

As this polymer-thickened fluid was an experimental lubricant with unknown properties, a series of other tests and observations were carried out and these are reported in Chapter 7.

6.1.3 Standard Fluid Runs

This section describes and compares the fatigue results obtained from the range of fluids used HF-B, HF-A and HF-C.

The fluid used for the first standard run was 'Aquacent Light' described in detail in Table 6.2. The second run was carried out using a dilute emulsion, made up from hard water-compatible concentrate, 'Specification 19'. The properties of this fluid are given in Table 6.8. Both these two fluids are in current use in mining applications with British Coal (56). The results from the invert emulsion run are given in Table 6.7, whilst those of the dilute emulsion are listed in Table 6.9. The conditions employed during these two tests and in others under standard conditions are given in Table 6.5. Owing to difficulty in obtaining an aqueous glycol HF-C, testing of HF-C took place some seven months after the other two runs. The conditions employed were the same as for the dilute and inverse emulsions as given in Table 6.5.

Test No	Life/Millions of Orders	Failure Mode
1	16.08	Spalling
2	34.35	Spalling
3	39.48	Spalling
4	22.30	Spalling
5	60.74	Spalling
6	70.72	Spalling
7	85.05	Spalling
8	46.63	Spalling
9	12.07	Spalling
10	18.47	Spalling
11	30.37	Spalling
12	24.22	Spalling

Table 6.7

Results for "Aquacent Light" (Series 3)

Solcenic 3A	
Specification Classification	463/1981 Type 19
maximum $CaCO_3$ equivalence Cl^-/SO_4^{2-} pH Thames concentration	750 mg/dm^3 400 mg/dm^3 9 270 mg/dm^3
pH (dilute) Kinematic viscosity (dilute)	11.8 1 cSt
Concentrate relative density Kinematic viscosity hygroscopic	 1005 Kg/m^3 1200 cSt

Table 6.8

Properties of the HF-A

TEST No	LIFE/MILLIONS OF CYCLES	FAILURE MODE
1	4.95	Micropitting
2	8.52	Micropitting
3	15.67	Micropitting
4	3.02	Micropitting
5	2.45	Micropitting
6	24.08	Micropitting
7	7.43	Micropitting
8	42.02	Spalling & Micropitting
9	51.02	Spalling & Micropitting
10	54.39	Spalling & Micropitting
11	13.15	Micropitting
12	3.49	Micropitting
13	4.06	Micropitting

Table 6.9

Results for Dilute Emulsion (Series 4)

Glycent FRX Light	
Specification	
density, ρ_{16}/kg/m^3	1048
Kinematic viscosity at t/°C	cSt
0	211
25	49
40	26
50	18.5
60	13.6
Water Content	46%
Colour	clear hazy fluid
Operating Range	-23- +71°C
Corrosion tests	
Copper	Pass
Brass	Pass
Silver	Pass
Aluminium	Pass
Steel	Pass

Table 6.10

Properties of the Aqueous Glycol

The physical properties of this HF-C fluid, Century 'FRX Light' are given in Table 6.10. Fluids of this type are not widely used in the British Mining Industry except for a few low temperature applications where dilute emulsions are unsuitable. It was delivered as a ready-mixed solution containing 47% water by weight. A series of tests were carried out with the 'as received' fluid and the results are reported in Table 6.11.

The first fluid tested, the HF-B 'Aquacent Light', gave quite long fatigue lives, 12.00 to 86.00 millions of cycles which was considerably longer than anticipated because the previous run gave lives of 1.00 - 45.00 millions of cycles. The reason identified for this was the hardness of the bar specimens at approximately 780 Hv 50. The influence of specimen hardness on fatigue life is further discussed in Chapter 7.

The failure mechanism for the first three series on HF-B was spalling. The failure mechanism for the HF-A and HF-C runs were, however, both micropitting. This conforms the work of Wan (72), on the lack of elastohydrodynamic film thickness and that of Berthe and co-workers (10), and Tallian (11), with regard to the failure mechanism. The HF-B used produced an elastohydrodynamic film due to the presence of a continuous mineral oil phase, but the HF-A and the HF-C fluids failed to produce measurable films. Berthe and co-workers (10) and Tallian (11), as described in Section 2.2.4 showed that low film thickness caused pitting and very low film thickness gave rise to micropitting. This was confirmed by these results. This is further discussed in Section 7.5.

6.1.3.1 Statistical Examination of the Standard Test Runs

The results of the three runs were analysed by the methods described in Section 2.3. The statistical significances at L_{10} fatigue life level of the three sets of results were established. These results are given in Table 6.12.

Test No	Life/millions of cycles	Failure mode
1	15.72	Micropitting
2	18.19	Micropitting
3	17.86	Micropitting
4	30.60	Micropitting
5	35.41	Micropitting
6	3.41	Micropitting
7	41.98	Micropitting
8	52.35	Micropitting
9	3.17	Micropitting
10	10.65	Micropitting
11	4.53	Micropitting
12	11.37	Micropitting
13	6.12	Micropitting

Table 6.11

Results for the HF-C Fluid, ("Glycent FRX" @ 46% H_2O by Weight) (Series 8)

Fluids	Series	Degrees of Freedom	L_{10} ratio	Confidence Limits (@) Weibull Slope		Overall Limit
HF-A/ HF-B	3 and 4	132	8.52	e = 2.99 e = 0.82	> 99% > 99	> 99%
HF-B/ HF-C	3 and 8	132	4.89	e = 2.99 e = 1.00	> 99% > 99%	> 99%
HF-A/ HF-C	4 and 8	144	1.74	e = 0.82 e = 1.00	> 60% > 65%	> 62.5%

Statistical significance of the results for the standard test runs

Table 6.12

From the results given in Table 6.12 it is clear that statistical significance is achieved between 'Aquacent Light' (Series 3) and the aqueous glycol (Series 8) and the dilute emulsion (Series 4), but statistically these last two fluids are indistinguishable at the L_{10} fatigue level.

The confidence limits for the mean lives, again calculated from the method in Appendix 2 (17), are given in Table 6.13.

Fluids	Series	Degrees of Freedom	Mean Life ratio	Confidence Limits (@) Weibull Slope		Overall Limit
HF-A/ HF-B	3 and 4	132	1.71	e = 2.99 e = 0.82	> 99% 92%	~ 99%
HF-B/ HF-C	3 and 8	132	1.60	e = 2.99 e = 1.00	> 99% 90%	~ 95%
HF-A/ HF-C	4 and 8	144	1.07	e = 0.82 e = 1.00	> 55% 57%	54.5%

Table 6.13

Statistical significance for the standard runs at the mean life level

The figures for the overall confidence limit show that similar statistical significance has been achieved at the mean life level. From the figures, it would appear that this is due to the very high mean life for the invert emulsion against comparatively low lives for the aqueous glycol and for the dilute emulsion. The figures for Series 4 and 8 indicate that under the conditions employed, the dilute emulsion and the aqueous glycol will give virtually identical results. It was decided that these two fluids gave lives that were so close that no further testing would be carried out as it would not have been able to achieve statistical significance for the two fluids within a realistic number of tests.

To summarise, these three sets of results showed that the test method did give good test results in agreement with previous workers (27), (67).

6.1.4 Investigative Test Runs

In order to investigate the mechanism of premature rolling contact fatigue failure, a series of tests were carried out on the effect of varying external conditions on the four-head test rig.

6.1.4.1 Polarisation Effects

Whilst the aqueous glycol, HF-C, was on order, three tests series were carried out to investigate the effects of applied surface electrical potential across the bar specimen. The unpolarised test series using dilute emulsion was employed as the datum from which the effects of the polarisation would be measured.

Following the work of Leach and Talks (98), it was thought possible that protective lubricant films might be formed on the surface of the specimen by the polarisation of the contacting region. A small electrical device for polarising the contact was constructed and connected to the heads in operation, as described in Section 5.1.6.

Test No	Life/millions of cycles	Failure mode
1	9.23	Micropitting
2	11.86	Micropitting
3	14.20	Micropitting
4	25.46	Micropitting
5	4.11	Micropitting
6	31.79	Micropitting
7	35.39	Micropitting
8	40.43	Micropitting & Spalling
9	26.21	Micropitting
10	9.75	Micropitting
11	12.44	Micropitting
12	13.05	Micropitting
13	16.67	Micropitting
14	2.95	Micropitting

Table 6.14

Results for the polarised + 200mV (Series 5)

This gave a potential of plus or minus 200 mV on the surface of the specimen relative to earth. The first set of results with a potential of +200 mV is given in Table 6.14. The conditions being otherwise the same as in Table 6.5.

Series	Applied Voltage mV	Fatigue lives in millions of cycles				Weibull Slope, e	Number of failures
		L_{10}	Mean	L_{50}	$L_{62.5}$		
4	-	1.35	21.0	13.0	19.5	0.82	13
5	+200	4.5	19.5	16.5	20.5	1.45	14
7	-200	4.3	16.5	14.3	18.0	1.57	14

Influence of applied voltage on fatigue lives for the dilute emulsion

Table 6.15

The results for both applied voltage runs are superior to the dilute emulsion series at both L_{10} and L_{50} fatigue lives but the dilute emulsion is superior to the -200 mV series at the characteristic life, $L_{62.5}$. The failure method in all instances was by micropitting, and the failures all appeared similar under the optical microscope. No corrosion effects were detected visually.

As will be shown in Section 6.4.1, the growth of the thick films formed under the +200 mV, described in Section 6.1.2.5 was almost certainly due to the surfactant, whilst under the -200 mV the opposing potential almost certainly prevented the film from forming. Other predicted effects of the polarising current are included in Table 6.16.

	Film Formulation	Corrosion	Iron Dissolution	Hydrogen Formation
+200 mV	Promoted	Should be promoted	Promoted	Inhibited
-200 mV	Inhibited	Should be inhibited	Inhibited	Promoted

Predicted events caused by the applied potential

Table 6.16

It would appear from the results that these four effects appear to cancel each other out to some extent though the use of a polarising current does give improved life over the standard dilute emulsion. This is further discussed in Chapter 7.

The confidence limits for the L_{10} fatigue lives is given in Table 6.17.

Series	Degrees of Freedom	L_{10} ratio	Confidence Limits (@) Weibull Slope		Overall
4 and 5	156	3.33	@ 0.82	82%	89%
			1.45	96%	
4 and 7	156	3.19	0.82	80%	86%
			@ 1.57	92%	
5 and 7	169	1.05	1.45	54%	55%
			1.57	56%	

Statistical Significance and Confidence limits for the applied potential series at the L_{10} fatigue life (4 = O mV), 5 = +200 mV, 7 = -200 mV)

Table 6.17

Statistical significance for the dilute emulsion without applied potential between the +200 mV and between the -200 mV and applied potentials was almost achieved (a confidence limit of > 90% is required for statistical significance) at the L_{10} fatigue life. The results indicate that the polarisation of the surface does have an effect on the L_{10} fatigue lives for the dilute emulsion.

The confidence limits for the mean lives, again calculated from the method in Appendix 2 (17), and are given in Table 6.18.

Series	Degrees of Freedom	Mean Life Ratio	Confidence Limits (@) Weibull Slope		Overall
4 and 5	156	1.08	@ 0.82 @ 1.45	55% 65%	60%
4 and 7	156	1.27	@ 0.82 @ 1.57	75% 84%	77%
5 and 7	169	1.18	@ 1.45 @ 1.57	77% 78%	55%

Confidence limits for the applied potential series at the mean life (4 = 0 mV, 5 = +200 mV, 7 = -200 mV)

Table 6.18

From the overall confidence limits established in Table 6.18, it can be clearly seen that statistical significance of the mean life difference was not obtained.

6.1.4.2 Loading Effects

After the start of the -200 mV test series, a fault occurred on the pump system and three results had been obtained at the correct stress level, whilst six other results were obtained at a lower stress level. It was decided to run both conditions to a statistical number of failures. The results for the low stress level series is given in Table 6.19 and the results from the high stress level in Table 6.20. Series 6 and Series 7 were carried out under identical conditions except that the loading used for series 6 was only 1046 N instead of the usual 1570 N.

The results obtained are compared in Table 6.21.

Series	Load	L_{10}	L_{50}	Mean Life	e	N
6	1046	21.0	36.5	37.0	3.41	11
7	1570	4.3	14.3	16.5	1.57	14

Results for low and high load test series under -200 mV applied potential

Table 6.21

Test No	Life/Millions of Cycles	Failure Mode
1	34.43	Micropitting
2	34.83	Micropitting
3	35.58	Micropitting
4	22.08	Micropitting
5	24.07	Micropitting
6	40.30	Micropitting
7	53.47	Micropitting
8	59.02	Micropitting
9	40.04	Micropitting
10	28.60	Micropitting
11	29.64	Micropitting

Table 6.19

Results for the -200mV Series under low load (Series 6)

Test No	Life/Millions of cycles	Failure Mode
1	6.77	Micropitting
2	6.94	Micropitting
3	16.64	Micropitting
4	21.38	Micropitting
5	26.30	Micropitting
6	17.18	Micropitting
7	2.95	Micropitting
8	4.78	Micropitting
9	8.43	Micropitting
10	30.33	Micropitting
11	33.02	Micropitting
12	17.37	Micropitting
13	13.26	Micropitting
14	15.25	Micropitting
15	10.02	Micropitting

Table 6.20

Results for -200mV under the standard High Load (Series 7)

In both cases the failure method was micropitting, the only difference being failure under the lower load were easier to detect due to lower vibration levels prior to failure.

The confidence limits for the results at the L_{10} and mean life but below in Table 6.22, calculated from the method in Appendix 2.

Series	Degrees of Freedom	Ratio of Lives	Confidence Limits (@) Weibull Slope	Overall
L_{10}	130	4.88	@ e = 3.41 >99% @ e = 1.57 96%	~ 98%
Mean Life	130	2.24	@ e = 1.57 >99% @ e = 1.57 >99%	> 99%

Confidence limits for the high and low stress tests at -200 mV using dilute emulsion

Table 6.22

As can be seen from the above data, statistical significance is achieved at both the mean life and the L_{10} fatigue life. As was expected, the two sets of results have separate identities. The significance of these results is discussed in Chapter 7.

6.1.4.3 Dilution Effects

Tests were carried out to investigate the effect of excess dilution of commercial water-based hydraulic fluids. Stanton and Whitwell (54), tested chemically modified water by diluting it to half its recommended concentration. Baker and Riley (53), also tested dilute emulsion concentrates by diluting them to 98% water to simulate practices found in the mining industry of over-diluting the emulsions employed. It was to this aim that attempts were made to produce a dilute emulsion at 98% dilution. The emulsion was unstable and the oil fraction formed a layer on top of the water and bulk fluid was milky. An emulsifying machine was employed to promote particle dispersions but after agitating for 15 mins, settling out took place immediately.

Test No	Life/Millions of Cycles	Failure Mode
1	8.45	Micropitting
2	3.29	Micropitting
3	14.99	Micropitting
4	5.38	Micropitting
5	20.61	Micropitting
6	12.96	Micropitting
7	39.86	Micropitting
8	48.85	Micropitting
9	5.97	Micropitting
10	5.20	Micropitting
11	16.66	Micropitting
12	9.58	Micropitting
13	8.98	Micropitting
14	8.65	Micropitting
15	4.00	Micropitting

Table 6.23

Results for the HF-C Fluid mixed 50/50 by weight with water (water content 73.5%) (Series 9)

As the aqueous glycol is a solution and not an emulsion, it offered the best opportunity to test the hypothesis (122), that dilution has very little effect on the performance of very dilute fire resistant lubricants. Made-up aqueous glycol was diluted 50/50 by volume with distilled water and a full test run was carried out with the product. Distilled water was used in preference to tap water, as some severe scumming with the latter and deposition of solid matter took place. The diluted aqueous glycol contained 73.5% water by weight. The results obtained for this fluid are given in Table 6.23 and the conditions employed are the standard ones, shown in Table 6.5. The results obtained for both dilutions are given in Table 6.24.

Series	Dilution % H_2O	Fatigue Life/millions of cycles			Weibull Slope e	No of failures N
		L_{10}	L_{50}	Mean Life		
8	47	2.35	15.5	22.5	1.00	13
9	73.5	2.40	10.8	13.5	1.25	15

Table 6.24

Comparison of the results for the Aqueous Glycol at different dilution levels

The L_{10} fatigue lives are very similar, the only difference being, however, the number of failures below 10 million cycles, where the 47% water gave only 4 whilst the 73.5% water gave 9. Both fluids gave lives in the same range of 3 to 50 million cycles to failure. At the L_{10} fatigue life level no possible statistical significance could be established, whilst at the mean life, an overall confidence limit of 93% was established showing that statistical significance, with the more concentrated fluid being superior to the diluted one, was obtained. As the failure mechanisms were apparently identical and similar almost non-existent, elastohydrodynamic films were formed (72), the reasons for the difference in lives must be due to the extra water present.

Unfortunately, it was not possible, due to a lack of suitable cutting equipment, to section the specimens at the wear scar. The aim of this would have been to try to distinguish between micropitting and micro-corrosion pitting, as described in Section 2.2.4. The appearances of the two under scanning electron microscope are different, (125).

This influence of the extra water is quite significant for the understanding of which failure mechanism was operating when the failure occurred and is further discussed in Chapter 7.

6.1.4.4 Polymer-Thickened Fluid

The final type of fluid investigated was a polymer-thickened, dilute emulsion as described in section 3.2. This fluid was not a commercial product but a pilot blend of a new fluid, intended for use as a replacement for invert or dilute emulsions. The fluid, despite containing 90% water, arrived in a ready-mixed condition. The properties of this polymer-thickened fluid are given in Table 6.25 and the results obtained are given in Table 6.26.

6.1.4.5 Comparison of the other classes of fluids with the polymer thickened fluid

It is of interest to compare the performance of this fluid with the other 3 main classes, HF-A, HF-B and HF-C to establish if the gap in the market, identified by the producers of the fluid, exists.

In Table 6.27, the tests results obtained in this study for the 4 fluids are given, together with their water contents.

Property	Results
Water Content	90% w/w
Viscosity	Not known
Refractive Index	Determined
EHD behaviour	In Section 7.3

Table 6.25

Properties of the Polymer-thickened fluid

Test No	Life/millions of cycles	Failure mode
1	27.19	Micropitting
2	22.81	Micropitting
3	11.71	Micropitting
4	24.93	Micropitting
5	12.32	Micropitting
6	14.35	Micropitting
7	46.69	Micropitting
8	69.02	Micropitting and spalling
9	18.45	Micropitting
10	24.47	Micropitting
11	27.08	Micropitting
12	38.98	Micropitting
13	16.07	Micropitting
14	29.16	Micropitting
15	36.75	Micropitting

Table 6.26

Results for the polymer thickened dilute emulsion @ 90% water (Series 10)

Fluid Type	Series	% Water	Fatigue Lives/millions of cycles			Weibull Slope e	No. of failures N
			L_{10}	L_{50}	Mean Life		
HF-B	3	40	11.5	35	36.0	2.99	12
HF-A	4	95	1.35	13.0	21.0	0.82	13
HF-C	8	47	2.35	15.5	22.	1.00	13
PTF	10	90	11.2	27.0	28	2.14	15

Table 6.27

Comparison of the performance of three varieties of fluids with the polymer-thickened fluid

A comparison of their relative performance is given in Figure 6.17 where the plots of all four fluids are drawn. This plot clearly shows that the performance of the HF-B and the polymer-thickened fluid are very similar and are an order of magnitude better than the performance of the dilute emulsion and the aqueous glycol. Comparative figures for the confidence limits for the L_{10} fatigue lives for each fluid with the polymer-thickened fluid are given in Table 6.28.

Series	Degree of Freedom	L_{10} Life Ratio	Confidence Limits (@) Weibull Slope		Overall
3 & 10	154	1.03	@ 2.99	60%	58%
			@ 2.14	57%	
4 & 10	168	8.30	@ 0.82	96%	~98%
			@ 2.14	> 99%	
8 & 10	168	4.77	@ 1.00	90%	~95%
			@ 2.14	> 99%	

Table 6.28

Statistical significance between HF/A, HF/B, HF/C and the Polymer-thickened fluid at L_{10} level

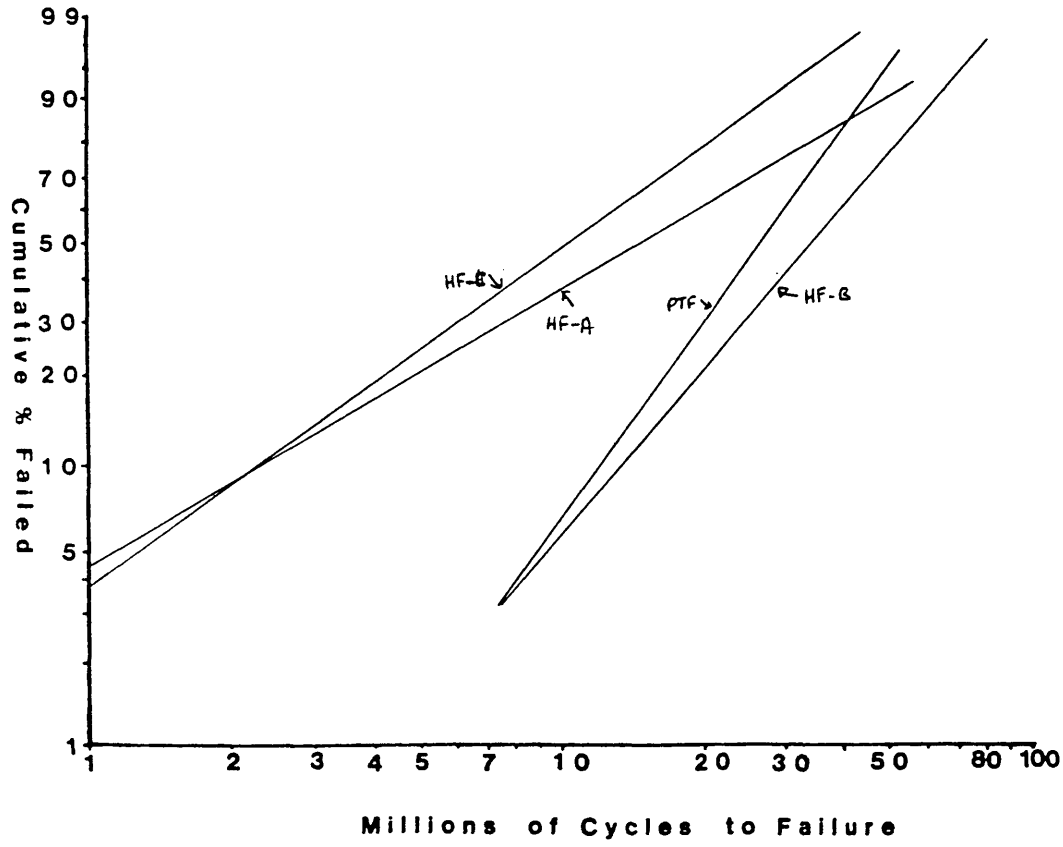

Comparison of the performance of the HF/A, HF/B, HF/C and the the polymer-thickened fluid

Figure 6.17

At the L_{10} fatigue life, statistical significance is achieved between the polymer thickened fluid and both the dilute emulsion and aqueous glycol. The overall confidence limit for the invert emulsion and the polymer-thickened fluid is only 58%, indicating that there is only a .58 probability that the HF-B gives a better performance than the polymer-thickened fluid, in terms of its 90% survival probability. The mean lives are compared in Table 6.29 with overall confidence limits established.

Series	Degree of Freedom	Mean Life Ratio	Confidence Limits (@) Weibull Slope		Overall
3 & 10	154	1.29	@ 2.99	93%	92%
			@ 2.14	91%	
4 & 10	168	1.33	@ 0.82	80%	86%
			@ 2.14	> 92%	
8 & 10	168	1.70	@ 1.00	92%	95%
			@ 2.14	> 97%	

Table 6.29

Statistical significance between HF-A, HF-B, HF-C, and polymer-thickened fluid at the mean life level

At the mean life time, statistical significance is achieved between the invert emulsion and the polymer-thickened fluid with the invert emulsion giving the better performance. For the dilute emulsion and the polymer-thickened fluid, significance is not quite achieved, again due to the very long mean life at low Weibull slope for the dilute emulsion. With the aqueous glycol and the polymer-thickened fluid, the polymer-thickened fluid achieved statistical significance for the results for its better performance than the aqueous glycol.
The reasons for the surprisingly good performance of the polymer-thickened fluid are examined in detail in the next chapter.

6.2 AOL VERTICAL FATIGUE RIG TEST RESULTS

As described in section 5.2, the AOL vertical fatigue rig was used solely for the generation of failed specimens for use in infra red (IR) spectroscopic, scanning electron microscope (SEM), and Secondary Ion Mass Spectroscopic (SIMS) analysis.

It was intended to generate a large series of failures using each type of fluid but this proved not to be possible.

The first fluid used to test the rig was "Aquacent Light" a water-in-oil emulsion described in Table 6.2. Only one successful failure was obtained from five attempts. Two specimens suffered cage failures whilst in two of the results the majority of the water was lost from the fluid and the fluid became an oil rather than an emulsion. The failed sample was run for almost 1 week (15 million cycles) at the standard load of 6670 N and 1500rpm. The failure, pictured in Fig 6.18 was not the same type of pitting as seen in the four-head rig but a longer, flatter pit. The reason for this is unclear but may be due to the geometry of the contact which produced a stress field which propagated the crack as described in section 2.2.4.1. The other possibility is that this type of pitting was caused by poor specimen quality (116). In section 2.2.4.1, the difference between surface and subsurface initiated pits initiated pits was described. The type of shallow flat pit formed is probably surface initiated. The type of pitting is shown in fig 6.18.

The cage failure was caused by the continued wearing of the balls against the cage over a period of days. Because of this it was decided to use the dilute emulsion for testing as the failures were obtained in a relatively short time (less than 5 days continuous running). The only cage failures that occurred when the dilute emulsion was used were either under very high applied load (about 10,000N) or when the pump system failed. The sectioning of the

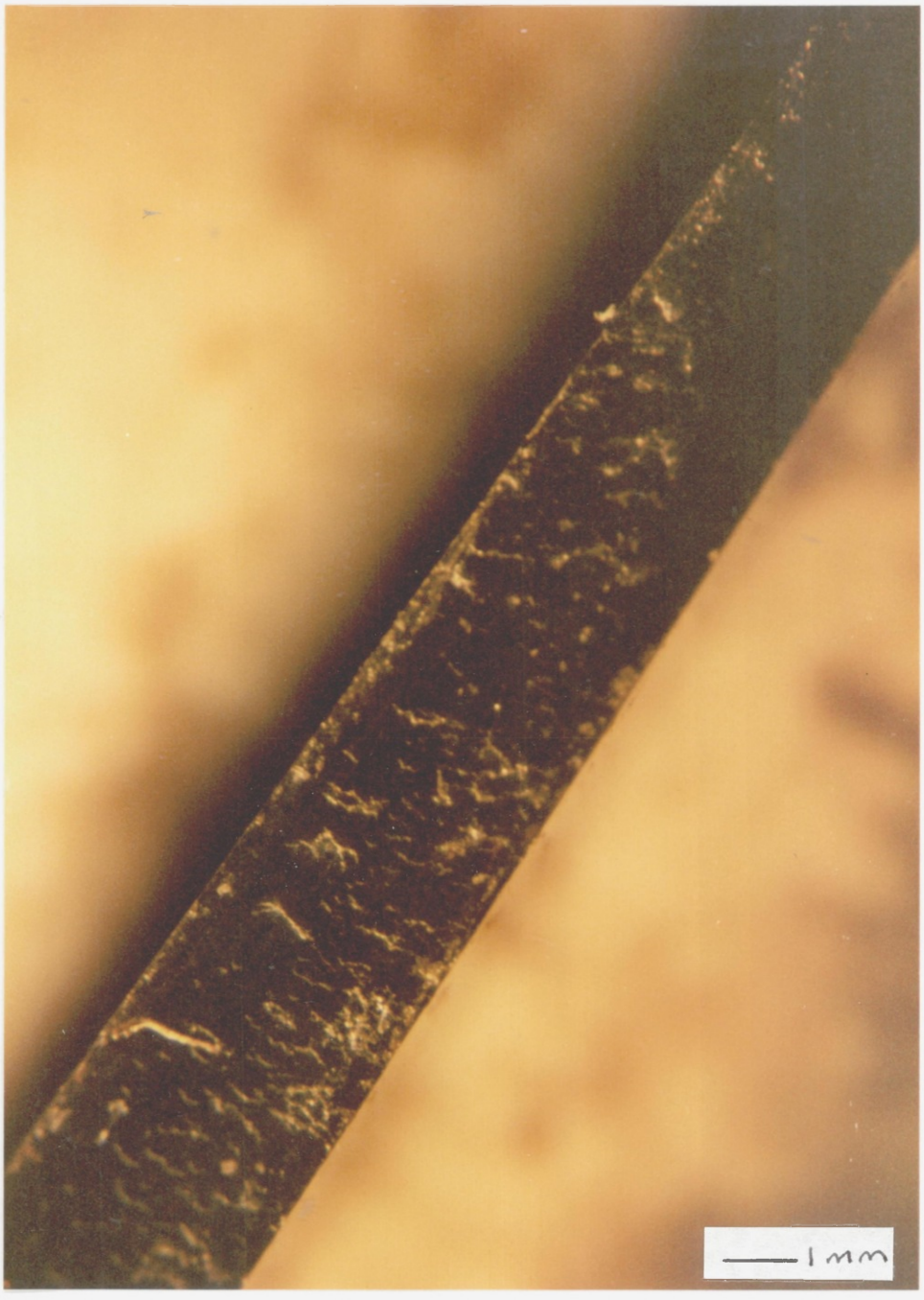

Figure 6.18

Failed AOL Raceway

dilute emulsion failures is discussed in the next section. As the method of obtaining the dilute emulsion failures had been successful, the same method was applied to obtain three failures with the aqueous glycol.

No sensible results were obtained with the polymer-thickened fluid, because the fluid had a much higher viscosity than the dilute emulsion, it would not flow. The running of the specimens caused the loss of water from the fluid and the formation of a plastic residue on cooling. Some micropitting was obtained but the failed specimen had to be washed in a soxhlet apparatus using a mixture of hot chloroform ($CHCl_3$), acetone (C_3H_6O) and toluene (C_7H_8) to remove the plastic residue.

The dilute emulsion lubricated failed specimens were used to develop the sectioning technique and for further work.

The slicing and grinding techniques used are described in the next section.

6.2.1 Preparation of Failed Specimen Raceways

The failed raceway was located in the specimen holder and fastened into position in a grinder cutter. The specimens were cut at 1000 rpm disc speed and approximately 1 cm/hour feed speed. This feed speed was a compromise between rate of cut, which was extremely slow at lower speeds and disc fracture and wear which occurred at higher speed.

Initially a cutting fluid recommended by the manufacturer was used to assist in the grinding of specimens. The first problem discovered that the fluid was producing a deposit on the surface of the raceways. Under a slightly lower feed speed of about 0.5 cm/hour, so that the specimen did not get too hot without the assistance of cooling, dry cutting was attempted. However, SEM examination of surfaces cut by this method showed that the surface of the raceway section was covered with fragments of the cutting disc. When

cutting, sparks occasionally flew from the disc and it was assumed that white hot metal and disc fragments melted into the surface. As each raceway had to undergo several cuts, the entire section surface became covered in fragments.

The only other option was to coat the specimen raceway with grease or petroleum jelly. This lubricated the cutting and also prevented hot fragments from embedding themselves in the specimen surface. The grease or petroleum jelly was removed by washing in the same manner as cleaning before use.

The actual slicing sequence is depicted in Fig 6.19.

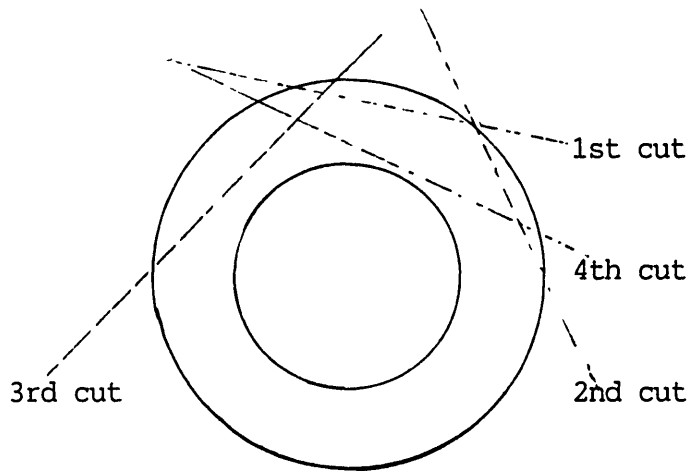

Fig 6.19 specimen slicing technique

This resulted in a sliced specimen which was almost flat and did not have any raised edges.

Another technique, which was tried was, to use a surface grinder "Metaserv" to slowly grind of the outside rim of the raceway, removing, the need for the first three cuts as described above and then using the same fourth cut as above. This technique was quite difficult as at low speed grinding was very slow and at high speed the grinding paper slipped. Again the raceways were ground wet using a cutting fluid. This also caused deposited films on the specimen. It was for these reasons the cutting of the specimen raceways was carried out with the grinder cutter and using grease or light petroleum jelly as a protector and lubricant.

Problems associated with the slicing of these specimens are further discussed in Section 6.4.

6.2.2. Other AOL Test Work

As well as carrying out tests on the four types of water-based fire resistant hydraulic fluids a series of other tests were attempted to add data to the results obtained elsewhere and to hopefully assist in the lubrication of the mechanism. Two tests were carried out in the complete absence of any lubricant. This was to try to prove the hypothesis of Way, (2), that a lubricant was required for pitting. The first test bearing suffered a cage failure after only 67000 cycles whilst the second was halted after only 45000 cycles with signs of imminent cage failure. In both cases, severe wear and oxidation of the balls and raceways had taken place with the specimen holder partially filled with ferric oxide debris. When this debris was cleaned off the raceways no sign of pitting or micropitting under optical microscope examination. This is further discussed in Chapter 7.

An attempt was also made to quantify effects of fluids and running on the surface microhardness of the specimens. Because the raceway specimens are grooved it proved impossible to get the objection lens focusing on the diamond microhardness indent and the study had to be abandoned.

Two tests were also carried out using a 1% by weight solution of sodium stearate ($CH_3(CH_2)_{14}COO^-Na^+$). One test suffered a cage failure but the other suffered micropitting. The surface of the raceway was coated in a thin white residue. This was examined by infra-red spectroscopy and is further described in Section 6.4.1.

6.2.3. Summary of AOL Results

Several good failures using the dilute emulsion were obtained but with most of the other fluids, problems prevented more than one or two failures from being obtained. The use of these specimens, once sliced is discussed in connection with analytic techniques in Section 6.4. The use of results from the two dry runs are also referred to in the mechanistic discussions in Section 7.5.

6.3 ROTATING-BENDING FATIGUE RIG RESULTS

As described in Section 5.3.4, rotating-bending tests used alternating high and low load test cycles on standard hour-glass specimens, Figure 5.9. Ten tests were carried out altogether with varying degrees of success. Of these tests, two were used to set the rig up as described in Section 5.3.4; two were run-outs with no failure or sign of initiation after 20 million cycles (approximately 1 week running), and one was bent by the load after the rig failed leaving the specimen highly loaded. The remaining five gave some useful information into crack propagation of steels in fire-resistant lubricant environments. During the tenth test the rig failed due to fatigue of the specimen holder. The holder contained a spring collet which had worn away part of the holder and itself was worn such that a specimen could not be gripped. Detailed examination of the components by the manufacturer of the rig was carried out. It was suggested that the repairs would be extremely expensive to the holder and also the supplier of the spring collet had ceased trading. This meant that the study had to be terminated with no comparison carried out with the other fluids to confirm ranking of fluids in Table 3.20. Only those specimens giving sensible results are discussed, in detail, in the sections below.

6.3.1 Measurement Protocol

All fatigue outer diameter measurements were carried out using a 0-25 mm micrometer with measurements lined-up by sight. All measurements were taken from above with the specimen base flat to reduce parallax error. The centre hour-glass specimens had been sectioned using a large grinder-cutter so that flat bases had been obtained for the this, Figure 6.20.

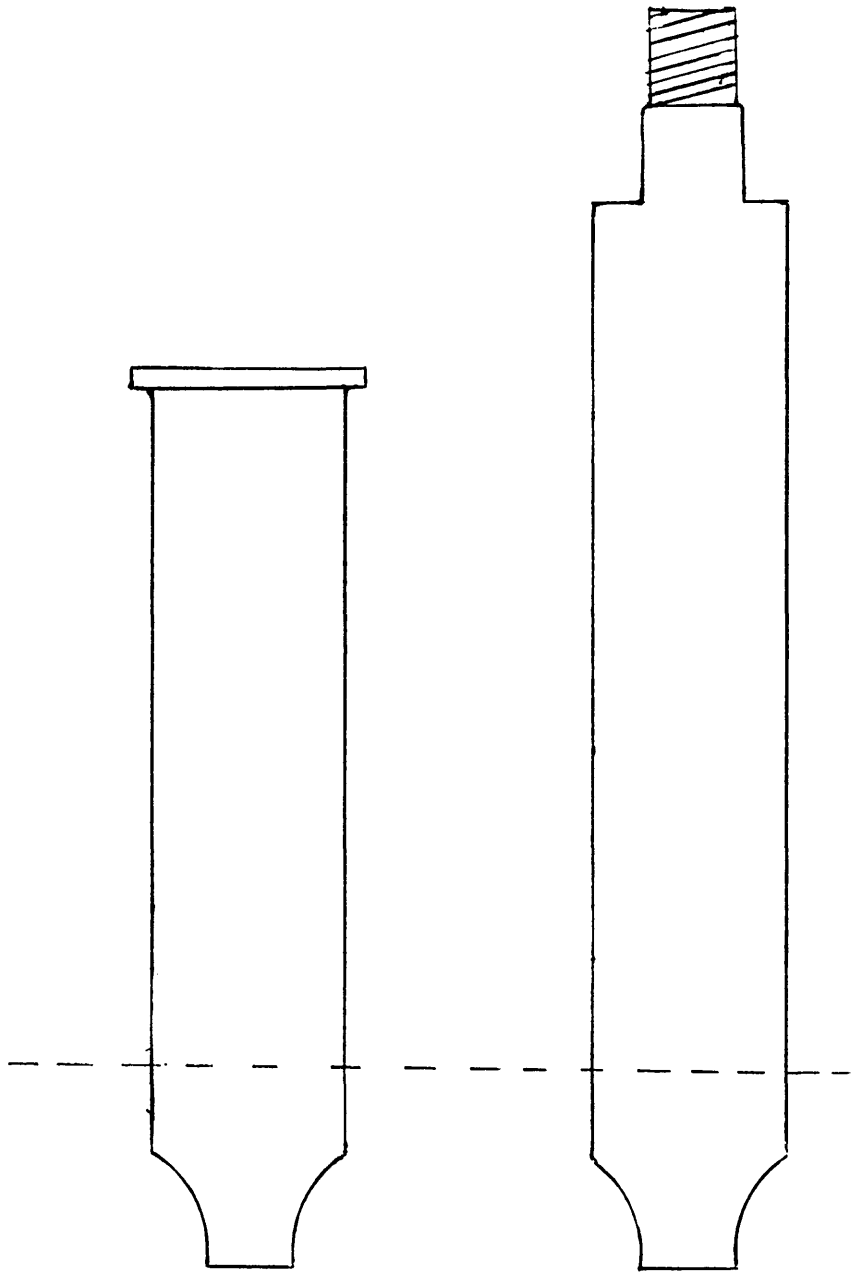

Figure 6.20

Sectioning of Rotating-bending Specimens

Owing to the difficulty of separating the light and dark loading bands on a photograph, it was decided for the purpose of illustration in this thesis to sketch them with dimensions indicated and place this adjacent to a photograph of the failed cross-section of the specimen, so all descriptions of cross-sections will have both a photograph and a sketch.

The fluid used for all tests was 'Aquacent Light' which was described in Table 6.2.

The stress intensity factors described in the following sections have been calculated from Neuber theory (120). The reason for this is that the stress intensity factor calculations of Harris (121), Eistenstadt and Fuller (118), and of Paris and Erdogan (13), were in Imperial units with constants also in Imperial units but without any identifiable conversion factors.

The calculations for load, bending stress and stress intensity factor are given in Appendix 8.

After the first specimen was run at a variety of loads without failure, a visual method of checking the running specimen every hour was used to try to estimate if the end of the initiation process had been reached. This method consisted of using the horizontal, unbent, position of the bar as a datum. When the specimen was loaded up, a certain amount of bending took place. The amount of bending during running was noted. If a change in the amount of bending was detected the load was removed and the rig was stopped, then examined. This process was carried out every hour or every two hours depending on how long the specimen had run for. If no sign of initiation having begun was visible, the fluid chamber was refilled and the rig restarted.

The five sensibly failed specimens are described in the next five sections.

6.3.2 Specimen Failure No. 1

This was the first specimen run from a new batch of six specimens manufactured to Figure 5.9. It was run for 9 hours at a high load of 1.8 kg then 66 minutes at low load 0.5 kg. Two minutes, 20 seconds after reloading for the second high load phase, failure occurred. The results of this failure are pictured in Figure 6.21. From Figure 6.22 the values of the band widths are obtained. These are given in Table 6.30. Crack propagation data for the first band is discussed in Section 6.3.7.

Position	Band Width/mm
A	0.70
B	0.73
C	1.06
D	0.94
E	0.71
F	0.74
G	1.12
H	0.87
Min	0.70
Max	1.12
Mean	0.86

Table 6.30

First Band Widths for Specimen No. 1

For the low load stage, values between 0.20 and 0.40 mm were obtained for the crack band width. The number of cycles was 200,000 and this gives a range of crack propagation rates of 1 to 2 x 10^{-6} mm/cycle.

Failure for the second high load stage occurred after about 140 s after its application. This represents only 7000 cycles and gives a mean crack propagation rate of about 1×10^{-3} mm/cycle. It does not appear from the end view of the specimen to show where steady state crack propagation finished and where fracture started. This figure equates to the fracture rates of the order of 10^{-3} mm/cycle found by Paris and Erdogan (13).

6.3.3 Specimen Failure No. 2

Because the specimen which was run immediately prior to this one suffered no failure after 2×10^{7} cycles with a load of 2 kg, it was decided to raise the load to 3 kg. Failure occurred after $5\frac{1}{4}$ hours during the first loading sequence. The end failure diagram and photograph are given in Figure 6.23 and 6.24 whilst the measured band widths are given in Table 6.31.

Figure 6.21

Photograph of the failed cross-section Specimen 1 unnotched

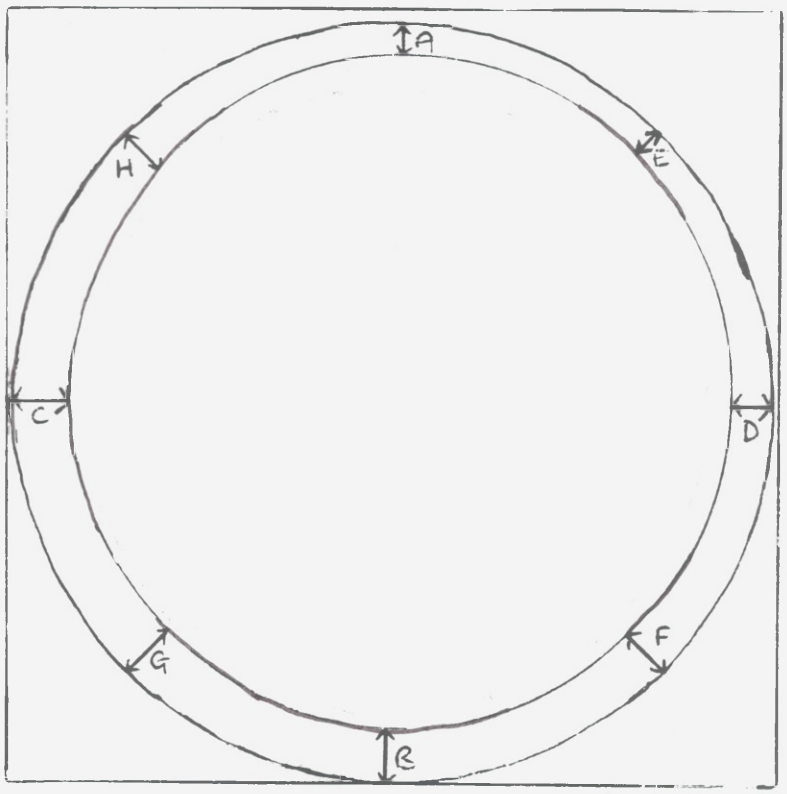

Figure 6.22

Diagram of the failed cross-section Specimen 1

Figure 6.23

Failed cross-section Specimen No. 2
notched

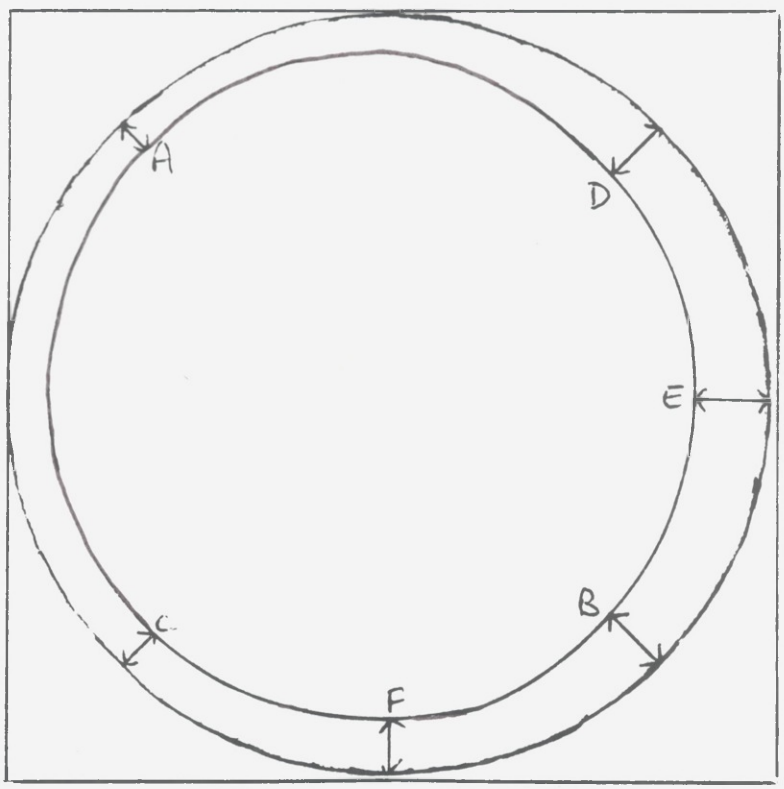

Figure 6.24

Schematic failed cross-section Specimen No. 2

Position	Band Width (mm)
A	.25
B	.56
C	.45
D	.46
E	.71
F	.70

Table 6.31

Measured Band Widths Specimen 2

These band widths indicate where the crack propagation rate changed from steady-state to fracture. The data obtained from this test is used to estimate crack propagation rates for this first period in Section 6.3.7 and for the estimates for m and C in Section 6.3.8.

6.3.4 Specimen Failure No. 3

This specimen was run at a high load of 2.5 kg for 16 hours when signs of initiation were noted. It was then run for 66 minutes at .5 kg load. On restarting at the high load (2.5 kg) fracture occurred almost immediately, (40 seconds) after restarting. The wide first band was measured; the results are given in Table 6.32, but the narrow dark band was difficult to measure with estimates of its width ranging from 0.20 to 0.40 mm being obtained. The mean value was taken to be 0.30 mm.

The end failure is pictured in Figure 6.25 and the diagram in Figure 6.26.

Figure 6.25

Failed cross-section Specimen No. 3
notched

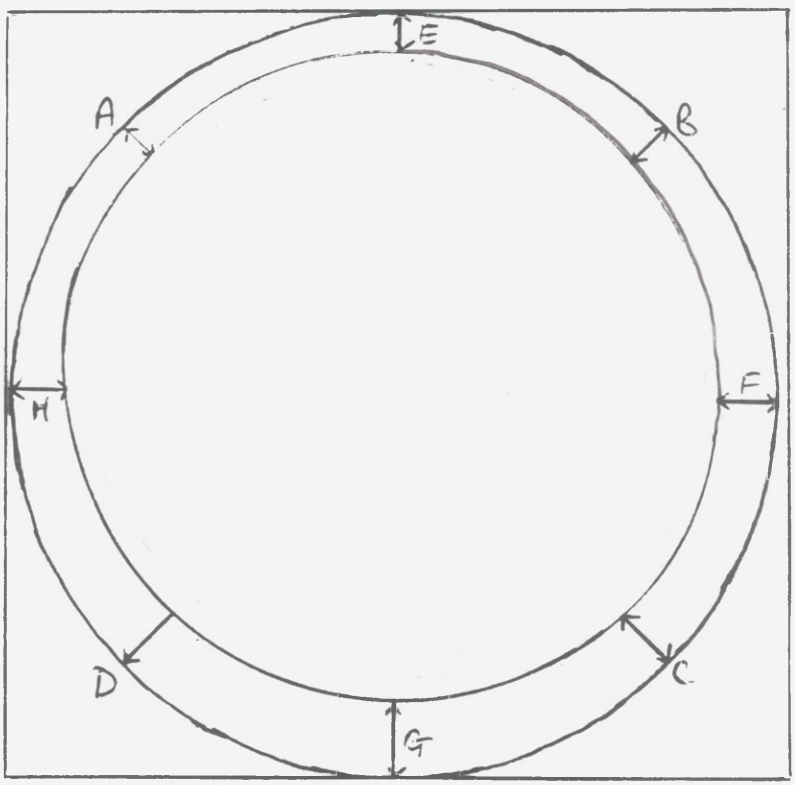

Figure 6.26

Schematic cross-section Specimen No. 3

Position	Band Width/mm
A	.54
B	.80
C	.82
D	.70
E	.67
F	.98
G	1.04
H	0.51

Table 6.35

First Band Widths Specimen 3

These failure bands are pictured in Figure 6.21.

The use of the data obtained from this first band is described in Section 6.3.7. The second low load band gives crack propagation rates of 1 to 2 x 10^{-6} mm/cycle. The failure of the second high load stage after 40 s (2000 cycles) gives a mean crack propagation rate of approximately 3 x 10^{-3} mm/cycle. This is a similar rate as found with specimen No. 1. The results for the low load cycle are used to estimate m and C in Section 6.37.

6.3.5 Specimen Failure No. 4 This specimen was run after the previous one and was very similar to it except that the load used was slightly lower, 2 kg instead of 2.5 kg. Unexpectedly, initiation occurred after 14 hours instead of the expected 20 hours. After initiation a low load band of 0.5 kg was achieved but again failure occurred almost immediately, 90 seconds after applying the high level load. This was despite the lowering of the high load to only 1.8 kg

instead of 2 or 2.5 kg as has been employed earlier. Measurements were more easily made on this second low load band because of its darker appearance in places. Lower width values were obtained than for the previous run, but the propagation rates obtained were of the same order of magnitude.

Results for the bands are given in Table 6.33 and these bands are pictured in Figures 6.27 and 6.28.

Band	Position	Width
1	A	.73
	B	.72
	C	.66
	D	.68
	E	.78
	F	.74
	G	.80
	H	.68
2	R	.18
	S	.25
	T	.25
	U	.23

Table 6.33

Band widths for Specimen Failure No. 4

The change between steady-state propagation and fracture cannot be identified. The failure after 90 seconds (4500 cycles) gives a crack propagation rate of approximately 1.4×10^{-3} mm/cycle. This is in agreement with the rates found for Specimen No. 1 and No. 3.

The figures for the crack propagation rates for the second (low load) are given in Table 6.34.

Figure 6.27

Cross-Section of failed Specimen No. 4
unnotched

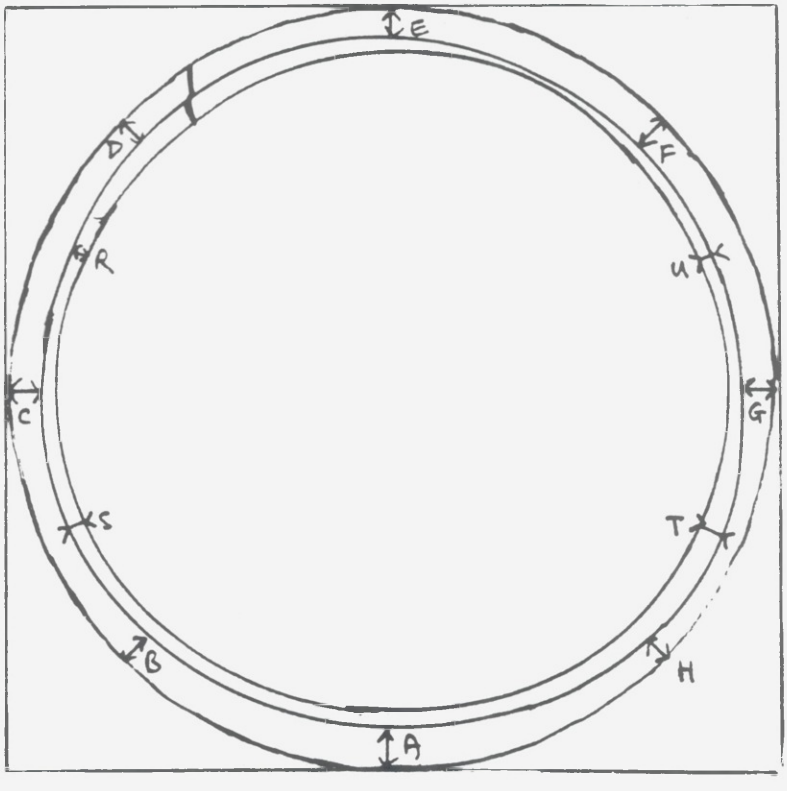

Figure 6.28

Schematic cross-section of failed Specimen No. 4

Distance Cracked		No. of Cycles	Crack Propagation Rate
Value	mm		mm/cycle
min	.18	200,000	0.90×10^{-6}
max	.27	200,000	1.35×10^{-6}
average	.23	200,000	1.15×10^{-6}

Table 6.34

Crack propagation rates for the low load band, Specimen No. 4

The use of this data for further calculations is described in Section 6.3.7 and Section 6.3.8.

6.3.6 Specimen Failure No. 5

When the test rig was delivered, six standard specimens were supplied. Subsequently a new batch of six specimens, made to Figure 5.9 were supplied. These newer specimens were used for the previous four failures. It was decided to try the technique on one of the older specimens. These older specimens were considerably softer (650 Hv 50) than the new batch (800 Hv 50). As the specimen was softer, its fatigue limit would be lower and so a lower load of 1.8 kg was used for the high load stages. This test was reasonably successful with four bands, two high load and two low load bands being obtained before fracture occurred soon after the start of the third high load band. The band failure section is pictured in Figures 6.29 and 6.30.

Figure 6.29
unnotched
Failed cross-section of failed Specimen No. 5

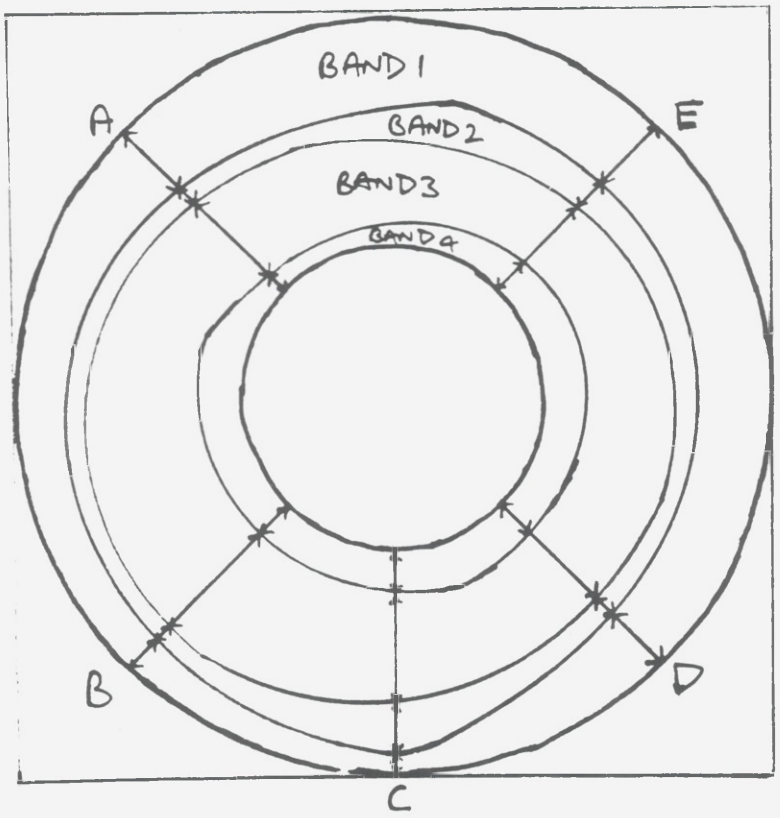

Figure 6.30

Schematic cross-section of failed Specimen No. 5

The band widths are given below in Table 6.35.

Band Width/mm	1	2	3	4
A	.81	.77	1.64	.34
B	.45	-	1.25	.30
C	.52	.60	-	.59
D	.74	.60	1.54	.20
E	.95	.90	1.81	-
min	.45	.60	1.25	.20
max	.95	.90	1.81	.59
average	.69	.72	1.56	.36

Table 6.35

Band Widths for Specimen No. 5

Deciding where one band ends and another starts was quite difficult, but Figure 6.30 illustrates that the examination of the failure bands was reasonably successful.

Failure of the specimen after 70 seconds (3500 cycles) after the start of the third high load band gave the specimen a fracture rate of 1.1×10^{-3} mm/cycle. Again this is the same order of magnitude as the previous specimens.

The crack propagation rates for three of the load levels are presented in Tables 6.36, 6.37 and 6.38.

Distance Cracked		No. of cycles	Crack Propagation Rate
Value	mm		mm/cycle
min	.60	200000	3.0×10^{-6}
max	.90	200000	4.5×10^{-6}
average	.72	200000	3.6×10^{-6}

Table 6.36

Crack propagation rates for the first low load band Specimen No. 5

Distance Cracked		No. of cycles	Crack Propagation Rate
Value	mm		mm/cycle
min	1.25	50000	2.50×10^{-5}
max	1.81	50000	3.62×10^{-5}
average	1.56	50000	3.12×10^{-5}

Table 6.37

Crack propagation rates for the second high load stage, Specimen No. 5

Distance Cracked		No. of cycles	Crack Propagation Rate
Value	mm		mm/cycle
min	.20	200000	1.00×10^{-6}
max	.59	200000	2.95×10^{-6}
average	.36	200000	1.80×10^{-6}

Table 6.38

The crack propagation rates for the second low load stage

Specimen No. 5

6.3.7 Analysis of Results

It can be seen that the tests were just beginning to yield useful results with multiple bands when final failure of the test rig occurred. This was somewhat unfortunate and reflects the difficulty in finding an appropriate load level/specimen hardness combination to yield crack growth rates neither too rapid nor too slow for testing. In this section the use of crack propagation rates to evaluate propagation rate constants will be discussed. Prior to that, the use of first band data will be considered.

6.3.7.1 Initiation Bands

A limitation of the current study is, due to the tendency for most of the specimens tested to fracture almost immediately after application of the second high load stage, there was only very limited crack band-width information.

In all tests a clearly defined initial band was formed, at high loads. However, analysis of this was difficult since, as with other fatigue bands it was not known when this started to develop ie exactly when a crack started to propagate. Since this initial band information formed the bulk of data available, it was decided to attempt to analyse it, despite the uncertainties as to the time of initiation. Some assumptions were therefore made about the start of crack propagation as follows.

It has long been believed in rolling contact fatigue that the majority of the time to failure consists of the initiation phase (13),(14), with the fracture at the end taking negligible time. Values for the propagation phase of between 1 and 10% of the time to failure have been suggested. Recent work by Yoshiaka and Fujiwara (15), and by Goto and co-workers (126), suggested that the propagation phase only lasts about 2% of the time to failure. In this analysis it is assumed that the specimens have initiated after a certain fixed fraction of the total number of cycles of the first high load stage of the fatigue test. The propagation phase is this remaining fraction. Exact

knowledge of this fraction which is propagation is not available, so estimates of the crack propagation time to failure of 1,2, and 10% of the total life to failure, are used. Table 6.39 shows calculated results.

Specimen No	Total cycles to Initiation/ failure	Assuming % is propagation		
		1%	2%	10%
1	1.62×10^6	16200	32400	162000
2	0.945×10^6	9450	18900	94500
3	2.88×10^6	16200	28800	288000
4	2.52×10^6	25200	50400	252000
5	1.08×10^6	10800	21600	108000

Table 6.39

Number of cycles for each specimen at 1, 2, 10, 100% of life

Using the estimates for the propagation period, and the distance cracked in the first band described in the previous sections, the crack propagation rates for all specimens are calculated below.

10% of life crack propagation rates

The crack propagation rates on the assumption that propagation takes up 10% of the life, in terms of their minimum, maximum and mean cracked distances, are given below in Table 6.40.

Specimen No	min cracked distance rate 10^{-6} mm/cycle	max cracked distance rate 10^{-6} mm/cycle	mean cracked distance rate 10^{-6} mm/cycle
1	4.3	6.9	5.3
2	2.7	7.5	5.5
3	1.8	3.6	2.6
4	2.6	3.2	2.9
5	4.2	8.8	6.4

Table 6.40

Crack propagation rates for all specimens at 10% propagation life

Values obtained are all of the same order of magnitude

2% of life crack propagation rates

The crack propagation rates for each specimen at the 2% of life level at minimum, maximum and mean cracking distances are given below in Table 6.41.

Specimen No	min cracked distance rate 10^{-5} mm/cycle	max cracked distance rate 10^{-5} mm/cycle	mean cracked distance rate 10^{-5} mm/cycle
1	2.2	3.5	2.7
2	1.3	3.8	2.8
3	0.88	1.8	1.3
4	1.3	1.6	1.4
5	2.1	4.4	3.2

Table 6.41

Crack propagation rates for all specimens at 2% propagation life

The values are again all the same order of magnitude and, as to be expected, five times higher than those of the 10% life.

1% of life crack propagation rates

The crack propagation rates for the assumption that propagation takes only 10% of the life time to failure, are given below in Table 6.42.

Specimen No	min cracked distance rate 10^{-5} mm/cycle	max cracked distance rate 10^{-5} mm/cycle	mean cracked distance rate 10^{-5} mm/cycle
1	4.3	6.9	5.3
2	2.7	7.5	5.5
3	1.8	3.6	2.6
4	2.6	3.2	2.9
5	4.2	8.8	6.4

Table 6.42

Crack propagation rates for all specimens at 1% propagation life

As expected the results are one order of magnitude higher for the 10% higher than the 1% propagation life level.

Interpretation of initiation data

It is clear from the results that initiation and propagation do not occur instantaneously. There is a finite time for initiation which appears to be between 90 and 99% of life (14). Propagation takes between 10 and 1% of life although in some cases, depending on the stresses involved may be even faster ie less than 1% of time to failure. In the cases studied, the propagation does take a measurable time. The crack propagation rates obtained under the high load are all much faster than under the low load. This ties in with the Paris equation (Eq. 2.3) that crack propagation rate depends on the stress intensity factor. The use of the Paris equation and the recent work of Goto and co-workers (126), is further presented in the next section.

6.3.7.2 Evaluation of crack Propagation Rate Parameters

The Paris equation, Eq. 2.3, involves two materials constants C and m. The evaluation of these parameters for specimens of one specimen batch and for the four bands of the softer specimen, were calculated from the method given in Appendix 9. No result was calculated for one of the failures because only one failure band was obtained. For the softer specimen with four bands, it was possible to obtain m and C from a graph of da/dN versus Δk. The results for m and C are given in terms of their maximum and minimum values based on the averages for values of da/dN and Δk. The results are given in Table 6.43.

Specimen No	Constant m		Constant C	
	max	min	min	max
1	3.83	3.04	5.47×10^{-5}	1.68×10^{-4}
3	7.69	4.18	7.3×10^{-5}	3.62×10^{-4}
4	2.54	1.62	1.14×10^{-6}	2.42×10^{-5}
5	2.94		4×10^{-5}	

Table 6.43

Values of Paris Equation parameters (13) m and C

The main problems in calculating m and C was the extensive calculation that had to be made on each of the variables in order to obtain estimates of the parameters.

6.3.7.3 Short Crack Calculations

Recent work Goto and co-workers (126), suggested that for small fatigue and lengths, the Paris equation was not valid but instead Eq. 6.1 should be used, where σ_n the stress amplitude is used, instead of Δk.

$$\frac{dl}{dN} = C (\sigma_n)^m l \qquad \text{Eq. 6.1}$$

The terms are the same as in Equation 5.3.

Rearranging equation 6.1 and integrating between initial and final crack lengths, the modified equation 6.2 is obtained -

$$\ln \left(\frac{l_2}{l_1}\right) = C (\sigma_n)^m (N_2 - N_1) \qquad \text{Eq. 6.2}$$

where the subscripts define the initial ($_1$) and final states ($_2$)

This can only be applied to specimens No. 1, 3 and 4 as a whole and to the three inner bands of Specimen No. 5.

When the results were put into the equation 6.2, completely diverse results were obtained such that it was impossible to draw a straight line through the points with any degree of certainty. There was insufficient further analysis by this method.

One reason for the strange results is probably due to the suggestion of Goto and co-workers (126), that their modified equation (Eq. 6.1) is only valid for very small cracks of the order of 1 mm long. In this study the crack lengths were between 0.7 and 3.6 mm long.

In the next section these results are compared to those of previous workers and in the last section the validity of the test method is discussed.

6.3.8 Comparison of Crack Propagation Data with Previous Work

As Eisenstadt and Fuller (118), used a different type of steel, carried out their tests in air and used different loads, no direct comparison can be made for the two sets of results. One feature of the work of Eisenstadt and Fuller (118), was that a lot more failure bands were obtained for each specimen than in the current study. This was almost entirely due to the lower loads and shorter loading cycles used. The steels used may also have been less brittle, but this cannot be confirmed.

The results from the six specimens from the same batch are plotted on an S/N fatigue plot, Figure 6.31.

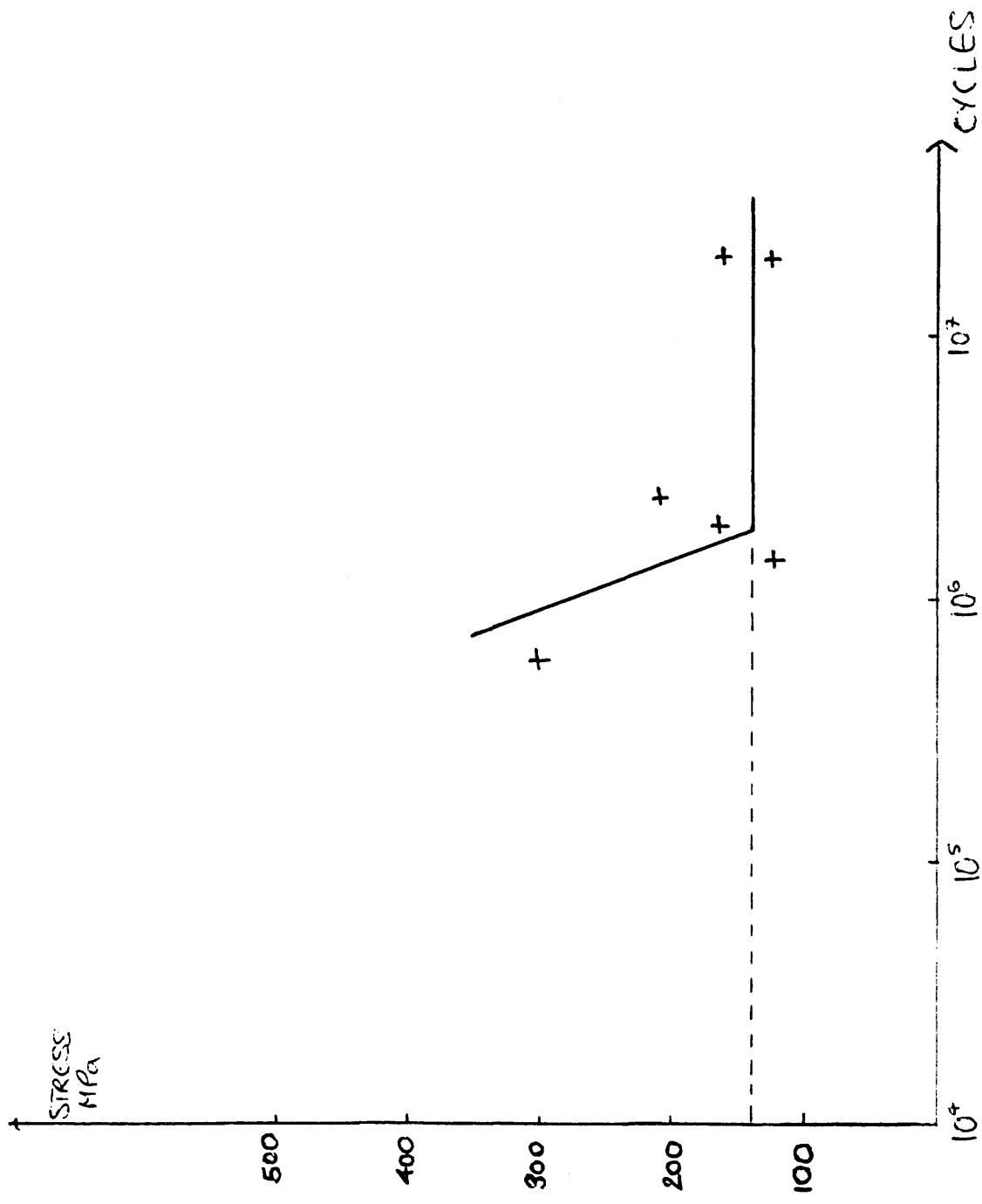

Figure 6.31

A load/life plot for the Rotating-Bending Specimens

An estimate of the fatigue limit is about 140 MPa. This figure is smaller than the results obtained by Armstrong and co-workers (82), using a similar specimen design for an SAE 20 mineral oil of about 720 MPa without water and 300 MPa containing 0.05% water (500 ppm). The differences are probably due to different surface treatments of the specimens and the influence of the extra water and surface active additives used in the Aquacent Light.

Eisenstadt and Fuller (118) also carried out some orthodox rotating-bending fatigue tests using similar equipment to that used by Armstrong and co-workers, (82). They found similar results for two mineral oils both with and without water. A test was also carried out using distilled water as the test fluid. This gave similar results to the mineral oils with added water at high stress levels, but at low stress levels the water failed to give a fatigue limit and the plot was as described by Harris (119).

When the values of m and C are compared with the results of others working in the field, reasonable correlation is obtained. Zheng and Hirt (127), in their review of the propagation of fatigue cracks in steels, suggested that most workers had found values of m to be in the range of 2 to 4 with C being the true material parameter. Other workers had suggested that the value of m was in the range 1.4 to 9.66. The results obtained in this study are in this range, but there are no quantitative details about the influence of water in the paper by Zheng and Hirt (127).

In 1974, Polk and co-workers (16), used the interrupted stressing technique to measure crack propagation rates for hardened and soft AISI 52100 steels in media with and without water. The values of crack propagation rates obtained by Polk, Murphy & Rowe technique were

considerably higher than those obtained in this study but this is because the values of Δk used by Polk and co-workers (16), were considerably higher. The values of constants m, and C obtained were 2.63 and 2.13 x 10^{-4} $mm^{3/2}$/MPa/cycle respectively. These values are very similar to those obtained in the current study by the Paris method. The main difference was, however, that Polk and co-workers used a drip lubrication method whilst in this study an immersion lubrication method was used. The influence of this difference in lubrication method on the crack propagation rate is not known. The validity of the test method and other influences on the results are discussed in the next section.

6.3.9 Validity of the Rotating-bending Test Method

In the following sections the rotating-bending test method, its use in the current study and analysis methods are reviewed and discussed.

6.3.9.1 Comparison with Contacting Methods

In section 4.8, non-contacting test methods were described but no comparison between them and contacting test methods as made. Contacting test methods are influenced by the factors described in table 2.4. In this study two different steels were used, S135 for the rotating-bending work and En31 (S82) for the rolling contact fatigue tests. The lubricant was the same in both types of test. The biggest difference between the two apart from the fact that one is contacting and the other is not is the loading cycle and hence the stress pattern.

In the rotating-bending situation, the normal loading follows a sinusoidal pattern as shown in Fig 6.32. The contacting method follows a cycle as shown in Fig 6.33. The stress pattern for the rotating-bending specimen follows a similar pattern to the loading cycle but in the contacting cycle the stress field is very complex. Also in the rotating-bending case the stress is directly responsible

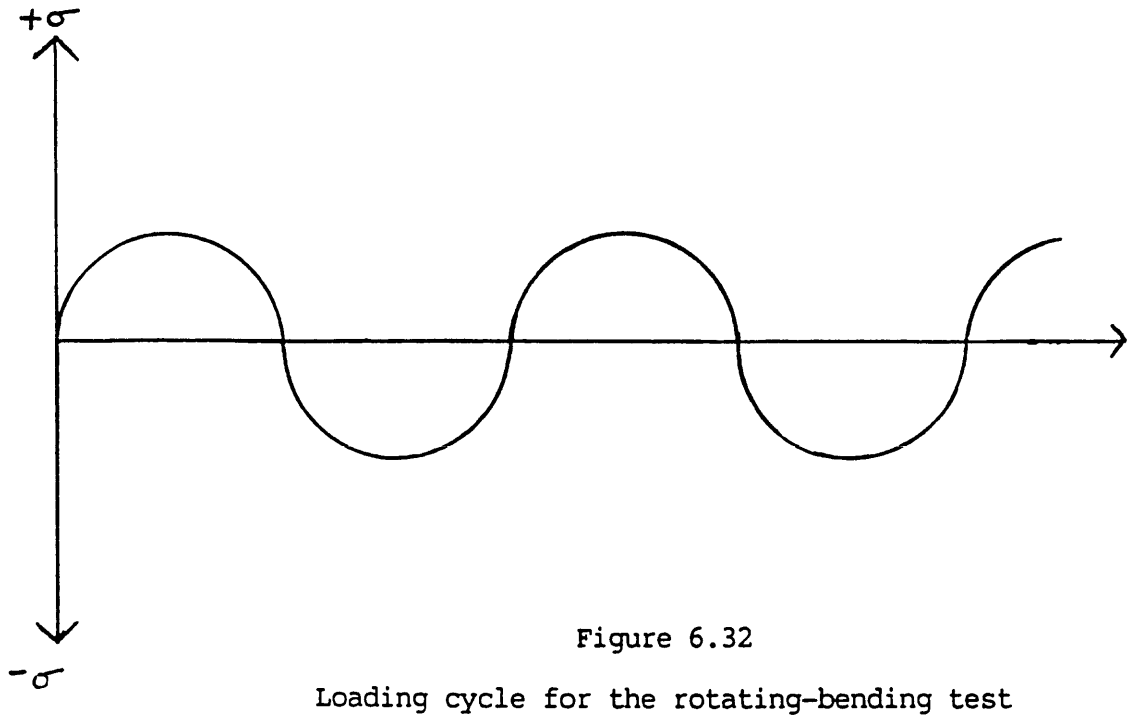

Figure 6.32

Loading cycle for the rotating-bending test

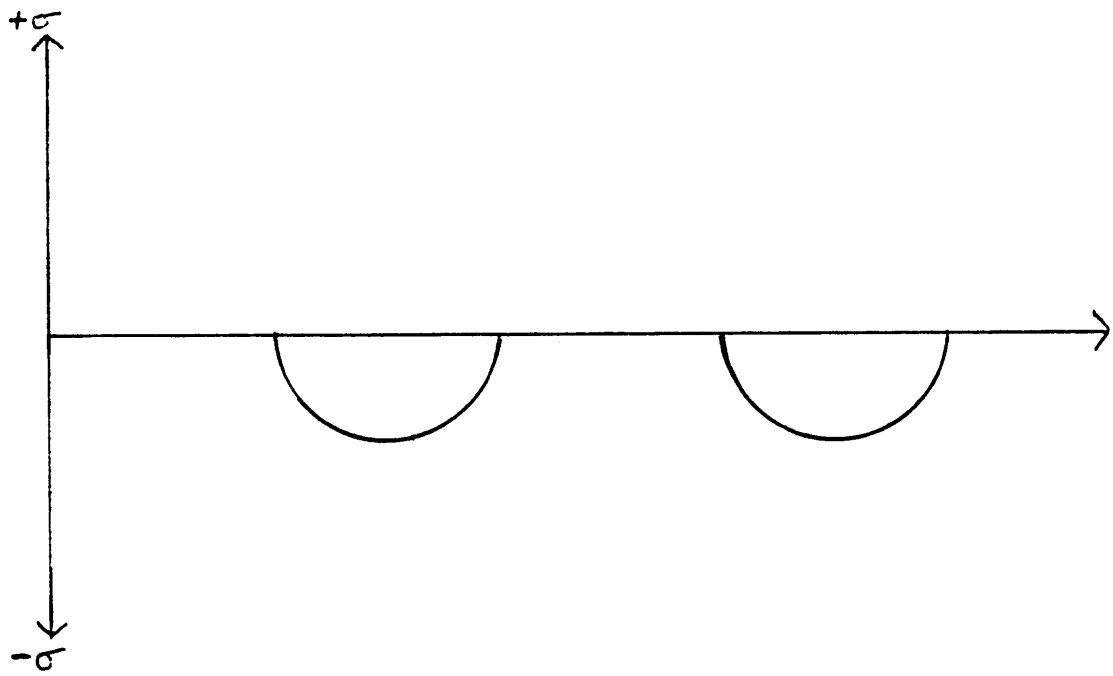

Figure 6.33

Loading cycle for a Rolling Contact

for crack propagation but the stresses causing crack propagation in the contacting region are very complex and not fully understood. The stresses in the contacting region are a mixture of normal, shear and orthogonal stresses plus the added elastrohydrodynamic pressure spike at the exit of the contact.

The stress in the rotating-bending situation has a maximum value of about 600 MPa whilst the contacting hertzian stress is one order of magnitude higher at about 6 GPa.

Crack propagation rates in both cases depend on the material and on the stress cycle. Overall fatigue lives for both types of fatigue test do depend on the lubricant environments but the lubricant appears to balance in different ways.

According to Goto and co-workers, (126), the presence of a lubricant in rotating-bending fatigue test work increases the fatigue limit by reducing the crack propagation rate by damping the sliding of the crack faces. From the work of Way,(2) and Murakami and co-workers, (39), the lubricant is the cause of pitting, without it, pitting would not occur. This was as in tests carried out on the AOL described in Section 6.2.2.

One area where the lubricant has a similar influence is when corrosion occurs. This is discussed in the next section.

6.3.9.2 Comparison of Corrosion Effects

In Chapter 3, the influence of corrosion on rolling contact fatigue was discussed. The influences were thought to be due to the presence of water and oxygen and surfaces where there is a potential difference. In both contacting and non-contacting methods corrosion appears to have an effect when the life to failure becomes long. The formation of corrosion pits in metal surfaces is a very time-dependent process. In Section 4.8 the influence of corrosion on the fatigue life of steel was discussed with the conclusion that long-life specimens have no fatigue limit because corrosion lowers the fatigue strength of the specimen, (119). When rolling contact fatigue tests are carried out above a limiting c/p value the specimen ought to have a near infinite life but failure always occurs due to corrosion causing a lowering of fatigue strength.

The use of specialist crack propagation reciprocating rigs other than rotating-bending fatigue rigs is further discussed in Chapter 9.

6.3.10 Summary of Rotating-bending Test Work

It was hoped that the test programme embarked on would have thrown a new light on the way that rolling contact fatigue and the presence of water influenced crack propagation. Unfortunately, due to the catastrophic rig failure described in Section 6.3.1. Only a few results were obtained. The results were analysed by the original methods of Paris and Erdogan,(13), and Polk and co-workers and by the newer method suggested by Goto and co-workers, (126). Good agreement was obtained with the results of Polk, but not so with the results of Goto. The validity of the method of Goto was not known because it does not yet appear to have been deeply analysed.

The results obtained on this rig are further discussed in the next chapter.

6.4 CHEMICAL ANALYTICAL TECHNIQUES

Three types of techniques were used to analyse the deposits and surfaces described in earlier sections. These were scanning electron microscopy (SEM) infra-red spectroscopy (IR) and secondary ion mass techniques are described in the following sections.

6.4.1 Infra Red Spectroscopy

The deposits grown on the bar specimen described in section 6.1.2.5 were first examined by reflective infra-red using a Perkin-Elmer machine. The uncleaned specimen bar was carefully positioned so that the infra red beam was reflected through the surface layer off the surface to the detector. Most films examined in this way showed similar results but the spectra obtained were not very good. The poor quality of the spectra obtained was due to the fact that when the films were fairly thin, only a small amount of absorbance was recorded except in bands arising from the water present. Where the layers were very thick, almost total absorption of the infra red was formed. To surmount these problems, some of the layer was scraped off and run in transmission mode between KCl plates. The resulting spectra is pictured in Fig 6.34.

The spectra again indicates the presence of a large amount of water, but seems to show the presence of organo sulphonates. Organo-sulphonates are used as the emulsifying agents to allow the oil to be dispersed throughout the water phase.

Infra red spectroscopy was also used to examine the plastic film on the bar specimen described in Section 6.1.2.8 from "as received" aqueous glycol film. The spectra in this case did not show anything of significance as the only bands seen were water and hydrocarbon-related. This is possibly due to the presence of the polyglycol polymer from the glycol and it could not be confirmed.

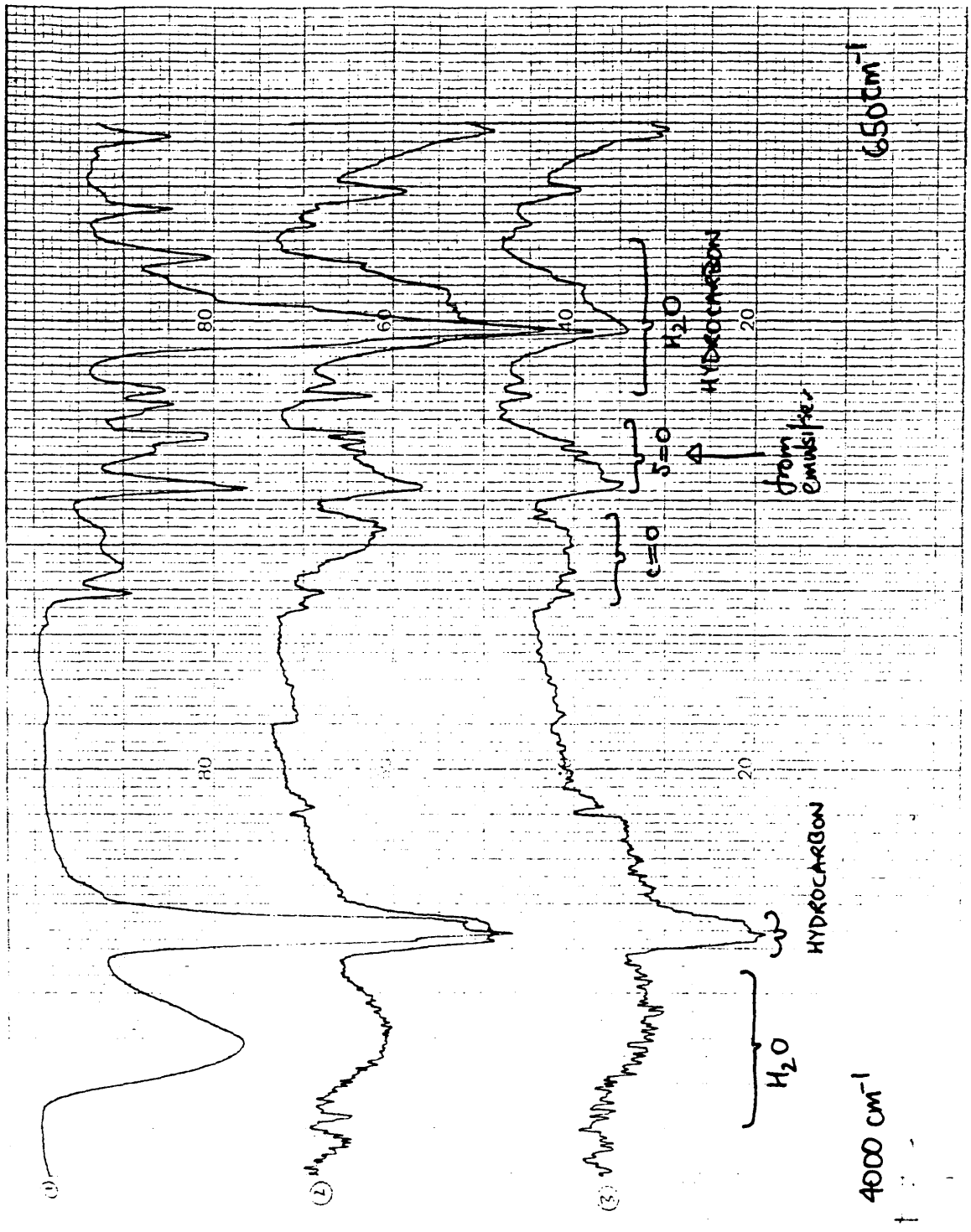

Figure 6.34

IR Spectra of the thick film residue

Growths from the polymer-thickened fluids were also examined but the results were similar to those found by the aqueous glycol, though because of the amount of water involved they were far more obscured than with the polyglycol. The presence of a zinc dialkyldithiophosphate was possibly detected with bands in the 1200 cm^{-1} region but this could not be confined. The raceway from the 1% sodium stearate solution run on the AOL rig described in Section 6.2.2 was also examined by infra red. The spectra obtained was of poor quality due to the very thin film formed but was comparable with a reference spectra of stearic acid, the difference being on a slight shift of the C=O and C-O bands. Water again interfered.

The main problem of using single beam infra-red spectroscopy to examine both water and oil based lubricants is the presence of the very large background water and oil bands. This is further discussed in Section 7.4.3.1.

6.4.2 Scanning Electron Microscopy

The scanning electron microscope has been used for a number of years to examine failures brought about by rolling contact fatigue. In 1965 Reichenbach and Syniata, (125), examined a whole series of rolling contact fatigue pits on balls from a rolling four-ball rig. After having used SEM to electron micrograph spalls they employed transmission techniques to view the structure of the balls and concluded that cracks initiated at grain boundaries. This work showed how valuable a powerful tool SEM could be.

Swahn and co-workers,(128), also looked at structural changes in balls caused by rolling contact. They concluded that the stressing caused changes in the structure and demonstrated this by a series of electron micrographs.

Nakayama and Takano, (129), examined the crack tips of sheet specimens having undergone cyclic stressing in corrosive environments. They tried to examine the mechanism behind stress corrosion cracking (SCC) and hydrogen embrittlement (HE) in stainless steel specimens and concluded that hydrogen embrittlement operated by a different mechanism to SCC. Nakayama and Takano, (129), concluded that HE was the prime cause of fatigue cracking in martensitic stainless steels. In Chapter 7 the role of hydrogen embittlement is further examined.

In a recent paper by Jahanmir, (130), worn camshafts from a Taxi fleet were examined by a variety of analytical techniques including SEM. SEM illustrated the presence of cracks in the camshafts and to show the presence of carbon layers on the surface. The paper illustrated that for some uses, especially elemental analysis by back scattering techniques, SEM has been superseded by more modern, more sophisticated techniques such as Auger Electron Spectroscopy (AES) Electron Diffraction and X-ray (EDAX) and Secondary Ion Mass Spectroscopy (SIMS).

In this study SEM was used to examine failed specimens prior to SIMS analysis to ensure that problems such as the presence of grinding disc fragments were not present. The electron micrograph in Fig 2.1 was taken of a failed ball specimen from series 1. The micrograph below illustrates the problems of debris on failed raceways, Figure 6.35.

6.4.3 Secondary Ion Mass Spectroscopy

Secondary Ion Mass Spectroscopy is a technique where ions, either Cs^+ or O_2^+, are fired at a surface from an ion gun and this results in the removal of the surface and subsequent examination by mass/charge ratio in the mass spectroscopy.

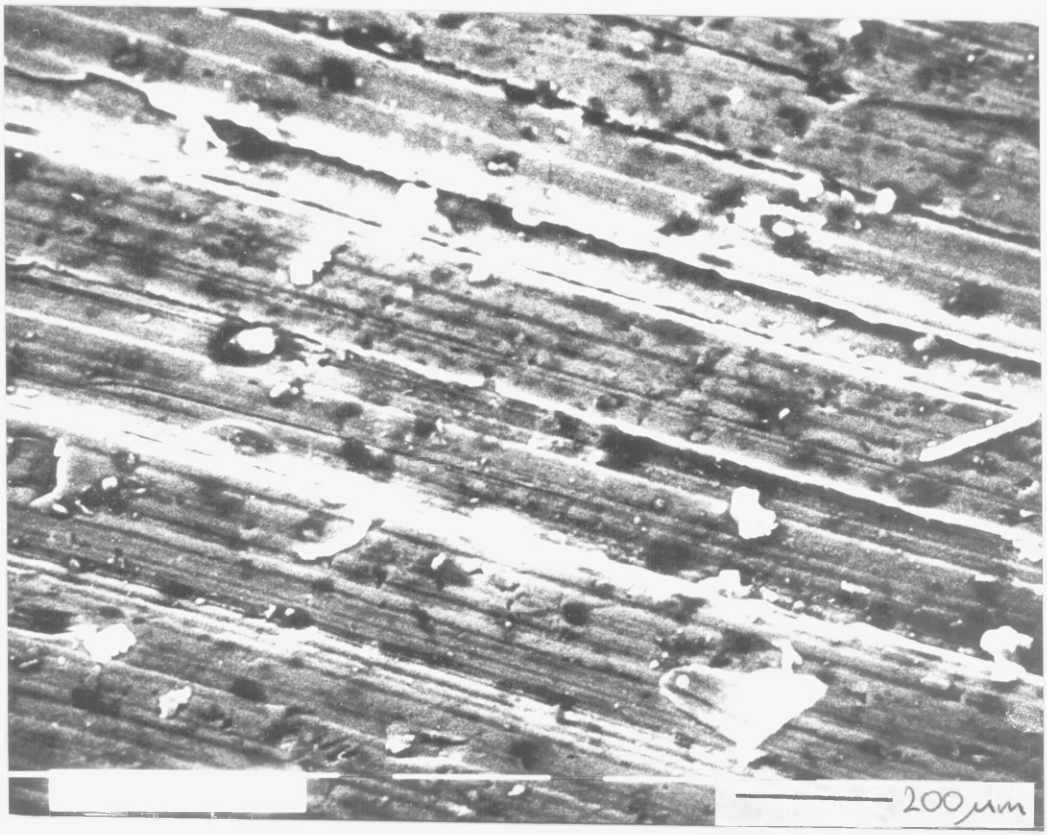

Figure 6.35

A micrograph of a failed raceway illustrating the problem of debris

In 1980, Zinner, (131), described the use of SIMS for depth profiling. Depth profiling is a technique where the secondary ion gun is used to rapidly remove surface layers such that the layered composition of the surface may be examined. This technique has been extensively used for the examination of wafers for silicon chip production.

In 1984, Suzuki and Ohtsubo, (132), described the detection of hydrogen in steels by SIMS in order to arrive at a quantitative method to measure the hydrogen content of steels. It was possible to measure hydrogen easily in some other metals but steel had proved difficult. The aim of the work was to enable a better assessment of hydrogen embrittlement to be made. It was observed that the choice of primary ion was important in that caesium (Cs^+) gave reproducible results generally and oxygen (O_2^+) produced scatter. Oxygen appeared to be better for the detection of organic material, (133). A problem in the qualification of hydrogen was the requirement of a ultra high vacuum of 10^{-9} Torr against the usual 10^{-7} Torr. This technique offered possible uses for mechanistic studies.

As described in the previous section, Jahanmir, (130), used SIMS to examine taxi camshafts with depth profiling to 150μm. The surface layers found to consist largely of ion oxides but below this there were large amounts of the additive elements, especially in surface cracks. Where these cracks extended deeper into the surface, additive elements were also found at greater depths.

This work offered some good pointers to possible uses of SIMS in this current study.

This is described in the next section.

6.4.3.1 Use of Sims in this Study

The mechanisms for rolling contact fatigue were described in Chapter 3. One possible mechanism, the hydraulic mechanism, describes how lubricant is forced into surface cracks and transmits the contact pressure to the crack tip to cause propagation. Another possible mechanism describes how the lubricant penetrates crack opening and reacts with the fresh metal surfaces, - the chemical mechanism.

In order to try to prove either of these two mechanisms it was decided to use SIMS depth profiling to investigate the presence of lubricant additives and water in cracks in the specimens. If the failure mechanism is the hydraulic one it should be possible to find water trapped in the crack as the depth is explored down to an estimated 20μm. If however, the chemical method dominates, the water and additives which penetrated the crack would have reacted with the fresh metal surface to produce hydrogen and corrosion products. One of the ways in which this should be detectable is the presence of methane. Chandler and Walter, (134), described how hydrogen, generated in this case from the lubricant, reacted with carbon in high carbon steels to produce methane which formed voids in between grain boundaries and weakened the structure (reactive hydrogen embrittlement). One possible problem described by Suzuki and Ohtsubo, (137), was the high incidence of background water, linked to the O_2^+ ion, which may influence the results. One way of getting round this problem would be to use either ^2D_2O or $H_2{}^{18}O$ as the water in the emulsion although this would evoke considerable expense. The actual results obtained are described in the next section.

6.4.3.2 Sims Results - 1st Series

Three specimens were set in mounting plastic and scanned by the VG IONEX SIMS using O_2^+ as the primary ion in the order 1, 2, 3 as per Figure 6.36. The results for each of the three specimens are given in Figure 6.37 and Figure 6.39. The depth profiling was not used because of problems due to the mounting plastic and curvature of the specimens. The three specimens had been run for 2×10^6, 6×10^6 and 10×10^6 cycles visually there was no difference between appearance of three specimens and the SIMS results all give approximately the same results. The plastic in which the specimens were mounted also gave off gas which appeared to interfere with data collection and so the surface surrounding the specimens was coated with silver so as to prevent this gassing. It was recommended for future specimens that larger sections attached to metal discs, as per the SEM analysis, be used, (135).

6.4.3.3. Sims Results - 2nd Series

The second series of results were also carried out using a "VG IONEX" SIMS. Three specimens the spectra of which are given in figs c, b and 6. The first two specimens were on raceways run in the dilute emulsion whilst the third had been run in a 1 % by weight sodium stearate solution. All three specimens had been run for 10×10^6 cycles under the standard load of 6670 N. The surfaces showed similar appearance to that of Fig 2.5.

The results of both sets of results are discussed in Section 7.4.3 and the implications of the results for the mechanisms discussed in Section 7.5.

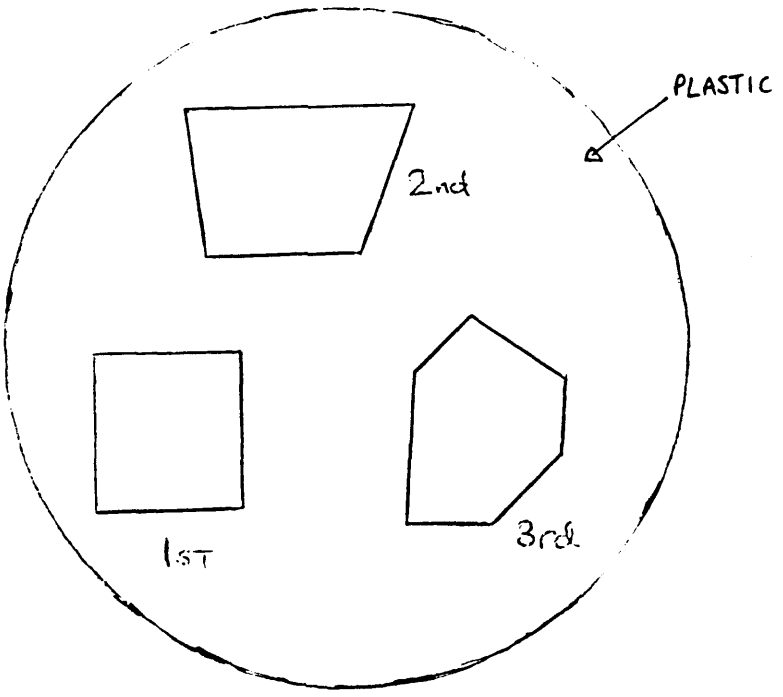

Figure 6.36

Specimens from the first SIMS Series

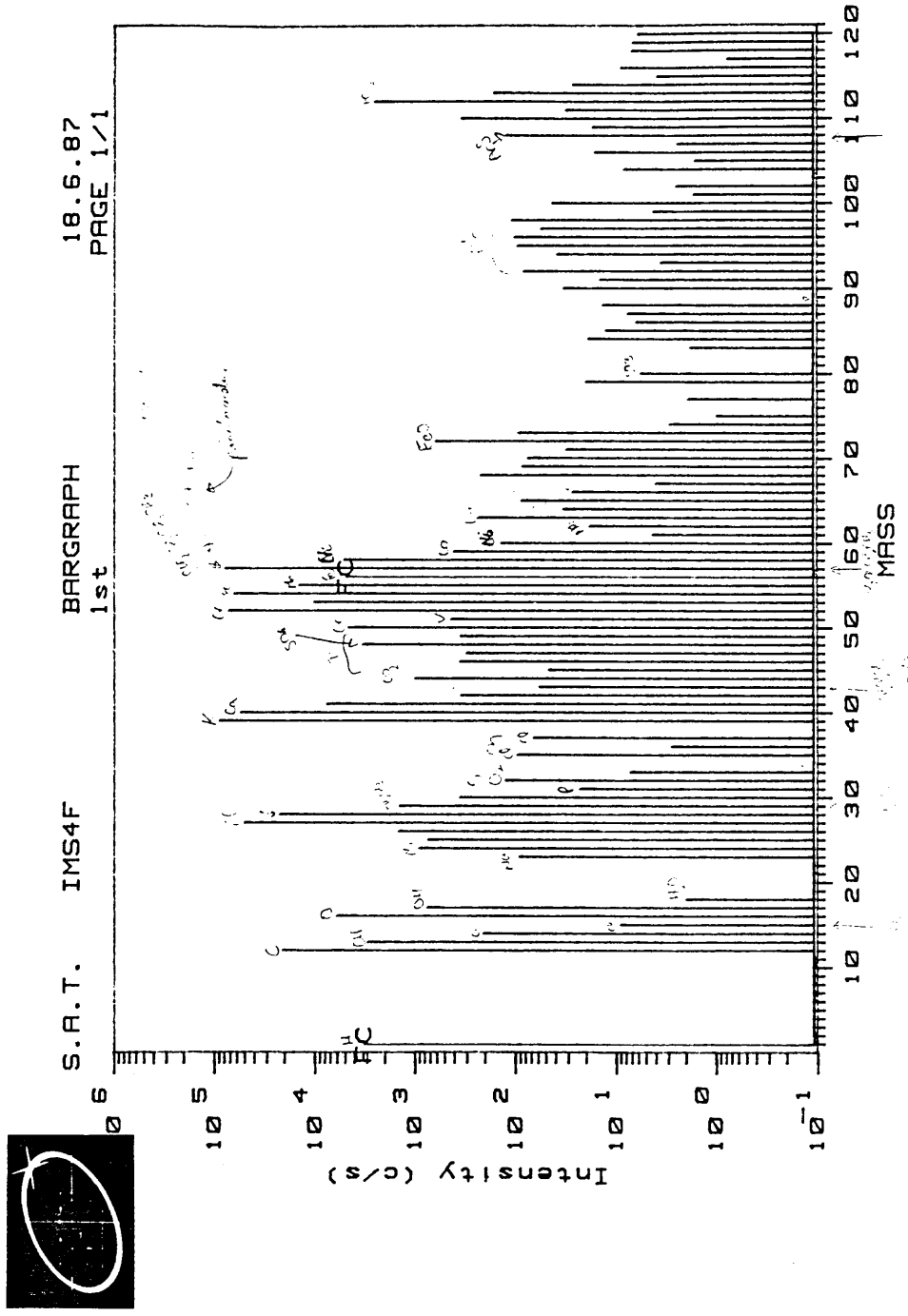

Figure 6.37

SIMS bargraph series 1, specimen 1

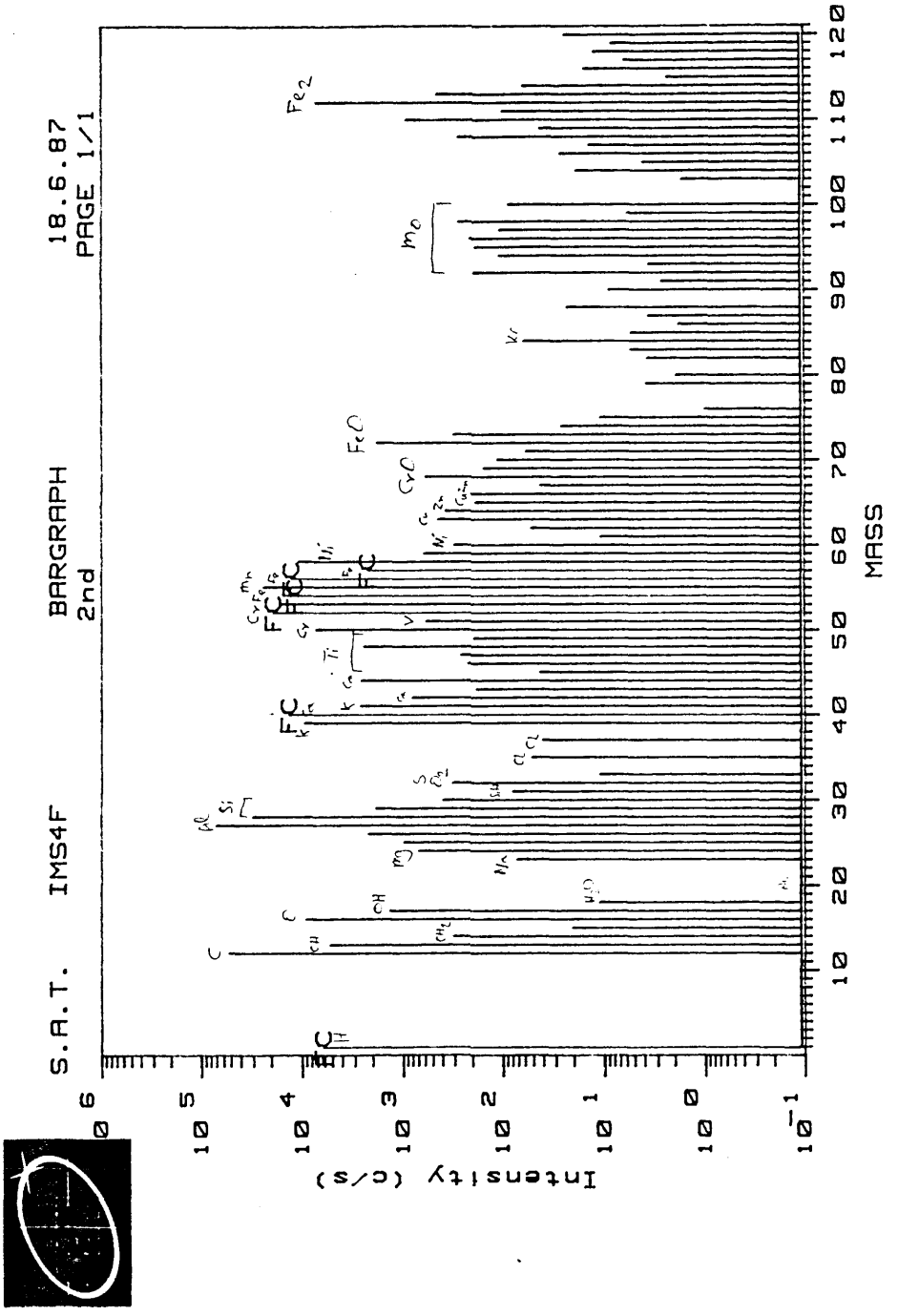

Figure 6.38

SIMS bargraph series 1, specimen 2

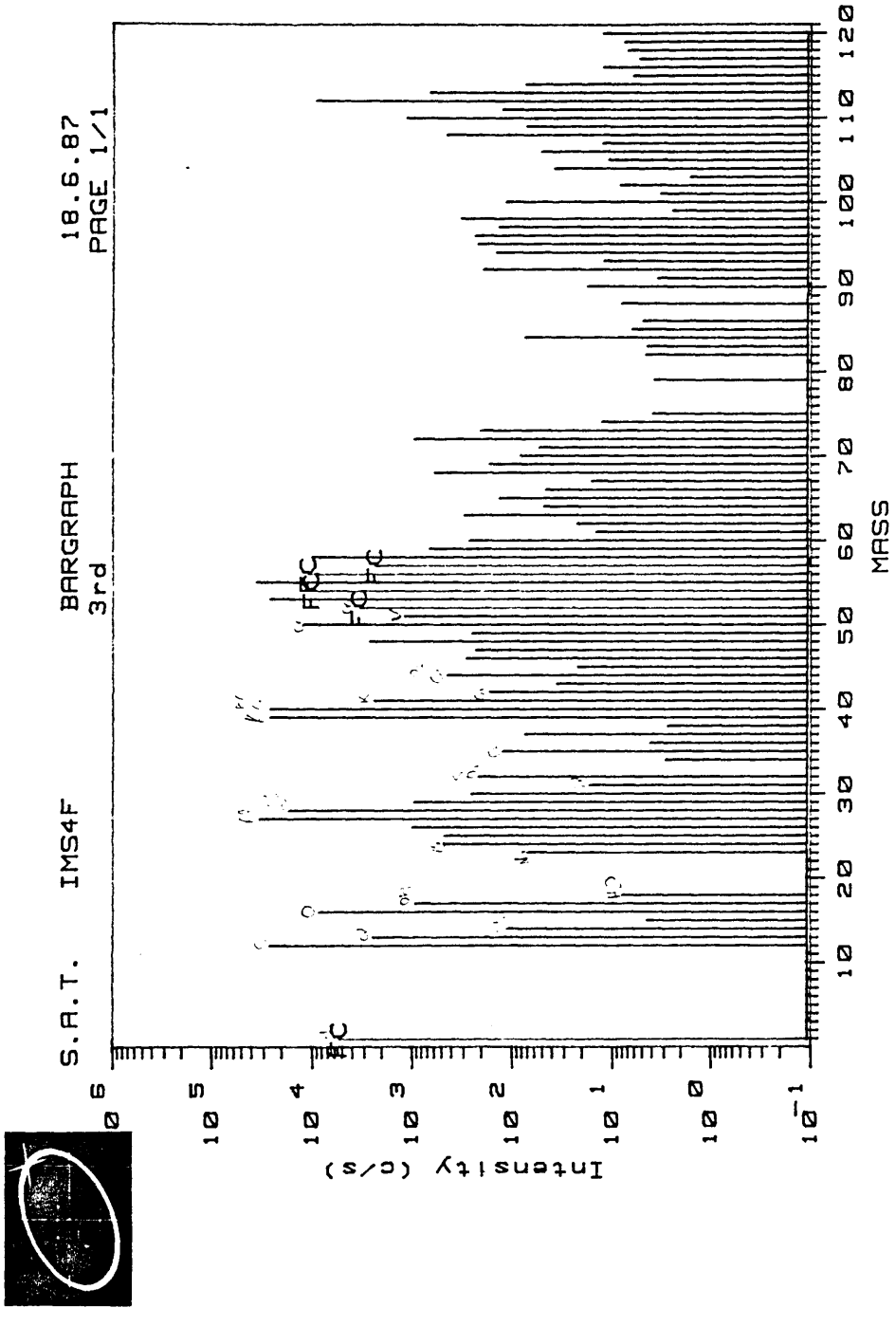

Figure 6.39

SIMS bargraph series 1, specimen 3

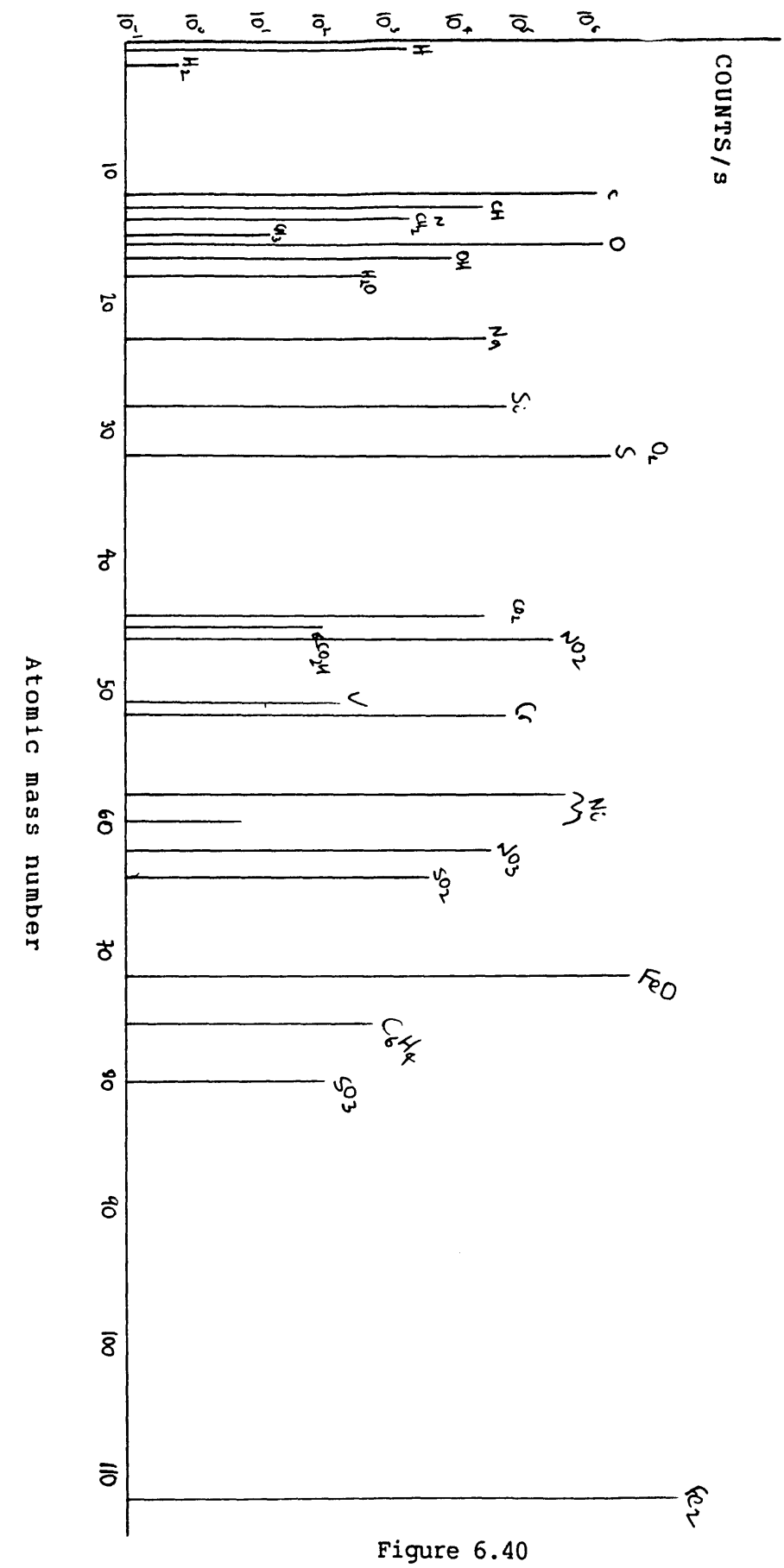

Figure 6.40

SIMS bargraph series 2, specimen 1

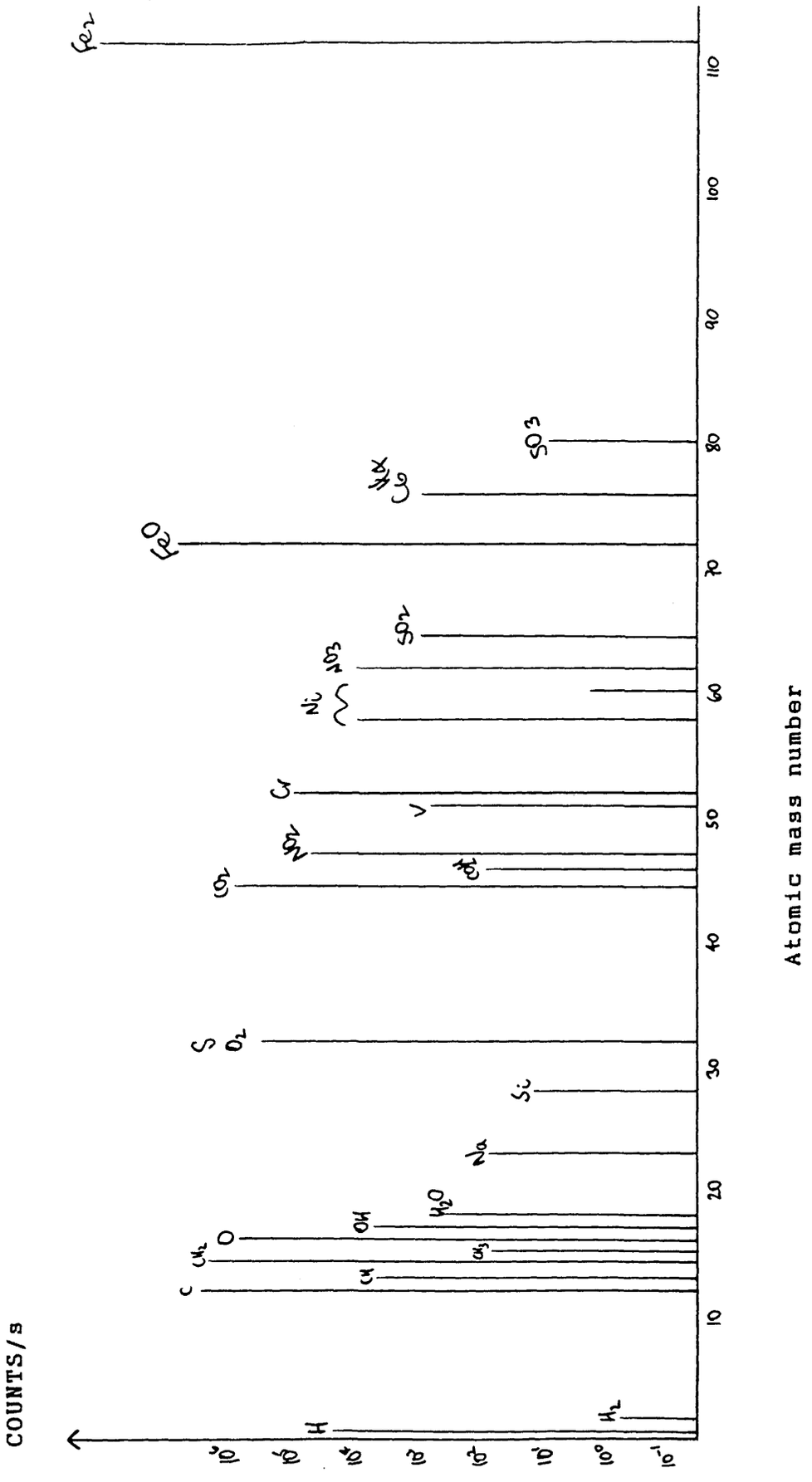

Figure 6.41

SIMS bargraph series 2, specimen 2

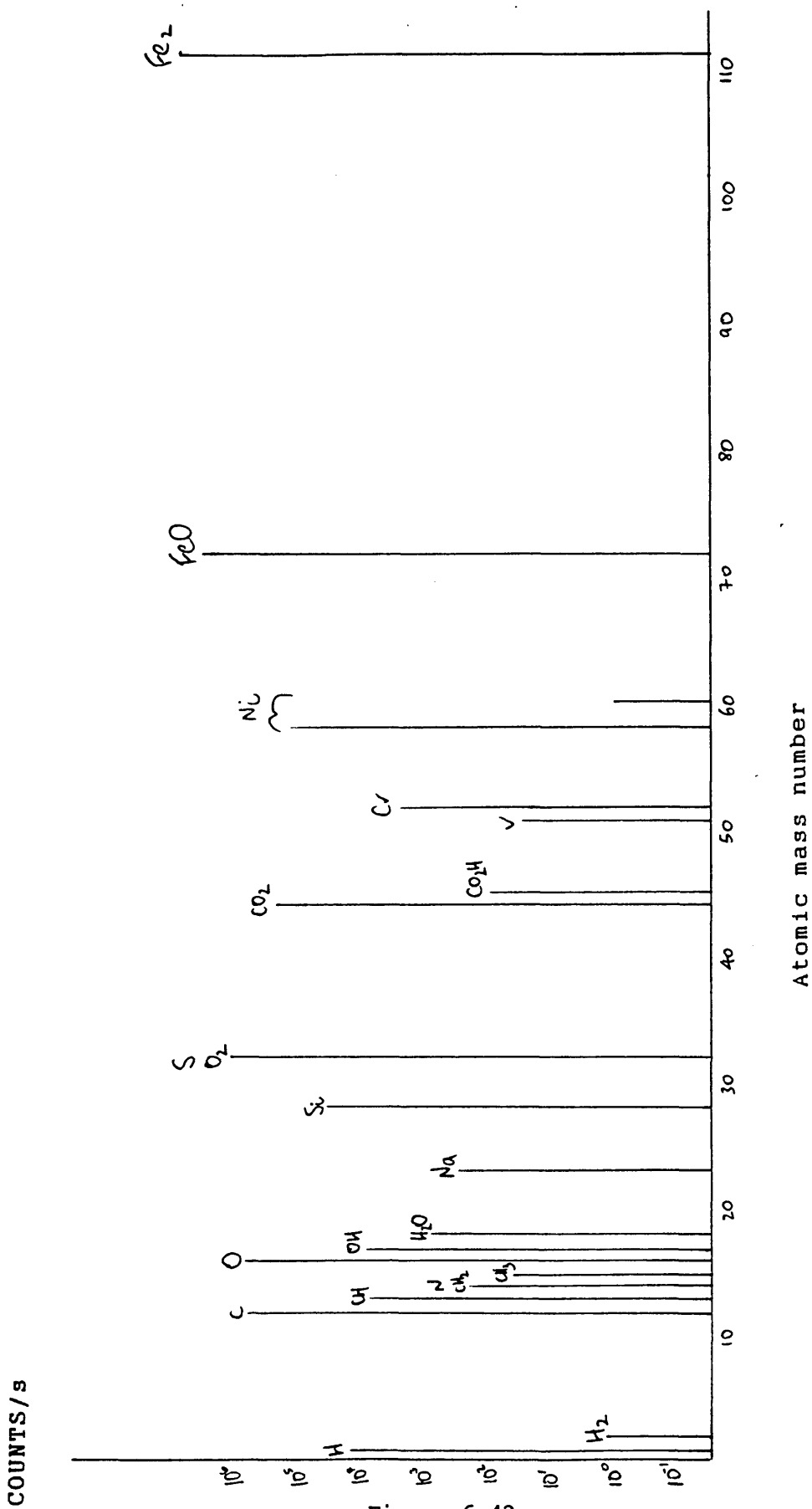

Figure 6.42

SIMS bargraph series 2, specimen 3
(sodium stearate solution)

7. DISCUSSION

In this chapter, the results described in the previous chapter are discussed and interpreted. Attention is focussed up on likely mechanisms operating when premature failure of bearing steels occurs.

7.1 THE EFFECT OF APPLIED STRESS

The results of the first four-head rig fatigue test series, table 6.3, indicated that specimen hardness had a greater influence on fatigue life than did combined stress at the level applied. This may however result from the effect of conforming due to wear as suggested by Nakajima, (123). Such conformation can override the reduction in fatigue life caused by the combined stress. Olver, (124), who analysed a similar contact situation of combined stresses, suggested that the way the combined stress was applied would have no influence on the fatigue life of the bearing steel and that the hardness of the two surfaces were the important factors. The reason offered by Olver, (124), was the maximum shear stress of the bending force was not in the correct direction to promote fatigue crack growth of the microcracks formed in the contact. The fatigue lives for the first three series are compared in table 7.1 together with the values of hardness of the specimens. The table is not a true comparison of the results but does give a qualitative feel for the influence of specimen hardness and combined stress.

Series	Hv 50	L_{10}	L_{50}	e	Bending Moment
3	780 $\pm$ 20	11.5	35	2.99	-
2	650 $\pm$ 20	0.73	6.4	1.42	-
1	770 - 850	2.3	21.0	1.39	20 Nm

Table 7.1

Weibull characteristics and hardness values for each batch of specimens run in 'Aquacent Light' on the four-head rig.

Ranking Fluid

% Statistical Significance, (18) between the two series at the L_{10} fatigue life level.

		% Water	IE	PTF	DE	AG	DAG
1.	Invert Emulsion (IE)	40	-	59	> 99	> 99	> 99
2.	Polymer Thickened Fluid (PTF)	90	58	-	95	98	99
3 =	Dilute Emulsion (DE)	95	> 99	95	-	N/A	N/A
3 =	Aqueous Glycol (AG)	47	> 99	98	N/A	-	N/A
3 =	Dilute Aqueous Glycol (DAG)	73.5	> 99	99	N/A	N/A	-

N/A = statistically significance was ~ 50%
and so the results were essentially the same.

RANKING OF THE FLUIDS AND THEIR STATISTICAL SIGNIFICANCE

Table 7.2

The application of combined stresses of the type used by Donsinas, (25), appeared to have no significant effect on the fatigue life of bearing steels. The most important effects appear to be specimen hardness and geometry for a given load and lubricant.

7.2 AGREEMENT OF FATIGUE LIVES OBSERVED WITH PREVIOUS RESULTS

The method of ranking fluids used in this study was as suggested by Kenny, (27), and by other workers (59), (64), was to compare their L_{10} fatigue lives. As shown in the previous chapter L_{10} fatigue lives per se, are not sufficient for ranking purposes and the statistical significance between sets of results must be taken into account. This is illustrated in table 7.2 which is a matrix displaying ranking and statistical significance of all the sets of results.

As described in chapter 3, the performance of mineral oils and phosphate esters had been compared in the past to those of fire resistant fluids and numerous other workers (27), (59), (64), (65), (67) are given in table 7.3.

Rank	Fluid
1	Mineral Oil
2	Phosphate Ester
3	Invert Emulsion
4 =	Dilute Emulsion Aqueous Glycol

The ranking of all classes of fluids

Table 7.3

No tests were carried out in this program on mineral oils nor on phosphate esters as it was anticipated that the fatigue lives would have been so long that it would have taken the order of nine months to produce a full Weibull plot for each fluid. When the L_{10} lives for the HF-A, HF-B and HF-C fluids obtained on the four-head rig are compared to the theoretical L_{10} lives of the three fluids from the adjusted formulae of Kenny and co-workers, (27), Eq 5.4, the current lives are considerably longer than the ones predicted by Kenny's equation. In Section 5.1.5, the dynamic capacity of the four head rig was shown to be 2043N and in table 5.2 the theoretical L_{10} fatigue life for a mineral oil at the capacity used in the four-head rig was given as 2.2 millions of cycles. However the values obtained for the invert emulsion aquacent light far exceeded this figure and was an order of magnitude greater than the reduced fatigue life of invert emulsions estimated by Kenny, (27), (table 7.4).

	Predicted from Kenny Formula $L_{10}/10^6$ cycles	Found in current study $L_{10}/10^6$ cycles	Ratio theoretical:actual
Invert Emulsion	0.767	11.5	1 : 15.0
Dilute Emulsion	0.248	1.35	1 : 5.4
Aqueous Glycol	0.342	2.35	1 : 6.9

Table 7.4

Comparison of Actual to theoretical lives for the three classes of fluid.

The actual trend is consistent with "Aquacent Light" still giving by far the best performance and the aqueous glycol giving a slightly better but similar L_{10} fatigue life to the dilute emulsion. The most likely explanation for the disparity of the current results with those of Kenny is that the latter were obtained over 10 years ago, and it is likely that products in use will have been developed and improved since then. A recent paper by Baker and Riley (53) showed that this was the case with respect to dilute emulsions. Company literature obtained in 1985 described slightly different properties for the same HF-C fluid used in the study to literature obtained in 1987 in terms of density and viscosity. This would clearly indicate that the fluid has been modified since its introduction to meet the 1981 Coal Board Specifications, (56).

This information, however, may not account for the increase in life by one order of magnitude and its longer fatigue life than with a mineral oil. The reasons for this increase are not clear, but possibilities are listed in table 7.5.

Improved Fluid Performance
Better Specimen Integrity
Invalid Application of theory
Scaling Factors, K, n Incorrect

Table 7.5

Possible influences on increased fatigue life

The four parameters listed above have been carefully examined and possible reasons for the discrepancies are outlined. The first two reasons would appear to contribute something to the increased life but one of the influences may be the resulting increased film thickness caused by improved formulation of the fluids. When the elastrohydrodynamic film thickness is increased only marginally between low levels of operation the increase in fatigue life is very marked, fig 3.1 (36). The theory used is the same as that used by previous workers. Equation 5.4 showed that the reduction of load reduced test severity but the factors n and k should take this into account as they were calculated from a weighted average of four-ball (C/P ratio 0.41) (63) and unisteel (C/P ratio 1.71) (65). The C/P ratio for the four-head rig is 1.3.

The above shows that the error must be caused by the first two factors listed in table 7.5 which resulted in far longer lives than theory predicted. These findings bring into play the question of the influence of the mechanism on fatigue life. This is further discussed in section 7.5.

7.2.1 Influence of Water Content on Ranking Position

The most noteworthy aspect of the ranking of the fluids relates to their water content table 7.2. The fluids did not rank with the least water giving the best performance. The aqueous glycol and the dilute aqueous glycol should, if water content were the only criterion for fatigue, give much better lives than the dilute emulsion or the polymer-thickened fluid. To account for the anomalies in the ranking order, a series of short studies were organised to try to elucidate the reasons for the superior performance of the polymer-thickened fluid. These studies are described in section 7.3.

7.2.2 Influence of applied potential on ranking

In section 6.1.4.1 the results for the three series using applied potentials were examined. The two series with applied potentials of +200 mV and -200 mV gave better results than with no potential for the dilute emulsion, table 7.6.

Test series	applied potential mV	% Statistical significance		
		4	5	7
4	None	-	89	86
5	+200	89	-	55
7	-200	86	55	-

Table 7.6

Influence of applied potential on dilute emulsion results

In table 6.16 the predicted influences of applied potential were outlined. The film formation effect was found to be correct with the films formed in series 5 but not in series 6 and 7. The corrosion, iron dissolution and hydrogen formation effects were described in section 3.5, (92).

The events predicted in table 6.16 are a fairly simplistic view but further experiments were beyond the feasible scope of the project. Some of the properties of the fluids and events were investigated by other methods, some of which were described in sections 6.4 and 7.3. The influence of these tests on the elucidation of mechanisms is discussed in section 7.5.

7.2.3 Influence of load on rankings

As described in chapters 2 and 5 the load generally has a significant influence on the fatigue life of bearing steel.

Using the load-life calculations described in section 5.1.5 and the factors introduced by Kenny and co-workers, (27), estimates for the predicted L_{10} and L_{50} fatigue lives are given in table 7.7.

Series	LOAD/ NEWTON	C/P RATIO	Predicted Fatigue Lives/millions of cycles			
			Mineral Oil		Dilute Emulsion	
			L_{10}	L_{50}	L_{10}	L_{50}
6	1046	1.95	7.45	22.35	0.56	1.69
7	1570	1.30	2.20	6.61	.248	0.74

Table 7.7

Predicted lives for the high and low load with dilute emulsion

One problem, which could not be accurately predicted due to a shortage of data, was the influence of the applied -200mV on the fatigue lives at the lower stress level. From the table 6.21, it can be seen that life under the high load increased by approximately three fold compared to the low load series but were of the same order of magnitude at the L_{50} fatigue life stage. Applying this to the theoretical lives did not give sensible answers and estimates for the life was not possible.

The theoretical lives for the two series were plotted on a Weibull graph paper fig 7.1. Values of mean life, Weibull slope, degrees of freedom based on 15 failures each were drawn up and overall confidence limits for these theoretical lives established. For both mean and L_{10} fatigue lives, confidence limits of 90% were calculated indicating that the L_{10} and mean lives of the low load stage were statistically significantly longer than those of the high load stage. As two identical runs apart from load had been carried out, analysis of the L_{10} lives to establish the K,n constants from the adjusted load-life equation eg 5.4. Two simultaneous equations of the form Eq 5.5 were set up from eq. 2.1 and eq. 3.2 and solved for the results obtained from series 6 and 7. Values of n = 3.905 and K = 0.896 are quite different from those

$$\log_{10} L_{10} = n\log_{10} C - n \log_{10} KP \qquad \text{Eq 5.5}$$

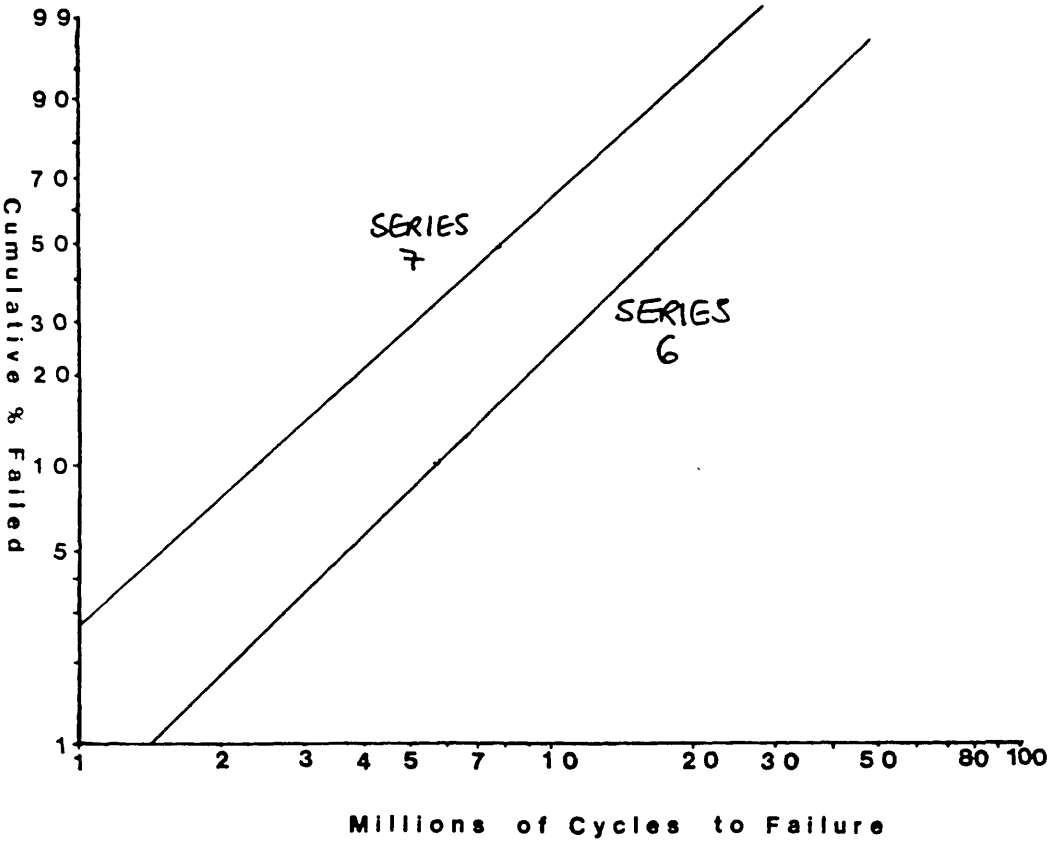

Theoretical Lives for high and low load Series

Figure 7.1

suggested by Kenny and co-workers, (27), of n=2.021 and k=2.591. The reason for this discrepancy is not clear but a conclusion similar to that reached in section 7.2.1, that improvement in specimen integrity and fluid performance gave rise to longer lives, was drawn. This is further discussed in section 7.5.

7.2.4 Influence of Dilution on Ranking

The very dilute aqueous glycol gave several more early failures than the "as received" fluid. There was no statistical significance achieved at the L_{10} fatigue life, but as described in section 6.2.5 there were more failures below 10 million cycles. One mechanism of failure, the influence of very low elastohydrodynamic film thickness, is not likely to be influenced by the water content in the fluid as according to Wan, (72), the film thickness formed by both fluids is very thin such that very low lambda values are obtained. In sections 6.1.2.8 and 6.1.2.9 the presence of thin plastic films on the surface of the specimens were noted. These deposits are formed on the wear tracks and may have some influence on fatigue lives of the specimens. The more dilute aqueous glycol has a much lower amount of film-forming additives present in solution and would therefore have a lower rate of film formation and it may well be this that influences the difference in fatigue lives found between the two levels of water content. This is further discussed in section 7.5.

7.2.5 Scatter from Previous Results

As outlined in section 7.2.1 there is an order-of-magnitude difference between the results obtained in this study and those of Kenny, (27). The reasons for this may be entirely dependent on the improvement of the specimens, especially as a lot of the data used by Kenny was based on Unisteel and rolling four-ball fatigue rigs. The performance of

these rigs appears to have improved considerably in the last five years, largely due to improved specimens, (136), (137), but also due to improved fluid performance. it would appear that in order to make a proper comparison a factored equation, like eq 2.9, (26) consisting of a variety of factors for increased or reduced fatigue lives should be used instead of the simple equation used by Kenny (27). An example of this is given in Eq 7.1.

$$L_{10} = F_1 \cdot F_2 \cdot F_3 \left\{\frac{C}{KP}\right\}^n \qquad \text{Eq 7.1}$$

where F_1 = relates to specimen integrity

F_2 = film thickness/fluid factor

F_3 = Corrosion Index, related to the corrosive nature of the lubricant.

A modified equation of this form would hopefully take into account of improved fluid and specimen performance. This is further discussed in Chapter 8.

7.3 SPECIAL STUDIES ON THE POLYMER THICKENED FLUID

As very little was known about this new and experimental fluid, considerable work had to be carried out on the fluid to assess its physical properties in order that it could be properly compared with other commercial fluids.

7.3.1 Physical Properties of the Fluid

The physical properties of the other commercial fluids are well documented but no data was available for the polymer-thickened fluid.

7.3.1.1 Viscosity

The most important property of a lubricant so far as its lubricating ability is concerned is generally its viscosity. A Ferranti-Shirley cone-on-plate dynamic viscometer was used to measure the viscosity of the fluid at various temperatures, under different shear rates and at different water contents. Water content was varied because of a report by Fosberg and Hughes, (55), that polymer-thickened fluids were prone to large viscosity increases due to loss of water. A " Titrimetric " automatic 'Karl Fischer', described in Appendix 5, was employed to measure the water content of all the fluids. The water loss suffered by the fluid during viscosity testing was also monitored as the initial results and those of Fosberg and Hughes indicated that the water content of the fluid in the sump had to be tightly maintained. The first result is of dynamic viscosity versus shear rate for the fresh sample of the fluid. The trend is given in Fig 7.2. A graph of the shear rate versus shear stress for the same fluid under the same conditions is also given, Fig 7.3. The increase in viscosity at the very high shear rates can be identified as being caused by the loss of water from the fluid. The water content of the fluid was measured after the viscosity test and was found to have decreased from 90 to 85%. A fresh sample was then placed on the viscometer at room temperature and low shear rate viscosities determined. The temperature was then raised and determinations were carried out at 30°, 35° and 40°C. The results are given in table 7.8.

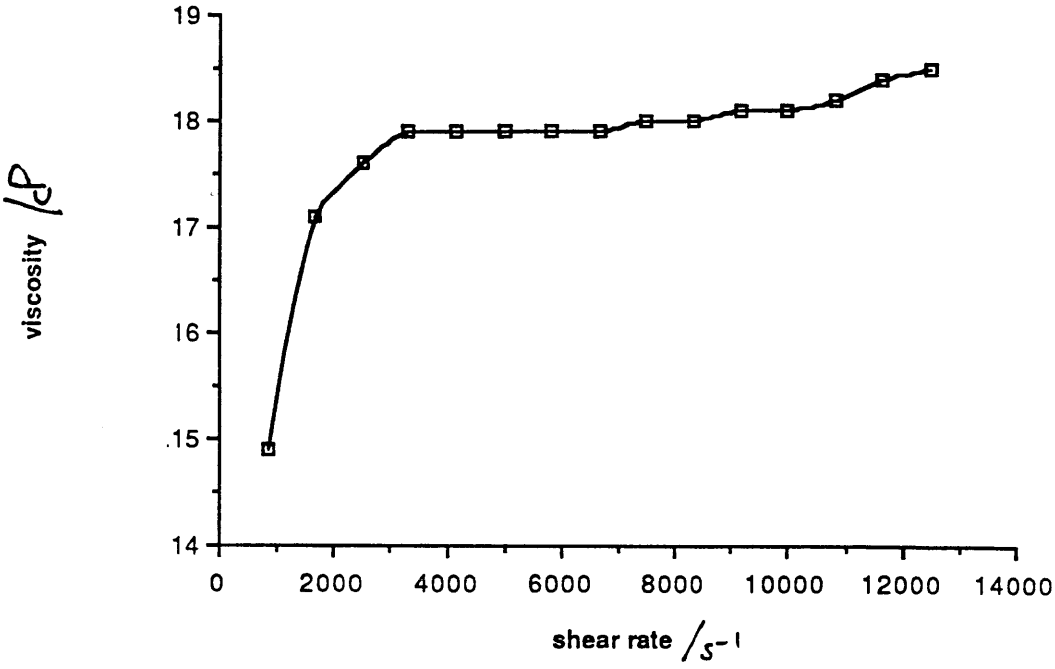

Viscosity versus Shear Rate for the Polymer-Thickened Fluid

Figure 7.2

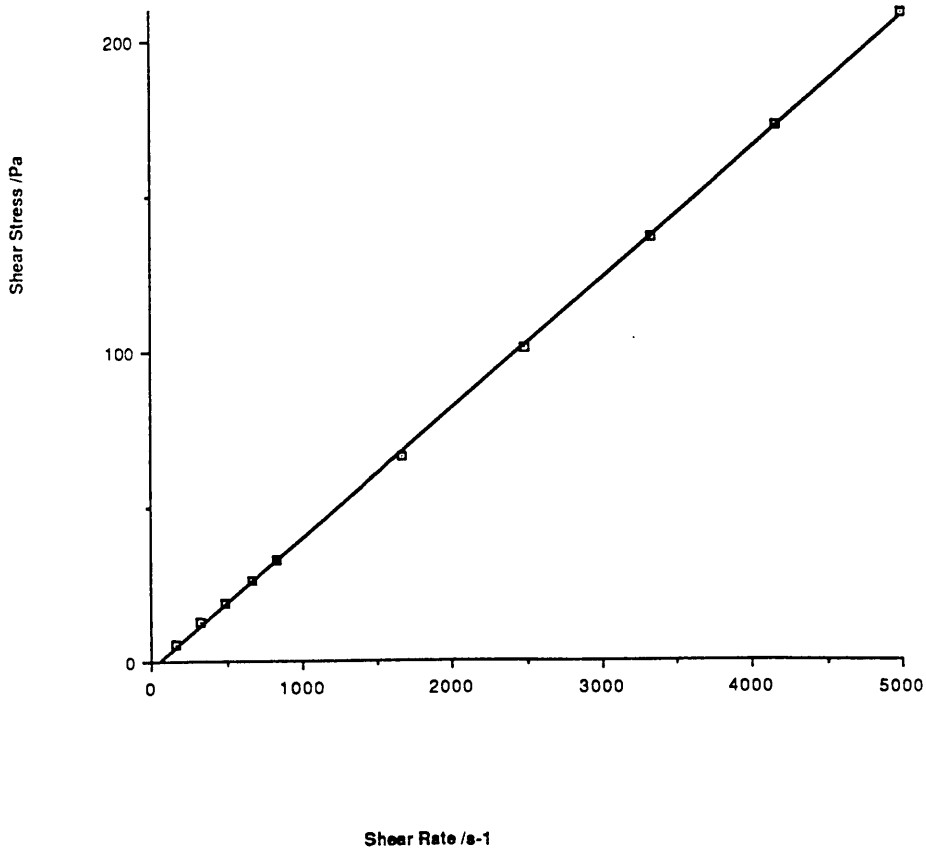

Figure 7.3

Shear Stress versus Shear Rate for the Polymer-Thickened Fluid

TEMP - VISCOSITY/CP				
Shear rate s^{-1}	21°C	30°C	35°C	40°C
250	17.1	15.4	15.4	10.3
500	19.3	17.1	17.1	13.7
750	20.0	18.6	20.0	14.9
1000	20.4	20.4	20.4	15.0
1250	20.6	20.6	21.4	16.3
1500	21.1	20.7	20.7	17.1

Table 7.8

Viscosity of the polymer-thickened fluid at a range of temperatures.

At the end of testing, which was carried out as fast as the temperature could be stabilized, the fluid was retested for water content. No measurable difference was found between the initial and final viscosities. However when the specimen on the viscometer was retested 1 hour later at 40°C the water content had fallen to 85%. In view of this a final series of tests were carried out which involved taking samples of the fluid and heating them by varying amounts and for different time durations. The results indicated an exponential decay of viscosity as water content increased. This is illustrated in Fig 7.4.

This graph clearly illustrates the problem of correct water content for polymer-thickened emulsions. If allowed to drop too low, the viscosity increase is large for only a slight decrease in water content. Conversely if the dilution is greater, there is only a slight loss of viscosity but there may be added complications such as corrosion.

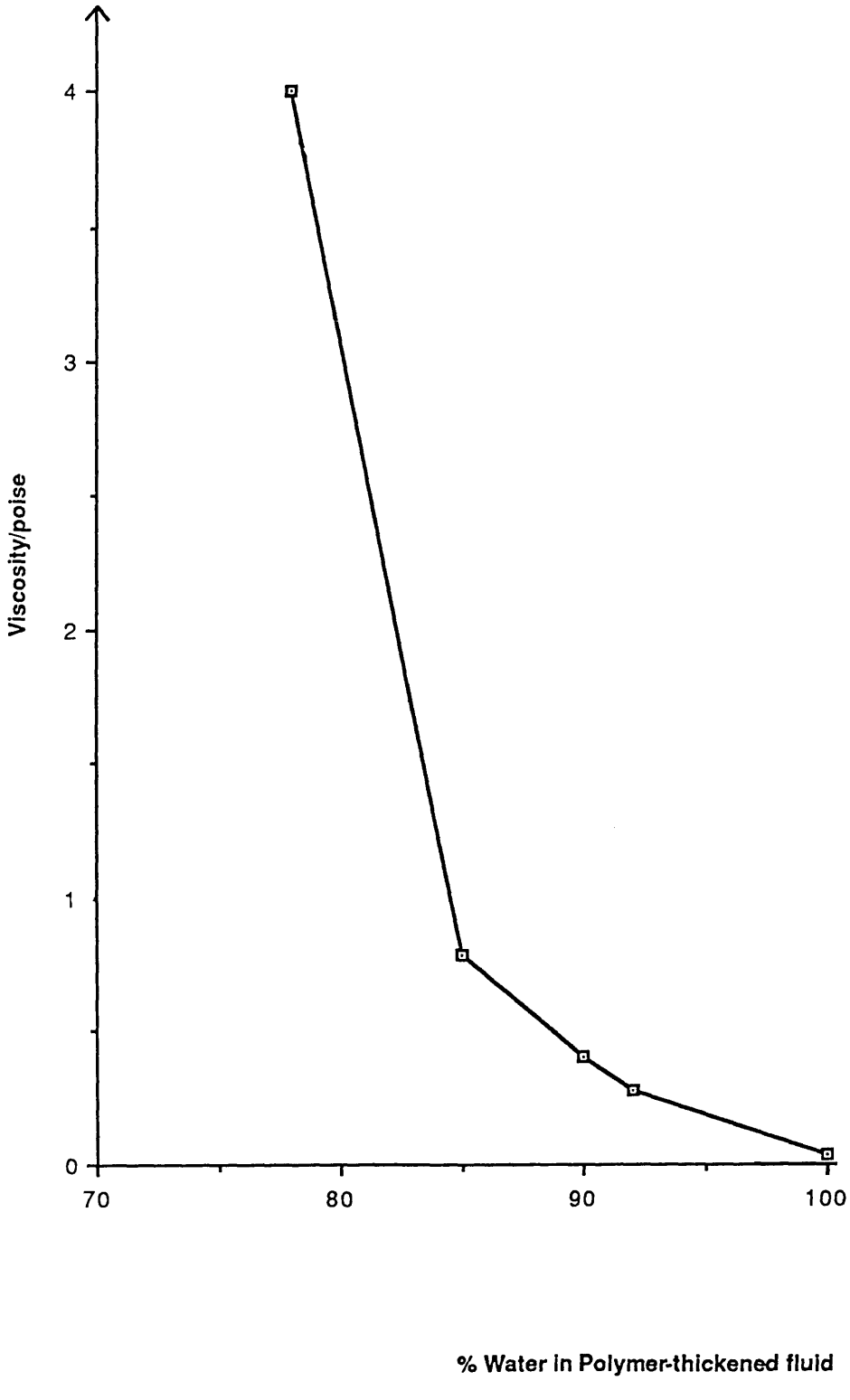

Figure 7.4

Viscosity versus Water Content for the Polymer-Thickened Fluid

7.3.1.2 Refractive Index

In order to carry out optical elastohydro-dynamic determinations of film forming ability and thence pressure-viscosity coefficient, the refractive index of the fluid must be established. The refractive index of water and the fluid at various water concentrations were measured at 25°C, using a temperature controlled refractometer. An approximate straight line plot of refractive index versus water content was obtained, Fig 7.5. The data obtained was used for the optical elastrohydrodynamic tests described in the next section.

7.3.2 Elastrohydrodynamic Lubrication Properties

One of the simplest methods for evaluating the elastrohydrodynamic performance of lubricants is to use an optical ehd rig to directly measure film thickness. This rig was devised by Foord and co-workers (138) and others over 15 years ago and its operation is very simple. More recently Wan, (72), used this method to evaluate the elastrohydrodynamic performance of "Aquacent Light", a dilute emulsion and a water glycol. A diagram of the rig and its theory is given in Appendix 7. The simplest way of using the rig is to calibrate it by measuring the film thickness formed by an oil of known performance and then to compare this with the test fluid. Because the fluid appeared to lose water fairly easily and increase its viscosity markedly, it was decided to adopt a schedule for testing similar to that used when testing greases, (139), Table 7.9.

(i)	Apply Fluid: Run immediately take readings.
(ii)	Allow to run for 2 minutes: then take readings.
(iii)	Allow to run for 10 minutes: then take readings.
(iv)	Switch off for 1 hour: restart then take readings.

Table 7.9

Protocol for testing the polymer-thickened fluid

The resultant fringes obtained for the calibration oil are given in Table 7.10.

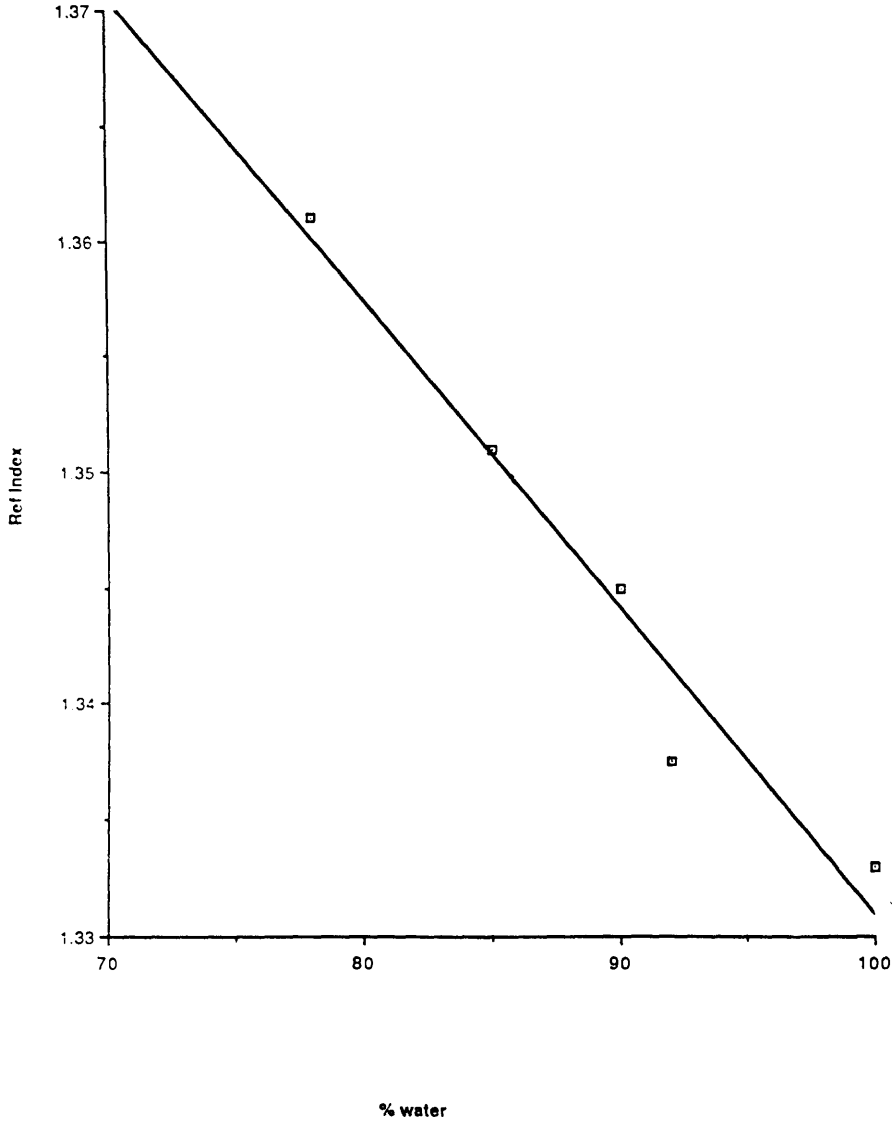

Figure 7.5

Refractive Index versus Water Content for the Polymer-Thickened Fluid

Fringe Order	Colour	h_{opt} /10^{-7}m	Speed/Ms^{-1} at load 5 lb	10 lb	15 lb
1	Yellow	2.0	0.028	0.032	0.035
1	Red	2.7	0.059	0.058	0.063
1	Blue	3.4	0.069	0.077	0.082
1	Green	4.3	0.100	0.100	0.125
2	Yellow	4.7	0.125	0.125	0.132
2	Red	5.6	0.145	0.150	0.155
2	Blue	6.1	0.170	0.190	0.188
2	Green	6.7	0.190	0.200	0.220
3	Yellow	7.6	0.210	0.230	0.250
3	Red	8.6	0.250	0.280	0.290
3	Blue	9.0	0.290	0.305	0.315
3	Green	9.6	0.320	0.325	0.350

Table 7.10

Calibration Data for the Reference Mineral Oil using the Optical EHD rig

When the polymer-thickened fluid was put on the disc and measured no immediate film was measured and the ball appeared to damage the reflective chromium layer. At the two minute mark the fluid appeared to give a yellow fringe but this appeared more at higher speed. By the end of the 10th minute most of the chromium coating on the track had been removed. The ball was moved to an adjacent track zone and the rerun result was identical to that at the 2 minute stage. At the one hour stage the result was also identical to the 2 minute stage. When fresh fluid was added during running no apparent effects were noticed. These results are summarised in Table 7.11.

Time stage	Film Thickness	Observations
Immediate	Nothing	Chromium layer being scraped off
2 minutes 10 minutes 60 minutes	Yellow Yellow Yellow	No change with speed, chromium layer scraped off, no effect of adding extra fluid

Table 7.12

Results for the polymer-thickened fluid in the Optical EHD rig

The appearance of a yellow central film thickness correlates to an optical film thickness of 0.2 μm and, using the refractive index calculated from the previous section, gives $h_{central}$ of 270nm. The interpretation of this result is discussed in Section 7.5.

7.3.2.1 Pressure-viscosity Coefficient

From Section 2.4.2 (30), it is clear that the pressure-viscosity behaviour of the fluid is very important. The usual method of measuring the pressure-viscosity coefficient is to do two or three optical determinations of the fluid at different loads. In this instance however, only one determination was possible as the elastrohydrodynamic film was very thin and testing damaged the glass discs.

As the film was produced over a range of speeds it was thought that this was due to a layer being formed on the surface of the disc. From the calibration aims assuming that the yellow fringe obtained was first order, $h_{opt} = 2.10 \times 10^{-7}$m approximate speed was 0.05m/s. From the equations in Appendix 10 a value of the pressure-viscosity coefficient for the fluid of 27.46 GPa^{-1} is obtained.

If the higher speed of 0.2 ms^{-1} is used then the value of the film thickness for the fluid is the same and the same calibrations are used a value of the pressure-viscosity coefficient of only 4.4 GPa^{-1} is obtained.

This indicates that either the shear rate has a very high influence on the viscosity or that the fluid does not behave like a mineral oil in that starvation takes place.

The most probable explanation for the fact that the fluid gives some sort of elastrohydrodynamic film is that fluid forms a layer on the surface of the disc and that is what it seems is seen in the interference fringe. This is further discussed in Section 7.5.

7.3.3 Chemical Tests

Further experiments were carried out in an attempt to understand the film thickness results. Wan,(72), had described how by making his dilute emulsion unstable, he was able to better study the surface effects of the emulsion. Similar techniques are outlined below.

7.3.3.1 The Stability of Test Fluids at High and Low pH

The stability of the dilute and invert emulsions, the aqueous glycol and the polymer-thickened film at high and low pH was investigated by the addition of either small amounts of either concentrated sulphuric acid or small pellets of sodium hydroxide which were stirred in and the pH measured using a conductimetric pH meter. These experiments consisted of (i) measuring the pH then (ii) the addition of the acid or the alkali, (iii) five minutes stirring using a magnetic stirrer bar (iv) measuring the pH again, (ii) to (iv) were repeated until a pH of either 1 or 14 was achieved. The liquid was then allowed to stand for up to 3 days as observations were made of effects such as phase separation or floculation of particles.

a. Invert Emulsion

The invert emulsion, which had an initial pH of about 8, reacted in the same way to both acid and alkali, resulting in phase separation. The end result after 1 hour was the formation of an oily layer on top of the beaker with an emulsified boundary layer and at the bottom a thick aqueous layer. No further change was recorded. After 3 days the fluid was re-emulsified but again after 1 hour the phases had separated.

b. Dilute Emulsion

A similar result occurred when sulphuric acid was added to the dilute emulsion, except that the oil layer at the top and the boundary layers were much thinner and the clear pale aqueous layer occupied about 80% if the depth of the fluid indicating a greater degree of emulsion breakdown.

With the addition of the alkali to the dilute emulsion, no apparent change took place even after 3 days. Restirring of the fluid caused the formation of soap like bubbles. Addition of large amounts of extra alkali caused the formation of a soapy deposit at the top of the beaker. This may be due to the over concentration of ions in solution causing the less soluble emulsifier molecules to "salt out".

c. Aqueous Glycol

With the addition of acid and alkali to the aqueous glycol, nothing was observed except for the formation of a "scum" on the surface of the fluid. No change took place after 3 days. This is similar to the effect of the addition of hard water to the aqueous glycol as described in Section 6.1.5.9.

d. Polymer-thickened Fluid

The addition of the acid and the alkali caused some interesting effects. The acid had no instantaneous effect but after 1 hour the fluid had separated out into three layers; a thick white globular layer at the top, a pale clear solution in the middle and a white particulate solid at the bottom of the beaker. A strong acrid smell was also detected. It may have been sulphur dioxide (SO_2) from the reduction of the sulphate ion (SO_4^{2-}) or dinitrogen tetroxide (N_2O_4) from the decomposition of the sodium nitrate ($NaNo_3$) corrosion inhibitor present. If the gas was sulphur dioxide it may also have come from the hydrolysis of a zinc dialkyldithiophosphate additive, which was known to be present in the formulation. Possible chemical reactions are given in equations 7.2 to 7.4.

$$H_2SO_4 \xrightarrow{\text{reduction}} SO_2\ (gas) + H_2O + O \qquad \text{Eq 7.2}$$

$$2NaNO_3 \xrightarrow[H_2SO_4]{\text{acid}} N_2O_4 + Na_2SO_4 \qquad \text{Eq. 7.3}$$

$$Zn\ S_2PO(OR)_2 \xrightarrow[\text{mechanism}]{\text{unknown}} SO_2\ (gas) + \text{unknown products} \qquad \text{Eq 7.4}$$

The study of the reactions of zinc dialkylthiophosphates is extremely complex and is beyond the scope of this thesis.

The particulate matter at the bottom of the beaker appeared to be the soluble polymer having come of solution or suspension.

With the addition of the alkali a similar 3 phase system developed but no acid gas was detected. The results of these tests indicate that the fluid appears to operate satisfactorily at normal pH but with slightly high acid or alkali severe instability problems occurred, which would almost certainly lead to a very much reduced fatigue life. However, the only way of measuring this would be to perform a full range of corrosion tests (IP 329), (97), or a whole range of different pH fluids.

7.3.3.2 Stability of Fluid under Heating

An attempt to obtain an infra-red finger print of the polymer-thickened fluid proved impossible as the water content masked all other bands. A low pressure distillation of the fluid was therefore undertaken. The reduced pressure was obtained from a top fitted vacuum pump and a water boiling temperature of about 68-70°C was obtained. The distillation was carried out slowly to try to prevent the hydrolysis of the ZDDP additive and the breakdown of the polymer. This distillation was halted when a value of about 10% of water in the thick solid was obtained. Some material was also carried over in the distillation which was thought to be co-solvent. An infra-red spectroscopic analysis was carried out on the concentrated

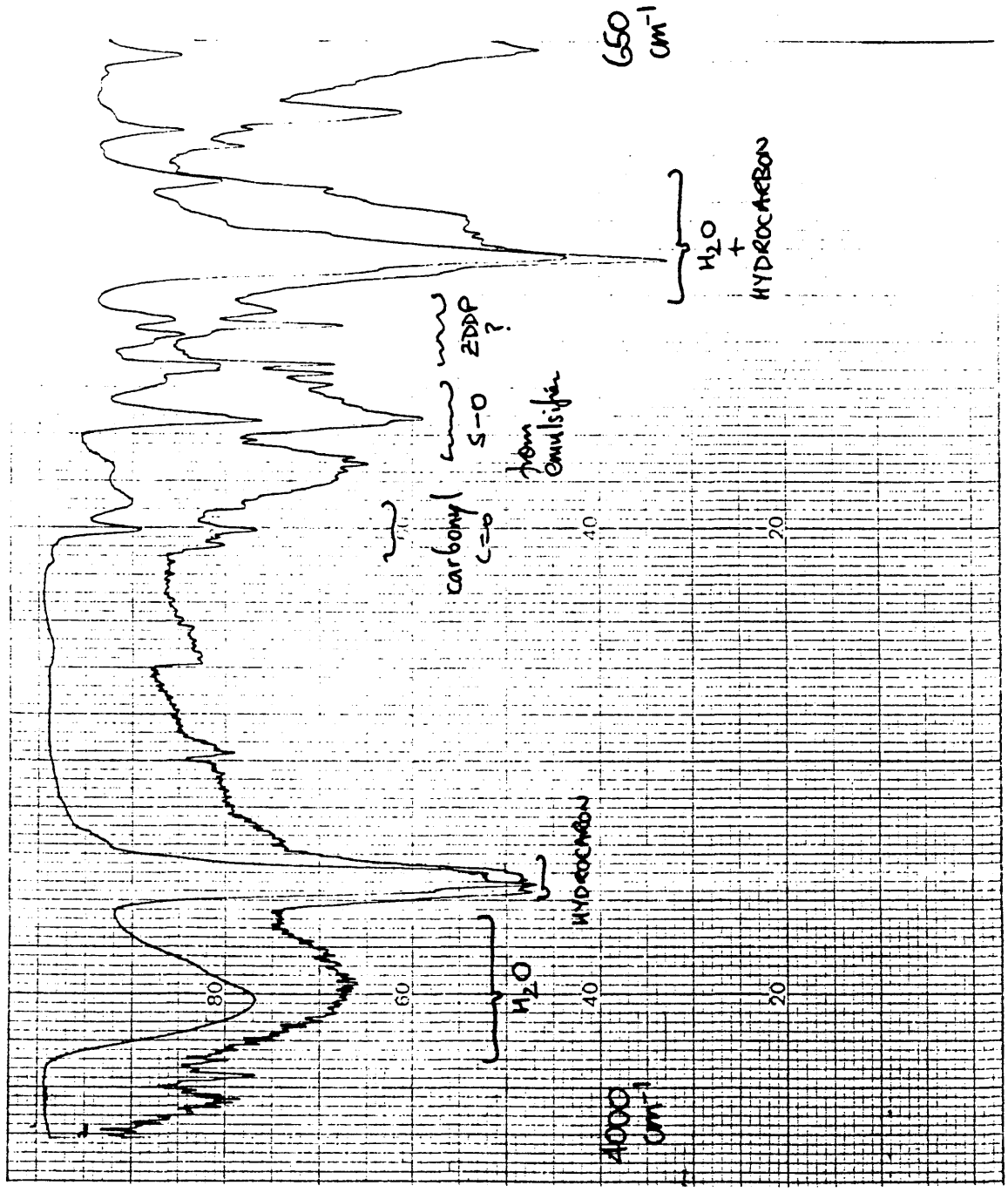

Figure 7.6

An Infra-Red Spectra of water-reduced
Polymer-Thickened Fluid

residue Fig 7.6 and the results discussed in Section 7.4. An attempt was also made to measure the viscosity of the residue. At room temperature the substance was solid at room temperature and at 70° was still too viscous to measure even at the lowest shear rate attainable.

7.3.4 Film Growth Studies

As a result of the deposited films found when polarizing the specimen described in Section 4.1.54 a simple experiment was set up to study the growth of these films on EN31 steel discs. The same polarizing equipment described earlier was once again used but instead of attaching slip rings, EN31 discs were cleaned, polished and soldered on to the wires as shown in Fig 7.7.

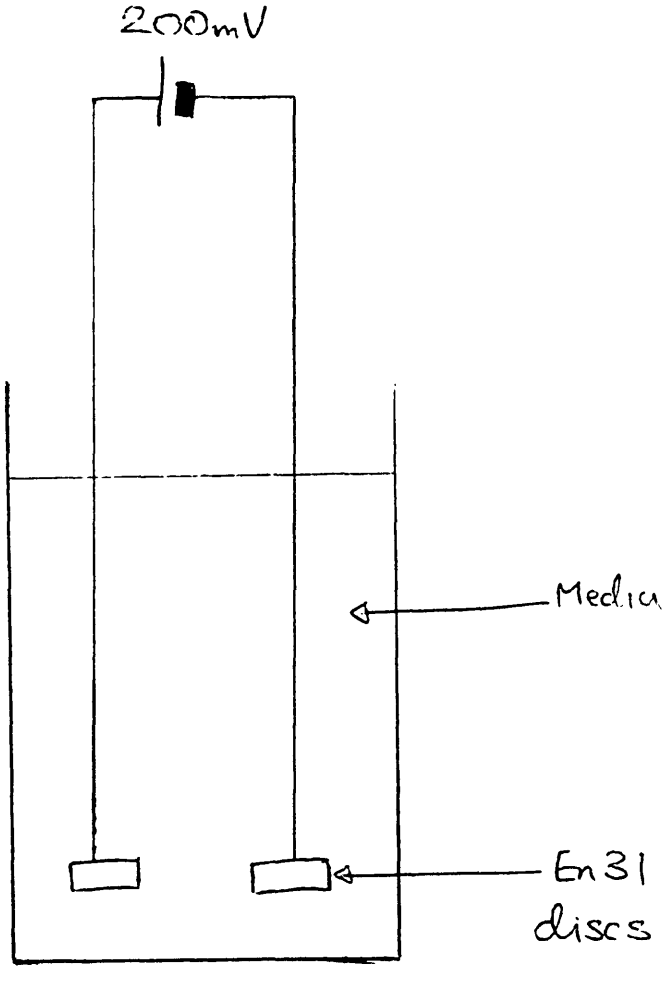

Figure 7.7

Schematic Diagram of the Film Studies Equipment

These tests were carried out on all the fluids under study. The tests consisted of mixing the emulsions to the appropriate concentration using the rotary emulsifier and then inserting the discs into the fluid. The electrodes were left in place for 1 week and then removed and examined. The tests were carried out in the open at room temperature which varied from about 6°C (overnight) to about 20°C (max day time temperature). The influence of this lack of temperature control compared to the 35°C controlled temperature in the four head ring is uncertain, but as the temperature is of a similar order of magnitude, the effects were thought to be small. The fluids tested are given below along with any results and observations noted in Table 7.12.

Fluid	Film formed on EN 31 disc		Other observations
	+200mV	-200mV	
Invert Emulsion	None	None	Slight oil layer formed on top.
Dilute Emulsion (distilled)	None	None	None
Dilute Emulsion (tap water)	None	None	None
Aqueous glycol (as rec'd)	None	None	None
Dilute AG(distilled)	None	None	None
(tapwater)	None	None	Scum formed
Polymer-thickened	None	None	Gummed on wire

Table 7.12

Film growth observations for the various fluids

Film formation on EN31 discs polarized by ±200mmV in various fluids. As can be seen from table 7.13, in a fairly tightly controlled test set-up no films formed indicating that the build up of films in the rubbing contact is not solely due to the applied potential. One possible reason for the formation of films in the contact zone is the formation of fresh metal surfaces caused by the contact allowing some form of chemical reaction to take place. The presence of wear particles may somehow also promote the reactions. The constant aeration of the fluid in the test head may also contribute some unknown influence of the formation of these films. The activation of the lubricant by oxygen has been described by several workers in the past twenty years, (96), (42), (88), (92) but the effects have not been quantified.

The only other quantity that was recorded was the loss of water from all of the very dilute fluids.

The lack of sensible results from these film studies, highlighted a problem. The relationship between service use and laboratory tests. The films were seen to have formed on the test specimens in section 6.1.2.6 but without the exact conditions, film formation was not possible. This is further discussed in Chapter 8.

7.3.5 Gumming

One of the major problems noted in the polymer-thickened fluid was its instability which gave rise to the formation of gummy deposits on all exposed metal surfaces and in pipes. The gummy deposits also formed on the surface of the specimen bar after tests. In some areas, such as on the surfaces of moving parts such as in the pump they appear to be beneficial in terms of increased life and wear resistance but caused problems with seals as discussed in the next section. The mixing return pipe became coated with large gummy deposits which had to be scraped off. Once formed these deposits did not redissolve in the emulsion and did not dissolve in distilled water or the mixed fluid even when a high speed emulsifier was used.

7.3.6 Seal Compatibility

When new fluids are developed, extensive tests are usually carried out to determine the compatibility of the fluid with seals. No actual tests were carried out but it was noted that the seals between the bars specimen and the head at either side of the contact in the four head rig, had to be replaced much more frequently than during the other tests. The reason for this was the formation of gummy deposits in the seal contact area which reduced the effectiveness of the seals and appeared to cause seal wear. The formation of darker deposits of seal material and gum from the fluid was also noted.

7.3.7 Comparison of the Polymer Thickened Fluid with other Fluids

In this section, in light of the tests carried out on the polymer-thickened fluid (PTF) the properties of the polymer thickened fluid are compared with those of the Aqueous glycol and the dilute emulsion to establish the reason for the performance of the PTF.

7.3.7.1 Aqueous Glycol

The two fluids are similar in make up apart from the emulsifying agents present in the polymer-thickened fluid. A list of the different formulations is given in Table 7.13.

	Aqueous Glycol	Polymer Thickened
Water content %	47	90
High molecular Weight polymer	20%	4-5%
Monomer	30%	1-2%
Emulsifying agents	-	1-2%
Anti-corrosion additives	3%	2%
Anti-wear additives		1%

Table 7.13

Comparison of the formulations of the aqueous glycol with the polymer thickened fluid.

One possible chemical reason for the better performance of the polymer-thickened fluid is the presence of the very surface active emulsifying agents present, assuming that the polymers and monomers are the same type of compound, usually poly or mono-glycol where the monomer acts as a co-solvent or aids the formation of mycelles. Physically, the only difference between the fluids is that the aqueous glycol is a true solution whilst the polymer-thickened fluid is a two phase emulsion. It is thought that a combination of these surface chemistry effects and the differing physical properties giving rise to different elastohydrodynamics film thicknesses, that are responsible for the difference between these two fluids. This was discussed in Section 7.3.2.

7.3.7.2 Dilute Emulsion

The formulations of the dilute emulsion and the polymer thickened fluids are compared in Table 7.14.

	Dilute Emulsion	Polymer thickened fluid
Water content %	95	90
Emulsifying agents %	1-2	1-2
Mineral Oil %	1-2	?
Anti-corrosion additives %	1-2%	2%
Polymer thickener %	-	4-5%
Monomer %	-	1-2%
Anti-wear additives %		1%

Table 7.14

Formulations of dilute emulsions and polymer thickened fluids.

There are only slight differences, except in the presence of the monomer and polymer, between the fluids. The polymer was shown to promote films on contacting surfaces in section 7.3.2. This film promotion is not understood and further work is proposed in section 9.3. The influence of film thickness improvement on failure mechanism is further discussed in section 7.5.1.

7.4 DISCUSSION OF OTHER TECHNIQUES

In this section important points arising from chapter 6 are discussed.

7.4.1 AOL Vertical Fatigue Rig

Once operational, this rig proved to be a useful qualitative technique for the generation of a large number of fatigue raceways which were analysed by a variety of chemical techniques. The deficiency of the test rig, described by Hopkinson, (116), in terms of its large number of cage failures was found to be correct. This detracted from its use as did the problems of maintaining lubricant in the specimen holder. The two results using no lubricant, where severe wear but no fatigue failures occurred, are further discussed in section 7.5.

7.4.2 Rotating-Bending Fatigue Rig

This rig appeared to work quite well until its irrepairable demise. Only five useful results were obtained on the test rig. These were analysed in detail and the results presented in section 6.3. Good agreement with previous work in this area was achieved within the limitations of the test method. The major difficulty with this type of non-contacting crack propagation rate estimation work is relating the results to those seen in a contacting situation. The main differences appear to be in the stress fields experienced by the two situations. In the contacting case it has been suggested that crack propagation is driven by either the maximum shear stress, or by the maximum orthoganal stress whilst in the non-contacting case the bending causes the initiation and propagation. The stress fields in the Rotating-Bending situation are a lot more simple than in the contacting case. Using rotating-bending techniques is simpler and cheaper than bearing tests but, the use of vibrating plate specimens is a further simplification as described in section 4.8.1. A lot more research needs to be carried out in this area of the influence of lubricant on cracking to correlate contacting and non-contacting studies. This is further discussed in chapter 9.

7.4.3 Chemical Techniques

In Section 6.4 the analytical techniques used to analyse failed specimens and deposits were described. An appraisal of each of the techniques is given in the following sections.

7.4.3.1 Infra Red

Some interesting results using infra red spectroscopy were obtained but the main drawback in the use of infra red is water. Water shows strongly absorbing bands in the 3700-3100 wave number region and in the 1300 wavenumber region. Hydrocarbons also absorb strongly in the 2800-3000 wavenumber region and interaction between water and oil makes analysis by simple infra red instruments difficult.

The type of infra-red machine used, a Perkin-Elmer, was only a single beam machine. If a two beam machine had been obtainable then some of the interference caused by water could have been removed and greater use of the technique could have been made.

7.4.3.2 Scanning Electron Microscope

This technique was only employed to examine failed specimens prior to SIMS analysis. It was used to screen problems found in the sectioning of specimens such as grinding grit embedded into the surface and rusting caused by the cutting fluid. Further use might have been made of the EDAX (Electron Diffraction and X-ray) technique to look at surface films on failed specimens but the results would have given similar results to that obtained by infra red.

EDAX analysis of one raceway gave only non oxygen, chromium, hydrogen, carbon and nicken in any identifiable quantity.

Summarising, Scanning Electron Microscopy was a subsidiary technique employed as a screening method.

7.4.3.3 Secondary Ion Mass Spectroscopy

As described in section 6.4.3, the SIMS was not as successful as it was hoped to be but still provided a lot of useful information for the mechanism study described in section 7.5. One of the problems was the time delay between running the specimens and their examination. The first set was examined using a VG Ionex SIMS described in section 6.4.3.1. No depth profiling was achieved with this initial analysis and the results were presented in figs 6.37 to fig 6.39. From these figures nothing apart from metal oxides and a few organics were found in the surface layers of the three specimens rendering the first series. The traces for the three raceway segments run under different tests were all very similar indicating that some repeatability of the technique existed.

The second series of SIMS specimens were carried out at a later date on a different set of specimen failures. The results obtained indicated the presence of a variety of organic substrates in the surface layers of the specimens which could be assigned to the sulphomate emulsifying agents as well as the previously found organics from the cleaning solvents. The depth profiling technique described in section 6.4.3 again did not work very well. One problem was that the ionic weight of methane and oxygen action conflict. As oxygen is the primary ion it is not so easy to distinguish between the two ions. The presence of hydrogen was also noted in higher abundance than anticipated. When long chain hydrocarbon molecules are examined by mass spectroscopy, a series of peaks are obtained, each 14 Atomic mass numbers apart. This is caused by the elimination reaction of successive CH_2 groups.

This is usually a clear indication of the presence of alleged chains. For this reason it was thought that sodium stearate (CH_3 $(CH_2)_{14}$ COONa) would be able to be easily resolved. This proved to be not possible due to the presence of a large number of other ions. The biggest difference obtained was the presence of aromatics (76, 89 (92 + sulphur) in the subsurface layers. The degree of surface penetration was the most difficult to ascertain, with only the operator suggesting that a depth of about 10μm had been reached. Water was also found but it was not certain if this was background due to moisture or O^2/H^+ interaction. Kilner (133), suggested it was probably due to the pressure of moisture in the vacuum chamber rather than the presence of water in the subsurface layers. This tied in with the problems Suzuki and Ohtsubo, (132). Summarising the work using the secondary Ion Mass Spectroscopy technique, useful information used in the next chapter was obtained, despite problems of the technique not working as hoped.

The results from the SIMS analysis are used in the mechanism study in an attempt to prove the difference between the hydraulic and chemical mechanisms.

7.5 MECHANISMS

In section 3.5 the three mechanisms for the premature failure of bearing steels, lubricated by water containing fluids, were introduced and summarised in table 3.11. The chemical mechanism was subsequently expanded to include corrosion and hydrogen embrittlement effects giving four possible mechanisms. In section 3.5.1 through to section 3.5.5 these mechanisms were reviewed and the causes of premature failure examined. It was clear from this survey that the causes of failure are extremely complex and it is not possible to produce a simple hypothesis to explain the failure mechanisms. Several workers

appear to have hypothesised as to the failure mechanism and carried out experiments to prove it (39), (83), (64). Other workers have set out to prove that different mechanisms are operating and have again carried out experiments or bearing tests to determine certain results (80) (88) (83).

From the above it appears likely that the four mechanisms are interactive and the mechanism that dominates depends upon the operating conditions.

There is also some doubt as to the validity of one or two of the mechanisms. There are a number of problems trying to assess how the validity and operation of each mechanism might be investigated. These problems along with the discussion of each mechanism and tests are outlined in the following sections.

7.5.1 Thin film mechanism

As illustrated by Hamaguchi and co-workers, (69), and more recently by Wan, (72), dilute emulsions and aqueous glycols form only very thin elastrohydrodynamic films and techniques have only just been developed to measure such thin films (76). Unfortunately, as yet no results on these types of fluids have been published. Invert Emulsions, owing to the presence of a large amount of oil, have been shown to produce reasonably thick elastrohydrodynamic films. On the four-head test rig a specific film thickness λ, of 0.47 was calculated. The polymer-thickened fluid gave anomalous results for film thickness tests. This is best explained by the formation of a deposited layer of about 250nm thick (almost the 1st yellow band seen on the optical EHD rig) and the rest of the film is formed due to the pressure-viscosity behaviour of the fluid. This would appear to operate satisfactorily at low shear rates but at much higher shear rates, the deposited film is scraped

off leaving only relatively thin films formed. The point at which the film starts to be removed could not be examined using the optical ehd rig so no quantitative analysis of this was possible. Deposited films were also found under the +200mV regime but not under the -200mV which shows that effects other than lack of film thickness contribute to reduced fatigue life. This was illustrated in table 7.7. This formation of non-EHD deposited films complements well the concept of the use of additives to increase film thickness which should improve fatigue life.

One situation where water has been definitely shown to have an effect not attributable to a reduced film thickness is in the case of small amounts of dissolved water in oil (up to 500ppm). This rate has no effect on the elastohydrodynamic properties of the oil or phosphate ester (48), (69) but has been shown to reduce fatigue lives by up to 90% depending on the amount of water present. In this instance either the hydraulic mechanism or one of the chemical mechanisms must be operating.

In situations where water is not present, the influence of low specific film thickness has been shown to be quite large (36). The presence of such a low specific film thickness of 0.47, as in the case of the "Aquacent Light" is estimated to reduce fatigue lives by as much as 75% compared with a value of lambda of about 3.

To summarise, for situations where lubrication is entirely by water or emulsified oil in small quantities, as the case of dilute emulsions and aqueous glycols, the lack of elastohydrodynamic film thickness has a very large influence in promoting premature failure. It appears to promote earlier initiation or pre-conditioning of the surfaces such that propagation takes place much earlier in the fatigue life and the

overall life is considerably reduced. With dissolved water, premature failure appears to be caused entirely by chemical or hydraulic mechanisms. The limiting effects for the amount of water present appear to be the solubility limit in oil (about 500 - 750 ppm) and above this limit it influences the physical properties of the oil. This is summarised in chapter 8.

7.5.2 The Hydraulic Mechanism

Way, (2), hypothesised that for pitting to take place a lubricant must be present, and it was the presence of this lubricant being forced into surface cracks which caused pitting. In section 3.5.2, the hydraulic mechanism was reviewed. The hydraulic mechanism has been suggested as a cause of pitting without the presence of water. The only difficulty is proving the mechanism. Michan and co-workers (81), carried out test on surface crack specimens in oil and found that when the crack was not in contact, oil was forced out of the crack and the crack appeared to propagate. No systemmatic examination of this was carried out and no details of how the hydraulic mechanism might cause surface microcracks to develop into bigger cracks has been given. The cracks used by Michan (81) were quite large to begin with. Murakami and co-workers, (39), showed a theoretical basis for the hydraulic mechanism but no experiment proof has been obtained. Sullivan and Middleton, (83), attempted to show that water from aqueous glycols caused crack propagation by entering microcrack openings. The hypothesis was that water is less compressible than oil and this transmits the stressing of the surface down through the crack to force crack extension. One of the problems with this work was that no analysis for water in the crack tips was carried out and there was no method devised and employed for the proving or otherwise this pressure pulsing effect.

To this aim, in the current study, the depth profiling technique of SIMS, was used in an effort to find water present in the subsurface layers of bearing raceway. The problem with the SIMS technique outlined in section 7.4.3, was the presence of background moisture to influence the results. Additives and oil particles were found in the subsurface layer, along with oxygen and hydrogen but it cannot be said with any certainty that water was present. As there were also additives present, it would be reasonable to assume the presence of water in the crack but it cannot be inferred that this had been completely reacted, promoting one of the chemical mechanisms.
The hydraulic mechanism almost certainly promotes failure in water free systems, but it has not been proved to have any influence on the premature failure of water-based lubricant systems.

7.5.3 Chemical Effects

The premature failure of bearings lubricated by wet mineral oils and the discovery of the presence of hydrogen in the balls, (5), showed clearly that the chemistry of the lubricants has a very significant influence on this failure. Further evidence of chemical effects is given by the apparent time dependence of fatigue failure as well as the number of cycles to failure in the presence of water, (42). The three chemically related mechanisms (i) Chemical promotion of crack growth (ii) hydrogen embrittlement and corrosion and (iii) the rebinder effect are examined and discussed in the next three sections.

7.5.3.1 Chemical promotion of crack growth

Water may influence either of the three pre-failure stages of the fatigue process. As was shown in section 6.3.8, it appears to have very little direct influence in rotating-bending type of fatigue testing but the large margin of error in the data obtained may prevent any of the effects from being discovered. Water was shown by Harris (119) to have an influence on the fatigue limit of S-N testing

results, but no data on crack propagation effects was provided. Armstrong and co-workers (82), and Polk and co-workers, (16), showed that water had some effects on the crack propagation rates under the conditions tested, but only a few tests were carried out. Lockwood and co-workers, (14), showed that water did not appear to have much influence on crack propagation but it appeared to have an influence on the stress level or critical crack size from which steady-state propagation started.

The influence of water on overall fatigue lives appears to be significant from the data collected but no direct evidence was obtained that it influenced the crack propagation rate. The greatest effects appear to have been in the pre-initiation and initiation stages, as outlined earlier in section 7.5, and from the work of various authors, these are the most important areas of prevention of premature failure caused by rolling contact fatigue (14) (24) (42). If the pre-initiation conditioning or the initiation can be prevented or slowed down then longer fatigue lives would result.

7.5.3.2 Hydrogen Embrittlement and Corrosion

These two effects, although appearing to be separate mechanisms, are closely interrelated and in the presence of water cannot be distinguished. It was clear from the work of Grumberg and Scott (5), that hydrogen was formed during the running of balls and appeared to be responsible for the failure. However further tests by Ciruna and Szieleit (88) and by Schatzberg and co-workers (42) (43) showed that oxygen had to be present for premature failure. This would suggest a mixed mechanism that presence of oxygen somehow promoted the production of hydrogen from the water and the lubricant and this hydrogen caused the embrittlement of the steel. In section 3.5.4, the previous work on hydrogen embrittlement was reviewed. In high carbon

steels (1% by weight) the hydrogen would react with the carbon and produce methane (CH_4) which could hopefully be detected in the subsurface layers (87). Ions were identified by SIMS analysis which had the correct weight but they might have come from a source other than methane. If the hydrogen did not react (reversible hydrogen embrittlement) then the hydrogen gas would have been found, but due to the nature of the analysis was not positively detected.

Evidence of corrosion was only seen in a few of the very long lived specimens. This ties in with the work of Evans (92), that corrosion is a time dependant process which shows only after a considerable running time. The major reaction products of corrosion are metal oxides and hydrogen which may cause the embrittlement of the steel.

The influence of the uptake of hydrogen was shown by Grunberg and co-workers (85) when the uptake of hydrogen in a bearing steel and in a stainless steel, was linked to the failure of the bearing steel which had absorbed a considerable amount more of hydrogen.

Evidence of the influence of hydrogen embrittlement and corrosion is strong. Numerous workers detected it, and several have hypothesised that corrosion and hydrogen embrittlement are the formulation problems of water fluids, (93), (84).

The resulting mechanistic picture appears to be that in most situations, the lack of film thickness causes asperity interaction on a micro or macro-scale, which results in microcracks opening on the surface into which the lubricant is forced. The water in the lubricant reacts with the fresh metal surface, produces hydrogen which leads to hydrogen embrittlement and a faster crack growth to the initiation crack length and the propagation as described in section 2.2.4.2. The evidence for this is that oxides are found at a much

deeper level than expected from purely surface oxidation. Hydrogen ions in the SIMS were found in the subsurface layers but it cannot be ascertained where the hydrogen came from. In section 3.5.4, it was hypothesised that the hydrogen ought to be detectable by using deuterium instead of hydrogen, but previous workers had found that the deuterium exchanged with the lubricant and again no discrimination would have been achieved. A better method would have been to use $H_2{}^{18}O$ but the cost of running specimens in fluid consisted of this was financially prohibitive.

To summarise hydrogen embrittlement, appears not to be a direct cause of premature failure but is the most important secondary effect. Corrosion, is only a minor secondary effect, which becomes important when the specimens live about 40 million cycles, when it helps to promote rusting and hydrogen embrittlement.

7.5.3.3 Rebinder Effect

As described section 3.5.5, the Rebinder effect (99) does appear to exist with the reduction of lives caused by the lowering of surface energy in rotating-bending fatigue tests but its influence on rolling contact fatigue cannot easily be established. Stepurenko and co-workers, (47) (102), and Lobioko and co-workers (100) (101) published conflicting evidence for the effect but this seemed to stem from a misinterpretation of test results, where water was not counted as a surfactant by Lobioko (100), and not measured by Stepurenko, (102).

To summarise, the Rebinder effect, (99), appears not to have any measurable effect on the premature failure of bearing steels, because the reduction in surface energy cannot be measured under the conditions tested. The link with the premature failure of steels and the reduction of surface energy appears to be tenuous and may even be discounted as the other effects described above may be the influential mechanism.

7.5.4 Mechanism Summary

Taking into account the details above, the major influence in the premature failure of bearings caused by lubrication with water-based fluids appears to be the influence of the lack of elastohydrodyanmic film. Once the lack of film has been established, asperity interaction takes place and lubricant is forced into the resultant micro-crack openings. Once in the crack, the water reacts with the fresh metal surface and corrosion and hydrogen embrittlement, aided by the stressing take over.

In the case of water dissolved in small quantities, it is the surface active properties of the water which allow it to absorb onto the surface and then into surface microcracks and then follows on as described above.

With low stress systems, as in the case of the four-head rig series 6, corrosion appears to be the important mechanism where the formation of corrosion pits allows initiation to begin at much lower stress levels.

The hydraulic mechanism appears to be not applicable in the case of water fluids but no absolute proof of this has yet appeared practicable.

The chemical influence on the crack propagation rate appears to be small. Far more important is the influence of the water on pre-initiation conditioning of the surface and on the initiation of fatigue cracks.

Similarly to the hydraulic mechanism, the Rebinder effect is not proven, but does not appear to be important when considering the influence of water on the premature failure of bearing steels.

8. CONCLUSIONS

The conclusions drawn from the work carried out as part of this project are listed in the following paragraphs.

8.1 APPLIED STRESS

Stress of the type applied in the first test series on the four-head test rig had no apparent effect on the fatigue lives of bearing steel specimens lubricated by an invert emulsion. It was thought that the hardness of the specimens and the conforming size of the specimens had a greater influence on rolling contact fatigue.

8.2 RANKING OF FLUIDS

The Rolling Contact fatigue four-head test method was proved when the three classes of Fire Resistant Fluids HF-A (dilute emulsion) HF-B (invert emulsion) and HF-C (Aqueous Glycol) were ranked in the same order as previous workers. The test method was found to be less severe than the four-ball but more realistic. The Rig offered new possibilities for a fire resistant fluid test method, but it was not very realistic when compared to the lubricated bearings in a hydraulic fluid pump. As virtually no direct maintenance apart from maintaining the water content of the fluid could be achieved by further automation of the rig, it offers a relatively easy screening and monitoring method specifically for fire resistant fluids.

8.3 INFLUENCE OF THE OPERATING CONDITIONS ON FAILURE MECHANISM

From the work of previous investigators and that carried out during this study, it is clear that the operating conditions influence the failure mechanism greatly. When elastohydrodynamic films were formed such that $\lambda = 0.47$, the failure manifestation was pitting, but where unmeasurable film thickness was formed the failure manifestation was micropitting. This tied in with the work of Berthe and co-workers (12).

The longer the specimens survived, especially at low load, the more they suffered from corrosion as well as from fatigue initiated by lack of elastohydrodynamic film.

Where dissolved water or emulsified water is present in oil, there exists the problem of the water being more surface active than the oil and so surface active corrosion inhibitors must be added in reasonable quantities to prolong fatigue life.

The application of applied potential offered an improvement in fatigue lives but does appear to be a very practical method of improving fatigue lives in actual service.

From this work and that of others, the best way to prevent the premature failure of bearing steels lubricated by water containing fluids is to formulate additives to prevent corrosion, in largely oil containing systems and phosphate esters. In dilute emulsions and aqueous glycols the best way forward would be to add film promoting additives such as with the polymer-thickened fluids to ensure that asperity interactions were prevented and pre-initiation conditioning and initiation would be arrested and lives increased.

8.4 INFLUENCE OF WATER ON CRACK PROPAGATION

This part of the study, using the rotating/bending fatigue rig produced a few interesting results but did not add anything to an already confused picture. From this work and that of others, (14) (17), it would appear that the biggest influence of water is in the pre-initiation conditioning and in the initiation of failure phases.

8.5 CHEMICAL TECHNIQUES

The use of infra red spectroscopy, Scanning Electron Microscopy and Secondary Ion Mass Spectroscopy proved to be extremly useful. There were however problems associated with using new techniques for this type of examination. The theoretical uses for the techniques proved to be not surmountable at present. The major problems were the contamination of water in all infra-red spectra and the confusion of common ions in the SIMS analysis.

8.6 SUMMARY

The conclusions reached in the above paragraphs show that any attempt to study fully formulated lubricants is very difficult, but a new test method, the four-head rolling contact fatigue rig has been shown to provide useable information. The major problem with using, accelerated tests such as this, is that full correlation with field data must be achieved before any complete validity can be attached to the test. This is because effects seen in the field are often not reproduced in laboratory test methods.

9. PROPOSALS FOR FURTHER WORK

9.1 CORRELATION WITH FIELD DATA

Before the rolling contact fatigue four-head rig could be used as a test method for screening or testing fire resistant fluids, its correlation with field data should be established. Without this the test method would not have validity.

9.2 VERY THIN ELASTOHYDRODYANMIC FILMS

One of the most important effects identified in this work was the influence of the lack of reasonably thick films formed. Those formed currently could not be measured so before any work on polymer film thickness improvers, can be carried out, the films need to be measured. The new technique of Spikes and Guangteng (76), should be applied to the study of these very thin films.

9.3 DEPOSITED FILMS

Unstable emulsions (72), polymer-thickened fluids and +200mV polarised specimens have been shown to produce residual films on the surfaces. These films behave anomalously under elastohydrodynamic lubrication. This behaviour needs to be investigated as it would appear from this study that the use of additives to promote thicker films is the best approach to counter the deleterious behaviour of water based fluids. If the causes and properties of these residual films could be determined then improved performance could be achieved.

9.4 DEPTH PROFILES OF FATIGUE SURFACES

The technique of depth profiling using SIMS on this type of application has not been fully explored but it offers a reasonable approach if suitable instrumentation can be made available. A new technique Sputtered Neutral Mass Spectroscopy (SNMS) has recently appeared as a non-destructive depth profiling technique. The use of this technique is not possible or practicable at the moment but should be when the technique becomes more widely available.

9.5 FRACTURE MECHANICS

Because the use of the four-head rig takes a long time to produce a set of results and the rotating-bending rig is difficult to operate, a better approach to crack propagation studies would be to use the plate specimens described in section 4.8.1. The effect of water on crack growth could easily be investigated. As the use of fracture mechanics for fatigue data is increasing, a comprehensive study of the influence of water would lead to greater understanding of the effect of the media on crack growth rates.

10. REFERENCES

(1) Scott, D, "Lubricant Effects on Rolling Contact Fatigue","Rolling Contact Fatigue - The Performance Testing of Lubricants" Eds Tourret, R. and Wright, E. P., Institute of Petroleum, London, p 3-15, October 1976, (1977).

(2) Way, S., "Pitting Due to Rolling Contact", J Appl Mech, 2, A49-58, (1935).

(3) Lundberg, G and Palmgren, A. "The Dynamic Capacity of Roller Bearings, "Acta Polyt", Stockholm (Mechanical Eng, Series) 1947, No 7, (1947).

(4) Cordiano, H.V, Cochran, E.P. jnr, and Wolfe, R.J. "Effect of Combustion Resistant Hydraulic Fluids on Ball Bearing Fatigue Life", ASME 55-LUB-21, (1955).

(5) Grunberg, L. and Scott, D. "The Acceleration of Pitting failure by Water in the Lubricant", J. Inst. Petrol, 44, 406-10, (1958).

(6) Crook, A.W. "The Lubrication of Rollers" Phil. Trans. A. 250, 387, (1958).

(7) Dawson, P.H. "The Effect of Metallic Contact on the Pitting of Lubricated Rolling Surfaces", J. Mech. Eng. Sci., 4.1, 16-21, (1962).

(8) Rounds, F.G., "The Effect of Base Oil Viscosity and Type on Ball Bearing Fatigue "ASLE trans, 5, 172 - 82, (1962).

(9) McKelvey, R.E. and Moyer, C.A. "The Relation Between Critical Maximum Compressive Stress and Fatigue Life Under Rolling Contact", Proc I Mech E., "Fatigue in Rolling Contact", 28/3/63, 1-10, (1963).

(10) Dawson, P..H. "The Effect of Metallic Contact and Sliding on the Shape of the S-N Curve for Pitting Fatigue", Proc. I. Mech. E., "Fatigue in Rolling Contact", 28/3/63, 41-45, (1963).

(11) Tallian, T.E., "Rolling Contact Failure Control Through Lubrication", Proc I. Mech. E. 182 Pt 3A, 205-36, 1967-8, (1968).

(12) Berthe, D., Flamand, L, Foucher, D, and Godet, M. "Micropitting in Hertzian Contacts", Trans ASME, F, JoLT, 102, 478-89, (1980).

(13) Paris, P.C. and Erdogan, F. "Critical Analysis of Crack Propagation Laws", Trans ASME, D, J. of Basic Engrg., 85.4, 49-51, (1967).

(14) Lockwood, F.E., Cristodoulou, L. and Langan, T.J., "Anti-fatigue Additives", Proc. Additives for Lubricants and Operational Fluids", 5th Int Coll Eslingen, Ed. Bartz, W.J. 14-16/1/86, (1986).

(15) Yoshioko, T. and Fugiwara, T. "Measurement of Propagation Initiation and Propagation time of Rolling Contact Fatigue Crack by Observation of Acoustic Emission and Vibration". Paper presented to the Leeds-Lyon Symposium, Sept 1987.

(16) Polk, C.J., Murphy, R.W and Rowe C.N. "Determining Fatigue Crack Propagation Rates in Lubricating Environments through the Application of a Fracture Mechanics Technique" ASLE Trans, 18.4, 290-8, (1975).

(17) Polk, C.J. and Rowe, C.N., "Crack Growth Rate: Its Measurement and a Controlling Factor in Rolling Contact Fatigue", ASLE Trans, 19, 23-32, (1976).

(18) Johnson, L.G. "The Statistical Treatment of Fatigue Experiments", Elsevier Publishing, New York, 1964.

(19) Weibull, W. "A Statistical Distribution Function of Wide Applicability", J. Appl. Mech., 18, 293-97, (1951).

(20) Howes, M.A.H., Bhattacharyya, S. Bock, F.C., and Parikh, N.M., "Chemical Effects of Lubrication on Contact Fatigue. Part 1: The Test Programme, Data and Metallurgical Observations", Trans ASME, F, J.o.L.T., 98, 286-98, (1976).

(21) British Standard 970, En31, Steel, British Standards Institute 1963.

(22) Littmann, W.E. and Widner, R.L., "Propagation of Contact Fatigue from Surface to Subsurface Origins"., Trans ASME, D, J.o. Basic Engrg, 88, 624-36, (1966).

(23) Martin, J.A., Borgese, S.F. and Eberhardt, A.D., "Microstructural Alterations of Rolling-Bearing Steels Undergoing Cyclic Stressing", Trans ASME, D, J.o. Basic, Engrg, 88, 555-67, (1966).

(24) Martin, J.A. and Eberhardt, A.D. "Identification of Potential Failure Nuclei in Rolling Contact Fatigue", Trans ASME, D, J.o. Basic Engrg 89, 932-42, (1967).

(25) Donsinas, N. "Rolling Contact Fatigue of Steel Operating Under Tensile Stress", Diploma of Imperial College Thesis, (1983).

(26) Harris, T.A. "Rolling Bearing Analysis, 2nd Edition, "Wiley, New York (1984).

(27) Kenny, P., Smith. J.D., and March, C.N. "The Fatigue Life of Ball Bearings When Used with Fire-Resistant Hydraulic Fluids", "The Performance Testing of Hydraulic Fluids", Eds Tourret, R. and Wright, E.P., Institute of Petroleum, Chapter 33, 495-519, 1978, (1979).

(28) Johnson, K.L., Inelastic Contact: Plastic Flow and Shakedown", Proc "Contact Mech and Wear of Rail/Wheel Systems", University of Waterloo, Vancouver, 6-9/7/82 (1982).

(29) Goldblatt, I.L. "Model for Lubrication Behaviour of Polynuclear Aromatics", I&EC Product R and D, 10, 270-278 (1971).

(30) Dowson, D and Hamrock, B.T., "Isothermal Elastohydrodynamic Lubrication of Point Contacts - Part III. Fully Flooded Results", Trans ASME, F, J.o.L.T., 99, 262-76, (1977).

(31) Bhargava, V., Hahn, G.T. and Rubin, C.A. "An Elastic-Plastic Finite Element Model of Rolling Contact. Part 1 Analysis of a Single Contact.", J. Appl. Mech., 52, 67-74, (1985).

(32) Meerwin, J.E. and Johnson, K.L., "An Analysis of Plastic Deformation in Rolling Contract, Proc I Mech E", 177, 676, (1963).

(33) Bhargava, V., Hahn, G.T. and Rubin, C.A., "An Elastic-Plastic Finine Element Model of Rolling Contact, part 2. Analysis of Repeated Contacts", J Appl. Mech, 52, 75-82., (1985).

(34) Tallian, T.G. "A Unified Model for Rolling Contact Fatigue", Trans ASME, F, J.o.L.T., 104, 336-46, (1982).

(35) Chow, L.S.H. and Cheng, H.S., "The Effect of Surface Roughness on the Average Film Thickness Between Lubricated Rollers" Trans ASME, F, J.o.L.T., 98, 117-24, (1976).

(36) "Life Adjustment Factors for Ball and Roller Bearing "An Engineering Guide Sponsored by the Rolling Elements Committee, The Lubrication Division of the ASME, (1971).

(37) Keer, L.M., Bryant, M.P. and Haritos, G.K. "Subsurface and Surface Cracking Due to Hertzian Contact" Trans ASME, F, J.o.L.T., 104, 347-51, (1982).

(38) Keer, L.M. and Bryant, M.D. "A pitting model for Rolling Contact Fatigue", Trans A.S.M.E., F, J.o.L.T., 105, 198-205, (1983).

(39) Murakami, Y., Kaneta, M. and Yatsuzuka, H. "Analysis of Surface Crack Propagation in Lubricated Rolling Contact", ASLE trans, 28.1, 60-68, (1985).

(40) Grunberg, L. and Scott, D., "The Effect of Additives on the Water Induced Pitting of Ball Bearings", J. Inst. Petrol, 46, 259-66, (1960).

(41) Mantel, E.R., Robinson, G.H., and Thomson, R.F. "Influence of Atmospheric Moisture on Fatigue of Hardened Steel", Eng. Met. Q., 2.1, 57-61, (1961).

(42) Schatzberg, P. and Felsen, I.M., "Effects of Water and Oxygen During Rolling Contact Lubrication", Wear, 12, 331-42, (1968).

(43) Schatzberg, P. and Felsen, I.M. "Influence of Water on Fatigue - Failure Location and Surface Alteration During Rolling Contact Lubrication", Trans ASME, F, J.o.L.T., 91, 301-7, (1969).

(44) Felsen, I.M., McQuaid, R.W. and Marzani, J.A. "Effect of Seawater on the Fatigue Life and Failure Distribution of Flood Lubricated Angular Contact Ball Bearings" ASLE Trans, 15, 8-17, (1972).

(45) Penfold, R.E., "A Six-Station Vertical Rolling Fatigue Rig", Admiralty Oil Laboratory Technical Memorandum, No 64, Admiralty Oil Laboratory, Cobham, Aug 1972, (1972).

(46) Eastaugh, P.R. and Ritchie, J. "Improved Fluids for Submarine Hydraulic Systems", Wear, 34, 355-371, (1975).

(47) Stepurenko, V.T., Proskuryakov, G.T., Sakharov, M.G. and Oleinik, V.N. "Water in Mineral Oils on the Durability of steels", Zaschita Metallov (Protection of Metals), 11.2, 155-8, (1975).

(48) Cantley, R.E., "The Effect of Water in Lubricating Oil on Bearing Fatigue Life", A.S.L.E. Trans, 20.3, 244-248, (1976).

(49) Scott, D., "Further Data on the Effect of Additives on the Water Induced Pitting of Ball Bearings", J. Inst. Petrol., 48, 23-4, (1962).

(50) Schatzberg, P., "Inhibition of Water-Accelerated Rolling Contact Fatigue" Trans ASME, F, J.o.L.T., 93, 231-35, (1971).

(51) Rowe, C.N. "Lubricant Factors in Rolling Contact Fatigue", National Bureau of Standards Publication, 584, 301 - 312, (1980).

(52) Blanplain, G., "The Use of Polyglycols in French Coal Mines" "Performance Testing of Hydraulic Fluids", Eds Tourret, R. and Wright, E.P., Institute of Petroleum, 10/77, London, Chapter 27, 389-403, (1978).

(53) Baker, P. and Riley, N.H. "Development of Specialized Lubricants for Use in Critical Applications", "Friction, Lubrication and Wear, Tribology 50 Years On" Proc I Mech E, C215/87, 461-72 (1987).

(54) Stanton, T.F. and Whitwell, R., "The Possible Use of Chemically Treated Water as an Alternative to Dilute Oil in Water Emulsions in Hydraulic Powered Roof Supports", "Performance testing of Hydraulic Fluids", Inst of Petrol., Eds Tourret, R., and Wright, E.P., Chapter 29, 415-29, (1980).

(55) Hughes, D.G. and Forsberg, J.W., "Laboratory Parameters for High Water Based Hydraulic Fluid Testing" Proc Symposium Eslingen, 14-16/1/86, ed Bartz, W.J. (1986).

(56) Coal Specification (formerly National Coal Board) 463/1981 (1981).

(57) Mattison, R., Lloyd, G.I., and Schofield, J." Fatigue Effect on EN3 Steel Balls of Microbially Degraded Soluable Oil Emulsion," Trib. Int, 8.6, 253-255, (1975).

(58) Wan, G.T.Y. and Spikes H.A. "The Elastohydrodynamic Lubricating Properties of Water - Polyglycol Fire-Resistant Fluids", ASLE Trans, 27, 366-372, (1984).

(59) Hobbs, R.A. and Mullett, G.W. "Effects of some Hydraulic Fluid Lubricants on the Fatigue Lives of Rolling Bearings.", Proc I.Mech.E, 183Pt3P, 21-27, (1968-9).

(60) Turski, A.B., "Studies of Engineering Properties of Fire Resistant Hydraulic Fluids for Underground Use, Part 1 Mining & Mineral Engrg, Dec 1968, 48-58, (1968).

(61) Turksi, A.B. ibid, Part 2, Feb 69, 50-9, (1969).

(62) Bietowski, R., "Ball Bearing Lubricants - Use of Fire Resistant Hydraulic Fluids.", Colliery Guardian, May 1971, 235-9, (1971).

(63) Kenny, P. and Yardley, E.D. "The Use of Unisteel Rolling Fatigue Machines to Compare the Lubricating Properties of Fire Resistant Fluids" Wear, 20, 105-121, (1972).

(64) Hobbs, R.A. "Fatigue Lives of Ball Bearings Lubricated with Oils and Fire-Resistant Fluids", "Elastohydrodynamic Lubrication Symposium 1972, Proc I. Mech E. (1972).

(65) Yardley, E.D., Kenny, P., and Sutcliffe, D.A. "The Use of Rolling - Fatigue Test Methods Over a Range of Loading Conditions to Assess the Performance of Fire-Resistant Fluids", Wear, 28, 29-47, (1974).

(66) March, C.N., "The Evaluation of Fire-Resistant Fluids Using the Unisteel Rolling Contact Fatigue Machine"., "Rolling Contact Fatigue - Performance Testing of Lubs", Int Symp, Eds Touret, R. and Wright, E.P. Oct 1976 Inst Petrol, 217-230, (1977).

(67) Knight, G.C. "Suitability of Hydrostatic Pumps and Motors", "Rolling Contact Fatigue Performance Testing of Lubricants" Eds Tourret, R and Wright, E.P., Inst Petrol, 10/76, 193-215 (1977).

(68) Culp, D.V. and Widner, R.L., "Effect of Fire Resistant Hydraulic Fluids on Tapered Roller Bearing Fatigue Life", SAE paper 770748 (1977).

(69) Hamaguchi, H., Spikes, H.A. and Cameron, A. "Elastohydrodynamic Propeprties of Water-in-Oil Emulsions", Wear, 43, 17-24, (1977).

(70) Dalmaz, G. and Godet, M. "Film Thickness and Effective Viscosity of Some Fire Resistance Fluids in Sliding Point Contacts, ASME Trans, F, J.o.L.T., 100, 304-8, (1978)

(71) Tokarzewski, L., Zakrzewski, J., Wachowicz, J., and Szczepaniak, S., "Phosphoryl Tris (Diethanolamide) (DAP) - A New Additive for Water-based and Ethopene Glycol Based Hydraulic Fluids and Lubricants"., Wear, 50.2, 365-9, (1978).

(72) Wan, G.T.Y. "The Elastohydrodynamic Properties of Water-based Hydraulic Fluids" Ph.D. Thesis, University of London, 1983.

(73) Wan, G.T.Y., Kenny, P., and Spikes, H.A., "Elastohydrodynamic Properties of Water-based Fire Resistant Hydraulic Fluids". Trib Int, 17, 309-315, (1984).

(74) Taylor, R and Wang, Y.Y., "Lubrication Regimes and Tribological Properties of Fire Resistant Hydraulic Fluids", ASLE Lub Engrg, 41.1, 44-50, (1985).

(75) Kimura, Y. and Okada, K. "Film Thickness at Elastohydrodynamic Conjunctions Lubricated with Oil-in-Water Emulsions", Friction, Lubrication and Wear - Tribology 50 Years On", Proc I Mech. E, C176/87, 85-90, (1987).

(76) Spikes, H.A., and Guangteng, G., "Properties of Ultra Thin Lubricating Films Using Wedged Spacer layer Optical Interferometry. "Paper presented to the 1987 Leeds-Lyon Symposium (1987).

(77) Cameron, A. "On a Unified Theory of Boundary Lubrication" Proc 12th Leeds-Lyon Con, Eds Dowson D, Taylor, C., Godet, M., and Berthe, D. Lyon 1985, (1985).

(78) Yahagi, Y., "Sulphur Lubricant Additives for Oils and Emulsions", Ph.D. Thesis, University of London, (1979).

(79) Spikes, H.A. and Cameron, A. "Scuffing as a Desorption Process - An explanation of the Borsoff Effect" ASLE Trans, 17, 92-96 (1973).

(80) Littmann, W.E., Widner, R.L., Wolfe, J.O., and Stover, J.D., "The Role of Lubrication in Propagation of Contact Fatigue Cracks", Trans ASME, F, J.o.L.T., 90, 89-100, (1968).

(81) Michan, B., Berthe, D., and Godet, M., "Observations of Oil Pressure Effects in Surface Crack developments", Trib, Int, 1, 119-211, (1974).

(82) Armstrong, E.L., Leonardi, S.J., Wooding, P.S., and Murphy, W.R., "Evaluation of Water-accelerated Bearing Fatigue in Oil Lubricated Ball Bearings", Lubr. Engrg., 34.1, 15-21, (1978).

(83) Sullivan, J.L. and Middleton, M.R., "The Pitting and Cracking of SAE 52100 Steel in Rolling/Sliding Contact in the Presence of an Aqueous Lubricant". Proc ASME/ASLE Con 22-24/10/84, Paper No 84-LC-3C-4.

(84) Rudston, S.G., and Whitby, R.D., "Recent Developments in the Performance Properties of Water based Cutting and Hydraulic Fluids, J Synth Lubr, 2, 183-212, (1985).

(85) Grunberg, L., Jamieson, D.T. and Scoff, D. "Hydrogen Penetration in Water-Accelerated Fatigue of Rolling Surfaces"., Philos. Mag, 8.93, 1553-68, (1963).

(86) Grunberg, L., Jamieson, D.T., Scott, D and Lloyd, R.A., "Hydrogen Diffusion in Water Accelerated Rolling Surface Fatigue", Nature, 188, 1182-3 (1960).

(87) Gray, W. "Introduction to conference on Hydrogen Embrittlement" an ASTM STP 593 (1977).

(88) Ciruna, J.A. and Szieleit, H.J., "The Effect of Hydrogen on the Rolling Contact Fatigue Life of AISI 52100 and 400c Steel Balls", Wear, 24, 107-118, (1973).

(89) Ray, D., Vincent, L., Coquillet, B., Guirandoq, P., Chene, J., and Aucouturier, M., "Hydrogen Embrittlement of a Stainless Ball Bearing Steel", Wear, 65.1, 103-11, (1980).

(90) Frisch, B., and Thiele, W-R., "Tribologically Induced Effect of Hydrogen Effusion and Penetration in Steels", Wear, 98, 213-227 (1984).

(91) Cotton, F.A., and Wilkinson, G., "Advanced Inorganic Chemistry, 4th Ed", Chapter 15, John Wiley and Sons, Canada (1980).

(92) Evans, U.R. "The Corrosion and Oxidation of Metals", Arnold, London, (1960).

(93) Endo, K., and Komai, K., "Corrosion Fatigue Strength of a Steel Under Controlled Potentials and pH Values", Proc 13th Japanese Congr on Mats - Res. - Metallic Mats, 162-6, (1970)

(94) Endo, K., Komai, K., and Matsuda, Y. "Mechanical Effects of Corrosion Fatigue Crack Growth of a Steel", Bull J.S.M.E., 24.194, 1319-25, (1981).

(95) Vijh, A.K. "Electrochemical Mechanisms of the Dissolution of Metals and the Concomitant Oxidation of Lubricating Oils Under High Temperature Friction Conditions", Wear, 104, 151-6, (1985).

(96) Bjerk, R.O., "Oxygen - An 'Extreme Pressure' Agent", ASLE Trans, 16, 97-106, (1973).

(97) IP Test No 239 "Corrosive Properties of Water Based Fluids" IP Test Methods (1979) (1983).

(98) Leach, J.S.L. and Talks, M.G., "The Electrochemical and Cavitational Erosion Properties of Hydraulic Emulsions", Proc 9th Inf Congr on Metallic Corr., Toronto, Canada, 1, 352-8, (1984).

(99) Rebinder, P.A. "Influence of Changes in the Surface Energy on Clearage Hardness and Other Properties of Crystals" Proc 6th Con. Rns Physicists, Gosident, Moscow, 29, (1928).

(100) Lobioko, V.I., and Karpenko, G.V., "Effect of a Limited Number of Alcohols on the Kinetics of Crack Development and the Energy of a Steel U8A", Mekhanika Materialov (Sov Mater Sci), 12.4, 51-5, (1975).

(101) Lobioko, V.I., Karpenko, G.V., and Vasilenko, I.I., "Absorption Fatigue of Structural Steels (Used for Ball Bearings) in the Presence of Alcohols". Mekhanika Materialov (Sov Mater Sci), 12.1, 21-25, (1976).

(102) Stepurenko, V.T., Sakharov, M.G., Stepurenko, Y.V., and Proskuryakov, G.T., "Influence of the Medium on the Endurance of Steel (Fatigue Testing in Air Distilled Water, Water with Monoethanolamine, and moist and dehydrated oil)", Zaschita Metallov (Protection of Metals), 14.6, 706-9, (1978).

(103) Riddei, V., Pacov, P. and Appledorn, J.K., "Cavitation Erosion and Rolling Contact Fatigue". Wear 27.1, 99-108, (1974).

(104) Okada, T., Awazu, K., and Kawasaki, H. "Influence of Cavitation Erosion on Corrosion Fatigue and the Effect of Surface Coatings on Resistance". Wear, 63, 51-70, (1980).

(105) Institute of Petroleum Test Method No 239. "Extreme Pressure Properties. Friction and Wear Tests for Lubricants: four ball Machine" IP test methods 239/79 (1981).

(106) Institute of Petroleum test method No 300 "Rolling Contact Fatigue Tests for Fluids in a modified four-ball machine" IP test methods 300/79 (1981).

(107) Institute of Petroleum Test Method No 305. "The Assessment of lubricants by Measurement of their Effect on the Rolling Fatigue Resistance of Bearing Steel Using the Unisteel Machine" IP Test Method 305/79 (1981).

(108) Kenny, P. "The Development of IP Test Method 305/74 Tentative - The Assessment of Lubricants by Measurement of Their Effect on the Rolling Fatigue Resistance Bearing Steel Using the Unisteel Machine", "Rolling Contact Fatigue - Performance Testing of Lubricants" Eds Touret, R and Wright, E. P. Institute of Petroleum, October 1976 (1977).

(109) Onions, R.A. "An Investigation into the Possibility of Using Fire-Resistant Hydraulic Fluids for Royal Naval Systems", Performance Testing of Lubricants", Eds Touret, R., and Wright, E.P., Institute of Petrol., Chapter 30, 439-458, (1980).

(110) Parker, R.J., Zaretsky, E.V. and Bambarger, E.N., "Evaluation of Load-Life Relation with Bearings at 500°F" ASME paper 73-lub-7' (1973).

(111) Stickels, C.A., "Rolling Contact Fatigue Tests of 52100 Bearing Steel Using a Modified NASA Ball Test Rig", Wear, 98, 199-210, (1984).

(112) Institute of Petroleum test Method No 281 "Anti-wear properties of Hydraulic Fluids - Vane Pump Test" IP Test Methods 281/80 (1981).

(113) Galvin, G.D. and Naylor, H. "Effect of Lubricants on the Fatigue of Steel and other Metals, Proc I. Mech E, 179.1.27, 857-71. (1964-5).

(114) Law, D.A. "The Development and Testing of an Advanced Water in-oil Emulsion for Underground Mine Service". ASLE Lub Engrg, 37.2, 82-90, (1981).

(115) Rowell, J.R. "The State of the Art with 5/95 Dilute Emulsions in Transmissions and Roof Support Applications in Coal Mining". Performance Testing of Hydraulic Fluids, "Eds Tourret, R, and Wright, E.P. Chapter 28, Inst of Petrol, 405-13 (1980).

(116) Hopkinson, N. Principal Scientific Officer, Petroleum Chemistry and Technology Division, (formerly Admiralty Oil Laboratory), Private Communication.

(117) Eastaugh, P.R., "Use of Accelerated Tests to Establish the Lubricant-Steel Interaction on Bearing Fatigue Life", "Rolling Contact Fatigue Testing of Bearing Steels", Ed Hoo JCC, ASTM STP 771, 219-36, (1982).

(118) Eisenstadt, R. and Fuller, W.D. "Generation of Crack Propagation Data on Notched Rotating Beam Specimens by Means of an Interrupted Stressing Technique" Trans ASME, D, J.O. Basic Engrg, 92, 183-192, (1970).

(119) Harris, W.J., "Significance of Fatigue" Oxford University Press, P14, (1976).

(120) Neuber theory of stress concentration factors "Mechanical Engineers Reference Book" 11th Edition Eds Parrish, A., Chapter 7, Butterworth, London (1973).

(121) Harris, D.O., "Stress Intensity Factors for How Circumferentially Notched Round Bars, "Trans ASME, D, J.O. Basic Engrg, 89.1, 49-51, (1967).

(122) Talks, M.G. (British Coal, HQ Technical) Private Communication.

(123) Nakàjima, A., "Effect of Asperity Interacting Frequency of Surface Durability". Int. Symp Gearing and Power Transmission, Tokyo, 1981, 401-6, (1981).

(124) Olver, A. V. "Wear of Hard Steel in Rolling Lubricated Contact" Ph.D. Thesis, University of London, 1986.

(125) Reichenbach, G.S. and Synita, W.D., "An Election Microscope Study of Rolling Contact Fatigue", ASLE Trans, 8, 217-33, (1965).

(126) Goto, M., Miyagawa, H. and Nisitani, H. "The Effect of Oil Environments of the Initiation of Fatigue Crack and Propagation of Small Crack in Plan Specimens" Eslingen Int Conf. Jan (1988) Ed Bartz, W.J. (1988).

(127) Zheng, X and Hirt, M.A. "Fatigue Crack Propagation in Steels", Engrg Fract. Mech, 18, 965-73 (1983).

(128) Swahn, H., Becker, P.C., and Vingsbo, E.T., "Electron Microscope Studies of Carbide Decay During Contact Fatigue in Ball Bearings", Metal. Sci., 10.1, 35-39, (1976).

(129) Nakayama, T. and Takano, M., "High Voltage Electron Microscope Observations of Crack Tip produced in Type 304 Stainless Steel by Stress Corrosion Cracking and Hydrogen Embrittlement", Corrosion, 38.1, 1-9, (1982).

(130) Jahanamir, S. "Examinations of Wear Mechanisms In Automotive Camshafts", Wear, 108, 235-54, (1986).

(131) Zinner, E, "Depth Profiling by Secondary Ion Mass Spectroscopy", Scanning, 3, 57-78 (1980).

(132) Suzuki, K-I and Ohtsubo, T. "Detection of Hydrogen in Steel by Secondary Ion Mass Spectroscopy., "Trans Iron and Steel Institute of Japan, 24, B-258, (1984).

(133) Kilner, J.A. (Surface Analysis Technology) Private Communication, (1986).

(134) Chandler, W.T. and Walter, R.J. "Hydrogen-Environment Embrittlement of Metals and its Control", "Hydrogen in Metals" A.S.M. Metals Park Ohio, 1057-1078.

(135) Kilner J.A. (Surface Analysis Technology), Private Communication (1987).

(136). Talks, M.G. (British Coal HQ Technical) Private Communication (1986).

(137) D.A. Yardley (ibid) Private Communication (1988).

(138) Foord, C.A., Hammann, W.C. and Cameron A, "Evaluation of Lubricants Using Optical Elastohydrodynamics" ASLE Trans, 11, 31-43 (1968).

(139) Spikes, H.A and Wan, G.T.Y., "Elastohydrodynamic Tests on Fire Resistant Greases", Report for N.C.B., TS008/84, March 1984, (1984).

(140) Diaconescu, E., "Pitting Under Traction in Heated Loaded Point Contacts", Ph.D. Thesis, University of London, (1975).

(141) ESDU "Tribology Series, 5, Contact Stresses" An ESDU publication No 78035, (1978).

11. APPENDICES

Appendix 1

Medium ranks for a number of failures.

Diaconescu, (140), gives the two formulae for the calculation of medium ranks for any number of failures above 20 equation A1.1 is used, below or equal to 20 the equatic A1.2 is used.

$$\lambda_n (r) = r - 0.30685 - 0.3863 \left(\frac{r-1}{n-1} \right) \qquad n > 20 \qquad \text{Eq A1.1}$$

$$\lambda_n (r) = 1 - 2^{(-1/n)} + \left(\frac{r-1}{n-1} \right) (2^{(1-1/n)} - 1) \qquad n < 20 \quad \text{Eq. A1.2.}$$

As all the failures are between 11 and 15 the medium ranks are given below in table A1.1.

	NUMBER OF FAILURES				
Failure Number	11	12	13	14	15
1	6.11	5.61	5.19	4.83	4.52
2	14.89	13.68	12.66	11.78	11.01
3	23.66	21.75	20.13	18.73	17.51
4	32.44	29.82	27.60	25.68	24.01
5	41.22	37.89	35.06	32.63	30.51
6	50.00	45.59	42.53	39.58	57.00
7	58.78	54.04	50.00	46.53	43.50
8	67.56	62.11	57.47	53.47	50.00
9	76.34	70.18	64.94	60.42	56.50
10	85.11	78.25	72.40	67.37	63.00
11	93.89	86.32	79.87	74.32	69.49
12	-	94.39	87.34	81.27	75.99
13	-	-	94.81	88.2	82.49
14	-	-	-	95.17	88.99
15	-	-	-	-	95.48

Table A1.1.

These cumultative percentage failures are plotted with the ordered lines on Weibull paper. From the graphs L_{10}, L_{50} are measured and the Weibull slope, e, is calculated.

A graph showing the variation in Weibull mean for a series of Weibull slopes is given in Figure A1.1.

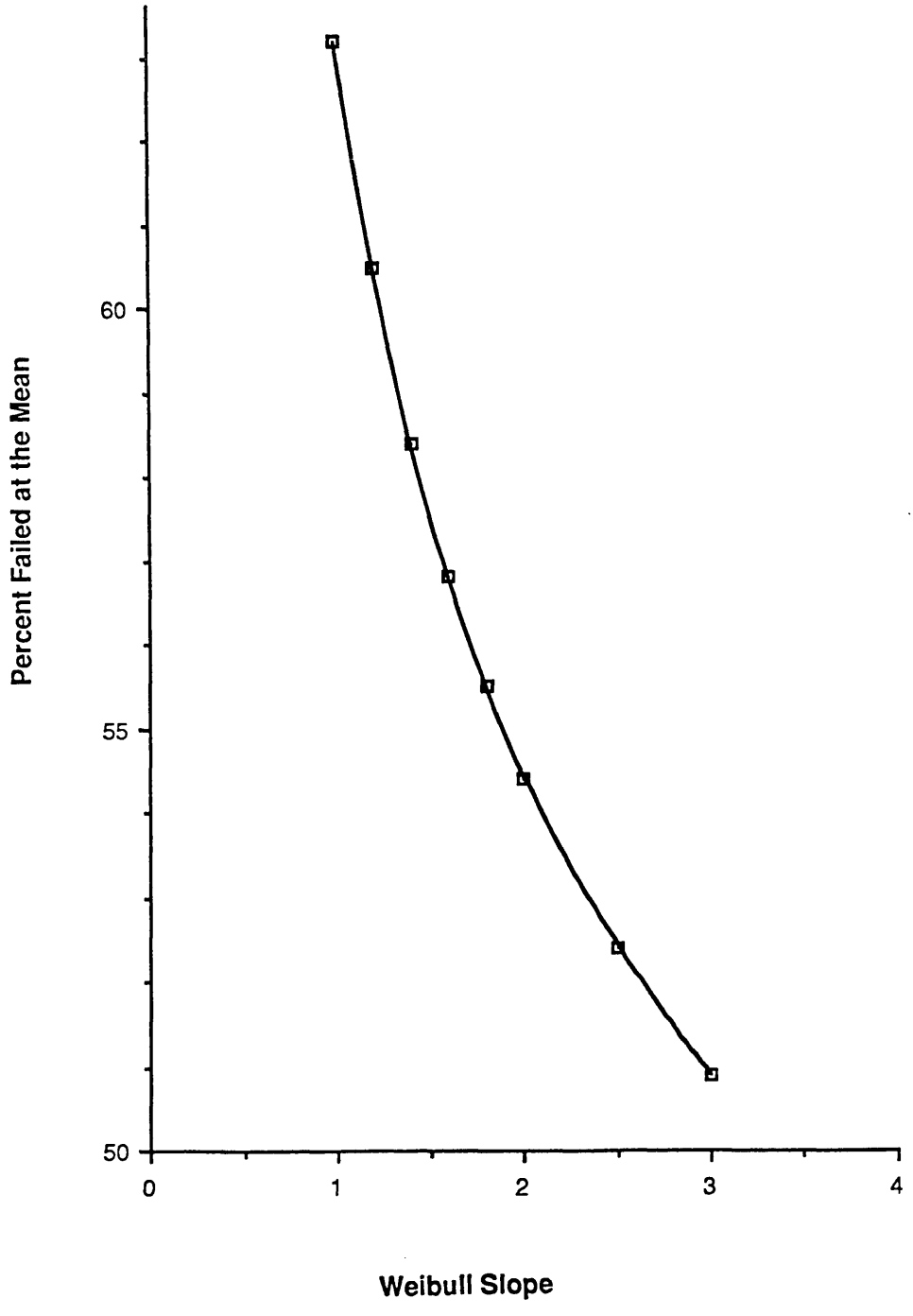

Figure A1.1

Variation of mean for different Weibull slopes (18)

Appendix 2

Calculation of Confidence Limits, (18)

In order to establish that two sets of results are different, 90% confidence must be established. This is achieved by the following method.

1. Weibull plots are drawn of the two sets of results and the Weibull slopes calculated.

2. The total degrees of freedom of the system must be calculated. This comes from the degrees of freedom for each of the two lots. if N_1, is the number of failures of first lot then the degrees of freedom are $(N_1 - 1)$ and the total degrees of freedom are $(N_1 - 1) \times (N_2 - 1)$.

3. The ratio of the mean lives (if mean lives are being compared) is calculated.

4. Using the life ratio and the degrees of freedom, these are applied to graphs taken from Johnson, (18), for the appropriate Weibull slope the confidence limit is obtained.

If the Weibull slopes are not equal the confidence limits are obtained at each of the Weibull slopes and then the average is taken of the two limits obtained.

The only problem with using the method of Johnson (18), is that only the mean lives can be compared assuming that Weibull slopes between 1 and 2 have been obtained. Outside this range approximations only may be made.

Appendix 3

Contact Stresses Calculations

Under dry static, smooth frictionless conditions the contact stress of the ball on the bar can be calculated using the method described below, (141). The contact for a ball on a bar is an elipse. The contact itself can be visualised in the x and y planes, Figure A3.1 and A3.2, A3.3.

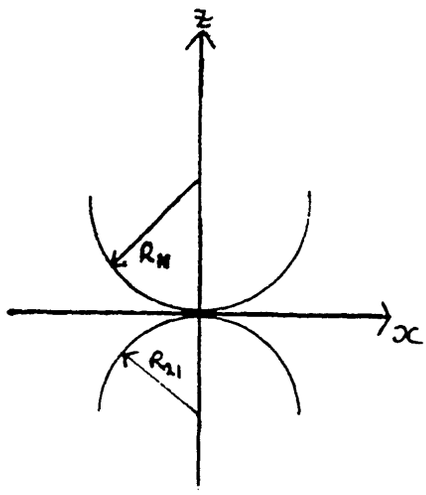

fig.A3.1
y plane

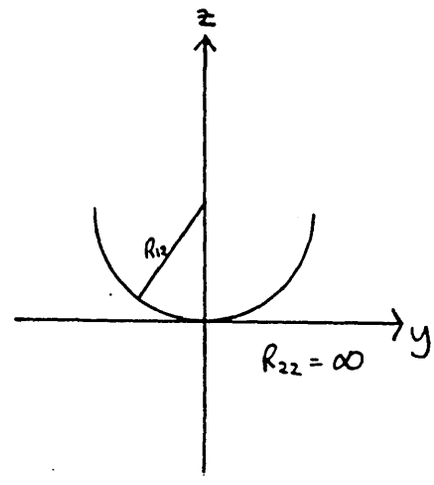

fig.A3.2
x plane

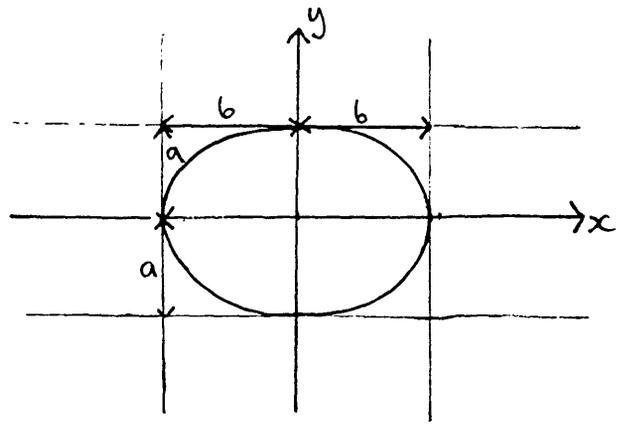

fig.A3.3
the contact

From these radii the curvature parameters A and B, used in the subsequent calculations must be used.

$$A = \frac{1}{2}\left(\frac{1}{R_{12}} + \frac{1}{R_{22}}\right) \qquad \text{Eq A3.1}$$

$$B = \frac{1}{2}\left(\frac{1}{R_{11}} + \frac{1}{R_{21}}\right) \qquad \text{Eq A3.2}$$

and the values of (A+B) and (A/B) are evaluated. The next evaluation is the reduced Youngs Modulus for each of the Bodies, Eq A3.3.

$$E_x' = \left(\frac{1 - \sigma_x^{\,2}}{\pi E_x}\right) \qquad \text{Eq. A3.3}$$

the load parameter W is the calculated, Eq 10.4.

$$W = \left[\frac{3\,P\,\pi}{4}\left(E_1' + E'_2\right)(A+B)^2\right]^{1/3} \qquad \text{Eq A3.4}$$

This is then used in the three equations to calculate the maximum compressive stress in the contact and the contact dimensions, a and b, where C_f, C_a, C_b are constants depending on the ratio A/B, (141).

$$\rho_{max} = -C_f \frac{2W}{\pi^2 (R_1 + R_2)} \qquad \text{Eq A3.5}$$

$$a = \frac{C_a W}{(A+B)}\left(\frac{A}{B}\right)^{1/3} \qquad \text{Eq A3.6}$$

$$b = \frac{C_b W}{(A+B)}\left(\frac{A}{B}\right)^{1/3} \qquad \text{Eq A3.7}$$

Values of a and b are then fed into equations A3.8 and A3.9 to obtain the value of the stress at any point in the elipse and the maximum direct stress.

$$P_o = \frac{1.5P}{\pi a b} = -f_z \qquad \text{Eq A3.8}$$

$$P = P_o\left(1 - \frac{x^2}{a^2} - \frac{y^2}{b^2}\right)^{1/2} \qquad \text{Eq A3.9}$$

Values of the Radii Youngs modulus and poissons ratio for the materials, and the normal load are given for the two bodies and from these values of P_o, a, b are obtained.

Appendix 4 - Film Thickness Equations

The elastohydrodynamic equations of Dowson and Hamrock, (30), are given below, Eq A4.1 is used to calculate the central film thickness and Eq A4.2 to calculate the minimum film thickness.

$$\frac{h_{central}}{R_x'} = 2.69 \left\{\frac{U\eta_o}{E'R_x'}\right\}^{0.67} (\alpha E')^{0.53} \left\{\frac{W}{E'(R'_x)^2}\right\}^{-0.067} (1-0.61e^{-0.73k})$$

Eq A4.1

$$\frac{h_{min}}{R_x'} = 3.63 \left\{\frac{U\eta_o}{E'R_x'}\right\}^{0.68} (\alpha E')^{0.49} \left\{\frac{W}{E'R'^2_x}\right\}^{-0.073} (1-e^{-0.68k})$$

Eq A4.2

Where

$$1/R_x' = \left\{\frac{1}{R_{11}} + \frac{1}{R_{21}}\right\}$$

$$1/Ry' = \left(\frac{1}{R_{12}} + \frac{1}{R_{22}}\right)$$

$$k = 1.03 \left\{\frac{R_y'}{R_x'}\right\}^{0.64}$$

U = mean speed of the two bodies $u = \left(\frac{u_1 + u_2}{2}\right)$

η_o = lubricant viscosity

E' = materials parameter, $\frac{2}{E'} = \left(\frac{1-\nu_1^2}{E_1}\right) + \left(\frac{1-\nu_2^2}{E_2}\right)$

E = Young modulus

ν = poissons ratio

α = pressure viscosity coefficient

W = normal load

subscripts 1, 2 indicate to which body they apply.

Appendix 5

Karl Fischer Water detecting equipment

At the start of the study a traditional titrating Karl Fischer water detector was used to assay the emulsions for water. An automatic electrical Karl Fischer was then purchased. The new machine was much safer to use and easier to operate. Details of both methods are given below.

The traditional method is based on the noxious substance pyridine and water is quantified by the reactions below.

$C_5H_5N.I_2$ + $C_5H_5N.SO_2$ + C_5H_5N + H_2O ⟶

pyridine-Iodine complex (titrant)	pyridine-sulphur dioxide complex	pyridine	water in a known weight of emulsion

$$2\ C_5H_5N.HI + C_5H_5N.SO_3 \xrightarrow{CH_3OH\ (methanol)} C_5H_5N.\ CH_3SO_4H \qquad \text{Eq A5.1}$$

The end point of the reaction is measured by a change in the resistance of the mixture and a known quantity of the solution is used to centralise the water and from this the amount of water is calculated.

The "coulomatic" method uses similar reactions to the above except that non-toxic amines and alcohols are used in the reaction. Instead of adding the iodine complex, the iodine is generated electrically in the cell and the amount of charge required to produce the iodine to neutralise the water is measured. From the amount of emulsion added the concentration of water is calculated. The end point is again measured by a conductance/resistance method. The reactions are given below.

$I_2 + H_2O + SO_2 +$ ROH (alcohol) + 3R'N (amine) ⟶

$$2R'N.HI + R'N.\ HSO_4.R \qquad \text{Eq A5.2}$$

A diagram of the cell is given below, Figure A5.1

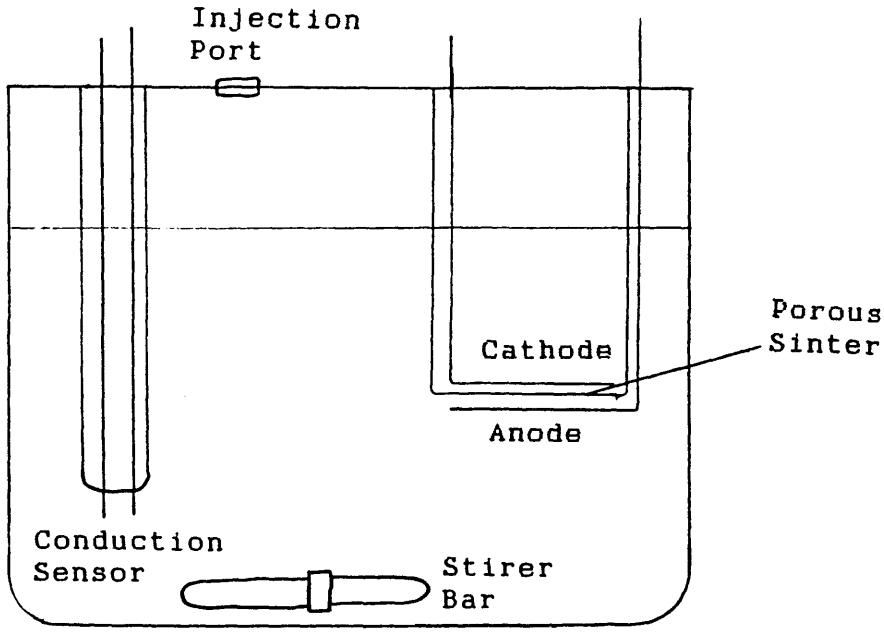

Fig A5.1

Appendix 6

Dynamic Capacity of the Bearing System.

Using the formula direct from Harris, (26), P455 Eq 14.58

$$Ca = A\left[\left(\frac{2R}{D}\right) \cdot \left(\frac{r}{r-R}\right)^{0.41} \frac{(1+\nu)^{1.39}}{(1-\nu)^{1/3}} \frac{(1-\nu)^{1.39}}{(1+\nu)^{1/3}} \left(\frac{\nu}{\cos\alpha}\right)^{-0.73}\right] D^{1.8} Z^{1/3}$$

Eq A6.1

Where A = materials constant (Nmm)
r = inner groove radius (mm)
R = ball contour radius (mm)
D = ball diameter (mm)
R = D/2
α = contact angle
dm= pitch diameter (mm)
$\nu = \cos\alpha / d_m$
Z = number of balls

In the system employed α = o, d_m = 17.84mm
r = oo, r/(r-R) = 1
R = 6.35mm A = 98.1 Nmm
Z = 1 , D = 12.7mm

This gives the value for the system of

Ca = 2043 N

Appendix 7

Optical Interferometry

This technique was developed to look at the elastohydrodynamic performance of oils, (138). More recently Wan (72) used it to investigate the lubricating properties of water based fluids, fig A7.1. A loaded steel ball is run against a glass disc coated with chromium. Light is shined on the contact and viewed through an optical microscope. The light reflected from the ball interferes with light reflected from the chromium. From the differences in path length (h opt) the film thickness in the contact can be calculated.

For monochromatic light

The optical path difference, S, between the two beams for normal incidence, Eq A7.1.

$$S = 2nh \qquad \text{Eq A7.1}$$

for oblique incidence, Eq A7.2.

$$S = 2nh \cos \varnothing + \phi \qquad \text{Eq. A7.2}$$

where ϕ = correction factor for phase change on reflection. Light fringes are seen where s is an integral number of wavelengths, Eq A7.3.

$$K\lambda = 2nh \cos \varnothing + \phi \qquad \text{Eq A7.3}$$

where k = 0,1,2,3, the fring order

dark fringes are seen where s is integral number of wavelengths plus a half of a wavelength (destructive interference) Eq A7.4.

$$(K + \tfrac{1}{2})\ \lambda = 2nh \cos \varnothing + \phi \qquad \text{Eq A7.4}$$

for white light

Chromatic interferometry gives a series of colour fringes because the different wavelengths give difference phase differences for the same path length.

Change in film thickness for successive maxima Eq A7.5.

$$\Delta h = \frac{k' \lambda}{2n \cos \phi}$$

A definite order of colours is seen as the film thickness changes. Small changes in h gives big colour differences ie greater resolving power, variation of colour is checked by calibration.

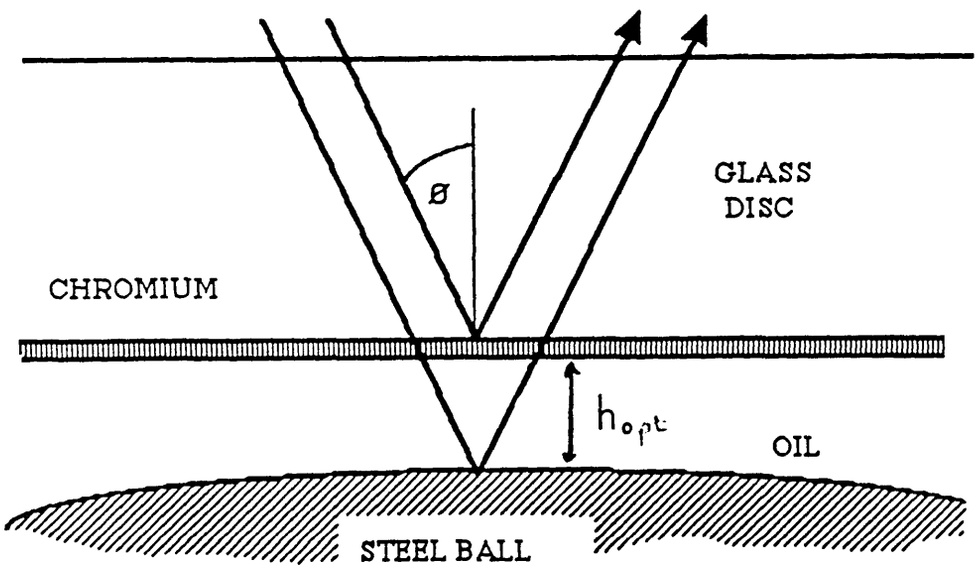

Figure A7.1

Optical Interferometric EHD Rig

Appendix 8

Stress Intensity Factors

As described in section 6.3, the calculation of stress intensity factors was not possible from the work of Harris (121) or from Eistenstadt and Fuller (118) because of empirical factors used in their equations. A better approach was to use Neuber theory (120).

The bending stress σ_b is calculated from the bending moment, M, and the cross-section area Eq A8.1.

$$\sigma_b = \frac{M.y}{I} = \frac{M}{Z} \qquad \text{Eq A8.1}$$

y = distance from axis to outermost fibre/mm
Z = sectional modulus / mm^3 = $I/y = \pi d^3/32$
I = 2nd moment of area/mm^4

$$\sigma_b = \frac{M}{(\pi d^3/32)} \qquad \text{Eq A8.2}$$

The stress intensity factor, K_t, is calculated from the ratio D/d and r/d from fig A8.1. This is used to calculate ΔK as per equation Eq A8.3.

$$\Delta K = 2K_t . \sigma_b \qquad \text{Eq A8.3}$$

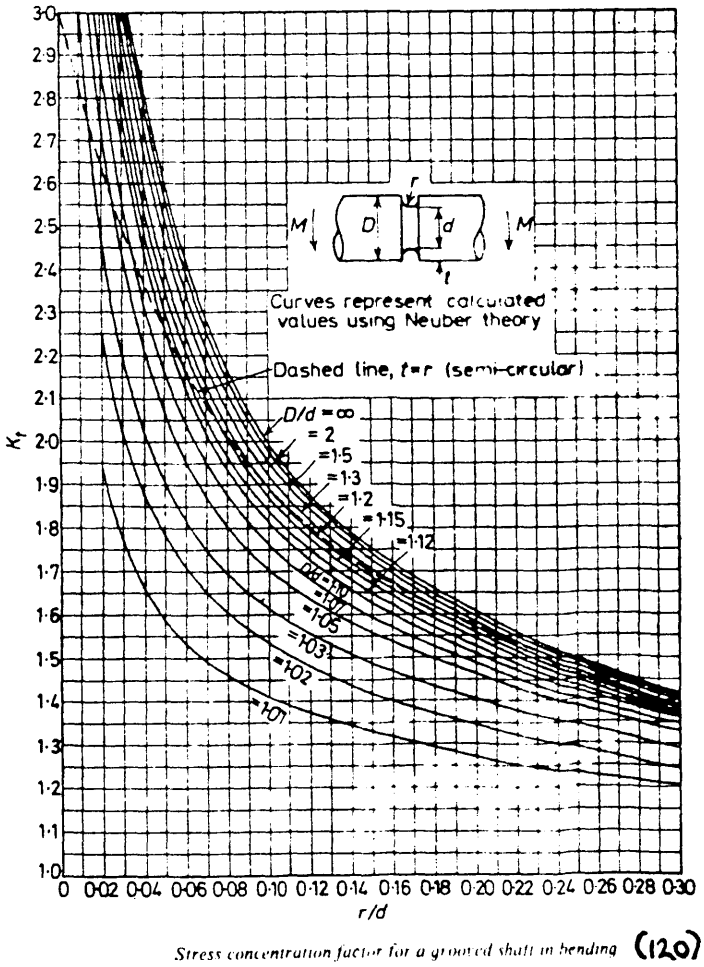

Stress concentration factor for a grooved shaft in bending (120)

Figure A8.1.

Appendix 9

Calculation of crack Propagation rates

The Paris law of crack growth (13), Eq 2.6, the steady state crack propagation rate is calculated.

$$\frac{da}{dN} = C\,(\Delta K)^m \qquad \text{Eq 2.6}$$

rearranging and integrating.

$$\int_{A_1}^{A_2} dA = C\,(\Delta K)^m \int_{N_1}^{N_2} dN \qquad \text{Eq A9.1}$$

$$A_2 - A_1 = C(\Delta K)^m\ [\,N_2 - N_1\,] \qquad \text{Eq A9.2}$$

Where 2 indicates final state and 1 indicates initial state.

For a true statement of the crack propagation rate, the stress intensity factory ΔK, varies with crack length. Because this introduces several complexities into the method, a simplification of calculating ΔK at the start of the load stage and at the end of the load stage and taking an average.

C and n were calculated by plotting log (da/dN) versus log (ΔK), the slope being n and the intercept n log C.

Appendix 10

Calculation of α

$$h_{opt} = k\ (U\eta_o)^{0.7}\ (\alpha)^{0.5} \qquad \text{Eq. A10.1}$$

By the method described in appendix 4, H_{opt} is calculated for both the reference oil and for the test oil.

Setting up two equations at the same speed and level

$$h_{ref} = K\ (U\eta_{o\ ref})^{0.7}\ (\alpha_{ref})^{0.5} \qquad \text{Eq. A10.2}$$

$$h_{test} = K\ (U\eta_{o\ test})^{0.7}\ (\alpha_{test})^{0.5} \qquad \text{Eq. A10.3}$$

The same conditions eliminate K and U on combination.

$$\frac{h_{test}}{h_{ref}} = \left\{ \frac{(\eta_o)^{0.7}\ (\alpha)^{0.5}\ test}{(\eta_o)^{0.7}\ (\alpha)^{0.5}\ ref} \right\} \qquad \text{Eq. A10.4}$$

rearranging

$$\alpha_{test} = \left[\frac{(h_{test})}{(\overline{h_{ref}})}\ \frac{(\eta_{o\ ref})^{0.7}}{(\overline{\eta_{o\ test}})}\ (\alpha_{ref})^{0.5} \right]^2$$

Eq. A10.5


4
A
B
C
D
E
5
6
8
10
11
12
13
14
15
DATUM

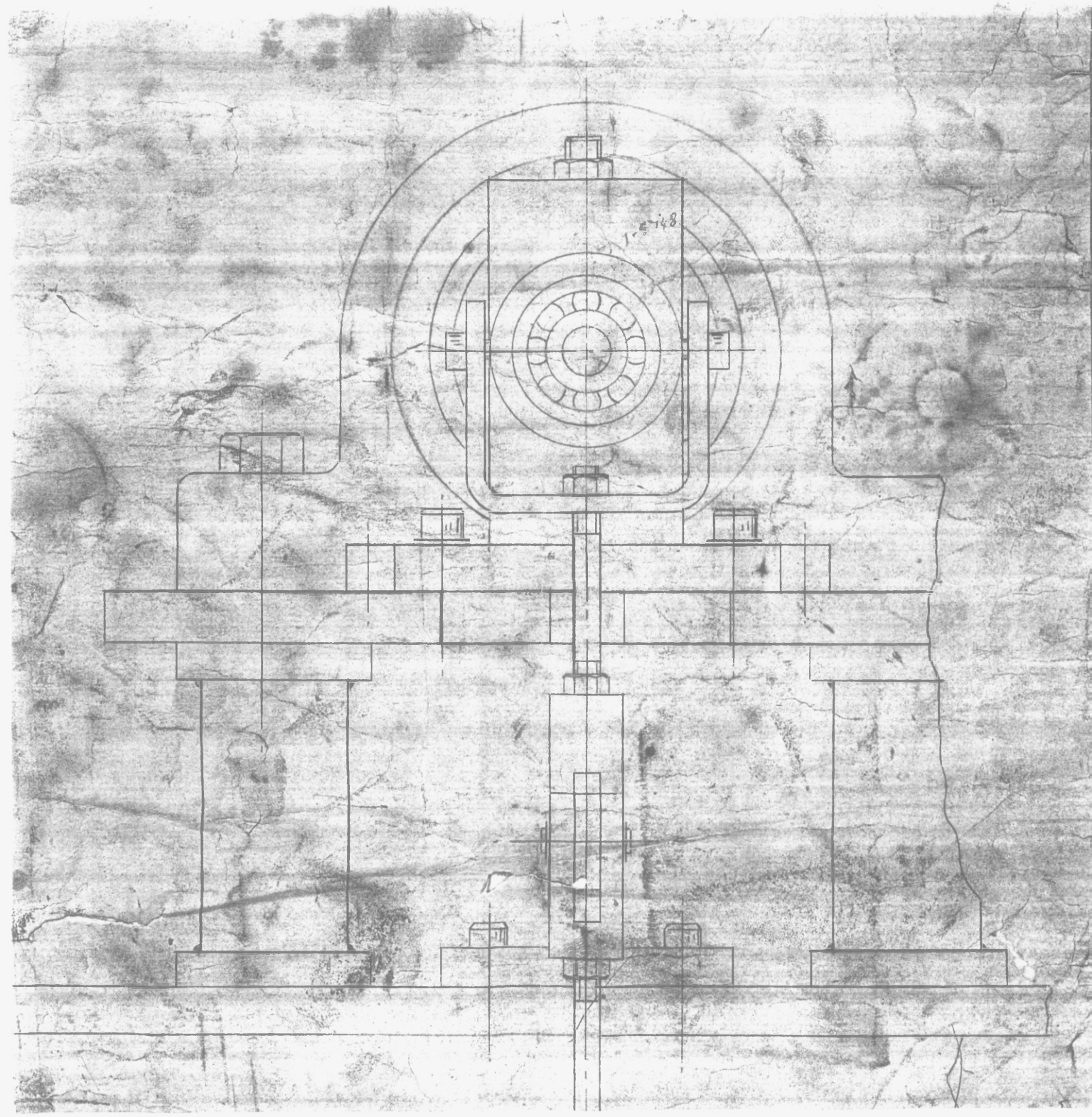

L	1	ANTIVBRATION MOUNT	'LAMA' MOUNT Nº 1
K	1	CONTROLLER	'NECO' 2AF 200
J	1	MOTOR	'NECO' 1 hp D.C. THIR. CONT.
I	1	PULLEY	20L075F 1108 ϕ1"
H	1	PULLEY	40L075F 1310 ϕ·75"
G	1	BELT	L075 367L
F	1	BEARING BLOCK	'ASAHI' UCW 201-8
E	1	CONNECTOR	3/8" BSP
D	2	LIP SEAL	'WESTERN' W08705025R4
C	1	LOCKING BUSH	'DOKO' 100/16 Ø10
B	1	PLUMMER BLOCK	'ASAHI' UKP 211+HE2311
A	1	PLUMMER BLOCK	'ASAHI' UKP 206+HE2306
25			
24			
23			
22	1	MAIN FRAME	STEEL
21	1	MOTOR GUARD	MESH
20	1	BELT GUARD	"
19	1	WEIGHT GUARD	STEEL
18	1	HANGER PAN	ALLOY
17	1	HANGER ROD	SILVER STEEL
16	1	LEVER	STEEL
15	1	TIE BAR	SILVER STEEL
14	3	CLEVIS PIN	" "
13	2	CLEVIS	STEEL
12	1	BRACKET	"
11	1	HANGER	"
10	1	CLAMP	"
9	1	BEARING HOUSING	"
8	1	DRAIN PIPE	COPPER
7	1	SPANNER	STEEL
6	1	BALL HOUSING	STEEL
5	2	GUIDE	"
4	1	SPACER	"
3	1	SUB-BASE	"
2	4	PILLAR	"